Synthesis and Self-Assembly of Multiple Thermoresponsive Amphiphilic Block Copolymers

A dissertation submitted to

University of Potsdam
Department of Chemistry

for the degree of
"doctor rerum naturalium"
(Dr. rer. nat.)

in Macromolecular Chemistry

Presented by

Jan Weiß

Supervisor Prof. A. Laschewsky

Potsdam 2011

Published online at the
Institutional Repository of the University of Potsdam:
URL http://opus.kobv.de/ubp/volltexte/2011/5336/
URN urn:nbn:de:kobv:517-opus-53360
http://nbn-resolving.de/urn:nbn:de:kobv:517-opus-53360

Danksagung

Mein Dank geht an Prof. Dr. A. Laschewsky für die Möglichkeit meine Doktorarbeit in seiner Gruppe anfertigen zu können und für die Unterstützung und Diskussionen während dieser Zeit. Ferner möchte ich Dr. J. van Heijst und Dr. H. Rüegger, der das Ende dieser Arbeit aufgrund tragischer Umstände leider nicht mehr miterleben kann, für die Möglichkeit danken, temperaturabhängige NMR Spektren an der ETH Zürich messen zu können, Dr. C. Böttcher für die TEM Messungen, Prof. Dr. S. Beuermann und Herrn S. Prentzel für SEC Messungen, Dr. N. Hildebrandt und Dr. S. Stufler für den Zugang zum Fluoreszenzspektrometer sowie Prof. Dr. J. Beckmann und Prof. Dr. H. Frauenrath für hilfreiche Diskussionen.
Ausserdem möchte ich Dr. Achille Bivigou-Koumba für die zahlreichen Diskussionen und die praktischen Ratschläge, besonders in der Anfangsphase meiner Promotionszeit und Maike Lukowiak für den Zugang zu einiger Literatur danken.
Des Weiteren möchte ich Dr. Nezha Badi für die hilfreichen Diskussionen, Korrekturen dieser Arbeit, die Unterstützung sowie für die wundervolle Zeit auch neben der Arbeit, die meine drei Jahre in Potsdam unvergesslich macht, von ganzem Herzen danken.
Zu guter Letzt geht noch ein besonderer Dank an meine Familie, insbesondere an meine Mutter für ihre fortwährende Unterstützung in jeglicher Hinsicht.

List of Publications

Parts of this Ph. D. thesis were published in scientific journals and were presented in oral presentations as well as on posters at several occasions by the author of this thesis.

Publications (peer-reviewed)

[1] "Universal Polymer Analysis by ^{1}H NMR Using Complementary Trimethylsilyl End Groups", M. Päch, D. Zehm, M. Lange, I. Dambowsky, J. Weiss, A. Laschewsky, *J. Am. Chem. Soc.*, **2010**, *132*, 8757-8765.

[2] "Self-Assembly of Double Thermoresponsive Block Copolymers End-capped with Complementary Trimethylsilyl Groups", J. Weiss, C. Böttcher, A. Laschewsky, *Soft Matter*, **2011**, *7*, 483-492.

[3] "Temperature Induced Self-Assembly of Triple Thermoresponsive Triblock Copolymers in Aqueous Solution", J. Weiss, A. Laschewsky, *Langmuir*, **2011**, *27*, 4465-4473.

[4] "Ferrocenyl (Meth)Acrylates in RAFT Polymerization", C. Herfurth, D. Voll, J. Buller, J. Weiss, C. Barner-Kowollik, A. Laschewsky, submitted to *J. Polym. Sci. Part A: Polym. Chem.*

Publications (to be submitted)

[5] "Water-soluble Random and Alternating Copolymers of Styrene Monomers with Adjustable Lower Critical Solution Temperature", J. Weiss, A. Li, E. Wischerhoff, A. Laschewsky*, to be submitted.

[6] "Facile One-Step Synthesis of Double Thermosensitive Diblock Copolymers", J. Weiss, A. Laschewsky*, to be submitted.

Oral Presentations

[1] "A Trimethylsilyl-labeled RAFT-Agent as NMR Probe for Reversible Block Copolymer Self-Assembly", 13.07.2010, 43rd IUPAC World Polymer Congress, Glasgow, UK.

[2] "Multistep Self-Assembly of Thermoresponsive Block Copolymer Surfactants", 03.05.2011, 45th International Detergency Conference (IDC), Düsseldorf, Germany.

Poster Contributions

[1] "Temperature Induced Self-Assembly of Triple-Responsive Triblock Copolymers in Aqueous Solutions", PhD Student's Workshop *Functional Soft Matter*, Potsdam, Germany, 2010.

[2] "Temperature Induced Self-Assembly of Triple-Responsive Triblock Copolymers in Dilute Aqueous Solution", 43rd IUPAC World Polymer Congress, Glasgow, UK, 2010.

[3] "Self-Assembly of Triple-Thermoresponsive Triblock Copolymers in Dilute Aqueous Solution", Polymers in Biomedicine and Electronics - Biannual Meeting of the GDCh-Division Macromolecular Chemistry and Polydays 2010, Berlin, Germany, 2010.

[4] "Improving the IQ of Intelligent Block Copolymer Surfactants: Designs for Multiple Switching", 6th European Detergency Conference, Fulda, Germany, 2010.

[5] "Sequential Self-Assembly of Multiple Thermoresponsive Block Copolymers", Makromolekulares Kolloquium, Freiburg, Germany, 2011.

Summary

In the present thesis, the self-assembly of multi thermoresponsive block copolymers in dilute aqueous solution was investigated by a combination of turbidimetry, dynamic light scattering, TEM measurements, NMR as well as fluorescence spectroscopy. The successive conversion of such block copolymers from a hydrophilic into a hydrophobic state includes intermediate amphiphilic states with a variable hydrophilic-to-lipophilic balance. As a result, the self-organization is not following an *all-or-none* principle but a multistep aggregation in dilute solution was observed. The synthesis of double thermoresponsive diblock copolymers as well as triple thermoresponsive triblock copolymers was realized using twofold-TMS labeled RAFT agents which provide direct information about the average molar mass as well as residual end group functionality from a routine ^{1}H NMR spectrum. First a set of double thermosensitive diblock copolymers poly(N-n-propylacrylamide)-*b*-poly(N-ethylacrylamide) was synthesized which differed only in the relative size of the two blocks. Depending on the relative block lengths, different aggregation pathways were found. Furthermore, the complementary TMS-labeled end groups served as NMR-probes for the self-assembly of these diblock copolymers in dilute solution. Reversible, temperature sensitive peak splitting of the TMS-signals in NMR spectroscopy was indicative for the formation of mixed star-/flower-like micelles in some cases.

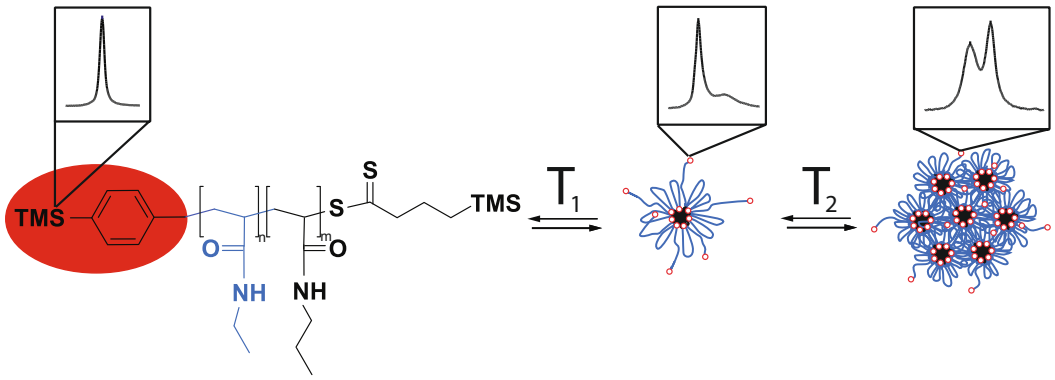

Moreover, triple thermoresponsive triblock copolymers from poly(N-n-propylacrylamide) (A), poly(methoxydiethylene glycol acrylate) (B) and poly(N-ethylacrylamide) (C) were obtained from sequential RAFT polymerization in all possible block sequences (ABC, BAC, ACB). Their self-organization behavior in dilute aqueous solution was found to be rather complex and dependent on the positioning of the different blocks within the terpolymers. Especially the localization of the low-LCST block (A) had a large influence on the aggregation behavior. Above the first cloud point, aggregates were

only observed when the A block was located at one terminus. Once placed in the middle, unimolecular micelles were observed which showed aggregation only above the second phase transition temperature of the B block. Carrier abilities of such triple thermosensitive triblock copolymers tested in fluorescence spectroscopy, using the solvatochromic dye Nile Red, suggested that the hydrophobic probe is less efficiently incorporated by the polymer with the BAC sequence as compared to ABC or ACB polymers above the first phase transition temperature.

In addition, due to the problem of increasing loss of end group functionality during the subsequent polymerization steps, a novel concept for the one-step synthesis of multi thermoresponsive block copolymers was developed. This allowed to synthesize double thermoresponsive di- and triblock copolymers in a single polymerization step. The copolymerization of different N-substituted maleimides with a thermosensitive styrene derivative (4-vinylbenzyl methoxytetrakis(oxyethylene) ether) led to alternating copolymers with variable LCST. Consequently, an excess of this styrene-based monomer allowed the synthesis of double thermoresponsive tapered block copolymers in a single polymerization step.

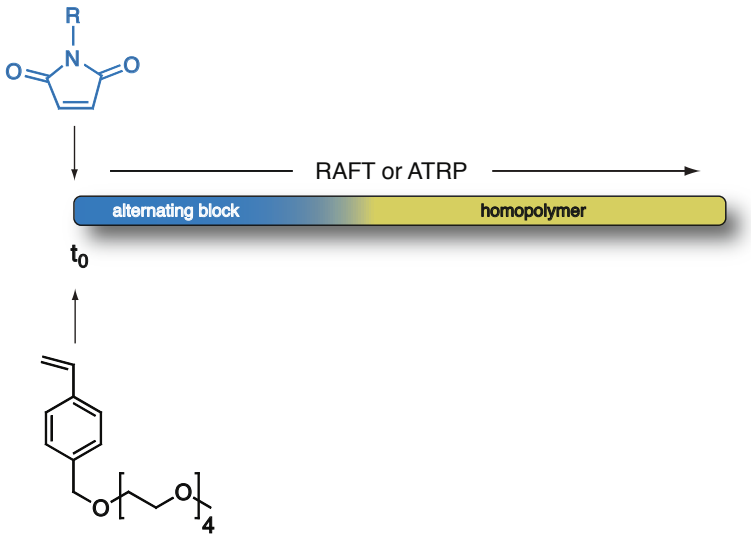

Furthermore, by using bifunctional initiators, even double thermosensitive binary triblock copolymers could be synthesized. Both types of polymers showed an aggregation behavior similar to the one of block copolymers obtained by the classical step-wise approach indicating the successful one-step synthesis of multi responsive block copolymers.

Zusammenfassung

Im Rahmen der vorliegenden Arbeit wurde die Selbstorganisation von mehrfach thermisch schaltbaren Blockcopolymeren in verdünnter wässriger Lösung mittels Trübungsphotometer, dynamischer Lichtstreuung, TEM Messungen, NMR sowie Fluoreszenzspektroskopie untersucht. Die schrittweise Überführung eines hydrophilen in ein hydrophobes Blockcopolymer beinhaltet ein oder mehr amphiphile Zwischenstufen mit einstellbarem hydrophilen zu lipophilen Anteil (HLB). Dies führt dazu, dass die Selbstorganisation solcher Polymere in Lösung nicht nur einem Alles-oder-nichts-Prinzip folgt sondern ein mehrstufiges Aggregationsverhalten beobachtet wird. Die Synthese von doppelt thermisch schaltbaren Diblockcopolymeren und dreifach thermisch schaltbaren Triblockcopolymeren wurde durch sequenzielle RAFT Polymerisation realisiert. Dazu wurden zweifach TMS-markierte RAFT Agentien verwendet, welche die Bestimmung der molaren Masse sowie der verbliebenen Endgruppenfunktionalität direkt aus einem ^{1}H NMR Spektrum erlauben. Mit diesen RAFT Agentien wurde zunächst eine Serie von doppelt thermisch schaltbaren Diblockcopolymeren aus Poly(N-n-propylacrylamid)-*b*-Poly(N-ethylacrylamid), welche sich lediglich durch die relativen Blocklängen unterscheiden, hergestellt. In Abhängigkeit von der relativen Blocklänge wurde ein unterschiedliches Aggregationsverhalten der Diblockcopolymere in verdünnter wässriger Lösung beobachtet. Des Weiteren wirken die komplementär TMS-markierten Endgruppen als NMR-Sonden während der schrittweisen Aggregation dieser Polymere. Reversible, temperaturabhängige Peakaufspaltung der TMS-Signale in der NMR Spektroskopie spricht für eine Aggregation in gemischte stern-/blumenartige Mizellen, in denen ein Teil der hydrophoben Endgruppen in den hyrophoben Kern zurückfaltet.

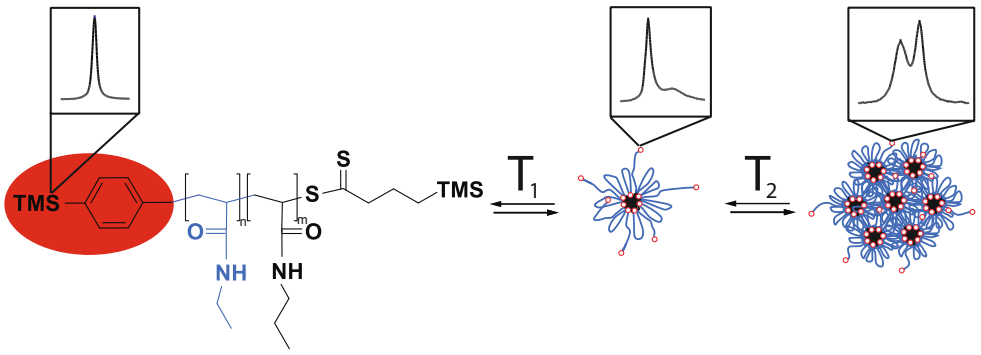

Obendrein wurden dreifach thermisch schalbare Triblockcopolymere aus Poly(N-n-propylacrylamid) (A), Poly(methoxydiethylen glycol acrylat) (B) und Poly(N-ethylacrylamid) (C) in allen möglichen Blocksequenzen (ABC, BAC, ACB) durch schrittweisen Aufbau mittels RAFT Polymerisation erhalten. Das Aggregationsverhalten dieser Polymere in verdünn-

ter wässriger Lösung war relativ komplex und hing stark von der Position der einzelnen Blöcke in den Triblockcopolymeren ab. Besonders die Position des Blocks mit der niedrigsten LCST (A) war ausschlaggebend für die resultierenden Aggregate. So wurde oberhalb der ersten Phasenübergangstemperatur nur Aggregation der Triblockcopolymere beobachtet, wenn der A Block an einem der beiden Enden der Polymere lokalisiert war. Wurde der A Block hingegen in der Mitte der Polymere positioniert, entstanden unimere Mizellen zwischen der ersten und zweiten Phasenübergangstemperatur, welche erst aggregierten, nachdem der zweite Block (B) seinen Phasenübergang durchlief. Die Transportereigenschaften dieser Triblockcopolymere wurden mittels Fluoreszenzspektroskopie getestet. Dazu wurde die Einlagerung eines hydrophoben, solvatochromen Fluoreszenzfarbstoffes, Nilrot, in Abhängigkeit der Temperatur untersucht. Im Gegensatz zu den Polymeren mit der Blocksequenz ABC oder ACB, zeigten die Polymere mit der Sequenz BAC eine verminderte Aufnahmefähigkeit des hydrophoben Farbstoffes oberhalb des ersten Phasenübergangs, was auf die fehlende Aggregation und die damit verbundenen relativ kleinen hydrophoben Domänen der unimolekularen Mizellen zwischen der ersten und zweiten Phasenübergangstemperatur zurückzuführen ist.

Aufgrund des zunehmenden Verlustes von funktionellen Endgruppen während der RAFT Synthese von Triblockcopolymeren wurde ein neuartiges Konzept zur Einschrittsynthese von mehrfach schaltbaren Blockcopolymeren entwickelt. Dieses erlaubt die Synthese von mehrfach schaltbaren Diblock- und Triblockcopoylmeren in einem einzelnen Reaktionsschritt. Die Copolymeriation von verschiedenen N-substituierten Maleimiden mit einem thermisch schaltbaren Styrolderivat (4-Vinylbenzylmethoxytetrakis(oxyethylene) ether) ergab alternierende Copolymere mit variabler LCST. Die Verwendung eines Überschusses dieses styrolbasierten Monomers erlaubt ferner die Synthese von Gradientenblockcopolymeren in einem einzelnen Polymerisationsschritt.

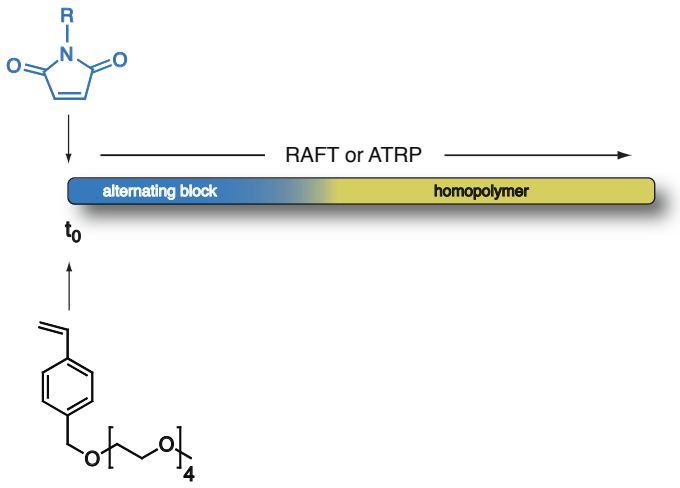

Bifunktionelle Initiatoren ergaben, dem gleichen Reaktionsprinzip folgend, doppelt schaltbare binäre Triblockcopolymere. Die so hergestellten Blockcopolymere zeigten ein vergleichbares Aggregationsverhalten in verdünnter wässriger Lösung wie Blockcopolymere, die durch klassiche sequenzielle kontrolliert radikalische Polymerisation erhalten werden.

List of Abbreviations

AGET	activator generated by electron transfer
anal.	analysis
ARGET	activators regenerated by electron transfer
ATRP	atom transfer radical polymerization
b	broad signal (NMR)
calcd	calculated
CP	cloud point
CRP	controlled radical polymerization
CTA	chain transfer agent
d	doublet (NMR)
δ	chemical shift (NMR)
DCM	dichloromethane
DBPO	dibenzoyl peroxide
DIEA	diisopropylethylamine
DIPA	diisopropylamine
DMF	*N*,*N*-dimethylformamide
DMSO	dimethylsulfoxide
DP	average degree of polymerization
EI	electron impact ionization
eq.	equivalents
ESI	electrospray ionization
FRP	free radical polymerization
GPC	gel permeation chromatography
^{1}H NMR	proton nuclear magnetic resonance
^{13}C NMR	^{13}carbon nuclear magnetic resonance
HMDS	hexamethyldisilazane
HRMS	high resolution mass spectrometry
HV	high vacuum
IR	infra red
J	J coupling constant (NMR)
LFRP	living free radical polymerization
m	multiplet (NMR)

M	molar
$[M]^+$	molecular ion (MS)
MDEGA	methoxydiethylene glycol acrylate
M_n	number average molecular weight
NDM	N-decylmaleimide
NEA	N-ethylacrylamide
NMM	N-methylmaleimide
NMP	nitroxide mediated polymerization
NMR	nuclear magnetic resonance
NPA	N-propylacrylamide
NPM	N-propylmaleimide
NPEGM	N-PEG_{750}-maleimide
NSM	N-ethylthiomethyl maleimide
NSOM	N-ethylsulfoxymethyl maleimide
NtBAlaM	N,N-maleoyl-L-alanine *tert.*-butylester
NtBGlyM	N,N-maleoyl-L-glycine *tert.*-butylester
NTESM	N-(3-triethylsilyl)propargyl maleimide
NTMSM	N-(3-trimethylsilyl)propyl maleimide
PDI	polydispersity index
PEG	poly(ethylene glycol)
PEO	poly(ethylene oxide)
ppm	parts per million (NMR)
PS	polystyrene
RAFT	reversible addition fragmentation chain transfer
R_f	retention or retardation factor (thin layer chromatography)
s	singlet (NMR)
t	triplet (NMR)
TBAF	tetrabutylammonium fluoride
TEA	triethylamine
TEM	transmission electron microscopy
TEMPO	2,2,6,6-tetramethylpiperidinyloxyl
TES	triethylsilyl
TFA	trifluoroacetic acid
THF	tetrahydrofuran
TLC	thin layer chromatography

TMS	trimethylsilyl
TMS_R	TMS group on the R group of a TMS-labeled RAFT agent
TMS_Z	TMS group on the Z group of a TMS-labeled RAFT agent
TEGDME	triethyleneglycol dimethylether
UV	ultraviolet
VBTOE	4-vinylbenzyl methoxytetrakis(oxyethylene) ether

Contents

1 Scope and Motivation

Hierarchically structured nanomaterials, as often present in biological systems, are typically obtained using a combined "bottom-up" and "top-down" approach.[1] The "top-down" approach, although still dominating in today's industries, will face increasing technological challenges and might reach its physical limitations in the near future. By contrast, the "bottom-up" approach aims to build up ordered structures from (macro)molecular precursors, attempting to benefit from their built-in information for higher structure formation. The propensity to hierarchical structure formation, thus, is programmed on the molecular level and translated into building blocks with a defined shape on the supramolecular level. Accordingly, the self-organization of appropriate macromolecular building blocks is a promising "bottom-up" route toward well-defined nanomaterials.[2–4]

Within this context, amphiphilic block copolymers in aqueous media represent an interesting class of self-organizing molecules since they are known to form a variety of aggregates such as spherical micelles, worm-like (*i.e.* cylindrical) micelles, as well as vesicles in dilute aqueous solution.[5–10] Especially, stimuli responsive polymers, also often referred to as "smart", found increasing attention in the last decade due to their potential application in industry ranging from biomedical to material science.[6] The ability to control the aggregation behavior of stimuli-sensitive polymers may help to address future challenges in nanoscience and provides fundamental knowledge for the design of smart materials with tunable properties. This thesis aims at understanding how multi responsive block copolymers self-assemble in aqueous solution and tries to develop solutions for current limitations in polymer synthesis and characterization as well as investigation of the formed aggregates on a molecular level.

2 Introduction

2.1 Controlled Radical Polymerization Techniques

Free radical polymerization (FRP) is widely used in order to obtain high molecular weight polymers due to (*i*) the compatibility with a variety of monomers, such as (meth)acrylates, (meth)acrylamides, styrenics, dienes as well as other vinylic monomers; (*ii*) its tolerance against many functionalities within monomers and solvent, *e.g.*, OH, NR_2, COOH, $CONR_2$, SO_3; (*iii*) its high compatibility with various reaction conditions (*e.g.*, bulk, solution, emulsion, mini-emulsion, and suspension); (*iv*) its relatively low costs compared to other technologies. Although widely used in industry and research laboratories, FRP has a significant drawback. The variety of possible termination reactions result in limited control over molecular weight, molecular weight distribution as well as end groups and architecture of the desired polymers.[11] Moreover, block copolymers with defined block sequences and predetermined relative block lengths are practically not accessible by conventional free radical polymerization. In order to overcome these limitations and enable the synthesis of well defined block copolymers, several controlled radical polymerization (CRP) techniques were invented within the past two decades, such as nitroxide mediated polymerization[12] (NMP), atom transfer radical polymerization[13] (ATRP), or reversible addition-fragmentation chain transfer polymerization[14] (RAFT). Before the discovery of the CRP principle, living ionic polymerizations were one of the few available tools to achieve control over molecular weight and architecture with low polydispersities. The major disadvantages of ionic polymerizations, however, are the very stringent reaction conditions, typically the complete absence of oxygen and water, as well as the sensitivity to most functional groups.[15] The development of controlled radical polymerization techniques combined the best of both attempts, compatibility with a wide range of functional monomers, low polydispersities, and control over molecular weight and architecture. The key principle of controlled radical polymerizations is based on reversible chain termination (Scheme 1).

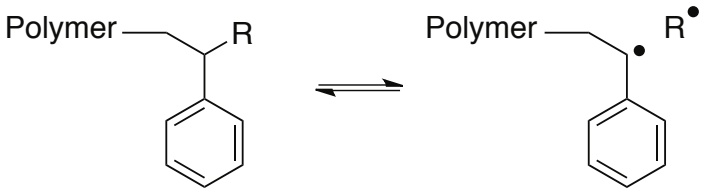

Scheme 1: Basic principle of Controlled Radical Polymerizations: Reversible interchange between dormant and active chain ends.

As a result, the polymer chains can grow simultaneously throughout the reaction with very low concentrations of free radicals present at all times during the polymerization process, thus minimizing irreversible termination reactions, such as recombination and disproportionation. However, controlled radical polymerization techniques are no "true" living systems[16–19] and termination reactions are not negligible. Nevertheless, they display important characteristics of a living polymerization such as (*i*) a linear relation between molecular weight and conversion, (*ii*) molecular weight equal or close to the theoretical molecular weight, (*iii*) low polydispersity, and (*iv*) defined end groups. For this reason, they are sometimes referred to as living free radical polymerization (LFRP) in the literature.

2.1.1 Nitroxide Mediated Radical Polymerization

Nitroxide mediated radical polymerization resulted from intentions of the australian Commonwealth Scientific and Industrial Research Organization (CSIRO) team around D. H. Solomon to study the initiation of free radical polymerizations by trapping the propagating radical.[20] The trapping agent used, 2,2,6,6-tetramethylpiperidinyloxy (TEMPO), does not react with heteroatom-centered radicals but adds to carbon-centered radicals with near diffusion-controlled rates.[21] The fact that trapped radicals with more than one monomer unit were found, in combination with the observed thermal instability of the formed alkoxyamines, led to the assumption that thermal dissociation and reversible trapping can lead to the controlled formation of oligomeric compounds.

Based on this initial work of Solomon, Rizzardo and Moad, low molecular weight polymers and oligomers were obtained at temperatures of 80-100°C.[22] Low polydispersity polystyrene was synthesized by further increasing the temperature to 130°C in bulk using dibenzoyl peroxide (DBPO) as initiator and TEMPO as mediator.[23] Since then ongoing research led to

improved nitroxides[12] which allow polymerization of many different monomer classes, e. g., acrylates, acrylamides, 1,3-dienes as well as acrylonitrile based monomers.

The polymerization mechanism of the nitroxide mediated radical polymerization is based on a kinetic phenomenon called *persistent radical effect*[24] (Scheme 2). After heterolytic cleavage of the initiator into the initiating radical $X^{\bullet}$ and the mediating radical $R^{\bullet}$, small amounts of the initiating radical will undergo radical-radical coupling. The mediating radical $R^{\bullet}$, however, cannot undergo homocoupling which results in an overall excess of mediating radicals compared to initiating/propagating radicals.

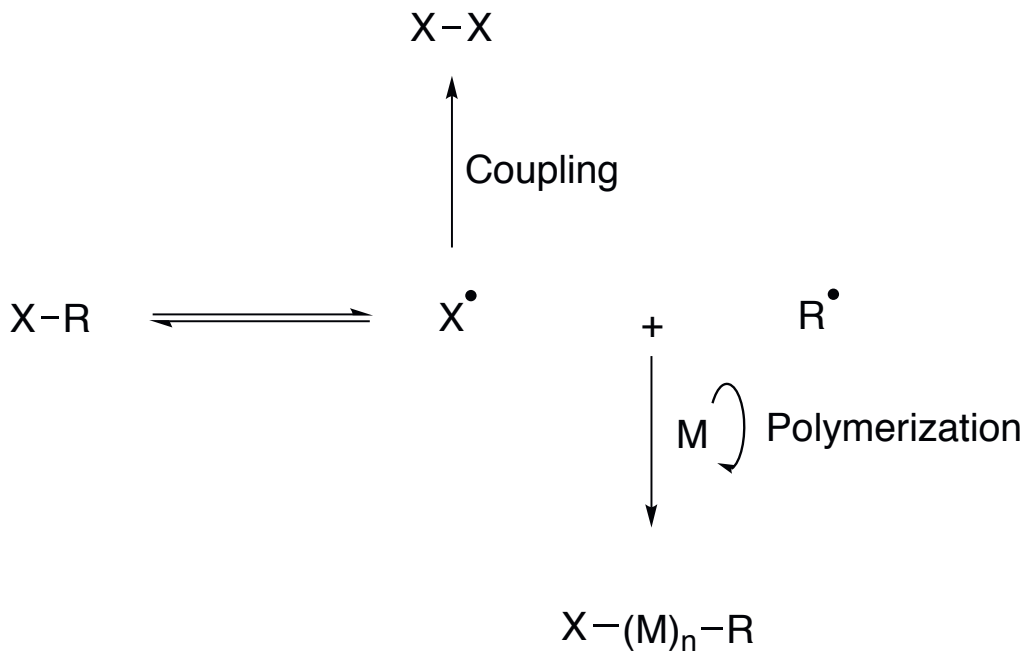

Scheme 2: Principle scheme for the nitroxide mediated radical polymerization.

The increasing efficiency of the formation of dormant chain ends with increasing excess of mediating radicals regulates this equilibrium. The resulting small quantity of propagating radicals with a large overall excess of dormant polymer chains gives rise to the persistent radical effect (PRE) and, hence, potential control over molecular weight and molecular weight distribution. The upper limit for controlled molecular weight lays at 150000-200000 g mol^{-1} for NMP polymerizations.[25]

2.1.2 Atom Transfer Radical Polymerization

The best established controlled radical polymerization technique to date is the transition metal catalyzed atom transfer radical polymerization (ATRP) which was independently discovered by Sawamoto *et al.* [26] and Matyjaszewski *et al.* [27] in 1995. The mechanism of ATRP (Scheme 3) is based on a reversible redox process which generates the active species, usually a Cu^{I}-complex. The oxidized species leads to a reversible abstraction of a halogen atom (Cl, Br) from the dormant species R-X to generate the active radical $R^{\bullet}$.

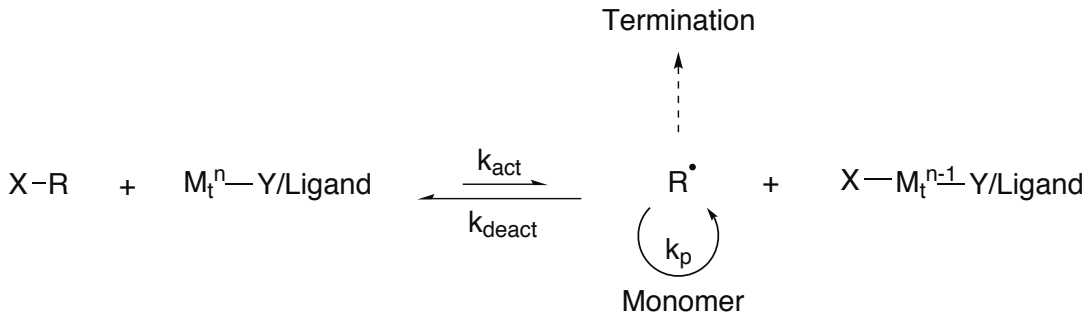

Scheme 3: General mechanism of the atom transfer radical polymerization.

Molecular weights up to 150000 g mol^{-1} have been successfully achieved by ATRP. However, at higher molecular weights increasing amounts of termination reactions suggest an upper limit for controlled radical polymer synthesis.[28] Such termination reactions mainly include recombination and disproportionation and result from interactions of Cu^{II} species with both the growing radical as well as its dormant species. In contrast to the normal ATRP, where the initiating radicals are formed from an alkyl-halide and a transition metal in its lower oxidation state, reverse ATRP uses classical initiators (e. g. AIBN) in combination with a transition metal-complex in its higher oxidation state.[29–31] Various monomer types have been polymerized by ATRP such as styrenes, (meth-)acrylates, (meth-)acrylamides and others.[13] However, some monomer classes are not accessible such as monomers containing acidic side chains, since they can protonate the ligands which form the corresponding carboxylates, as well as halogenated alkenes, alkyl-substituted olefines, and vinyl esters. In ATRP, likewise to other controlled polymerization techniques, the initiator should ensure a fast initiation step compared to propagation.

Therefore, some general considerations for the initiator design should be taken into account:

- The initiator quality decreases from tertiary to secondary to primary alkyl halides and addition of stabilizing groups, with relative efficiencies in the order CN > C(O)R > C(O)OR > Ph > Cl > Me, will improve the initiator quality.[32–34]
- Although the bond strength for alkyl halides decreases in the order R-Cl > R-Br > R-I and, hence, alkyl iodides should be the most efficient ATRP initiators, their use requires certain precautions. For instance, their light sensitivity can lead to the formation of metal iodide complexes (e. g., CuI_2 which is thermodynamically unstable) or heterolytic cleavage resulting in degenerative transfer reactions.[35] Accordingly, bromides and chlorides are preferentially used. Also pseudohalogens such as thiocyanates (SCN) have been used[36] but showed slow initiation for both styrene and methacrylate (MA).
- The choice of catalyst may also influence the initiation efficiency. For example, 2-bromoisobutyrophenone initiates the controlled polymerization of methylmethacrylate (MMA) when ruthenium or nickel complexes are used but turns out to be useless in the copper-mediated ATRP. This is ascribed to the reduction of the resulting electrophilic radical by the Cu^I species due to the lower redox potentials of copper-based catalysts.
- The order of reagent addition might be important. Upon slow addition of the catalyst to the initiator/monomer solution the rate of termination during the initiation period was found to be reduced.[13]

Beside the initiator and transition metal catalyst, the ligand is very important. Its major role is to provide solubility for the transition-metal salt in the reaction medium and to adjust the redox potential of the metal center. For the copper-mediated ATRP, nitrogen-containing chelating ligands have predominantly been used not least because of the much lower efficiency of sulfur, oxygen or phosphorus ligands due to unfavorable binding constants and/or improper electronic effects. In principle, the activity of an ATRP ligand decreases with decreasing nitrogen atoms and increasing linking carbon atoms.[37] The major disadvantage of ATRP is, beside the relatively high temperatures usually used, the high amounts of (generally toxic) transition metal catalysts needed. These metal contaminants have to be removed

from the products, especially in industrial use and, due to their toxicity, limit the use of ATRP derived polymers. Recent developments led to improved methods to conduct ATRP polymerizations. In the so called activator generated by electron transfer (AGET) ATRP process electron transfer is used instead of organic radicals to reduce the higher oxidation state transition metal.[38] This allows the use of ATRP catalyst systems in their more stable higher oxidation states since these are reduced *in situ* before adding the initiator. In addition, the amount of transition metals could be reduced to ppm quantities using activators regenerated by electron transfer (ARGET) ATRP.[39] Reducing agents such as ascorbic acid or tin(II) 2-ethylhexanoate can continuously regenerate Cu^{I} from Cu^{II} during the polymerization and, thus, ensure the catalytic amounts of transition metal needed.

2.1.3 Reversible Addition-Fragmentation Chain Transfer Polymerization

Reversible addition-fragmentation chain transfer (RAFT) polymerization was discovered at Australia's CSIRO in the late 1990s.[40–42] In parallel, a similar polymerization technique, macromolecular design by interchange of xanthate (MADIX) was invented in France.[14] Both RAFT and MADIX are based on an addition-fragmentation chain transfer mechanism.[43,44] While MADIX refers to polymerizations mediated by xanthates, RAFT is usually mediated by dithioesters or trithiocarbonates. Successful RAFT polymerization depends on the design of the RAFT agent. To date many different RAFT agents have been reported.[40,41,45–56] Both R- and Z-group allow for fine tuning of the performance of the RAFT agent. In principle the R-group should be a good leaving group and liberate a relatively stable free radical with the ability to initiate a polymerization. Therefore, the type and structure of the R-group can have tremendous impact on the polymerization kinetics and the overall control. In contrast, the Z-group is responsible for the ability of the C=S double bond to react with growing radicals and the mean lifetime of the resulting intermediate radical formed.

The RAFT process is basically a free radical polymerization carried out in the presence of a particular chain transfer agent, the so-called RAFT agent. Accordingly, traditional methods to generate radicals from commercially available initiators such as 2,2'-azobis(2-methylpropionitrile) (AIBN) or 4,4'-azobis(4-cyanovaleric acid) (V-501) are used. The initiation step can also be carried out by photoinitiators or gamma irradiation.[51,57–59] Neglecting

the solvent cage effect, the produced radical $I^{\bullet}$ can either add to a monomer to initiate a growing chain or add to the RAFT agent (Scheme 4). Due to the high transfer constants of the most RAFT agents it is unlikely that more than a few monomers add to a growing chain before the chain adds to a RAFT agent. Thus, *via* both pathways the intermediate radical is reversibly formed which then can either fragment to give the RAFT agent and the growing radical chain or cleave the R-group homolytically. The latter is the desired reaction pathway and requires the R-group to be a better leaving group than the oligomer or polymer chain and to be capable to initiate a polymerization. Hence, in the beginning of the polymerization, the so-called pre-equilibrium, all initial RAFT agents should be activated and converted into RAFT agents containing oligomeric or polymeric R-groups (macro-RAFT agents).

Pre-equilibrium:

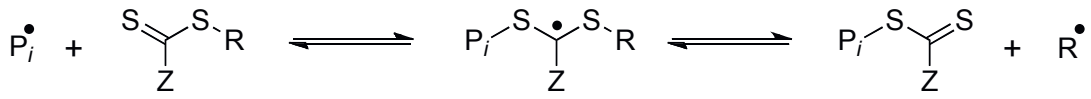

Main equilibrium:

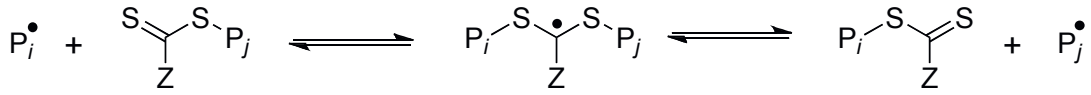

Scheme 4: Mechanism of the RAFT process.

The number of polymer chains is controlled by the amount of RAFT agents and not by the number of initiator radicals produced. Once all RAFT agents are converted into macro-RAFT agents, the main equilibrium starts. Here the reversible addition-fragmentation reactions are dominant with a high amount of dormant chain ends compared to free radicals. In an ideal RAFT polymerization all polymers are initiated by the R-group of the RAFT agent. As a result the degree of polymerization is controlled by the ratio of monomer to RAFT agent and the molar mass at a certain conversion can be calculated according to:

$$M_{n,theory} = \frac{[Monomer]_0 * M_{Monomer} * \rho}{[CTA]_0 + 2f[I]_0 * (1 - e^{-k_d t})} + M_{CTA} \tag{2.1}$$

where $[Monomer]_0$ stands for the initial monomer concentration, $M_{Monomer}$ is the molecular weight of the monomer, ρ is the conversion, $[CTA]_0$ is the concentration of RAFT agent, f is the initiator efficiency, $[I]_0$ is the initiator concentration, k_d is the initiator decomposition rate constant, and M_{CTA} is the molecular weight of the RAFT agent. If the ratio of $[CTA]_0/[I]_0$ is high, initiation of polymer chains by initiator radicals can be neglected and equation 2.1 simplifies to:

$$M_{n,theory} = \frac{[Monomer]_0 * M_{Monomer} * \rho}{[CTA]_0} + M_{CTA} \tag{2.2}$$

The dithiobenzoate mediated RAFT polymerization involves two possible rate retarding effects, (*i*) an *induction period* during the initial stage with almost no polymerization activity, and (*ii*) *rate retardation* in the following phase with polymerization rates slower than in conventional radical polymerization systems.[60] These effects depend on the concentration of RAFT agent. Rate retardation is only observed for polymerizations initiated by macro-RAFT agents. While the CSIRO team explained the rate retardation effect by slow fragmentation of the carbon-centered intermediate radical, Monteiro, Brouwer and Fukuda postulated a *cross-termination* of the intermediate radical with a growing radical chain.[60]
In all theoretical models the retardation effect increases with increasing stability of the intermediate radical. In dithiobenzoate mediated RAFT systems delocalization of the radical within the aromatic system is assumed to be responsible (Scheme 5).[61]

Replacing the phenyl group by a benzyl moiety led to significantly lower rate retardation effects since the delocalization of the radical center is effectively suppressed.[62] Furthermore, para-substituted dithiobenzoates showed significantly lower rate retardation effects.[63] This observation indicates delocalized radicals and potential side reactions since the para-position is less prone to radical attacks whereas the stability of the intermediate radical should remain unchanged using the substituted RAFT agent. In order to investigate the mechanistic aspects of the RAFT process, radical storage experiments were applied to cumyl

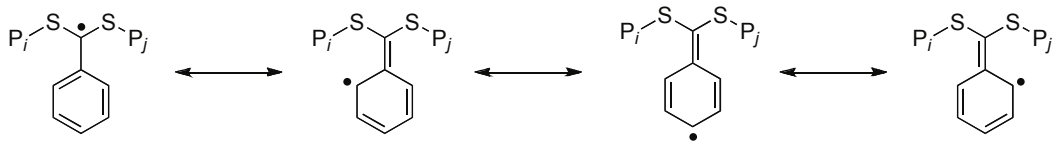

Scheme 5: Assumed resonance structures of the intermediate radical in dithiobenzoate mediated RAFT polymerizations.

dithiobenzoate (CDB) mediated styrene and methylacrylate systems[59,64] as well as to non-retarding RAFT agents.[65] Systems containing dithiobenzoate RAFT agents are capable to store radicals for a certain time and, moreover, can induce a polymerization afterward without the need of initiators. However, such experiments cannot be used to identify the chemical nature of these intermediates. In order to determine whether or not cross-termination occurs, electronspray ionization mass spectrometry (ESI-MS) was used. Until now, no star polymers could be detected by this technique.[66,67] This lack of experimental evidence for cross-termination reactions is a reason for continued debates about the origin of rate retardation in the RAFT mechanism. ^{13}C NMR measurements, in contrast, provided evidence about the existence of 3- and 4-arm star polymers when high initial concentrations of RAFT agents were used. This led to the assumption that the intermediate radicals undergo side reactions with growing radical chains.[68]

On the theoretical level, the RAFT process can neither be fully explained using the cross-termination model nor the slow-fragmentation model. The cross-termination model is in good agreement with the experimentally observed kinetic aspects of the main equilibrium but predicts significant concentrations of termination products which could not yet be detected. On the other hand, the slow-fragmentation model is in agreement with the non-stationary polymerization rate in the pre-equilibrium and the experimentally observed radical storage effects. However, the predicted intermediate radicals have not been observed in ESR spectroscopy and it is contradictory to the observations for the main equilibrium. A combined model which accounts for the differences in polymerization rate within the pre- and the main equilibrium and which also includes yet unknown mechanistic aspects of the RAFT process was developed by Buback who introduced the reversibility of the cross-termination reaction into the theoretical calculations.[69] This led to good results and explained the absence of star shaped polymers in the RAFT polymerizations. However, the

reaction mechanism still needs to be verified and these side reactions do not explain that carbazoles show similar behavior to dithiobenzoates. Recently, Perrier *et al.* combined these two conflicting models assuming reversible termination of the intermediate radicals only for low molecular weight species but the slow fragmentation to be prominent during the main equilibrium.[70] Termination of short intermediate radicals would explain the absence of 3-arm star polymers since the changes in molecular weight and hydrodynamic volume are negligible for low molecular weight species. Furthermore, matrix-assisted laser desorption/ionization time-of-flight (MALDI-TOF) spectrometry experiments proved the existence of such short cross-termination products.[71] The basis for this assumption is that cross-termination is diffusion controlled and, hence, small intermediates show much higher termination rate coefficients. In a following publication the same group predicted these short intermediates to be maximum dimeric suggesting that cross-termination occurs only in the very early stages of the RAFT process.[72]

In comparison to NMP and ATRP, RAFT polymerization is particularly robust and versatile and can be applied to many different monomer classes. However, the choice of RAFT agent, which commercial availability is limited, is crucial for successful polymer formation. Moreover, the sulfur containing end groups often result in red to yellow-colored polymers which limits the application of RAFT in industrial processes without special treatment.

2.2 Block Copolymer Self-Assembly

Self-assembly of amphiphilic molecules into aggregates of different size and shape is mainly determined by intermolecular interactions such as van der Waals, hydrophobic-hydrophobic, hydrogen-bonding, or electrostatic interactions.[73] Such systems are dynamic in nature and external changes (e. g., pH, temperature, concentration, etc.) can lead to changes of the formed aggregates. Both the thermodynamics of the self-organization process and intra-aggregate forces between molecules within the same aggregate determine the equilibrium structure formed. Considering the self-assembly of small amphiphilic lipids, two major forces govern the self-organization process, (*i*) hydrophobic attraction of the hydrocarbon part and (*ii*) hydrophilic, ionic or electrostatic repulsion of the head groups. Thus, at a certain head group area (Figure 1) the energy of repulsive interactions reaches a minimum.

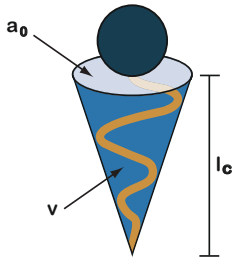

Figure 1: Schematic representation of an amphiphilic molecule with head group area a_0, chain volume v, and chain length l_c.[73]

The size of the formed aggregates is controlled by entropy which will favor the formation of particles with the smallest aggregation number. While larger structures will be entropically unfavorable, smaller particles will suffer from increased repulsive interactions of the head groups and, hence, be energetically disfavored. For low molecular weight lipids the value of the *packing parameter* $v/a_0 l_c$, where a_0 is the optimal head group area, v is the hydrocarbon volume, and l_c is the critical chain length, determines the shape of the resulting aggregates (Figure 2).[74]

Spherical micelles are formed only when the optimal head group area a_0 is large in comparison to the hydrocarbon volume v that the radius of the formed micelles does not exceed the critical chain length l_c. Geometrical considerations for a spherical micelle with radius r_m and aggregation number N give,

$$N = \frac{4\pi r_m^2}{a_0} = \frac{4\pi r_m^3}{3v} \tag{2.3}$$

which becomes

$$r_m^2 = \frac{3v}{a_0} \tag{2.4}$$

Hence, amphiphiles only assemble into spherical micelles if,

$$\frac{v}{a_0 l_c} < \frac{1}{3} \tag{2.5}$$

With decreasing size of head group cylindrical micelles, bilayers, vesicles or inverted micelles are formed (Figure 2). Changes in temperature can cause changes in both a_0 as well as l_c depending on the amphiphile.

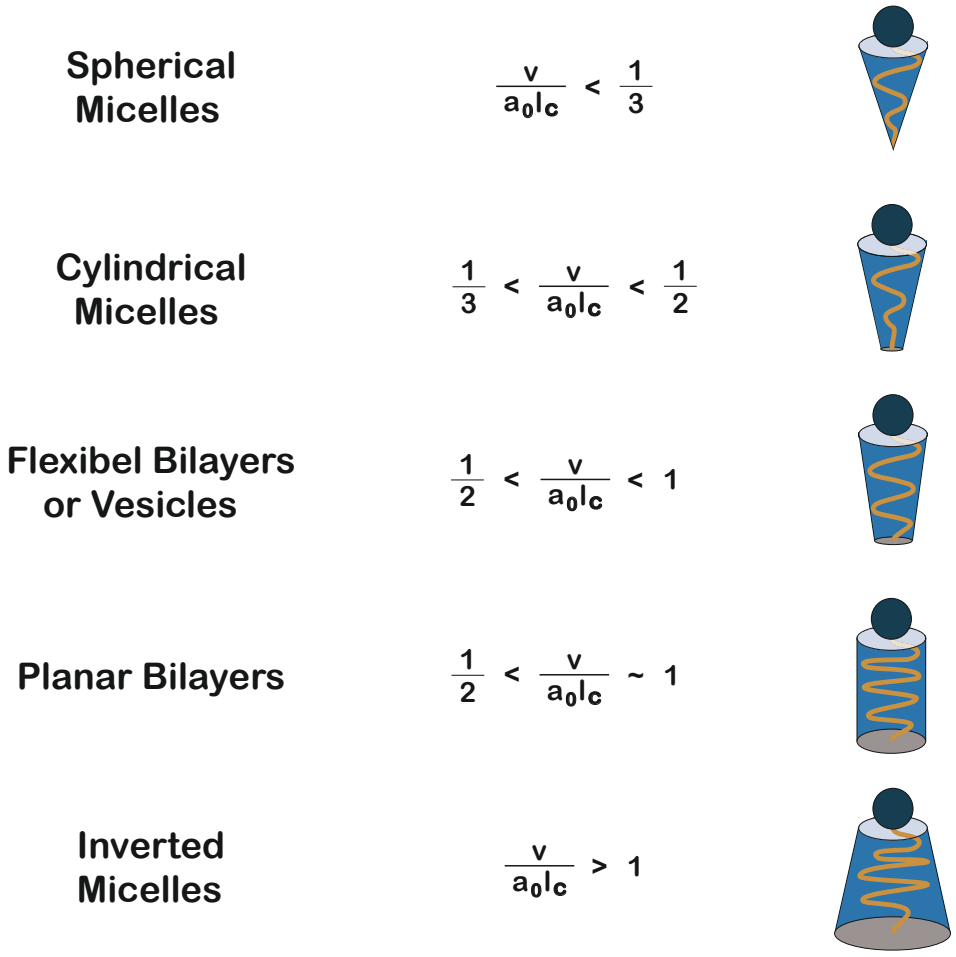

Figure 2: Relation between packing shape and resulting structure according to Israelachvili.[73]

Increasing temperature usually increases the motion of the hydrocarbon chain including trans-gauche isomerization and, accordingly, reduces the critical chain length l_c which increases the term $v/a_0 l_c$. Changes in a_0 depend on the type of head group. Poly(ethylene oxide) (PEO) head groups, for example, shrink with increasing temperature due to dehydration phenomena, whereas more hydrophilic head groups show an increase in a_0 at higher temperatures due to the increased intermolecular steric repulsion.[75] Spherical micelles formed from non-ionic amphiphiles generally increase in size with increasing temperature[76,77] whereas those formed from amphiphiles with charged head groups shrink.[78] In analogy to low-molecular weight surfactants, block copolymers self-assemble into similar structures when dissolved in selective solvents for one block or upon external changes in, e. g., temperature, pH or ionic strength. The insoluble block then undergoes phase separation and different structures such as spherical or worm-like (i. e., cylindrical) micelles, vesicles, or bilayers have been observed.[5–10,79,80] Figure 3 illustrates the formation of spherical

micelles, cylindrical micelles, and vesicles depending on the relative block length within AB diblock copolymers.

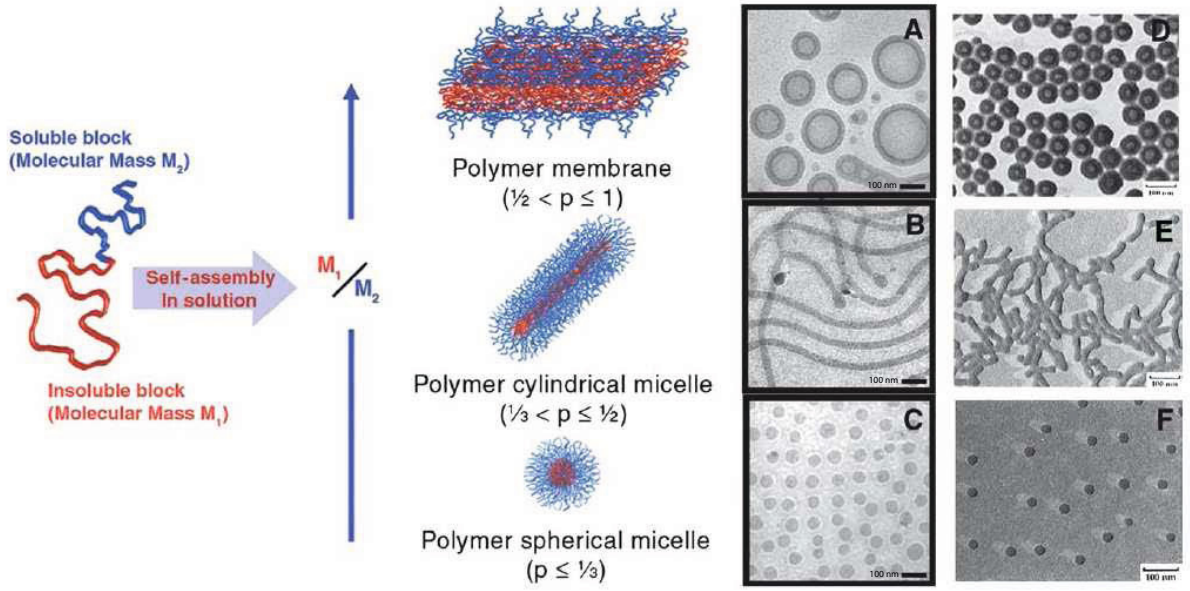

Figure 3: Left: Schematically shown self-organization of diblock copolymers into spherical micelles, cylindrical micelles, and vesicles; Right: (A-C) cryoTEM images of aggregates formed by PB-*b*-PEO; (D-F), TEM images of aggregates formed by PS-*b*-PAA. A and D show vesicles; B and E show cylindrical micelles; C and E show spherical micelles.[81]

Furthermore, two kinds of spherical micelles can be distinguished according to the relative lengths of the blocks in an AB diblock copolymer, (*i*) star-like micelles with a small hydrophobic core compared to the large corona, formed by the hydrophilic block, and (*ii*) crew-cut micelles with a large hydrophobic core and stretched short hydrophilic coronal chains (Figure 4). For simple amphiphilic block copolymers dissolution in a selective solvent for one block is the most straight forward method for the preparation of micelles. However, depending on the monomers used, non-equilibrium aggregates may be formed.[82] In order to obtain micelles closer to a thermodynamic equilibrium, the block copolymers are often dissolved first in a nonselective solvent followed by slow addition of a selective solvent for one block. The commercially available amphiphilic block copolymers from poly(ethylene oxide) and poly(propylene oxide) (PPO) are well-known to form micelles in aqueous solutions containing a PPO core surrounded by a dense PEO layer and dangling PEO chains forming the outer corona.[83]

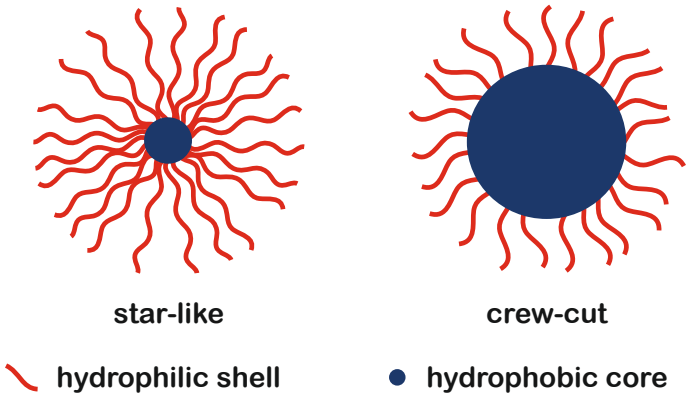

Figure 4: Schematic representation of a star-like (left) and a crew-cut (right) micelle.

In the case of diblock copolymers of polystyrene (PS) linked to PEO in aqueous solution, two populations with a hydrodynamic diameter D_h of 40 nm and 150 nm have been observed in TEM and light scattering studies.[84] The authors concluded that the small aggregates are regular micelles while the large particles consist of loose clustered micelles. Further investigations using SANS, DLS and SLS proved the formation of anisotropic clusters of PS-*b*-PEO micelles in aqueous solutions of up to 10 wt%.[85–88] These clusters may be the result of merging of initially formed micelles, as supported by controlled deaggregation of the clusters into micelles upon the addition of toluene or inorganic salts. The reason for cluster formation involves attractive interactions between the outer PEO chains such as hydrogen bonding or hydrophobic interactions.[89]

The key problem of all block copolymer assemblies is how to control the structure and its dimensions by choosing appropriately the length of each block and, moreover, how to trigger structural changes such as transitions from spherical into cylindrical micelles by external stimuli. Extensive theoretical and computational work indicates that especially the length of the hydrophilic corona forming block is crucial for the dimensions of the micelles formed.[90,91] Besides controlling the dimensions of spherical micelles, it would be highly desirable to control the morphology of block copolymer aggregates with view on potential applications in nanotechnology. Pioneering work of Eisenberg *et al.* demonstrated that for PS-*b*-PAA block copolymers with a constant polystyrene block (DP = 200), a decreasing degree of polymerization (DP) of the poly(acrylic acid) (PAA) block from DP = 21 to DP = 4 results in spherical, rod-like, vesicular, as well as crew-cut assemblies (Figure 5).[5]

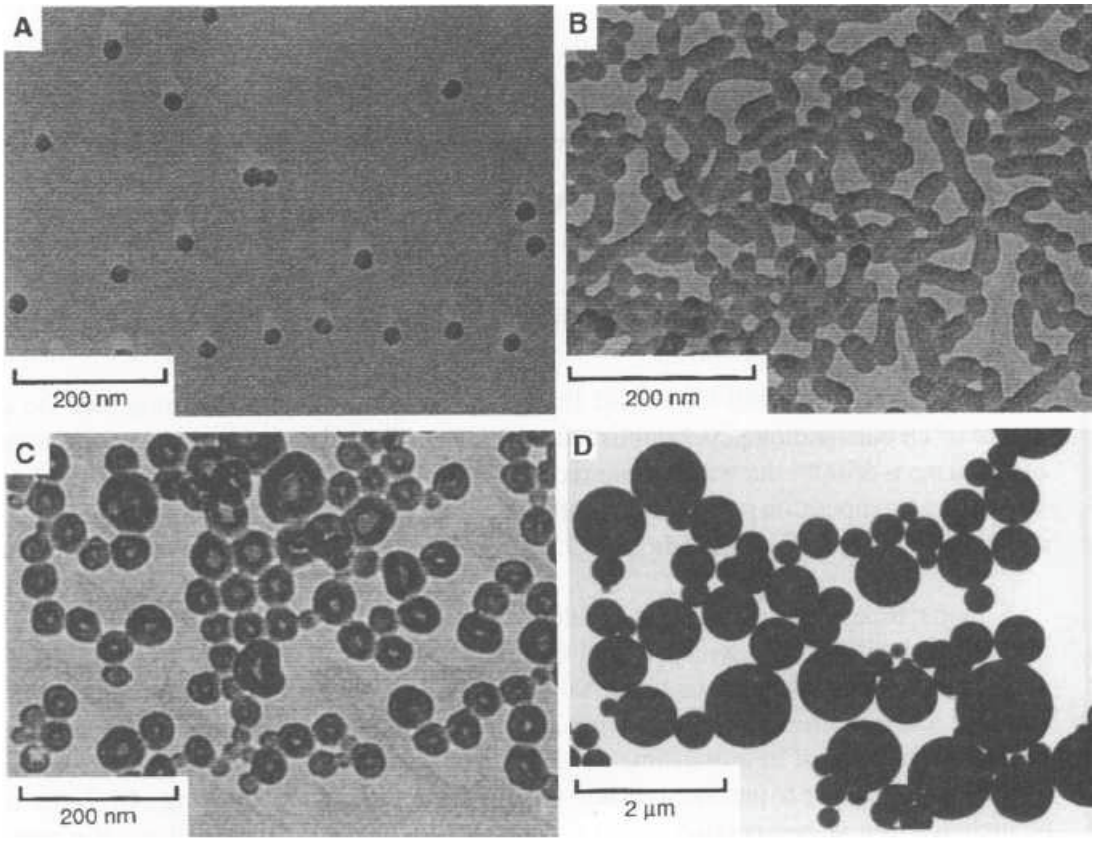

Figure 5: PS-*b*-PAA block copolymers forming a) spherical (PS_{200}-*b*-PAA_{21}), b) rod-like (PS_{200}-*b*-PAA_{15}), c) vesicular (PS_{200}-*b*-PAA_8), and d) crew-cut (PS_{200}-*b*-PAA_4) aggregates depending on the PAA content.[5]

The morphology depends on three main factors, (*i*) the streching of the core forming blocks, (*ii*) the core-corona interfacial energy, and (*iii*) repulsion between the corona forming blocks. Changes in one of these three factors will result in thermodynamic instability and lead to rearrangement into thermodynamically more stable morphologies.

Discher and Eisenberg proposed a general rule to predict the aggregate morphology from the block copolymer composition where $f_{hydrophilic}$ is the relative content of the hydrophilic block:[8]

- Spherical micelles are formed when $f_{hydrophilic} > 45\%$.
- Rod-like micelles are formed when $f_{hydrophilic} < 50\%$.
- Vesicles are formed when $f_{hydrophilic} \sim 35\%$.
- Inverted microstructures and crew-cut micelles are formed when $f_{hydrophilic} < 25\%$.

However, this rule has no universal validity. The chemical nature of the blocks used as well as the overall molecular weight of the block copolymers influence the aggregation in a way that is not yet fully understood.

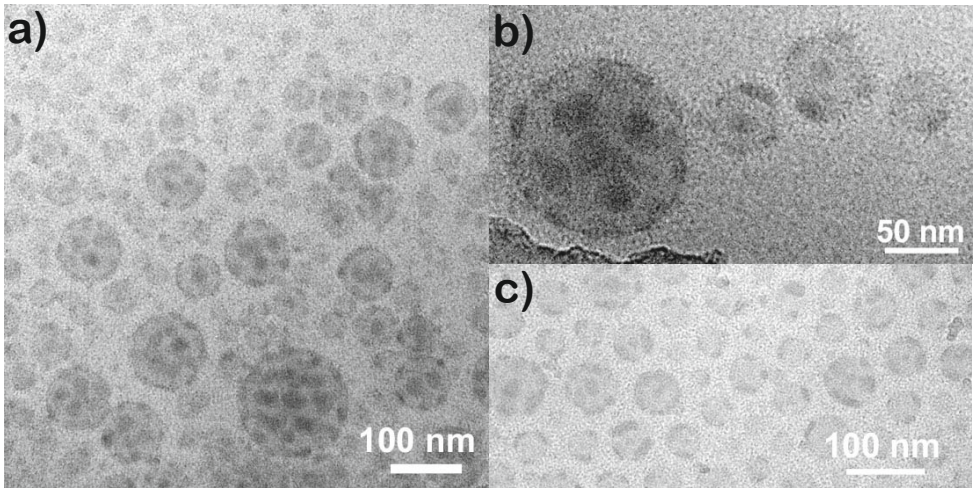

Figure 6: Cryo-TEM images of $PEHA_{120}$-*b*-$POEGA_{50}$-*b*-$PFDA_{40}$ at 0.5 wt% in aqueous solutions a) dispersed at 25°C; b) dispersed at 25°and annealed for 21d at 78°C; c) dispersed at 70°C.[92]

In addition, double hydrophobic ABC triblock copolymers containing two insoluble blocks assembled into core-shell-corona micelles with the two hydrophobic blocks forming the core and the shell and the hydrophilic block forming the solubilizing corona.[93–96] For polymers with the hydrophilic block in the middle, the aggregation behavior can be assumed to be similar to ABA triblock copolymers as long the terminal blocks have a similar degree of polymerization. In the case of double hydrophilic terpolymers, the insoluble block can be either in the middle or at one chain end. In the case of a terminal hydrophobic block, core-shell-corona micelles are expected. In contrast, when the hydrophobic block is located in the middle of the block copolymer, non-centrosymmetric micelles can be observed due to the heterogenous corona.[97,98] Recently, so-called multicompartment micelles, ABC triblock copolymers with a water-soluble shell and a segregated hydrophobic core have been published.[99,100] The hydrophobic core was composed of hydro- and fluorocarbon containing blocks which showed segregation and the formation of two distinct domains. For instance, cryo-TEM measurements of poly(ethylhexyl acrylate)-*b*-poly(oligoethylene glycol monomethylether)-*b*-poly(tetrahydroperfluorodecyl acrylate) ($PEHA_{120}$-*b*-$POEGA_{50}$-*b*-$PFDA_{40}$) showed the segregated dark fluorocarbon domains within the self-assembled

micelles (Figure 6).[92] Simultaneous, selective uptake of lipophilic and fluorophilic guest molecules into the corresponding hydrophobic polymer domains of multicompartment micelles was monitored by UV-vis[101] and NMR spectroscopy.[102,103] Besides spherical micelles and vesicular structures also helical[104,105] or disk-like[81] assemblies of block copolymers have been observed (Figure 7).

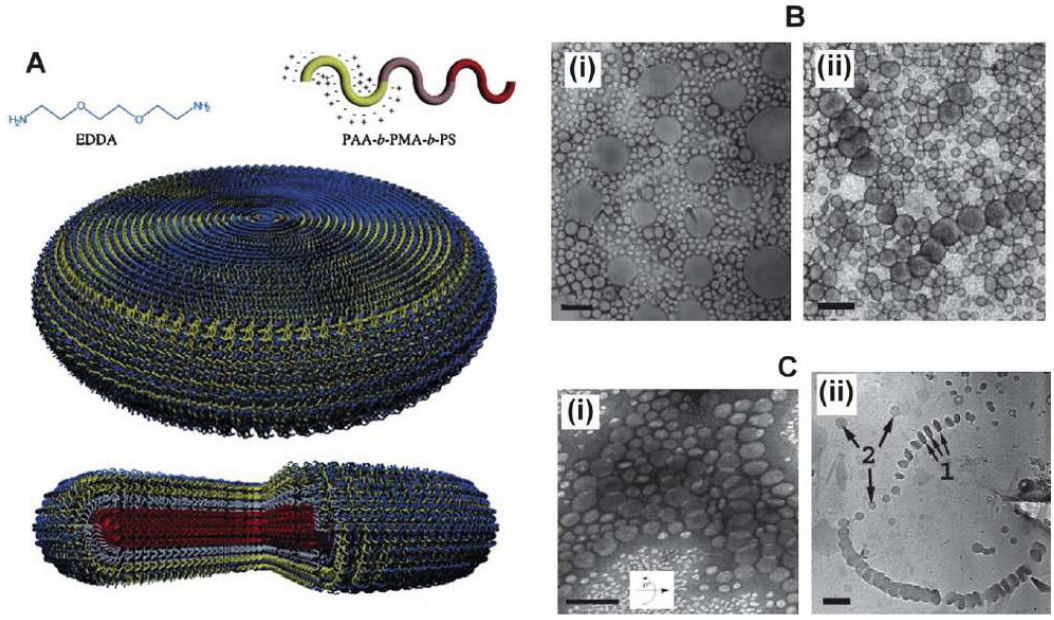

Figure 7: A) Schematic illustration of self-assembled ABC block copolymers into disk-like micelles, B) TEM images displaying disk-like micelles of PAA-*b*-PMA-*b*-PS triblock copolymers (amine/acid ratio 1/1) in a mixture of 40% water and 60% THF: (*i*) EDA as the counterion; (*ii*) EDDA as the counterion, C) (*i*) tilted TEM images of disk-like micelles (EDDA as the counterion, amine/acid ratio 0.3/1), (*ii*) CryoTEM images for the same sample where the disks are either parallel to the electron beam axis (arrows 1) or perpendicular to the electron beam axis (arrows 2). Scale bars = 200 nm.[81]

2.2.1 Stimuli Responsive Block Copolymers

In aqueous solution stimuli sensitive polymers are typically switched from a hydrophilic to a hydrophobic state or *vice versa*. Both physical (temperature, UV) and chemical (pH, redox) stimuli can be applied in order to change the hydrophilicity of polymers. In some cases polymers are even sensitive to more than one external stimuli. Poly(amine)s and poly(carboxylic acid)s undergo distinct changes in hydrophilicity upon protonation or deprotonation, respectively.[106] Thermoresponsive behavior of polymers, in contrast, may be distinguished by

two different types. Either polymers are soluble above a certain temperature, exhibiting an upper critical solution temperature (UCST), or they are soluble below a certain temperature, showing a lower critical solution temperature (LCST). In contrast to the UCST phenomenon which is caused by unfavorable enthalpy, the LCST is entropically driven.[107] Rushbrooke suggested already in 1938 that intermolecular hydrogen bonding may cause the LCST phenomenon.[108] In 1960 Freeman and Rowlinson reported that hydrocarbon polymers show a LCST in hydrocarbon solvents.[109] This finding was validated by a universal theory of Flory on the LCST behavior of polymers in solution.[110–112] LCST behavior is widespread among non-ionic hydrophilic polymers,[113–116] and is attributed to the balance of polymer-solvent hydrogen bonding and polymer-polymer hydrophobic interactions.

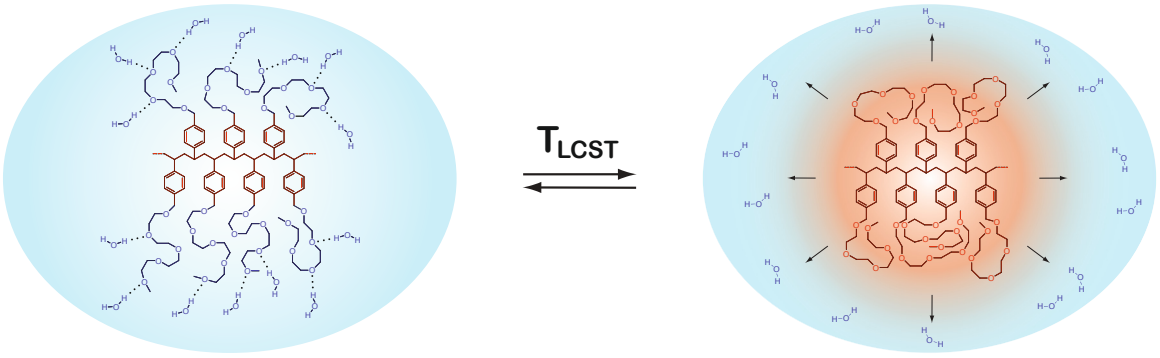

Figure 8: Phase transition of thermoresponsive polymers in water.

Nevertheless, the exact position of such a phase transition can not be predicted by simple hydrophilic-hydrophobic balance considerations.[115,117,118] Moreover, the exact phase transition temperature of a polymer depends on additional factors such as molar mass, architecture, end groups, concentration or added salts.[113,116,119,120] While the UCST increases, the LCST usually decreases with increasing molecular weight.[121] In addition, an increase in meso diads decreases the LCST while an increase in racemo diads increases the LCST of poly(isoproylacrylamide) (PNIPAM).[122,123] Isotactic PNIPAM was found to be more hydrophobic than atactic one with phase transition temperatures of about 24°C.[124] Thus, tacticity of polymers seems to play an important role on their phase separation behavior. Also the heating rate may effect the measured phase transition temperature markedly.[125] An increase of heating rate from 0.2 to 5 K/min can result in an increase in the apparent cloud point values of up to 10°C due to insufficient heat transfer.[121,126]

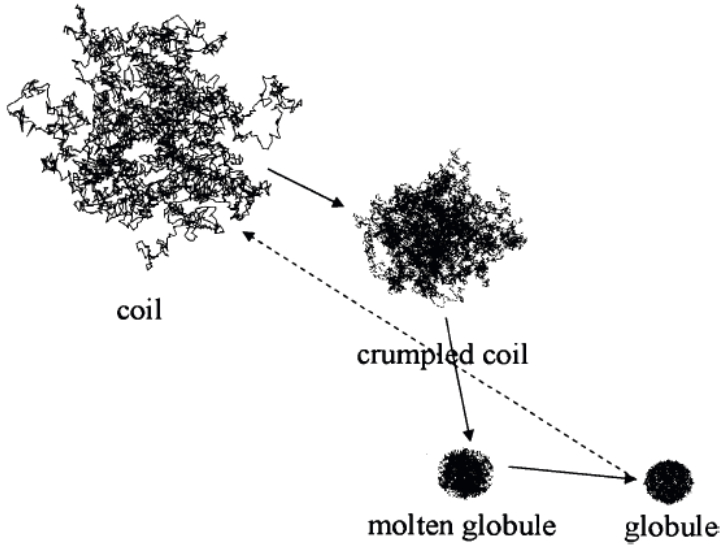

Figure 9: Thermodynamically stable random coil, crumpled coil, molten globule, and globule of homo-PNIPAM chains in aqueous solution during the thermally induced collapse.[127]

The collapse of single PNIPAM chains in dilute solutions was intensively studied by several analytical techniques. Though thermosensitive homopolymers usually precipitate above their LCST, they show the formation of kinetically stable mesoglobules in highly dilute solutions ($10^{-6}\,\mathrm{g\,mol^{-1}}$).[128,129] Wu and coworkers studied the coil-to-globule and globule-to-coil transition using dynamic and static light scattering.[128,130,131] After the coil-to-globule transition, which was observed by a decrease of R_g/R_h from 1.50 to 0.56, the average chain density ρ decreased to 0.34 g/cm^3 indicating that even the fully collapsed mesoglobules still contain about 66% water. The authors suggested, that between the coil and the globule two other thermodynamically stable states exist, namely the crumpled coil and the molten globule[127,130] (Figure 9). Winnik *et al.* used light scattering in combination with microcalorimetry for fluorescently labeled PNIPAM chains.[129] Fluorescence spectroscopy indicated that PNIPAM mesoglobules undergo a gradual transition from fluidlike particles into hard spheres. Liu *et al.* reported on the observation of a two-stage transition of pyrene labeled PNIPAM chains by a combination of fluorescence and stopped-flow techniques. A first fast transition of randomly coiled PNIPAM into crumpled chains was followed by a slow collapse into compact globules.[132] Also Aseyev and coworkers observed the formation of mesoglobules of PNIPAM, poly(N-vinyl caprolactam) (PVCL), and poly(vinyl methyl ether) (PVME) homopolymers.[133] Although theoretical calculations suggest that homopolymers which form mesoglobular aggregates should assemble into cylindrical structures rather that

spherical,[134] no such experimental observation has been made so far. A combination of static and dynamic light scattering, instead, excluded cylindrical aggregates for PVCL, PNIPAM, and PVME homopolymers but suggested spherical particles with relatively narrow size distributions.[133]

The simplest examples of stimuli-responsive block copolymers contain one permanently hydrophilic or hydrophobic block and one block which undergoes a phase transition from hydrophilic to hydrophobic when external stimuli such as temperature, pH, ionic strength or UV-light are applied. Perrier *et al.* , for instance, synthesized diblock copolymers from PNIPAM and poly(dimethylacrylamide) (PDMA) varying the length of the PDMA block.[135] The authors stated that not only the relative length of the blocks determines whether micelles or larger aggregates are formed but also the absolute length of the hydrophilic block. Moreover, they demonstrated that the formed micelles are able to reversibly incorporate hydrophobic dye molecules, in this case the relatively large 2,6-diphenyl-4-(2,4,6-triphenyl-N-pyridino) phenolate also known as Reichardt's dye (Figure 10). McCormick *et al.* synthesized block copolymers from PNIPAM and PDMA by aqueous RAFT polymerization at room temperature and observed reversible micelle formation by passing the phase transition temperature of PNIPAM.[136] An increase of the relative length of the PNIPAM block led to larger particles when the aqueous solutions were heated above 32-36°C. Tenhu *et al.* studied diblock copolymers from PNIPAM with hydrophobic blocks of polystyrene or poly(*tert*-butylmethacrylate) obtained from RAFT polymerization.[137] By variations of the length of the PNIPAM block similar observations as by Perrier *et al.* were made. Not only the relative length of the blocks is crucial for the formation of micellar aggregates. Longer PNIPAM chains led to larger aggregates which was interpreted in a way that the long PNIPAM chains destabilize the formation of hydrophobic cores of polystyrene or poly(*tert*-butylmethacrylate). Interestingly, even at prolonged elevated temperatures of 50°C for several days the formed particles remained stable and did not precipitate from solution. Marty, Destarac *et al.* synthesized PNIPAM-*b*-poly(butylacrylate) (PBA) diblock copolymers with varying length of the PBA blocks.[138] With increasing PBA length the observed aggregates showed increasing hydrodynamic diameters. This was explained by an increasing aggregation number N_{agg} of the formed micelles. Moreover, the PBA block led to a decrease of the phase transition temperature of the PNIPAM block by about 6°C. The cloud point was decreased even further when the length of the PBA block increased. Complementary results were obtained by Armes *et al.* for AB block copoly-

mers from methyl vinyl ether (MVE) and methyl triethylene glycol vinyl ether (MTEGVE).[139] The cloud points of the block copolymers increased from 18°C to 84°C with increasing length of the more hydrophilic polyMTEGVE block.

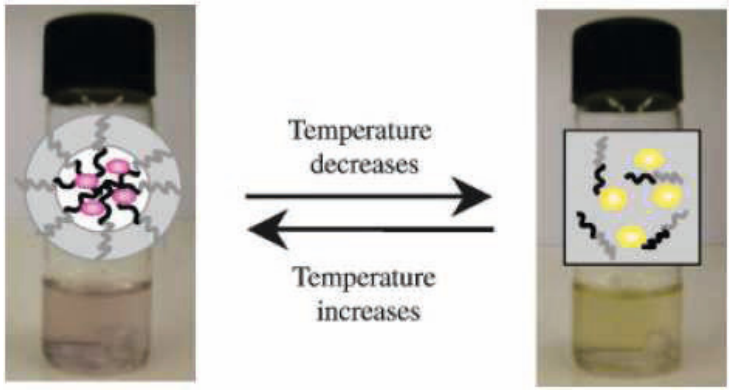

Figure 10: Bathochromic and hypsochromic shift of Reichardt's betaine dye in an aqueous solution of $PDMA_{58}$-*b*-$PNIPAM_{61}$ at a concentration of 1 w% upon heating and cooling between r.t. and 55°C.[135]

Especially block copolymers from PNIPAM and PEO found much attention throughout the recent years, because of the lower critical solution temperature of PNIPAM (32°C) close to human body temperature (37°C) and the biocompatibility of PEO.[113,140–143] Such block copolymers are expected to be interesting candidates for drug delivery and biomedical applications.[115,140,144–149] For instance, Feijen *et al.* synthesized PEO-*b*-PNIPAM block copolymers which self-assembled into spherical micelles in aqueous solution once the temperature was increased above the cloud point of the PNIPAM block at about 31°C.[141] Hennink *et al.* studied the self-aggregation of PEO-*b*-PNIPAM block copolymers in dilute aqueous solution, too.[150] With increasing PNIPAM chain length the particle size was found to decrease. These findings were interpreted in terms of increased dehydration of the thermosensitive block which results in more densely packed hydrophobic cores. These observations are in direct contrast to the results obtained by Marty and Desterac,[138] who found larger particles with increasing length of the hydrophobic block (*vide supra*). Moreover, the heating rate appeared to influence the size of the formed aggregates with a fast heating protocol resulting in smaller particles than observed for slow heating rates. In addition, the particles formed by fast heating had lower polydispersity indices than the ones from slow heating. Based on these finding the authors tested a *heat shock* protocol. Relatively small amounts of polymer solution below the cloud point temperature were added to water at 40°C, thus well above

the LCST of PNIPAM. Such rapid heating led to even smaller particles with a D_h of 50 nm and very low polydispersities around 0.04. Pispas *et al.* observed the same trend for different heating protocols of PEO-*b*-PNIPAM diblock copolymers.[125] Moreover, Shi *et al.* observed a concentration dependence of micellar size and size distribution of PEO-*b*-PNIPAM diblock copolymers. Surprisingly, higher concentrations led to smaller and more narrowly distributed aggregates than smaller concentrations at which loose micellar assemblies or even clusters appeared.[142]

More dynamic aggregation behavior was observed for double responsive diblock copolymers. By the use of orthogonal stimuli or by the combination of one LCST and one UCST block, so called *schizophrenic* block copolymers can be obtained in which micelles and reverse micelles can be selectively formed according to the external stimulus applied. For instance, double thermoresponsive block copolymers from PNIPAM and poly(3-[N-(3-methacrylamidopropyl)-N,N-dimethyl]ammoniopropane sulfonate) (PSPP) having a LCST and a UCST block, respectively, have been synthesized.[151] At low temperatures PSPP-core PNIPAM-shell micelles are obtained, at intermediate temperatures the block copolymers are molecularly dissolved whereas at high temperatures reverse micelles with a PNIPAM core and a PSPP shell are formed. Similar systems have also been reported by Maeda and Armes.[152,153] In addition, schizophrenic diblock copolymers sensitive to changes in pH values have been reported. A zwitterionic block copolymer of poly(4-vinylbenzoic acid) (PVBA) and poly(2-N-(morpholino)ethyl methacrylate) (PMEMA) showed PVBA-core micelles below pH 6. Increasing the pH above 6 led to dissolved polymers which aggregated into PMEMA-core micelles at elevated temperature or in the presence of Na_2SO_4.[154] In addition, even triple responsive diblock copolymers exhibiting a third redox[155] or sugar response[156,157] were published recently but especially the redox switch is often not reversible. Such schizophrenic block copolymers are especially interesting due to their ability to aggregate into different structures under changing conditions. Double responsive diblock copolymers with a thermo- and a pH-responsive block from PNIPAM and poly(N,N-diethylaminoethyl methacrylate) (PDEAEMA), respectively, could even be switched from micellar into vesicular aggregates in response to changes of the external conditions[158] (Figure 11).

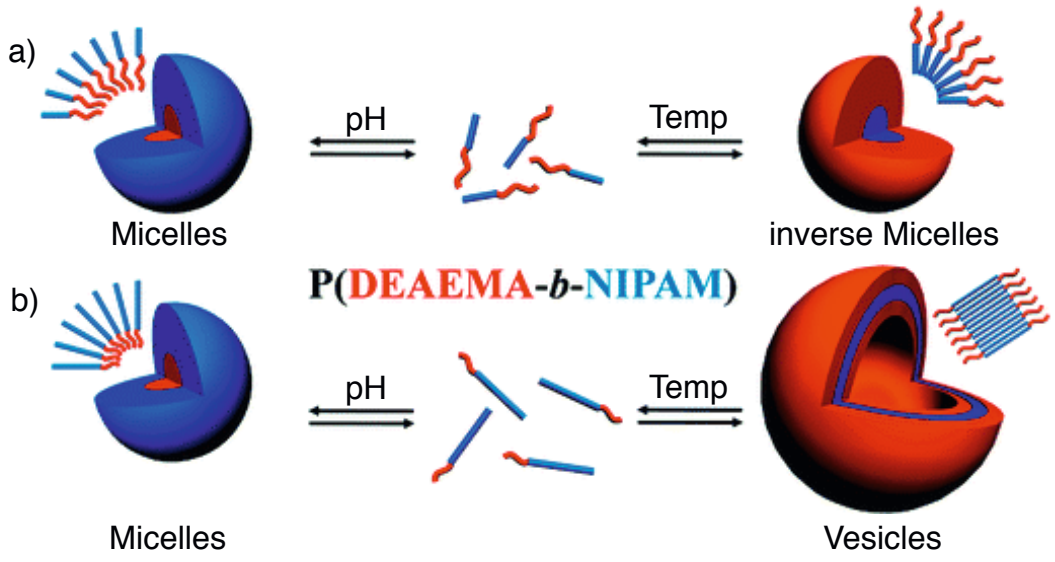

Figure 11: Schizophrenic aggregation behavior of (a) PDEAEMA$_{98}$-*b*-PNIPAM$_{209}$ and (b) PDEAEMA$_{98}$-*b*-PNIPAM$_{392}$. Adapted from ref.[158]

Beside diblock copolymers, multi responsive terpolymers with ABA or BAB sequence, containing a responsive block and a permanently hydrophilic B block, are well-known for their rich aggregation behavior. While BAB triblock copolymers often form spherical micelles with a core forming A block and corona forming B blocks, the situation becomes more complex for ABA systems. Theoretical discussion of the formation of flower-like micelles in which the dissolved middle block has to loop in order to incorporate both hydrophobic A blocks into the core were done by Tirrell and coworkers.[159] Calculations suggested that only polymers with very short hydrophobic A blocks will form flower-like micelles while for longer A blocks mixed star-/flower-micelles, with partially free dangling chain ends, are more probable. The assumption of flower-micelles formed by ABA triblocks was experimentally supported by the findings that the investigated aggregates had dimensions of those formed by diblock copolymers of half the molecular weight.[159,160] Moreover, when the relative block length of the middle block was decreased below the size of the hydrophobic A blocks, no aggregation was observed. Likewise to their diblock counterparts, changes in size and morphology of triblock copolymer aggregates can be induced by changes of the solvent qualities or upon introducing stimuli-sensitive blocks. Wang *et al.* synthesized poly(stearyl methacrylate)-*b*-PNIPAM-*b*-poly(stearyl methacrylate) (PSMA-*b*-PNIPAM-*b*-PSMA) triblock copolymers which showed morphological transitions from vesicular into micellar structures with increasing water content in THF/water mixtures.[161]

ABC triblocks with stimuli-sensitive blocks have been described by Eisenberg and coworkers who reported on the self-assembly of PAA_{26}-*b*-PS_{890}-*b*-$P4VP_{40}$ as function of pH in DMF/THF/H_2O mixtures.[162] At low pH, vesicles with the P4VP blocks forming the outer shell and PAA blocks forming the inner shell were formed. At intermediate pH values, spherical and ellipsoidal aggregates were found while at high pH again vesicles, this time with outer PAA and inner P4VP block, were observed. Thus, an interconversion of vesicles with either outer PAA or P4VP blocks was possible by changing the pH of the solution (Figure 12).

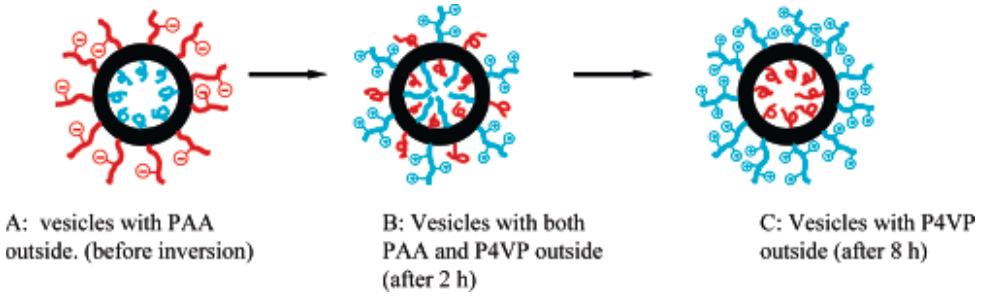

Figure 12: Schematic representation of the pH induced inversion of vesicles formed from PAA_{26}-*b*-PS_{890}-*b*-$P4VP_{40}$ triblock copolymers.[162]

$P2VP_{58}$-*b*-PAA_{924}-*b*-$PBMA_{48}$ terpolymers also showed morphological changes at different pH values and temperatures in aqueous solutions.[163] At pH 1, changes in temperature led to either mesoglobules (T < 20°C) or swollen micelles (T > 20°C). An increase in pH from 8 to 11 and then to 12 led to spheres, toroidal nanostructures and finally to microgels, respectively. Another example for double responsive ABC triblock coplymers is the aggregation of PEO-*b*-P4VP-*b*-PNIPAM in aqueous solution.[164] At 25°C a unimer-to-micelle transition occured when the pH was increased from 2 to 6.5. At elevated temperatures, above the cloud point of the PNIPAM block, micellar clusters could be converted into core-shell-corona micelles upon increasing the pH. Interestingly, even morphological changes from spherical into worm-like micelles were reported for double hydrophilic ABC triblock copolymers from PEO_{114}-*b*-PBA_{250}-*b*-$PDEAM_{135}$ (poly(diethyl acrylamide) (PDEAM)), upon changes of the solution temperature[165] (Figure 13). In addition, schizophrenic aggregation behavior of ABC triblock copolymers could be obtained from poly(2-(diethylamino)ethyl methacrylate)-*b*-poly(2-(dimethylamino)ethyl methacrylate)-*b*-poly(2-(N-morpholino)ethyl methacrylate) (PDEA-*b*-PDMA-*b*-PMEMA) by changes in pH and addition of Na_2SO_4.[166]

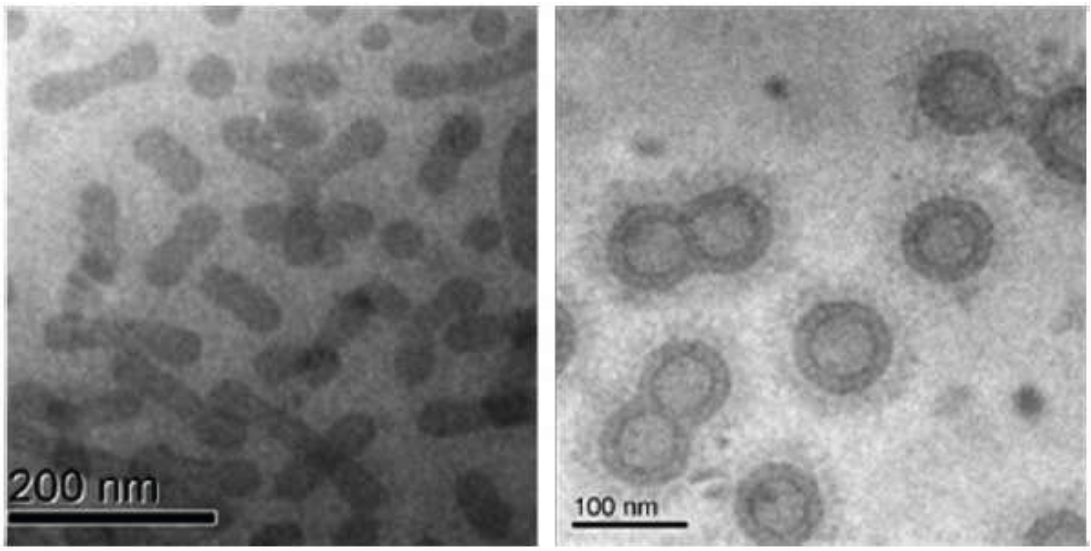

Figure 13: Worm-like and spherical micelles formed from double hydrophilic ABC triblock copolymers depending on the solution temperature.[165]

At pH 7.6 PDEA-core, PDMA-shell, PMEMA-corona micelles were formed which inversed to PMEMA-core, PDMA-shell, PDEA-corona micelles when Na_2SO_4 was added. Finally, ABC terpolymers can also form helical[105] or hamburger-like[167] superstructures under proper solvent conditions.

Consequently, triple responsive ABC triblock copolymers are assumed to provide even more opportunities to control the self-aggregation and, moreover, trigger morphological changes stepwise. However, until now only very few examples of triple responsive terpolymers have been reported, all of which comprising three temperature responsive blocks. Aoshima *et al.* reported on the synthesis and aggregation behavior of triple thermoresponsive block copolymers from 2-ethoxyethyl vinyl ether (cloud point 20°C), 2-methoxyethyl vinyl ether (cloud point 41°C) and 2-(2-ethoxy)ethoxyethyl vinyl ether (cloud point 64°C) obtained from sequential living cationic polymerization.[168] Such ABC polymers showed a multi-step aggregation process from unimers to micelles followed by physical gelation and finally precipitation upon increasing the temperature. More recently, Zhu *et al.* reported on the multi-step phase transitions of triple thermoresponsive terpolymers in dilute aqueous solutions and studied their self-assembly by a combination of dynamic and static light scattering, NMR spectroscopy as well as ultrasensitive differential scanning calorimetry.[169,170] ABC triblock copolymers with thermoresponsive blocks from poly(N-propylacrylamide) (PNPAM, cloud point 22°C), poly(N-isopropylacrylamide) (cloud point 32°C) and poly(N,N-

ethylmethylacrylamide) (PNEMAM, cloud point 56°C) showed a multi-step self-organization from unimers into micelles or micellar clusters depending on the chain length of the poly(N,N-ethylmethylacrylamide) block, i. e., only a long poly(N,N-ethylmethylacrylamide) block was able to stabilize micellar aggregates. Whereas the influence of the chain length of the terminal high-LCST block on the aggregation process has been studied, the effect of changing the block sequence has not been explained. However, although the triblock copolymers $PNPAM_{124}$-*b*-$PNIPAM_{60}$-*b*-$PNEMAM_{44}$ showed three changes in transmission intensity with increasing temperature, dynamic light scattering displayed only one thermal transition for homo-, di-, and triblock copolymers (Figure 14).

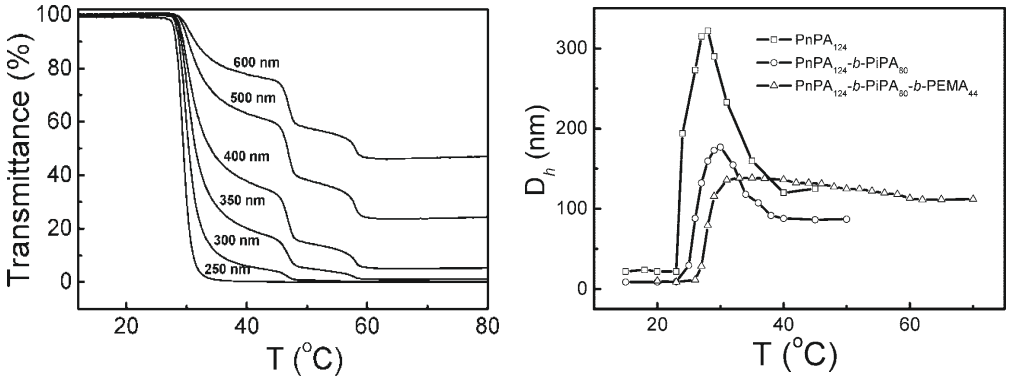

Figure 14: Turbidity (left) and dynamic light scattering (right) measurements of $PNPAM_{124}$-*b*-$PNIPAM_{60}$-*b*-$PNEMAM_{44}$.[169]

After passing the cloud point of the PNPAM block at about 24°C, aggregates with a D_h of ~ 150 nm were observed for $PNPAM_{124}$-*b*-$PNIPAM_{60}$-*b*-$PNEMAM_{44}$. Further heating led to a gradual decrease of D_h without any indication of a second pronounced change. Variations in the relative block length, $PNPAM_{124}$-*b*-$PNIPAM_{80}$-*b*-$PNEMAM_{44}$ and $PNPAM_{124}$-*b*-$PNIPAM_{80}$-*b*-$PNEMAM_{160}$, then led to better results and changes of the hydrodynamic diameter with temperature became visible upon heating their aqueous solutions from 15°-70°C (Figure 15).[170]

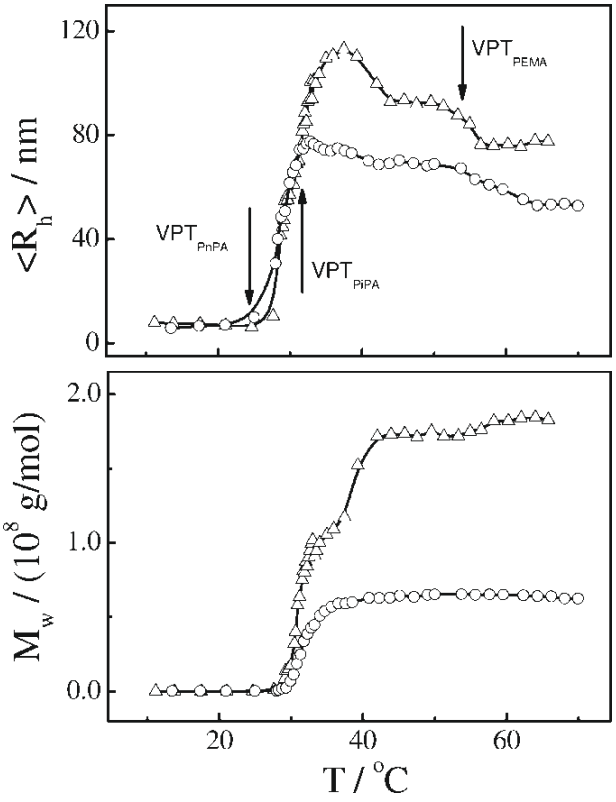

Figure 15: Hydrodynamic diameter (top) and apparent molar mass (bottom) of $PNPAM_{124}$-*b*-$PNIPAM_{80}$-*b*-$PNEMAM_{44}$ (△) and $PNPAM_{124}$-*b*-$PNIPAM_{80}$-*b*-$PNEMAM_{160}$ (∘) as function of temperature.[170]

While the dynamic light scattering curves show more than a single transition during the heating process the interpretation and proposed aggregation pathway (Figure 16) is questionable at least for the polymer with the shorter PNEMAM block . The smallest observed aggregates have a D_h of about 160 nm while its contour length is 62 nm. Thus, even in the fully extended state no single micellar aggregates with a hydrodynamic diameter of minimum 160 nm can be formed.

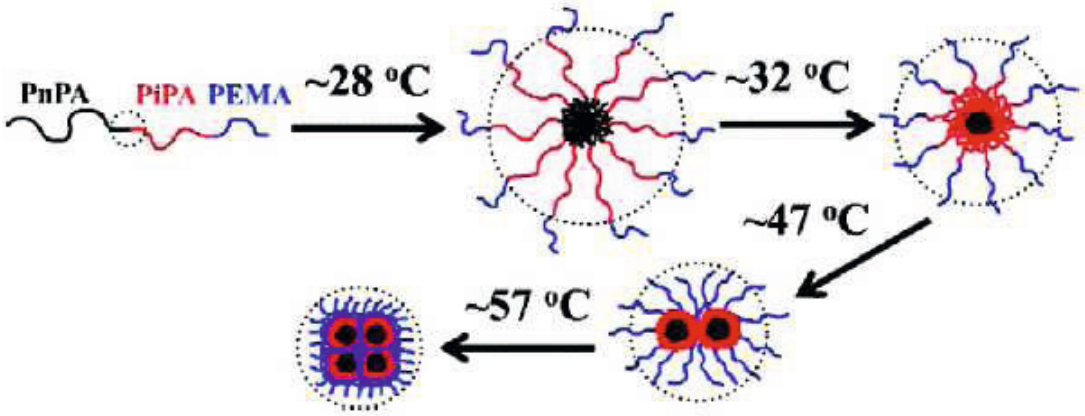

Figure 16: Proposed aggregation pathway of $PNPAM_{124}$-*b*-$PNIPAM_{80}$-*b*-$PNEMAM_{44}$.[169]

2.3 Alternating Copolymerization

Nylon 6,6 is maybe one of the most famous alternating copolymers due to the wide range of commercial applications. Nylon 6,6 can be obtained by polycondensation of the corresponding diamines and dicarboxylic acids. In principle, the polycondensation or step-growth polymerization of A-A and B-B monomers will always result in alternating copolymers since each monomer cannot react with itself. Thus, crosspropagation is the only possible polymerization pathway. In chain growth systems such as a common radical copolymerization of two monomers A and B, however, four different chain propagation reactions can take place, namely A as well as B can add either to an active chain of A or B. These four propagation pathways are governed by the propagation rate constants k_2^{ab}, k_2^{aa}, k_2^{bb} and k_2^{ba}. The resulting composition of the formed copolymers is then determined by the ratios of the corresponding propagation rate constants

$$\alpha = \frac{k_2^{ab}}{k_2^{aa}} \quad ; \quad \beta = \frac{k_2^{bb}}{k_2^{ba}} \tag{2.6}$$

Accordingly, if a copolymerization of A and B is started in a molar ratio of B/A, the molar ratio within the resulting polymer b/a can be calculated according to:[171]

$$\frac{b}{a} = \frac{B}{A} * \alpha * \frac{\beta B + A}{\alpha B + A} \tag{2.7}$$

Alternating copolymers are usually only obtained by radical polymerization, if the monomer pair is forming charge-transfer complexes (CTC) which then homopolymerize, or if the crosspropagation rate constants are much higher than the homopolymerization rates. N-Vinylcarbazole, for instance, was reported to form 1:1 alternating copolymers with fumaronitrile and diethyl fumarate.[172,173] Also alternating copolymers of styrene and acrylonitrile were synthesized by free radical polymerization in the presence of zinc chloride.[174] In the special case of styrene (A) and maleic anhydride (B), the latter does not undergo homopolymerization and, in addition, the propagation rate for styrene terminated polymers is much higher toward maleic anhydride than styrene monomers. As a result, k_2^{bb} becomes zero, thus, also β becomes zero and equation 2.7 simplifies to:

$$\frac{b}{a} = 1 + \frac{1}{\alpha} * \frac{A}{B} \tag{2.8}$$

2.3.1 Alternating Copolymers of Maleic Anhydride and Styrene

Since the 1940's the copolymerization of styrene and maleic anhydride (MAn) is known to proceed in an alternating fashion.[171,175] However, there is still disagreement about the origin of the alternating nature of this monomer pair. Mainly two, incompatible, explanations are discussed in the literature.[176] On the one hand the alternation is claimed to arise from charge-transfer-complexes which show higher reactivity against the growing radical than uncomplexed monomers.[177,178] On the other hand the alternating copolymerization of styrene and maleic anhydride is discussed in terms of different reactivities of the monomers resulting in marked preferences for crosspropagation reactions.[179] Sometimes it is argued that this general tendency is enhanced by donor-acceptor interactions between the growing radical chain ends and adjacent monomers. In the case of maleic anhydride and N-substituted maleimides with styrene, the very low tendency of maleic anhydride and

N-substituted maleimides toward homopolymerization and the extremely favored crosspropagation with styrene can be accounted for the alternating nature of the polymerization process.[180,181]

However, the former is still an issue of discussion since UV and NMR measurements proved the existence of styrene-maleic anhydride donor-acceptor complexes under usual polymerization conditions.[177] In solvents such as methyl ethyl ketone or DMSO competitive complexation of the monomers by the solvent molecules takes place. However, the alternating feature of the copolymerization alone cannot prove the involvement of CTCs. For instance, the relative reactivity of styrene and MAn with donor-type radicals, e. g., cyclohexyl radicals, was tested and showed that MAn was 850 times more reactive than styrene.[182] Likewise, acceptor type radicals, benzoyloxy radicals, reacted 50 times faster with styrene than with MAn.[183,184] Thus, the alternation can also arise from the different reactivities of the monomers favoring crosspropagation. Moreover, the question has to be addressed whether the CTCs have a higher reactivity toward a growing polymer chain than uncomplexed monomers since this cannot be assumed *a priori*. In fact, theoretical calculations are difficult for this problem since the structure of the formed styrene-MAn complex can only be assumed from ^{1}H NMR data but has large impact on the potential reactivity. Theoretical calculations, however, have shown that CTCs may indeed participate in the polymerization but only one reaction proceeds faster for the complex, namely the addition to an active styrene end. Electron spin resonance (ESR) spectroscopy as well as trapping of active radical chain ends was suggested to give further information about the polymerization mechanism. Indeed, by trapping styrene-MAn mixtures with 2-methyl-2-nitrosopropane at 50°C only styrene terminated molecules could be found in agreement with a polymerization of CTCs which add with their MAn side to the active styrene end.[185] However, the trapping agent used is not very efficient in trapping maleic anhydride radicals and, therefore, the observation made is not a proof for the proposed mechanism.[176]

The latter, in contrast, is accounted for by the penultimate unit model (PUM).[186] Here not only the terminal unit determines the crosspropagation rate constant but also the penultimate unit ($k_{iii} \neq k_{jii}$). Especially the decreasing content of alternation with increasing temperature was often used to support the complex participation model (CPM). However, copolymerizations in the absence of CTCs are known to proceed more randomly at higher temperatures and the temperature dependence of copolymer composition *vs.* monomer

feed can be described by both models (CPM and PUM). Thus, in order to rule out one of these two models other experimental data are required. Determinations of average propagation rate coefficients as function of comonomer feed compositions using pulsed laser polymerization were used by Klumperman *et al.* for the MAn-styrene system.[187] The observed increase of the rate coefficients with increasing MAn fraction could be explained using the PUM but not by the CPM. Reductive demercuration was used to generate benzyl radicals in N-phenylmaleimide (NPhM) styrene mixtures in order to investigate the concerted addition of a styrene terminated polymer to a CTC of a N-substituted maleimide and styrene.[188] The results showed almost exclusively single addition of styrene ruling out a concerted addition of a 1:1 maleimide-styrene complex. Further indication for the absence of CTC in RAFT-mediated styrene-MAn copolymerizations were reported using *in situ* ^{1}H NMR spectroscopy during the initiation period.[189] The results showed that, depending on the structure of the RAFT agent used, selective addition to a single monomer unit of either MAn or styrene takes place. Within the early stages of the copolymerization only one monomer unit adds to the growing polymer chain before termination takes place. In the case of complex participation, however, the styrene-MAn couple should be added to the chain end.

2.3.2 Copolymerization of N-substituted Maleimides with Styrene

Compared to maleic anhydride, the copolymerization of N-substituted maleimides with styrene is not strongly alternating[190–192] since the styrene content can be varied depending on the monomer feed.[176] This aspect is also important for the discussion of CTCs involved in the polymerization mechanism since styrene rich copolymers can arise only from incorporation of non-complexed monomers. Moreover, in contrast to MAn, N-substituted maleimides can be homopolymerized by anionic as well as radical polymerization.[193–196]

Many different N-substituted maleimides have been used as comonomers in order to increase the solubility and thermal stability,[196,197] or functionalize polymer chains.[180,181] Recent examples by Lutz *et al.* showed that the monomer sequence can be conveniently controlled even in radical polymerization when the kinetics are well known.[180,181,198–200] The sequential addition of various different maleimides to a growing styrene chain led to preprogrammed distributions of functional side chain groups and up to four different maleimides could be incorporated along one polystyrene chain (Figure 17).

This concept works because the maleimides are incorporated immediately after addition and result in very narrow domains of alternating copolymer parts.

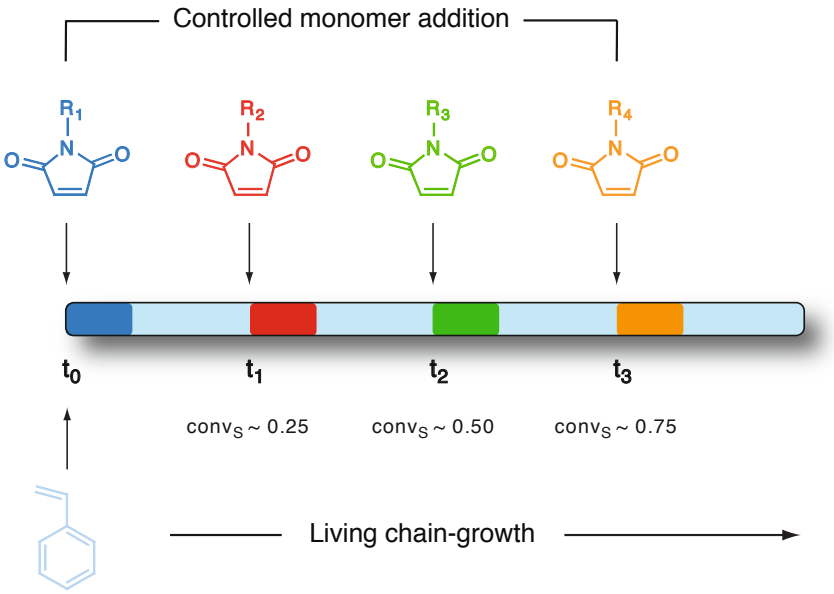

Figure 17: General concept for the sequential addition of various functional maleimides to the polymerization of styrene by ATRP according to Lutz *et al.* [201]

2.3.3 One-Step Synthesis of Diblock Copolymers

In comparison to commonly applied sequential synthesis of block copolymers by controlled radical polymerization techniques, the one-step formation of block copolymers would be a significant advantage. The aforementioned alternating copolymerization of styrene and MAn or N-substituted maleimides is a promising candidate within this context. Recently a few reports were published on the one-step formation of AB diblock copolymers. The NMP polymerization of a 9:1 mixture of styrene and MAn as reported by Hawker *et al.* produced a poly(styrene-*co*-MAn)-*b*-polystyrene (P(S-*co*-MAn)-*b*-PS) block copolymer.[202] During the initial phase of the polymerization the much faster crosspropagation takes place until MAn is consumed, followed by the homopolymerization of styrene. However, NMP did not result in an alternating block but in a copolymer with a 2:1 content styrene:MAn. By the use of RAFT, Li *et al.* obtained P(S-*alt*-MAn)-*b*-PS in a one-step synthesis.[203] Hydrolysis of the MAn units gave an amphiphilic block copolymer which formed spherical particles in aqueous solution. Recently, P(S-*alt*-MAn)-*b*-PS

was also obtained using BlocBuilder®-controlled (2-([*tert*-butyl-(1-(diethoxyphosphoryl)-2,2-dimethylpropyl)amino]oxy)-2-methylpropanoic acid)) NMP which can be carried out at 90°C rather than at 120°C.[204] ^{13}C NMR spectroscopy revealed that alternating copolymers were obtained at equimolar feed ratios. The copolymerization characteristics became more and more random with decreasing MAn fraction when the polymerization was carried out at 110°C while predominantly alternating polymers were obtained even at low MAn fractions at 90°C. In addition to the two expected ^{13}C NMR signals corresponding to styrene-MAn-styrene (SMS) and SSS triads the diblock copolymers exhibited small signals of SSM and MSS triads indicating the formation of tapered block copolymers.

2.4 Previous Investigations at Potsdam University

Since the development of controlled radical polymerization techniques, the synthesis of multiblock copolymers composed of almost all kind of monomers is possible. Especially the combination of different monomer classes within one block copolymer allowed to adjust the polymer properties in view of potential applications.[205] However, the analysis of such block copolymers is still not straightforward and standard techniques such as SEC are often not suitable for the determination of the molecular weight of multiblock copolymers bearing different kinds of monomers.

2.4.1 Twofold TMS-Labeled RAFT-Agents

Although a wide selection of different RAFT-agents were synthesized since the discovery of the RAFT process, analysis of (block) copolymers without existing SEC standard is still challenging. Especially for block copolymer synthesis, dormant polymeric intermediates are crucial and, therefore, the degree of end group functionality is very important. In principle, end group analysis is an elegant method for polymer characterization but it requires that the average number of end groups is known. In practice, however, this information is difficult to obtain. As an outstanding example, polymers synthesized by the RAFT process contain a defined initiating R- and terminating Z-group if the polymerization is conducted correctly.[45] The number-average molar mass M_n then can be calculated using the R- or the Z-group

$$M_n^{exp} = \frac{M_{monomer} \cdot [CRU]}{[R^{inc}]} + M_{CTA} \tag{2.9}$$

$$M_n^{exp} = \frac{M_{monomer} \cdot [CRU]}{[Z^{inc}]} + M_{CTA} \tag{2.10}$$

where $M_{monomer}$ and M_{CTA} are the molar masses of the monomer and the RAFT agent, respectively, and [CRU], [R^{inc}] and [Z^{inc}] are the concentrations of the constitutional repeat units (CRU), as well as the incorporated R- and Z-groups, respectively. In equation 2.9 the majority of polymer chains have to be initiated by the R-group and, hence, initiator derived polymer chains as well as uncontrolled chain transfer should be negligible. In contrast, in equation 2.10 additionally complete Z-group functionality is necessary. While the former requirements can be achieved by appropriate amounts of initiator[45,206] and solvent, the latter suffer from known side reactions of thiocarbonates and trithiocarbonates under RAFT conditions.[54–56,207–210] Due to the aforementioned confinements, the R-group should be preferred for molecular weight determinations of polymers by end group analysis.

Several methods for end group analysis and molar mass determination of synthetic polymers such as UV absorption,[52,54,55,151,211–215] SEC with UV-detection,[208,216] elemental analysis,[56,214] and ^{1}H NMR spectroscopy[56,214,217–229] have been applied. Among these, ^{1}H NMR spectroscopy might be the most promising due to its easy accessibility and short measurement times. However, although many examples for end group analysis by ^{1}H NMR spectroscopy can be found in the literature[220,222–224,229–232] the corresponding peaks appeared usually in the range from 0.8 to 8.0 ppm, i. e., the range where also common polymer signals show up and, moreover, often were broad and suffered from low intensities. Thus, these labeled RAFT agents were typically not universal in nature and valid only for certain types of monomers. For instance, the use of an aromatic end group label may be useful for, e. g., MMA polymers but will be useless for polystyrene. In addition, good molecular weights were only obtained for polymers with an M_n below 10000 g mol^{-1}. In order to overcome this limitation, trimethylsilyl (TMS) label were introduced into different RAFT agents[233,234] since the TMS group (*i*) is sufficiently stable when attached to carbon and (*ii*) gives rise to

nine equivalent proton signals in a spectral region that is usually NMR silent (0.0-0.5 ppm). The reinitiating benzylic R-group was TMS-labeled in 3- or 4-position and connected to the propyl-TMS label in the Z-group *via* either a dithiocarboxylate (CTA **1** and CTA **2**) or a trithiocarbonate moiety (CTA **3** and CTA **4**) as shown in Figure 18.[235] Since hydrophobic end groups can have marked influence on the solution behavior of water soluble polymers,[236] the end group markers should be as small as possible. Especially the detailed investigation of the self-organization behavior of multiresponsive block copolymers in dilute aqueous solutions may be affected by large hydrophobic end groups.

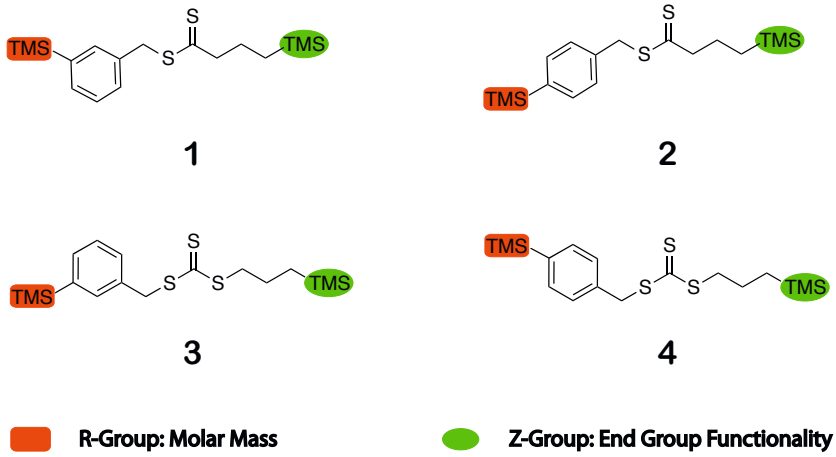

Figure 18: Structure of the four novel TMS-labeled RAFT-agents **1**-**4**.

These RAFT agents result in two well separated singlets at 0.00-0.05 ppm for alkyl bound TMS groups and at 0.2-0.4 ppm for TMS groups on aromatic rings. This downfield shift results from deshielding of aryl bound TMS groups due to ring current effects.[237,238] Furthermore, CTA **1**-**4** proved to be efficient for the polymerization of styrene and *n*-butyl acrylate as well as less trivial monomers.[235] The theoretical number average molar mass values M_n and the SEC results agreed well with M_n values obtained from ^{1}H NMR end group analysis using the TMS_R signal against a characteristic polymer peak. In addition, a comparison of the relative integrals of the TMS_R and the TMS_Z resonances gave information about the residual end group functionality within the polymer. Even high molecular weight poly(butylacrylate) of up to 10^5 g mol^{-1} could be analyzed with high precision. The easy determination of residual end group functionality additionally allowed the investigation of solvent suitability for RAFT polymerizations. Especially for polymerizations in THF a high loss of Z-group was observed even when freshly distilled THF was used. Thus, in order to obtain high quality polymers for

the preparation of multi block copolymers, THF should be avoided. These results were in agreement with recent degradation studies of RAFT end groups in THF.[210]

2.4.2 Mono and Double Responsive Triblock Copolymers

In previous investigations in Potsdam three double thermoresponsive triblock copolymers containing a permanently hydrophilic block of poly(N,N-dimethylacrylamide) (PNDMAM) and two thermoresponsive blocks, namely poly(N-acryloylpyrrolidone) (PNAP) and PNIPAM with cloud point temperatures of 56°C and 32°C, respectively, were synthesized. Three polymers, $PNDMAM_{64}$-*b*-$PNAP_{70}$-*b*-$PNIPAM_{110}$ (ABC), $PNAP_{69}$-*b*-$PNDMAM_{52}$-*b*-$PNIPAM_{110}$ (BAC) and $PNDMAM_{139}$-*b*-$PNIPAM_{52}$-*b*-$PNAP_{28}$ (ACB) were obtained by successive RAFT polymerizations.[239]

Their self-organization behavior was investigated by turbidity measurements and dynamic light scattering (Figure 19). The aggregation behavior of these polymers depended on the heating rate during the DLS measurement, i. e., appeared to be kinetically controlled. Moreover, the block sequence was found to be a major aspect influencing the thermoresponsive behavior. In more detail, the turbidity curve of aqueous solutions of $PNDMAM_{64}$-*b*-$PNAP_{70}$-*b*-$PNIPAM_{110}$, which contained the highest LCST block in the middle, dropped above 35°C accompanied with an increase in D_h observed from DLS measurements (Figure 19a) which was attributed to the phase transition of the terminal PNIPAM block. After an initial maximum of 500-600 nm stable colloids of about 200 nm were formed until 54°C. Further heating led to a second increase of the hydrodynamic diameter, interpreted as secondary aggregation due to the collapse of the PNAP block.
In copolymer $PNAP_{69}$-*b*-$PNDMAM_{52}$-*b*-$PNIPAM_{110}$, with the permanently hydrophilic block in the middle, the cloud point of the PNIPAM block induced an increase in D_h and a drop in transmittance above 35°C (Figure 19b). After an initial maximum of the hydrodynamic diameter the aggregate size became bimodal in DLS measurements but no clear indication for a second transition could be observed. Polymer $PNDMAM_{139}$-*b*-$PNIPAM_{52}$-*b*-$PNAP_{28}$ with the lowest LCST block in the middle showed only one thermally induced transition into aggregates of 40 nm above 38°C (Figure 19c).

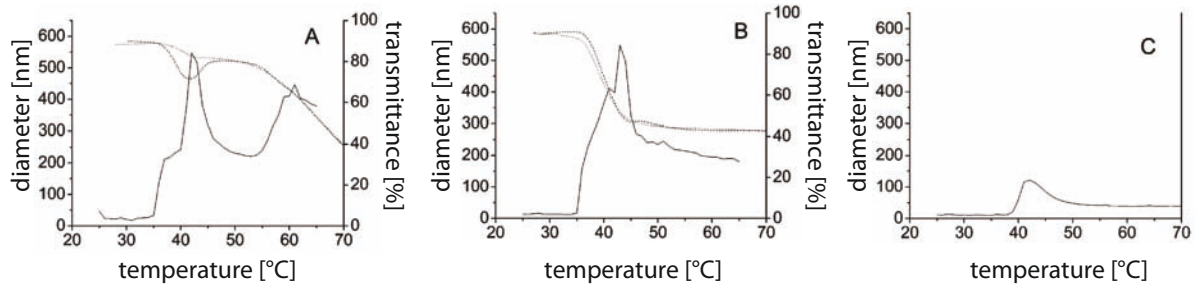

Figure 19: Temperature dependent dynamic light scattering (solid lines) and turbidity measurements (broken lines heating, dotted lines cooling curves) of A) $PNDMAM_{64}$-*b*-$PNAP_{70}$-*b*-$PNIPAM_{110}$ B) $PNAP_{69}$-*b*-$PNDMAM_{52}$-*b*-$PNIPAM_{110}$ C) $PNDMAM_{139}$-*b*-$PNIPAM_{52}$-*b*-$PNAP_{28}$ at 0.1wt% aqueous solution.[239]

The interpretation of the self-organization processes of these triblock copolymers were complicated by kinetic effects. The applied heating rate as well as aging phenomena had marked influence on the aggregation processes. Fast heating typically led to smaller aggregates. Temperature dependent ^{1}H NMR measurements in D_2O were performed to gain information of the self-organization process on a molecular level (Figure 20). For the polymers $PNDMAM_{64}$-*b*-$PNAP_{70}$-*b*-$PNIPAM_{110}$ and $PNAP_{69}$-*b*-$PNDMAM_{52}$-*b*-$PNIPAM_{110}$ an increase of the solution temperature to 45°C caused the attenuation of the PNIPAM side chain signals. Further heating to 65°C then also showed the vanishing of the proton resonances of the PNAP block (Figure 20a,b). These findings supported the picture obtained from turbidity and DLS measurements. In contrast, the signals of the PNIPAM and the PNAP block were both attenuated already at 45°C for $PNDMAM_{139}$-*b*-$PNIPAM_{52}$-*b*-$PNAP_{28}$, suggesting that the two phase transition temperatures of these two block are no longer resolved from each other (Figure 20c).

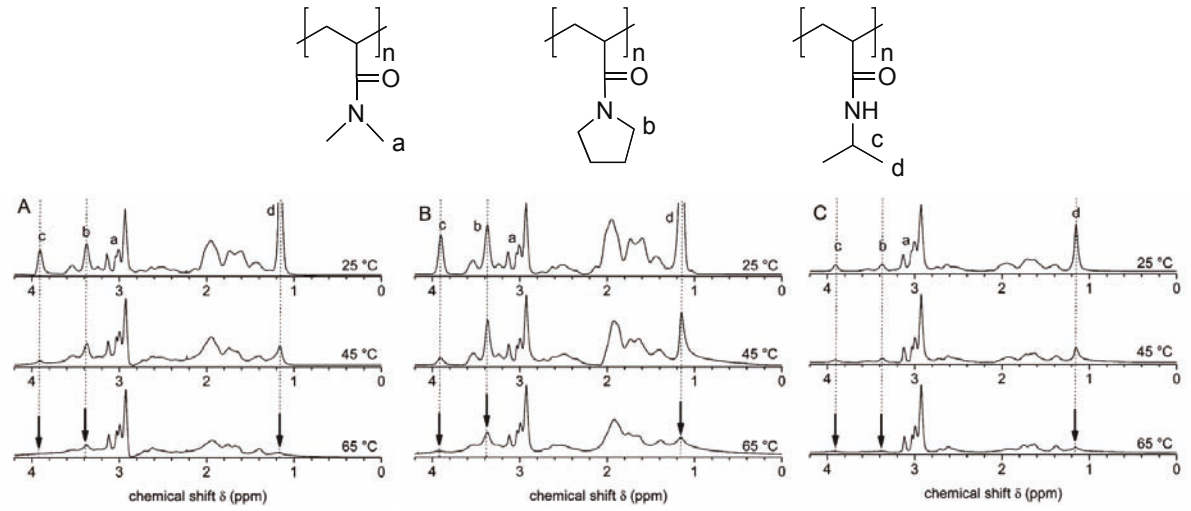

Figure 20: Temperature dependent ^{1}H NMR spectra of A) PNDMAM$_{64}$-*b*-PNAP$_{70}$-*b*-PNIPAM$_{110}$ B) PNAP$_{69}$-*b*-PNDMAM$_{52}$-*b*-PNIPAM$_{110}$ C) PNDMAM$_{139}$-*b*-PNIPAM$_{52}$-*b*-PNAP$_{28}$ in D_2O.[239]

Thus, only those block copolymers containing the high LCST block in the middle displayed two thermally induced, discernible transitions while for other block sequences only one transition could be observed.

2.5 Objectives of this Thesis

As outlined in the introduction, the aggregation behavior of smart block copolymers becomes more complex and dynamic in nature when the amount of responsive blocks is increased. For instance, the self-organization of double thermoresponsive terpolymers in dilute aqueous solution differed significantly from the one usually observed for double thermosensitive diblock copolymers.[239] Accordingly, the self-assembly of triple thermoresponsive triblock copolymers is expected to be even more complex and dynamic and may even allow for stimuli-triggered interconversion of one aggregate into another (e. g., spherical to cylindrical micelle). Thus, one major objective of this thesis was the synthesis of such triple thermoresponsive terpolymers in all possible block sequences (ABC, BAC, ACB) and to study the influence of the block sequence on their self-assembly in dilute solution. Different measurement techniques such as turbidimetry, dynamic light scattering, TEM measurements and NMR spectroscopy will be used for a detailed investigation. Furthermore, temperature dependent solubilization of a solvatochromic probe, will provide a first indication of

the “smart“ carrier abilities in dependence of the block sequence of such multi responsive block copolymers.

In addition, due to the limitations of the classical step-wise synthesis of smart terpolymers by controlled radical polymerization, e. g., increasing loss of end group functionality during the subsequent polymerization steps, the one-step synthesis of similar multi thermoresponsive block copolymers will be explored. A possible strategy is the use of the alternating copolymerization of a thermosensitive styrene derivative and different N-substituted maleimides. If the phase transition temperature of such a styrene derivative can be varied upon copolymerization with maleimides bearing hydrophobic or hydrophilic side chains, an excess of the styrene-based monomer will lead to the formation of tapered block copolymers which may show similar thermosensitive aggregation behavior than block copolymers obtained by a sequential approach.

3 Results and Discussion

3.1 Synthesis of RAFT-Agents and Monomers

In order to obtain triple thermoresponsive triblock copolymers which show three distinct transitions in dilute aqueous solutions, the three phase transition temperatures should be distributed as far as possible within the given temperature window in water. Furthermore, characterization of the polymers should be reliable and straightforward. Accordingly, for the sequential RAFT synthesis of triblock copolymers with three different LCSTs the twofold TMS-labeled RAFT agents were used which allow characterization of the homo-, di- and triblock copolymers by ^{1}H NMR spectroscopy. Within this context, the three monomers used should show distinct NMR signals even in the NMR spectra of the final triblock copolymers. This will allow to not only determine the average molar mass but also the composition of the obtained block copolymers for routine ^{1}H NMR spectra. However, neither the RAFT-agents nor appropriate monomers are commercially available and, thus, were synthesized according to literature procedures.

3.1.1 Synthesis of RAFT-Agents

4-(Trimethylsilyl)benzyl-3'-(trimethylsilyl)propyl-dithioate (CTA **1**) and 3-(trimethylsilyl)-benzyl-3'-(trimethylsilyl)propyl dithioate (CTA **2**) were synthesized starting from 3-chloropropyl trimethylsilane (Scheme 6). Dropwise addition of CS_2 and 4- (**5**) or 3-(trimethylsilyl)benzylbromid (**6**) in dry THF gave the desired twofold TMS-labeled RAFT agents **1** and **2**. Slight variations of the original synthesis protocol given in the diploma thesis of Maik Lange,[234] such as prolonged activation of the magnesium turnings and elevated reaction temperatures (44°C), led to an increase of the isolated yield after purification in column chromatography from about 30% to 69% and 77% for CTA **1** and CTA **2**, respectively.

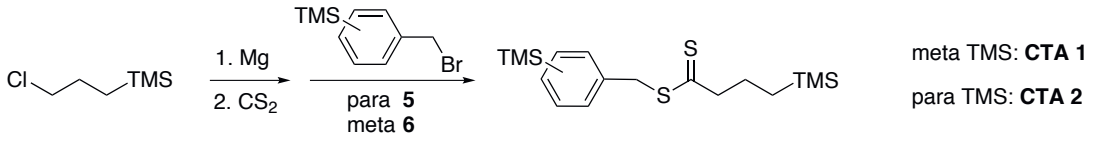

Scheme 6: Synthetic route to 4-(trimethylsilyl)benzyl 4'-(trimethylsilyl)propyl-dithioate (CTA **1**) and 3-(trimethylsilyl)benzyl-3'-(trimethylsilyl)propyl dithioate (CTA **2**).

3.1.2 Synthesis of Monomers

Three monomers, N-propylacrylamide (**7**), methoxydi(ethylene glycol) acrylate (**8**), and N-ethylacrylamide (**9**), with reported LCST values for their homopolymers of 20-25°C,[117] 39°C[240] and 70-80°C,[117] respectively, were synthesized according to literature procedures. Thus, N-propylacrylamide was obtained by the dropwise addition of acryloyl chloride to a basic solution of propylamine in dry benzene at 0°C (Scheme 7).

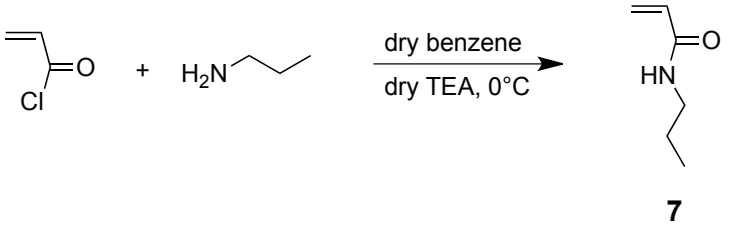

Scheme 7: Synthesis of N-propylacrylamide (**7**).

After distillation in vacuo at 105°C N-propylacrylamide was obtained as colorless liquid with moderate yields of 58%. N-Ethylacrylamide (**9**) can be synthesized analogously, however, since ethylamine, with a boiling point of 16°C, is a gas at room temperature, the reaction was carried out in dry DCM at -40°C (Scheme 8).

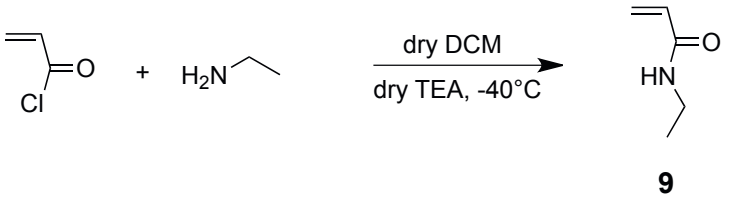

Scheme 8: Synthesis of N-ethylacrylamide (**9**).

Dropwise addition of acryloyl chloride to ethylamine in dry DCM and triethylamine (TEA), followed by distillation in vacuo at 100°C gave N-ethylacrylamide as a colorless liquid with moderate yield of 53%. Both N-propylacrylamide and N-ethylacrylamide solidified upon storage in the freezer that no addition of inhibitors was necessary.
In a similar way methoxydi(ethylene glycol) acrylate (**8**) can be obtained by dropwise addition of acryloyl chloride to a solution of dry TEA and di(ethylene glycol) monomethyl ether in dry DCM (Scheme 9). After aqueous work up and purification by column chromatography methoxydi(ethylene glycol) acrylate (**8**) was obtained in excellent yield of 96%.

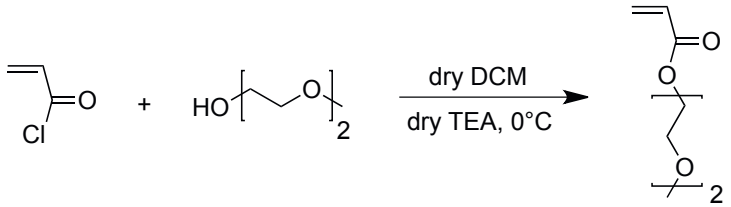

8

Scheme 9: Synthesis of methoxydi(ethylene glycol) acrylate (**8**).

3.2 TMS-Labeled RAFT-Agents and Styrenes

As outlined in the introduction (see Section 2.4.1), the two TMS-label on CTA **1**-**4** give rise to distinct, well separated singlets at about 0 ppm. Surprisingly, when the synthesis of thermoresponsive polymers based on styrene was intended, splitting of the TMS_R and TMS_Z resonances into broad multiplets was observed (Figure 21a). In contrast, the polymerization of acrylamides and acrylates led to the expected singlet signals (Figure 21b). Since a cleavage of the C-Si bond under usual polymerization conditions is not likely, the observed TMS-group splitting must have its origin from other than chemical side reactions. However, the multiplets of the TMS_R end groups of polystyrenes could still be used for the determination of the molar mass using ^{1}H NMR spectroscopy, suggesting that no cleavage of the TMS-label took place.

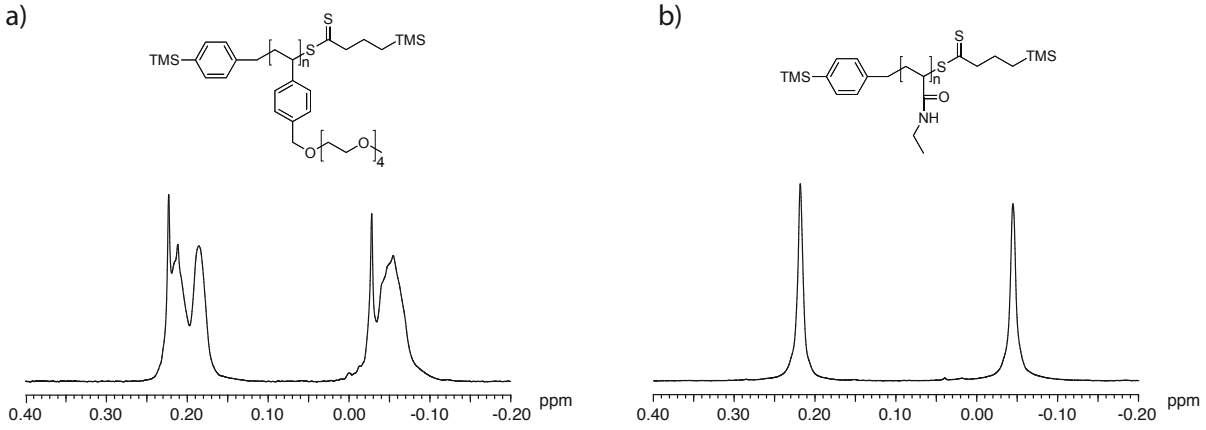

Figure 21: R- and Z-group TMS resonances of a) poly(4-vinylbenzyl methoxytetrakis(oxyethylene) ether) and b) poly(N-ethylacrylamide) obtained by RAFT polymerization using CTA **1**.

A detailed investigation of RAFT derived polystyrene[235] showed that the TMS resonances lead to different peak pattern depending on the one hand on the substitution of the R-group and on the other hand on the type of Z-group (Figure 22). Similar peak splitting was observed when styrene was polymerized using the intermediate TMS-aryl bromides **5** and **6** as ATRP initiators. One possible explanation for the observed peak splitting is stereoisomerism at the chain ends. Several reports on the influence of the chain end tacticity in poly- or oligostyrene on the NMR signal of end group substitution have been published.[241–243] A detailed NMR study of oligostyrene terminated with trimethylsilyl groups by Gibson *et al.* revealed that the complex signals observed in ^{1}H-, ^{13}C-, as well as in ^{29}Si NMR spectroscopy indeed resulted from stereoisomerism at the chain end. However, the TMS group was directly attached to the polymer chain end in this case while the TMS_R functionality in polystyrenes from CTA **1**-**4** is separated by nine bonds from the first stereocenter of the polymer chain. Therefore, the observed peak splitting might be rather explained by anisotropy effects of adjacent aromatic rings[237,244] somehow additionally influenced by stereoisomerism of the polymer chain than by chain end tacticity alone. In addition, chain extensions of RAFT-derived polystyrene with butylacrylate performed in our group[235] gave a sharp singlet for the TMS_Z-group while the complex peak pattern of the TMS_R-group remained unchanged. This control experiment indirectly proves the influence of the aromatic side chains on the peak shape of the TMS-resonances and furthermore reveals the absence of chemical side reactions during the polymerization.

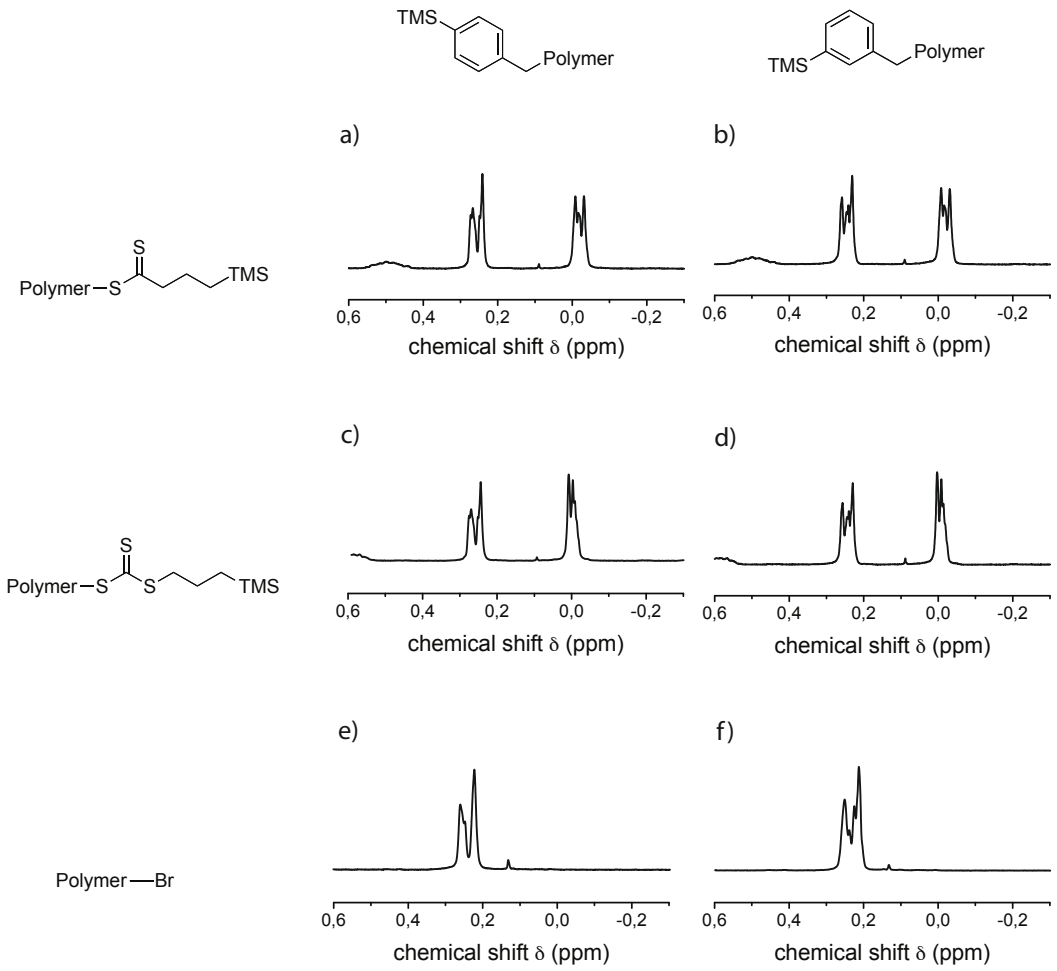

Figure 22: Comparison of the ^{1}H NMR signals of the TMS end group labels of polystyrene samples made with RAFT agents a) **1**, b) **2**, c) **3**, and d) **4**, or by ATRP using e) **5** and f) **6** as initiators.[235]

3.3 Sequential RAFT-Synthesis of Multiple Thermoresponsive Block Copolymers

As discussed in the introduction, the phase transition temperature of a given polymer can be influenced by an adjacent block in a block copolymer (see Section 2.2.1). Thus, the combination of one thermosensitive block and one hydrophobic block in a diblock copolymer can lower the cloud point in comparison to the homopolymer.[138,139] For multi thermoresponsive block copolymers the situation can become more complex when the cloud points of the different blocks are affected by each other, i. e., the cloud point of the low-LCST block increases while the cloud point of the high-LCST decreases. As a result blurring of the phase transition

temperatures and only one thermally induced transition may be observed. Therefore, first homopolymers of **7**, **8** and **9** were synthesized and their phase transition temperatures in dilute aqueous solution were studied by turbidimetry. Furthermore, combinations of these three monomers in diblock copolymers were synthesized in order to verify that each block still exhibits a distinct phase transition.

3.3.1 Synthesis and Solution Properties of Homopolymers

Homopolymers of **7**, **8** and **9** were synthesized by RAFT polymerization using CTA **1**. A combination of SEC and end group analysis in ^{1}H NMR spectroscopy revealed the successful synthesis of $PNPAM_{118}$, $PMDEGA_{115}$, and $PNEAM_{133}$. All three polymers show clear solutions below 15°C when dissolved in water at concentrations of $1.0\,g\,L^{-1}$. Heating their aqueous solution from 10°C to 90°C displayed cloud point temperatures of 16°C, 47°C, and 70°C, respectively (Figure 23).

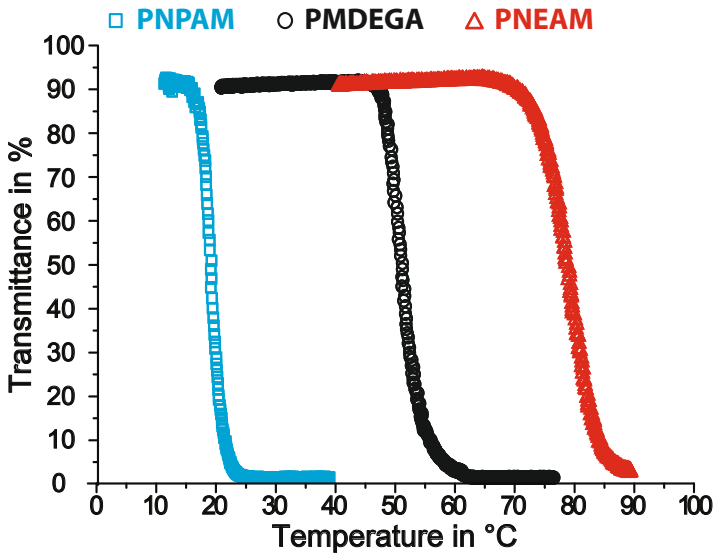

Figure 23: Plot of the transmittance (%) of aqueous solutions ($1.0\,g\,L^{-1}$) of $\mathbf{P7}_{118}$ (□), $\mathbf{P8}_{115}$ (◯), and $\mathbf{P9}_{133}$ (△) as function of temperature.

The observed phase transition temperatures are in reasonable agreement with literature values.[117,240] Slight deviations result from several factors such as degree of polymerization, end groups, concentration and others. Due to the possible shifting of the cloud point, the choice of monomers is crucial in order to avoid blurring of the phase transitions within block

copolymers. Accordingly, the three LCST values should be distributed as far as possible from each other within the given temperature window in water.

3.3.2 Double Thermoresponsive Diblock Copolymers

Double thermoresponsive diblock copolymers $PNPAM_{103}$-*b*-$PMDEGA_{29}$ (**P7**$_{103}$-*b*-**P8**$_{29}$) and $PNEAM_{64}$-*b*-$PMDEGA_{20}$ (**P9**$_{64}$-*b*-**P8**$_{20}$) were synthesized using CTA **1** (Figure 24). The obtained copolymers were characterized by a combination of SEC and ^{1}H NMR spectroscopy as summarized in Table 3.1. **P7**$_{103}$-*b*-**P8**$_{29}$ and **P9**$_{64}$-*b*-**P8**$_{20}$ were obtained in relative compositions of 3 : 1 with the PNPAM and PNEAM blocks being three times longer than the PMDEGA block.

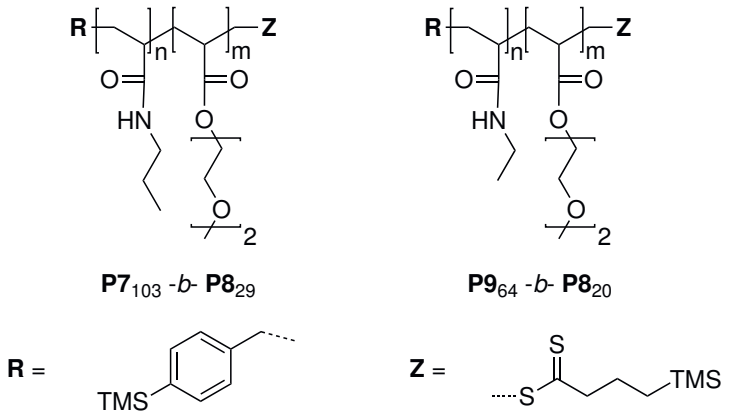

Figure 24: Structure and composition of $PNPAM_{103}$-*b*-$PMDEGA_{29}$ (**P7**$_{103}$-*b*-**P8**$_{29}$) and $PNEAM_{64}$-*b*-$PMDEGA_{20}$ (**P9**$_{64}$-*b*-**P8**$_{20}$).

The molar mass was determined directly from ^{1}H-NMR spectroscopy by integration of the TMS_R resonance against the CH_3 side chain resonances of PNPAM and PNEAM at 0.8 ppm and 1.0 ppm, respectively, as well as against the CH_2 signal adjacent to the ester functionality of PMDEGA at 4.2 ppm. Moreover, the comparison of the intensities of the TMS_R and TMS_Z signals revealed a loss of the Z-group in particular after the block copolymerization step from 90% to 10% (**P7**$_{103}$-*b*-**P8**$_{29}$) and 30% (**P9**$_{64}$-*b*-**P8**$_{20}$). Such a loss of the thiocarbonyl end group in THF has been reported recently and was attributed to an oxidative degradation by peroxides.[210] In the light of the precautions taken to purify the THF used, thus precluding from the presence of notable amounts of peroxides during synthesis and work up, the reasons for the loss of thiocarbonyl end groups seem yet unclear. Furthermore, such a high loss

in end group functionality renders the obtained diblock copolymers useless for the synthesis of triple thermoresponsive triblock copolymers.

Table 3.1: Synthesis data of $\mathbf{P7}_{103}$-*b*-$\mathbf{P8}_{29}$ and $\mathbf{P9}_{64}$-*b*-$\mathbf{P8}_{20}$. Polymerizations were carried out in dry THF for 5-6 h.

Polymer	CTA	Monomer	yield[a]	M_n[b]	Z/R	M_n[c]	PDI	DP
$\mathbf{P7}_{103}$	**1**	NPAM	57	12000	0.9	12700	2.26	70
$\mathbf{P9}_{64}$	**1**	NEAM	55	6700	0.9	8800	1.33	64
$\mathbf{P7}_{103}$-*b*-$\mathbf{P8}_{29}$	$\mathbf{P7}_{70}$	MDEGA	72	17000	0.1	9800	2.30	98
$\mathbf{P9}_{64}$-*b*-$\mathbf{P8}_{20}$	$\mathbf{P9}_{64}$	MDEGA	29	10200	0.3	11000	1.39	84

[a]Yield in % determined gravimetrically. [b] Calculated molar mass from ^{1}H NMR spectroscopy by integration or the TMS_R peak against a peak of the polymer (end group analysis). [c] Determined by size exclusion chromatography (SEC) using linear polystyrene standards.

The self-organization behavior of $\mathbf{P7}_{103}$-*b*-$\mathbf{P8}_{29}$ and $\mathbf{P9}_{64}$-*b*-$\mathbf{P8}_{20}$ in dilute aqueous solution was studied by turbidimetry and dynamic light scattering. Both double thermoresponsive diblock copolymers $\mathbf{P7}_{103}$-*b*-$\mathbf{P8}_{29}$ and $\mathbf{P9}_{64}$-*b*-$\mathbf{P8}_{20}$ show clear solutions below 24°C when dissolved in water at concentrations of 1.0 g L^{-1}. When heated from 15-80°C, aqueous solutions of $\mathbf{P7}_{103}$-*b*-$\mathbf{P8}_{29}$ and $\mathbf{P9}_{64}$-*b*-$\mathbf{P8}_{20}$ showed two distinct, temperature induced phase transitions. $\mathbf{P7}_{103}$-*b*-$\mathbf{P8}_{29}$, with a relatively long low-LCST block of PNPAM showed aggregation in DLS together with a drastic drop in transmittance when its aqueous solution was heated above 24°C (Figure 25a). After an initial maximum in D_h the hydrodynamic diameter leveled off at about 300 nm between 38°C and 50°C. Within this temperature range also the transmittance reached a plateau. These changes are attributed to the collapse of the PNPAM block and the formation of aggregates with hydrophobic PNPAM domains. Further heating then induced a second pronounced drop in DLS and turbidimetry above 50°C, the collapse temperature of the PMDEGA block. As a result, the formed particles shrank by 130 nm to about 170 nm.

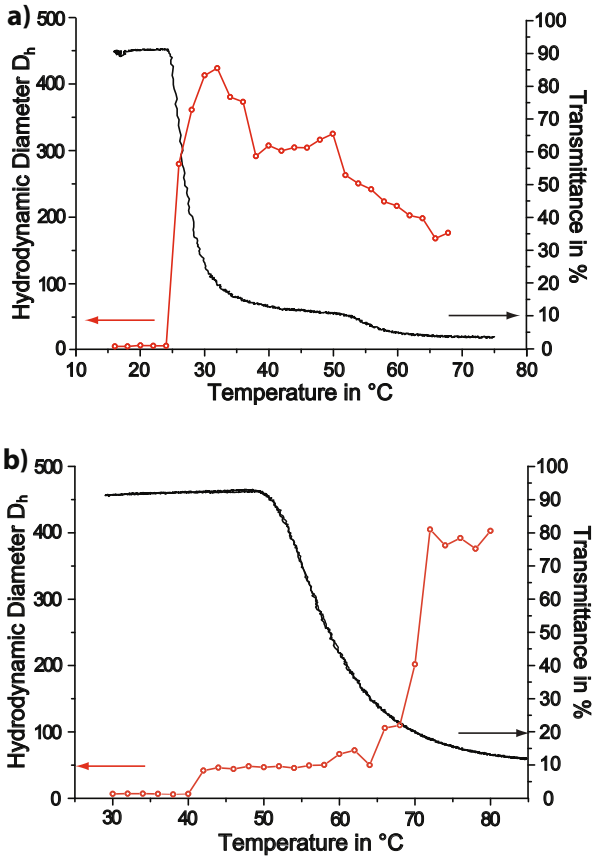

Figure 25: DLS (red dotted line) and turbidity measurements (black solid line) of aqueous solutions of a) $PNPAM_{103}$-*b*-$PMDEGA_{29}$ (**P7**$_{103}$-*b*-**P8**$_{29}$) and b) $PNEAM_{64}$-*b*-$PMDEGA_{20}$ (**P9**$_{64}$-*b*-**P8**$_{20}$) during the heating process from 10°to 80°C.

In contrast, **P9**$_{64}$-*b*-**P8**$_{20}$ with a relatively long high-LCST block of PNEAM showed aggregation only above 40°C, the phase transition temperature of the PMDEGA block. Between 42°and 60°C PMDEGA-core PNEAM-shell micelles with a D_h of 45 nm are observed by DLS (Figure 25b). Above 60°C, when the cloud point temperature of the PNEAM block is reached, secondary aggregation into micellar clusters of about 400 nm set in and turbidity measurements displayed a single transition (Figure 25b). Thus, the initially formed micelles seem to be too small to be detected by turbidimetry. Taking the contour length of **P7**$_{103}$-*b*-**P8**$_{29}$ and **P9**$_{64}$-*b*-**P8**$_{20}$ with 24.5 nm and 21 nm into account, the particles formed by **P7**$_{103}$-*b*-**P8**$_{29}$ are by means too large to be single micelles and, thus, are rather interpreted as clusters of micelles.

Interestingly, the temperature induced aggregation process of **P7**$_{103}$-*b*-**P8**$_{29}$ and **P9**$_{64}$-*b*-**P8**$_{20}$ was completely reversible. The cooling curve in DLS of **P7**$_{103}$-*b*-**P8**$_{29}$ was virtually identical to the heating curve shown in Figure 25a and even the clustering of micelles observed above

the second cloud point by **P9**$_{64}$-*b*-**P8**$_{20}$ was reversible during repeated heating-cooling cycles without any hysteresis (Figure 26a and b). Thus, both aggregation pathways seem to be thermodynamically controlled.

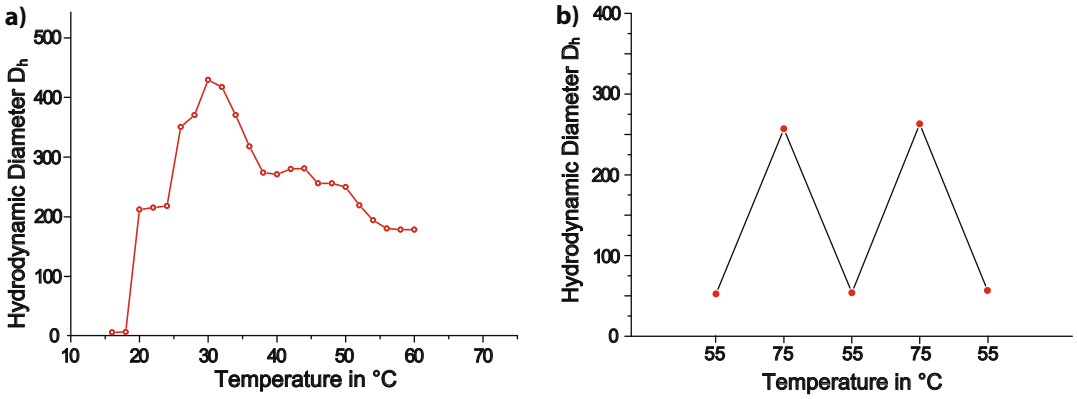

Figure 26: a) Cooling curve in DLS of **P7**$_{103}$-*b*-**P8**$_{29}$ and b) heating-cooling cycles between 55° and 75°C in dynamic light scattering of **P9**$_{64}$-*b*-**P8**$_{20}$ both in aqueous solution at a concentration of 1.0 g L^{-1}.

In addition, a set of double thermoresponsive diblock copolymers PNPAM-*b*-PNEAM was synthesized by sequential RAFT polymerization using CTA **1** (Figure 27). The resulting block copolymers only differed in their relative composition, i. e., PNPAM$_{137}$-*b*-PNEAM$_{67}$ (**P7**$_{137}$-*b*-**P9**$_{67}$), PNPAM$_{133}$-*b*-PNEAM$_{133}$ (**P7**$_{133}$-*b*-**P9**$_{133}$) and PNPAM$_{34}$-*b*-PNEAM$_{94}$ (**P7**$_{34}$-*b*-**P9**$_{94}$).

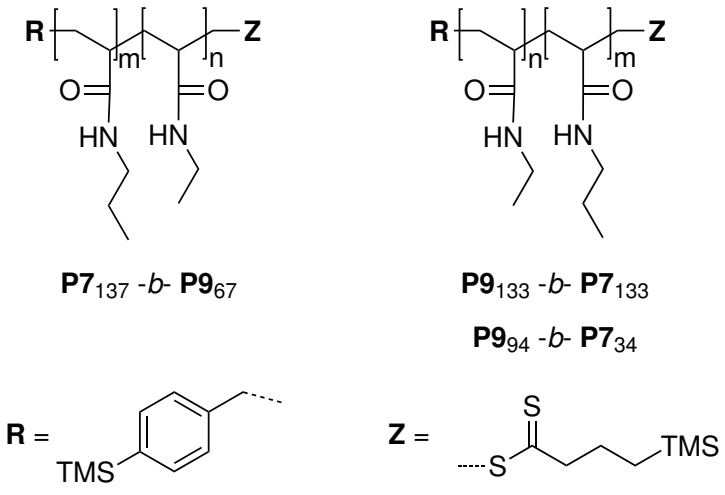

Figure 27: Structure and composition of PNPAM$_{137}$-*b*-PNEAM$_{67}$ (**P7**$_{137}$-*b*-**P9**$_{67}$), PNPAM$_{133}$-*b*-PNEAM$_{133}$ (**P7**$_{133}$-*b*-**P9**$_{133}$) and PNPAM$_{34}$-*b*-PNEAM$_{94}$ (**P7**$_{34}$-*b*-**P9**$_{94}$).

The molar mass and end group functionality was determined directly from ^{1}H-NMR spectroscopy by integration of the TMS_R and TMS_Z resonance against the CH_3 side chain resonances of PNPAM and PNEAM at 0.8 ppm and 1.0 ppm, respectively (Table 3.2). Again, the comparison of the intensities of the TMS_R and TMS_Z signals revealed a loss, although less pronounced, of the Z-group in particular after the block copolymerization step.

Table 3.2: Synthesis data of **P7**$_{137}$-*b*-**P9**$_{67}$, **P7**$_{133}$-*b*-**P9**$_{133}$ and **P7**$_{34}$-*b*-**P9**$_{94}$.

Polymer	CTA	Monomer	yield[a]	$M_{n,theor.}$[b]	M_n[c]	Z/R[d]	M_n[e]	PDI
P7$_{137}$	CTA **1**	NPA (**7**)	63	15000	15000	0.7	11700	1.41
P9$_{133}$	CTA **1**	NEA (**9**)	76	13800	13200	1.0	14100	1.33
P9$_{94}$	CTA **1**	NEA (**9**)	55	11000	9300	0.9	10000	1.32
P7$_{137}$-*b*-**P9**$_{67}$	**P7**$_{137}$	NEA (**9**)	69	21800	22100	0.5	14400	1.58
P7$_{133}$-*b*-**P9**$_{133}$	**P9**$_{133}$	NPA (**7**)	51	23500	28200	0.5	18700	1.68
P7$_{34}$-*b*-**P9**$_{94}$	**P9**$_{94}$	NPA (**7**)	60	14300	13200	0.6	12800	1.44

[a]Yield in % determined gravimetrically. [b] Determined gravimetrically. [c] Calculated molar mass from ^{1}H NMR spectroscopy by integration of the TMS_R peak against a peak of the polymer (end group analysis). [d] Determined by ^{1}H NMR spectroscopy using the TMS_R and TMS_Z group. [e] Determined by size exclusion chromatography (SEC).

All homo- and block copolymers give clear solutions in water at temperatures below 15°C. Upon heating, dilute aqueous solutions (1.0 g L^{-1}) of **P7**$_{137}$-*b*-**P9**$_{67}$, **P7**$_{133}$-*b*-**P9**$_{133}$, and **P7**$_{34}$-*b*-**P9**$_{94}$ from 15°C to 90°C, two thermally induced transitions are visible in turbidimetry as well as dynamic light scattering (Figure 28). A pronounced first transition occurs in the range of 15°C to 30°C, while a second transition is observed in the range of 60°C to 70°C. Even well above the second thermal transition, stable polymer aggregates are formed, though both blocks then turned hydrophobic. The remarkably stable colloids produced above the second phase transition is explained by the concept of mesoglobules.[116] Wu *et al.* found that fully collapsed PNIPAM globules still contained about 66% water suggesting that the PNIPAM chains investigated were not completely hydrophobic even well above the LCST.[127,128,130,131] **P7**$_{137}$-*b*-**P9**$_{67}$, **P7**$_{133}$-*b*-**P9**$_{133}$ and **P7**$_{34}$-*b*-**P9**$_{94}$ show individual aggregation behaviors, although they are based on the same polymers and have identical end groups. The differ-

ences must therefore result from the different relative sizes of the PNPAM block exhibiting the low LCST *vs.* the PNEAM block exhibiting the high LCST. In **P7**$_{137}$-*b*-**P9**$_{67}$, the PNPAM block is about twice as long then the PNEAM block. Turbidimetry displays a cloud point at 17°C paralleled by the abrupt increase of the hydrodynamic diameter D_h as seen by DLS measurements (Figure 28a).

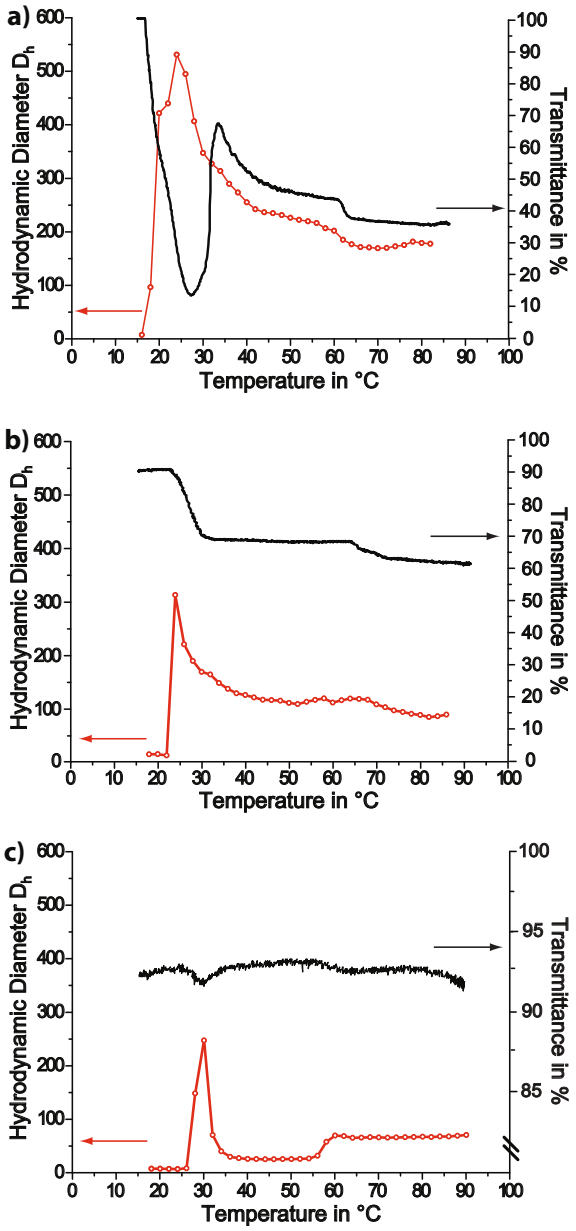

Figure 28: Turbidimetry (solid line) and DLS (dotted line) measurements of aqueous solutions of a) **P7**$_{137}$-*b*-**P9**$_{67}$, b) **P7**$_{133}$-*b*-**P9**$_{133}$ and c) **P7**$_{34}$-*b*-**P9**$_{94}$ at a concentration of 1.0 g L^{-1}.

Characteristically, turbidity and D_h pass through a maximum shortly above the cloud point, before leveling off and reaching a plateau value between 40°C and 60°C, to give stable aggregates with hydrodynamic diameters of about 200 nm. Further heating led to a sudden shrink of D_h about 160 nm around 62°C. This second thermal transition is also reflected by a small, distinct decrease in transmittance. In copolymers **P7**$_{133}$-*b*-**P9**$_{133}$ and **P7**$_{34}$-*b*-**P9**$_{94}$ the cloud point of the PNPAM block shifts with increasing relative length of the PNEAM block toward higher temperatures compared to **P7**$_{137}$-*b*-**P9**$_{67}$, namely to 23°C and to 27°C, respectively (Figure 28b and c). Overall, the solutions of **P7**$_{133}$-*b*-**P9**$_{133}$ and **P7**$_{34}$-*b*-**P9**$_{94}$ are much less turbid than those of **P7**$_{137}$-*b*-**P9**$_{67}$, pointing to smaller aggregates above the first phase transition temperature. In particular, in the case of **P7**$_{34}$-*b*-**P9**$_{94}$, the turbidity of the solution is hardly notable by the naked eye. Nevertheless, DLS measurements show a marked increase of the D_h for both **P7**$_{133}$-*b*-**P9**$_{133}$ and **P7**$_{34}$-*b*-**P9**$_{94}$ above the corresponding cloud point of the PNPAM block accompanied with a decrease in transmittance (Figure 28b and c). Like for **P7**$_{137}$-*b*-**P9**$_{67}$ D_h passes through a pronounced maximum before leveling off in the range of 40-60°C at plateau values of about 100 nm and 25 nm, respectively. Again, further heating results in a second thermal transition, as revealed by a second small, but notable drop in transmittance as well as marked changes of D_h. However, whereas D_h of the aggregates of **P7**$_{133}$-*b*-**P9**$_{133}$ decreases from about 100 nm to 85 nm at about 65°C, D_h of the aggregates formed by **P7**$_{34}$-*b*-**P9**$_{94}$ increases from about 25 nm to 65 nm when heating beyond 58°C. The two thermal transitions found agree with the LCST values reported for the two homopolymer blocks of PNPAM of 20-25°C, and of PNEAM of 70-80°C, respectively,[117,245–247] and therefore reflect the successive collapses of the PNPAM and PNEAM blocks in the copolymers. The increase of the cloud points of copolymers **P7**$_{137}$-*b*-**P9**$_{67}$, **P7**$_{133}$-*b*-**P9**$_{133}$ and **P7**$_{34}$-*b*-**P9**$_{94}$ with increasing relative length of the PNEAM block is explained by the increasing hydrophilicity of the end of the collapsing PNPAM block, which is known to often raise the thermal transition temperature.[136,213,218,248] The first transition induced by the collapse of the PNPAM block converts a double hydrophilic block copolymer into an amphiphilic one, while the second transition, caused by the collapse of the PNEAM block, turns the amphiphilic into a double hydrophobic structure (Scheme 10). The contour lengths of the block copolymers are 51 nm (**P7**$_{137}$-*b*-**P9**$_{67}$), 66 nm (**P7**$_{133}$-*b*-**P9**$_{133}$), and 32 nm (**P7**$_{34}$-*b*-**P9**$_{94}$).

Taking these values into account, the observed D_h values after the first thermal transition are consistent with the formation of polymeric micelles in the case of **P7**$_{133}$-*b*-**P9**$_{133}$ and **P7**$_{34}$-*b*-**P9**$_{94}$, whereas in the case of **P7**$_{137}$-*b*-**P9**$_{67}$, D_h is too large for individual micelles.

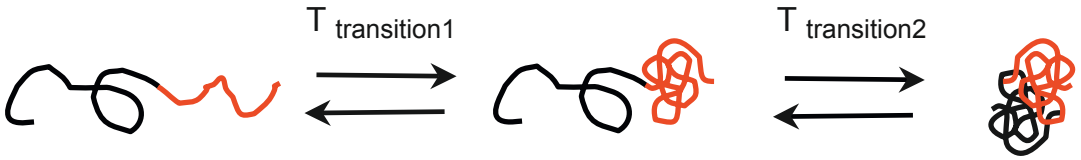

Scheme 10: Schematic behavior of double thermoresponsive block copolymers exhibiting two LCSTs in solution. At T < $T_{transition1}$, the polymer behaves as double hydrophilic (left), at $T_{transition1}$ < T < $T_{transition2}$, the polymer behaves as amphiphilic (center), while at T > $T_{transition2}$, the polymer behaves as double hydrophobic (right).

Transmission electron microscopy (TEM) at 45°C revealed the formation of spherical aggregates for all three polymers (Figure 29). **P7**$_{133}$-*b*-**P9**$_{133}$ formed spherical aggregates with a diameter of about 50 nm (Figure 29b), while **P7**$_{34}$-*b*-**P9**$_{94}$ showed small spherical aggregates of about 20 nm in diameter which partially align into *pearl-necklace type* aggregated during the drying process on the surface (Figure 29c). Hence, copolymers **P7**$_{133}$-*b*-**P9**$_{133}$ and **P7**$_{34}$-*b*-**P9**$_{94}$ indeed form polymeric micelles. The aggregate sizes observed by TEM are 30-50% smaller compared to the sizes determined by DLS studies. This can be explained by the dehydration of the solvated PNEAM corona of the micelles during the drying process involved in the sample preparation. In the case of **P7**$_{137}$-*b*-**P9**$_{67}$, however, TEM shows larger compact spherical aggregates of 160-180 nm in diameter, which coexist with some few small aggregates of about 32 nm in diameter (Figure 29a), suggesting that the major population observed by DLS are clusters of smaller entities, such as micelles. The tendency towards cluster formation is attributed to the relative short hydrophilic PNEAM block, which may either not be sufficient to stabilize isolated micelles, and/or may disfavour the formation of individual micelles with high curvature. The need of relatively long hydrophilic blocks compared to the size of the hydrophobic block in order to provide stable micelles of non-ionic amphiphilic block copolymers was reported before,[249,250] and contrasts with observations on ionic crew-cut block copolymer systems[251,252] which profit from additional electrostatic colloid stabilization. The observed secondary aggregation of **P7**$_{137}$-*b*-**P9**$_{67}$ and **P7**$_{103}$-*b*-**P8**$_{29}$ suggests the high tendency of such block copolymers for cluster formation when the rela-

tive composition is not adjusted with care. A minimum size ratio of about 1 : 1 between the hydrophilic and hydrophobic blocks seems necessary for efficient micellar stabilization.

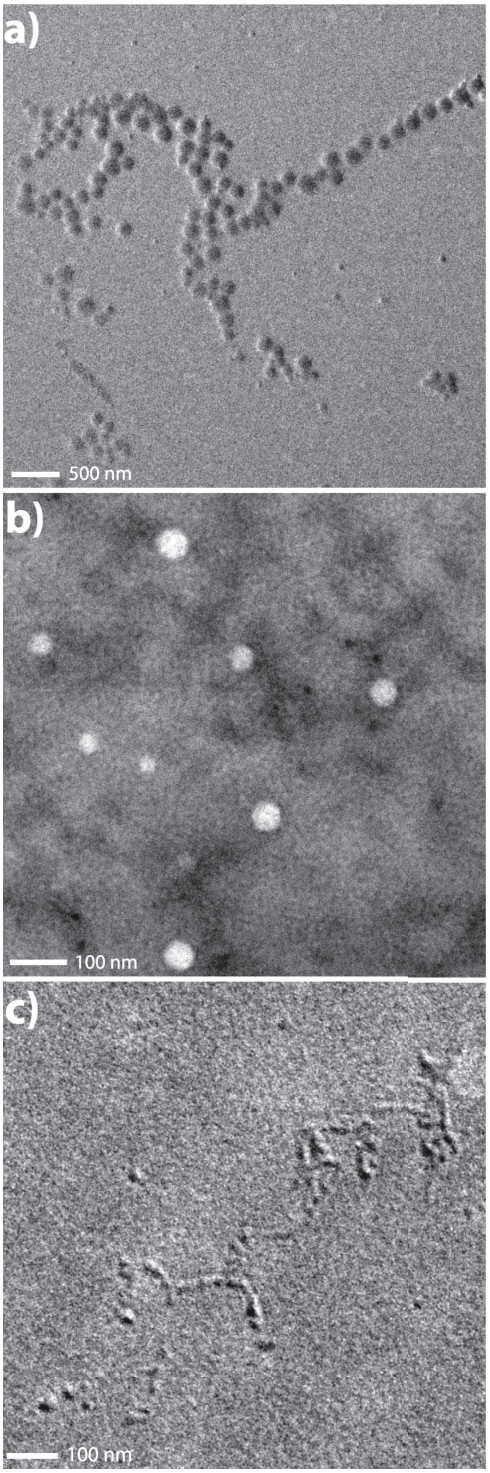

Figure 29: TEM images of **P7**$_{137}$-*b*-**P9**$_{67}$ (a), **P7**$_{133}$-*b*-**P9**$_{133}$ (b) and **P7**$_{34}$-*b*-**P9**$_{94}$ (c) at 45°C shadowed with Pt/C (a,c) or stained with 1% PTA (b).

Beside the expected spherical particles, *pearl-necklace type* aggregates where found for **P7**$_{137}$-*b*-**P9**$_{67}$ in very few cases in TEM (Figure 30). The existence of micelles within the observed linear/cylindrical aggregates indicates a fusion of micelles during the drying process resulting in linear arrangements. Such fusion processes were reported by Lee *et al.*[253] for poly(n-hexyl isocyanate)-*b*-poly(2-vinylpyridine). Light scattering data indicate that these kind of aggregates do not exist in solution and are formed only on the TEM grid during the drying process.

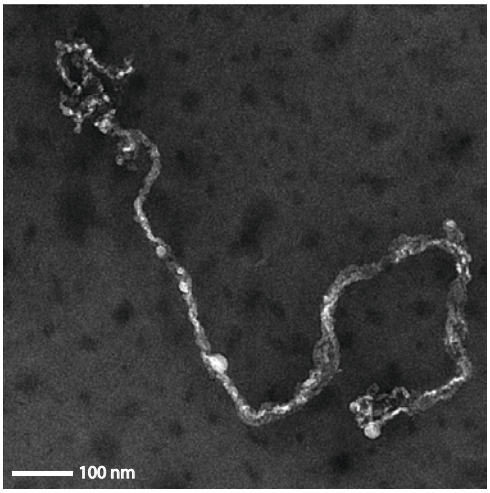

Figure 30: Pearl-necklace type aggregates formed by **P7**$_{137}$-*b*-**P9**$_{67}$ on the TEM grid.

Interestingly, the second thermal transition inducing the collapse of the PNEAM block in **P7**$_{137}$-*b*-**P9**$_{67}$, **P7**$_{133}$-*b*-**P9**$_{133}$ and **P7**$_{34}$-*b*-**P9**$_{94}$ does not lead to the precipitation of the now double hydrophobic copolymers, but results in stable aggregates. The size of the aggregates remained fairly stable even upon continued heating up to almost 90°C. This phenomenon is by no means trivial,[213] though often observed for thermoresponsive block copolymers, most typically for such containing PNIPAM, and is discussed in the context of mesoglobule formation.[116,129,133] Due to their chemical similarity to PNIPAM, the occurrence of mesoglobules of copolymers containing PNEAM and PNPAM is not surprising. As for the first thermal transition, polymers **P7**$_{137}$-*b*-**P9**$_{67}$, **P7**$_{133}$-*b*-**P9**$_{133}$ and **P7**$_{34}$-*b*-**P9**$_{94}$ exhibit individual aggregation behaviors upon passing the second cloud point, which can be correlated to the different size ratios of their low and high LCST blocks. For both **P7**$_{137}$-*b*-**P9**$_{67}$ and **P7**$_{133}$-*b*-**P9**$_{133}$, the hydrodynamic diameter decreased above the second thermal transition. This reflects the shrinking PNEAM coronas due to the thermal collapse in both cases, compacting the micellar clusters or individual micelles, respectively. The formation of more compact aggre-

gates of **P7**$_{137}$-*b*-**P9**$_{67}$ and **P7**$_{133}$-*b*-**P9**$_{133}$ is further indicated by the simultaneous decrease of transmittance and aggregate size. Contrary to **P7**$_{137}$-*b*-**P9**$_{67}$ and **P7**$_{133}$-*b*-**P9**$_{133}$, D_h increased above the second thermal transition in the case of **P7**$_{34}$-*b*-**P9**$_{94}$. This indicates the temperature induced clustering of micelles into aggregates which show a very narrow PDI according to DLS. These marked differences in aggregation behavior must result from the variation in relative block lengths of the polymers and is in agreement with the self-organization observed for **P7**$_{103}$-*b*-**P8**$_{29}$ and **P9**$_{64}$-*b*-**P8**$_{20}$ which have compositions comparable to **P7**$_{137}$-*b*-**P9**$_{67}$ and **P7**$_{34}$-*b*-**P9**$_{94}$ and, hence, show similar aggregation behavior (compare Figure 25 and Figure 28). While it is well documented that the transition of thermosensitive double hydrophilic block copolymers from unimers to micellar aggregates is reversible,[2,254] reversibility of the second transition, which can lead to macroscopic phase separation, is not obvious. Therefore, the second thermally induced transition was investigated by repeated heating-cooling cycles in DLS (Figure 31). Figure 31a illustrates the reversible shrinking of the micellar clusters formed by **P7**$_{137}$-*b*-**P9**$_{67}$ when cooled back from 75°C to 50°C. Although a slight reduction of the aggregate size was found after the first cycle, the values of D_h remained fairly constant at around 170 nm (50°C) and 150 nm (75°C) in the following cycles. The slight differences in the D_h values found by DLS in the cycling experiments compared to the continuous heating studies are attributed to the somewhat different heating rates, which are known to effect the size of the formed aggregates.[125,218,239] Also for **P7**$_{133}$-*b*-**P9**$_{133}$, the decrease in D_h above the thermal transition of the PNEAM block was found to be reversible. Upon cooling the aqueous solutions of **P7**$_{133}$-*b*-**P9**$_{133}$ from 80°C back to 50°C the hydrodynamic diameter increased by 6 nm (from 90 nm to 96 nm) due to the rehydration of the PNEAM shell (Figure 31b). Again, the hydrodynamic diameter was slightly smaller than observed for the slow heating protocols. Figure 31c demonstrates the complete reversibility of the aggregate sizes of **P7**$_{34}$-*b*-**P9**$_{94}$, too, when changing from individual micelles to micellar clusters and back upon repeated heating and cooling between 45°C and 75°C. Remarkably, the rate of heating had almost no effect on both the formed micelles as well as the sizes of the formed clusters. The fast reversible clustering, especially the very fast fission of the micellar clusters of **P7**$_{34}$-*b*-**P9**$_{94}$ without any changes in D_h somewhat rules out bridging of micelles during the second transition since such a mechanism is expected to give rise to more broadly distributed aggregates and hysteresis.

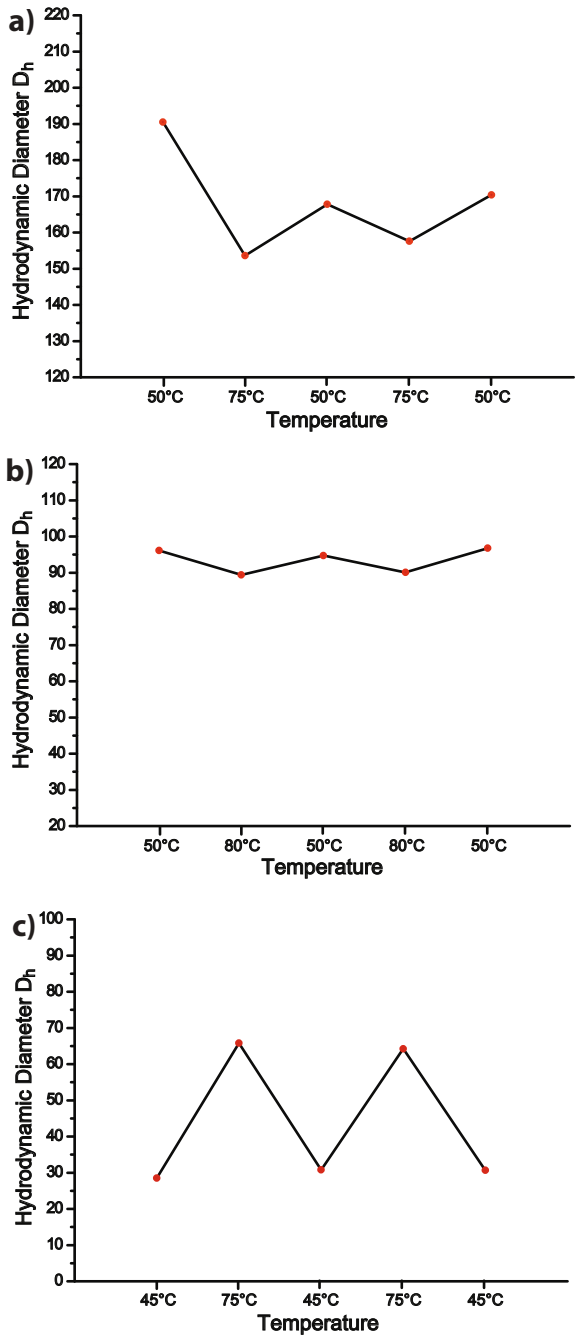

Figure 31: Cooling and heating cycles in dynamic light scattering showing the reversibility of the second thermally induced transition of a) **P7**$_{137}$-*b*-**P9**$_{67}$, b) **P7**$_{133}$-*b*-**P9**$_{133}$ and c) **P7**$_{34}$-*b*-**P9**$_{94}$.

The temperature dependent DLS and turbidity studies were complemented by temperature dependent ^{1}H NMR spectroscopy at concentrations of 10 g L^{-1} in D_2O (Figure 32). Most characteristically, the spectra showed the strong attenuation of the CH_3-signal at 0.8 ppm of the propyl moiety of the PNPAM block, when heating the aqueous solutions of **P7**$_{137}$-*b*-**P9**$_{67}$, **P7**$_{133}$-*b*-**P9**$_{133}$, and **P7**$_{34}$-*b*-**P9**$_{94}$ above the corresponding phase transition temperature.

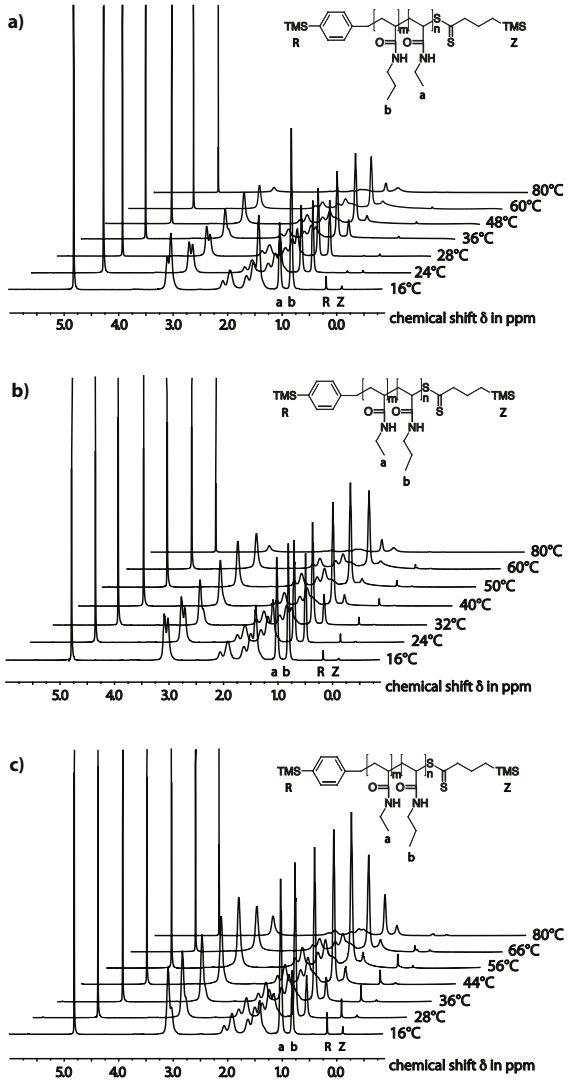

Figure 32: Temperature dependent ^{1}H-NMR spectra of a) **P7**$_{137}$-*b*-**P9**$_{67}$, b) **P7**$_{133}$-*b*-**P9**$_{133}$ and c) **P7**$_{34}$-*b*-**P9**$_{94}$ showing the CH_3-resonance of the PNPAM block at 0.8 ppm and the CH_3-resonance of the PNEAM block at 1.0 ppm.

This reflects the reduced mobility of these groups due to formation of PNPAM-core aggregates. In analogy, when heating above 60°C to induce the collapse of the PNEAM block, the intensity of the corresponding CH_3-signals at 1.0 ppm decreased in all three cases. The occurrence of two separate thermal transitions becomes particularly obvious, when comparing the relative evolution of the intensities of both CH_3-signals characteristic for the PNPAM and PNEAM blocks (Figure 33).

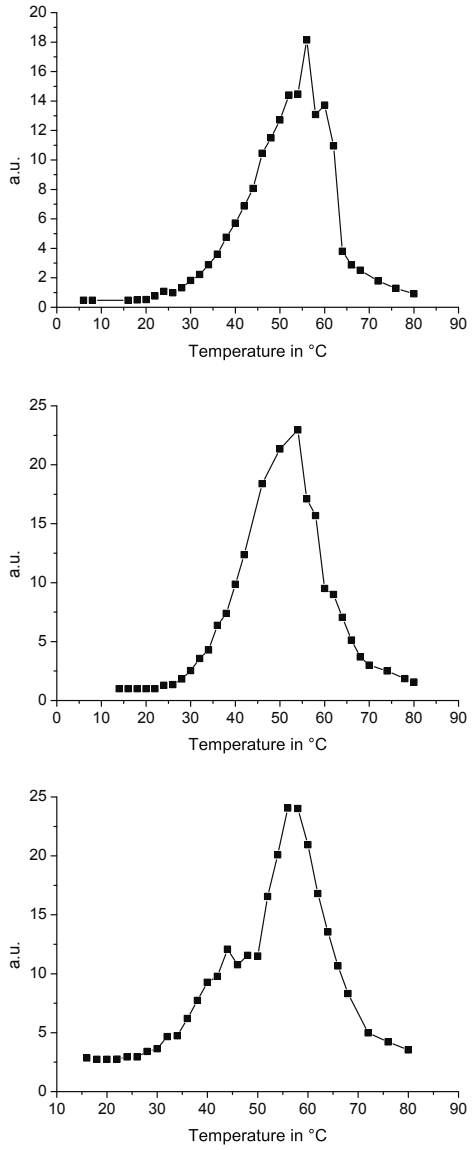

Figure 33: Ratio of the integrals of the signals of the methyl groups in the side chain of the PNEAM block compared to the ones of the PNPAM block, as a function of temperature for $\mathbf{P7}_{137}$-*b*-$\mathbf{P9}_{67}$ (top), $\mathbf{P7}_{133}$-*b*-$\mathbf{P9}_{133}$ (center) and $\mathbf{P7}_{34}$-*b*-$\mathbf{P9}_{94}$ (bottom).

Still, the attenuation of the PNEAM CH_3-signal was less pronounced in the case of copolymer $\mathbf{P7}_{34}$-*b*-$\mathbf{P9}_{94}$ when compared to $\mathbf{P7}_{137}$-*b*-$\mathbf{P9}_{67}$ and $\mathbf{P7}_{133}$-*b*-$\mathbf{P9}_{133}$. This finding suggests that the PNEAM block in copolymer $\mathbf{P7}_{34}$-*b*-$\mathbf{P9}_{94}$ is only partially collapsed in the temperature range studied, and might explain the stability of the observed clusters even at temperatures close to 90°C (*vide supra*). It should also be noted that the CH_3-signals of both blocks do not vanish instantly when passing the respective phase transition temperatures, but are gradually attenuated over a range of about 20°C (Figure 32 and 33). This observation

corroborates the findings of previous studies,[218,239] indicating the continuous dehydration of the collapsed polymer blocks over a considerable temperature range, instead of an instant (*all-or-none*) transition from dissolved random coils into a dehydrated collapsed state. Such a continuous dehydration process could also explain the intermediate maximum in D_h observed by passing the first phase transition temperature (see Figure 28). At the onset of (micro)phase separation of the collapsing block, the chains are still considerably hydrated, and only upon further heating, the water is increasingly expelled from the core of the aggregates.

The RAFT-agent used for the synthesis of the block copolymers contains a hydrophobic TMS-label on both the R- and the Z-group (Figure 27). Hence, the polymers are end-capped by two different hydrophobic groups that can be easily identified in ^{1}H NMR. Consequently, the two TMS-resonances might provide additional information about the temperature induced self-organization process of the copolymers. In polymer **P7**$_{137}$-*b*-**P9**$_{67}$, the aromatic end-group is fixed next to the PNPAM block, while the aliphatic end-group is placed at the end of the PNEAM block. Below the first cloud point, both signals are well visible in the NMR spectra when **P7**$_{137}$-*b*-**P9**$_{67}$ is dissolved in D_2O at concentrations of 10 g L^{-1} (Figure 34a). When the polymer solution is heated above the first cloud point to 24°C and further to 32°C, the aryl bound TMS-signal at 0.16 ppm gradually disappears and finally vanishes completely, revealing the formation of hydrophobic PNPAM domains. In contrast, the signal of the alkyl bound TMS-group, attached to the still water-soluble PNEAM block, at 0.13 ppm remains almost unchanged up to about 70°C. Further increase in temperature then also causes the attenuation of this peak in agreement with the collapse of the high-LCST block in this temperature range (Figure 34a). In contrast to the situation in **P7**$_{137}$-*b*-**P9**$_{67}$, the aromatic end group is located at the end of the PNEAM block for copolymers **P7**$_{133}$-*b*-**P9**$_{133}$ and **P7**$_{34}$-*b*-**P9**$_{94}$, while the aliphatic end group is now connected to the PNPAM block's end. Thus, the signal of the alkyl-bound TMS-group is increasingly attenuated upon heating above the first cloud point which causes the collapse of the PNPAM block, corroborating again the formation of micellar aggregates with a PNPAM-core and a PNEAM-corona in both cases (Figure 34b and c). Interestingly, a shoulder appears on the signals of the aryl-bound TMS-groups of **P7**$_{133}$-*b*-**P9**$_{133}$ and **P7**$_{34}$-*b*-**P9**$_{94}$ at 46°C and 40°C, respectively, which remains unchanged up to 60°C. Further heating until 80°C results in an increase of the shoulder, that finally two resolved peak maxima are observed (Figure 34b and c).

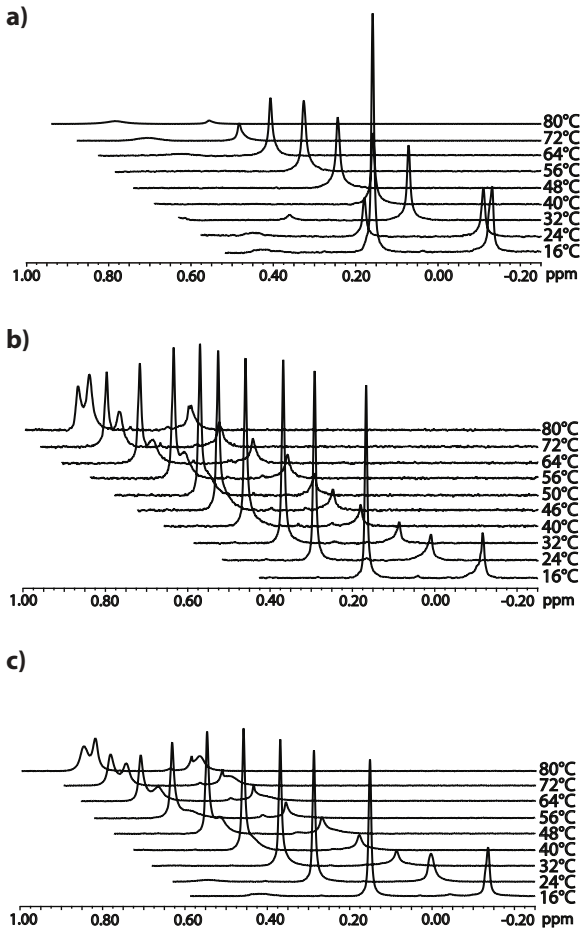

Figure 34: Temperature dependent ^{1}H-NMR measurements of a solution (10 g L^{-1}) of **P7**$_{137}$-*b*-**P9**$_{67}$ (a), **P7**$_{133}$-*b*-**P9**$_{133}$ (b) and **P7**$_{34}$-*b*-**P9**$_{94}$ (c) in D_2O. The signals at -0.15 ppm are the aliphatic TMS-resonances of the Z-group and the signals at 0.15 ppm are the aromatic TMS-resonances of the R-group.

This temperature induced peak splitting is completely reversible. In parallel, the complex signal is gradually attenuated above 60°C, i. e., above the second phase transition. Cooling the samples below 60°C, the relative intensity of the second peak is reduced to form the previously observed shoulder, and a singlet signal is reestablished when reaching 40°C. Thus, the aryl-bound TMS-signal at the end of the PNEAM-block is temperature sensitive and, consequently, this moiety participates in the self-assembly of **P7**$_{133}$-*b*-**P9**$_{133}$ and **P7**$_{34}$-*b*-**P9**$_{94}$. A normalized plot of the relative peak areas of the original aromatic TMS-signal R and the shoulder R' over temperature reveals that the peak splitting proceeds *via* two distinct steps for both **P7**$_{133}$-*b*-**P9**$_{133}$ and **P7**$_{34}$-*b*-**P9**$_{94}$ (Figure 35).

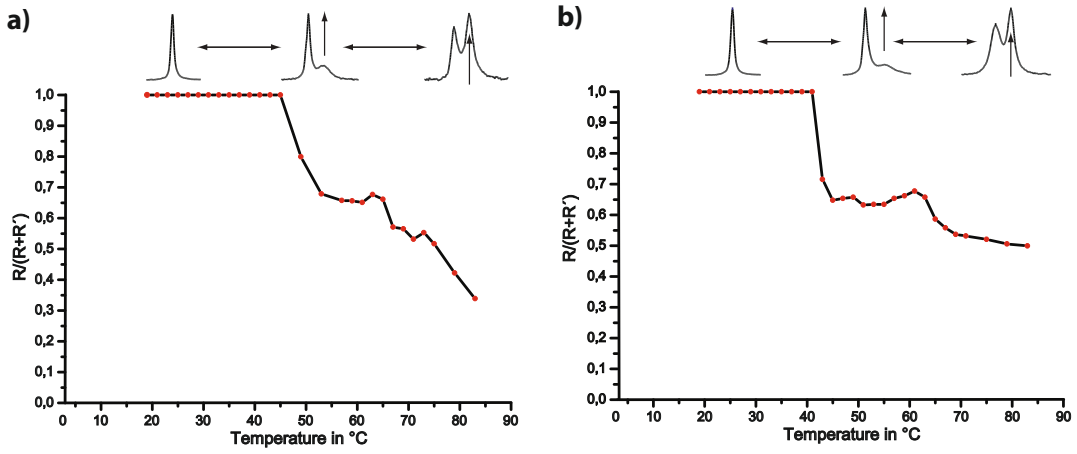

Figure 35: Plot of the normalized relative peak areas R/(R+R') over temperature of the aromatic TMS resonance in ^{1}H-NMR of **P7**$_{133}$-*b*-**P9**$_{133}$ (a) and **P7**$_{34}$-*b*-**P9**$_{94}$ (b). R represents the peak area of the original aromatic TMS resonance and R' the peak area of the shoulder which arose with temperature. The peak areas were obtained from MestReC by peak deconvolution.

The second step above 60°C is close to the collapse temperature of the PNEAM-corona, and suggests that the end groups get buried in the hydrophobic PNPAM-cores, as might be expected. Whether the aromatic end groups are also incorporated into adjacent cores to formed bridged clusters cannot be verified from the spectroscopic data obtained. In contrast, the appearance of the shoulder R' at 46°C and 40°C for **P7**$_{133}$-*b*-**P9**$_{133}$ and **P7**$_{34}$-*b*-**P9**$_{94}$, respectively, can on the first sight not directly be related to the thermal collapse of the PNPAM block, since it is shifted by more than 10°C to higher temperatures as compared to the collapse onset. However, the temperatures at which the shoulder appears are in good agreement with the temperature ranges in which the intermediate maxima of D_h seen in DLS level off and micellar aggregates with dense cores are formed (Figure 28b and c). Accordingly, the observed peak splitting can be attributed to the formation of micelles, in which the TMS-phenyl groups, fixed at the end of the water-soluble PNEAM block, partition between the micellar corona and the core. Hence, only a part of the TMS-groups remains to be located in the corona, while the rest enters into the hydrophobic micellar core. This implies that only a part of the PNEAM chains that are tethered at the surface of the hydrophobic cores has free dangling ends in the aqueous phase, while another part of the PNEAM chains folds back toward the core and, thus, describes a picture of an intermediate situation between a star and a flower-like micelle[255,256] (Scheme 11).

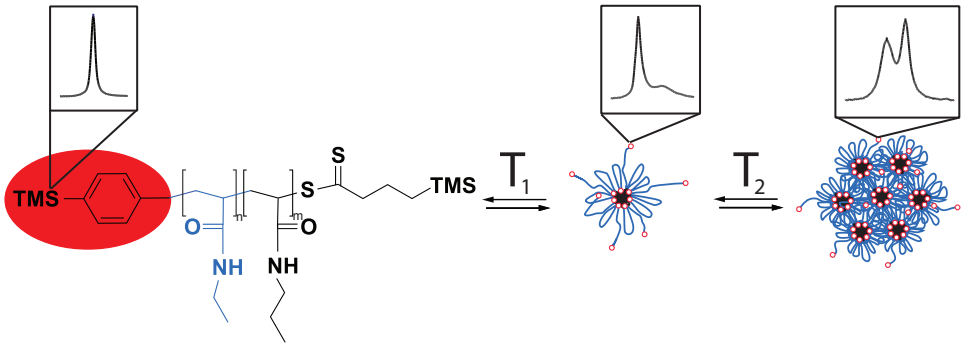

Scheme 11: Schematic representation of the formation of mixed star/flower-like micelles due to partial incorporation of the aromatic end groups into the hydrophobic core examplified on **P7**$_{34}$-*b*-**P9**$_{94}$.

With the partial collapse of the PNEAM-shell at high temperatures, the hydrophobic core grows which causes more hydrophobic TMS end groups to insert into the core, as indicated by the markedly increasing shoulder of the NMR signal. This temperature sensitive peak splitting, however, should not be confused with the observed peak splitting of the TMS$_R$ and TMS$_Z$ groups after polymerization of styrenes as described above. Here the changes of the peak pattern of the aromatic TMS-signal is a result of the temperature dependent aggregation process of the block copolymers. In order to verify the hypothesis of partial flower-like micelles, the evolution of the NMR signals of the aromatic protons of the TMS-phenyl end group of **P7**$_{34}$-*b*-**P9**$_{94}$ at 7-8 ppm was followed at different temperatures. The signals of the aromatic protons are markedly attenuated upon heating the solution of **P7**$_{34}$-*b*-**P9**$_{94}$ from 20°C to 55°C (Figure 36), indicating that the hydrophobic end groups are at least partially immobilized.

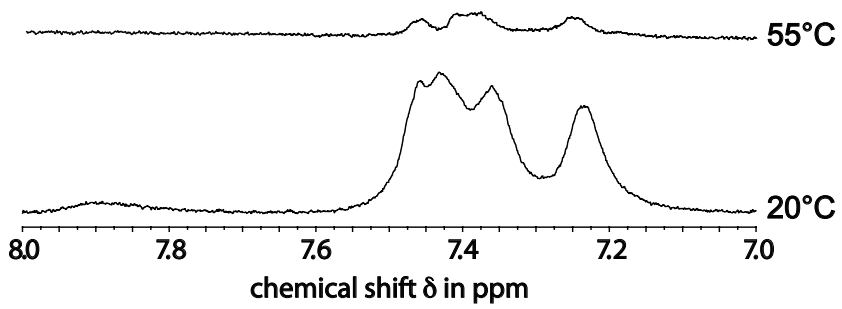

Figure 36: NMR spectra of the aromatic protons of the R-group of **P7**$_{34}$-*b*-**P9**$_{94}$ at 20°C and 55°C.

This effect strongly points to an attachment of a part of the aromatic end groups to the aggregates' hydrophobic cores, and supports a model of micelles with a mixed star-/flower-like structure in the temperature range between the first and the second thermal transition. A model of the self-assembly of the three double responsive diblock copolymers investigated is depicted in Scheme 12.

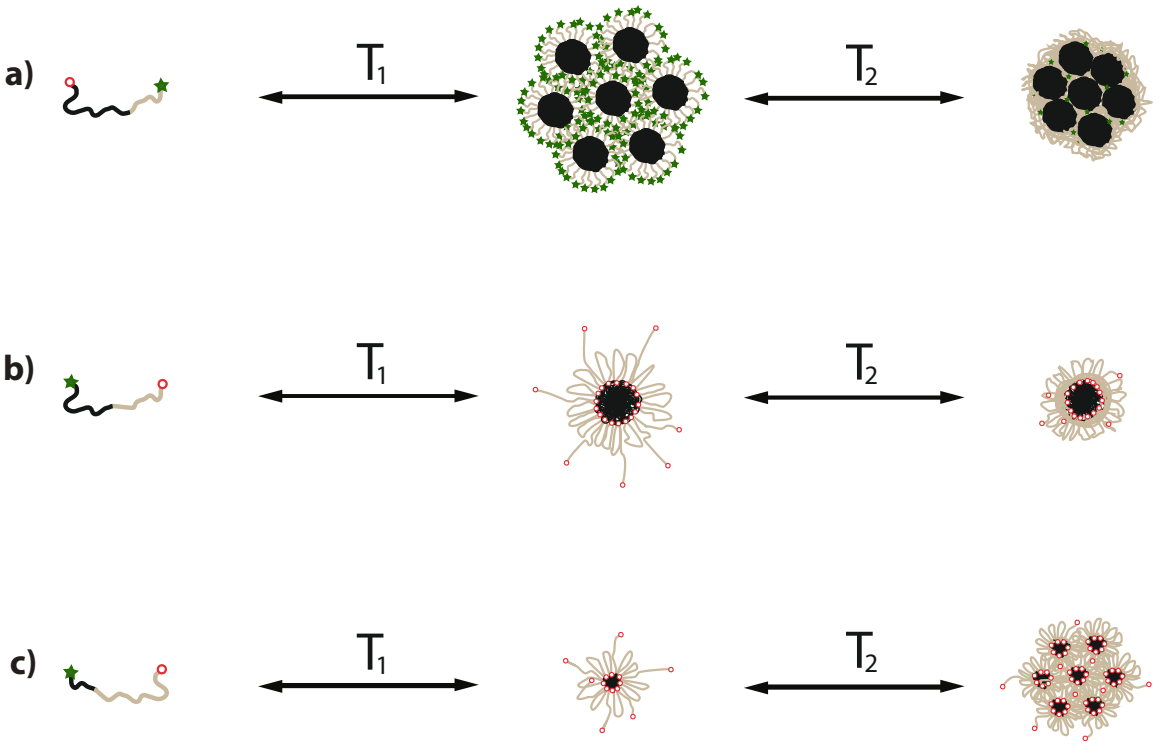

Scheme 12: Possible two-step self-assembling pathway of a) **P7**$_{137}$-*b*-**P9**$_{67}$, b) **P7**$_{133}$-*b*-**P9**$_{133}$, and c) **P7**$_{34}$-*b*-**P9**$_{94}$. The dark part represents the PNPAM block, the light gray part the PNEAM block and the red dots the aromatic TMS end group.

As the polymers **P7**$_{137}$-*b*-**P9**$_{67}$, **P7**$_{133}$-*b*-**P9**$_{133}$, and **P7**$_{34}$-*b*-**P9**$_{94}$ differ in the relative lengths of their blocks, they form different aggregates upon heating their aqueous solutions from 15°C to 90°C. **P7**$_{137}$-*b*-**P9**$_{67}$, i. e., the polymer with the longest PNPAM block, forms clusters of micelles above the first cloud point which show reversible dehydration when passing the second thermal transition (Scheme 12a). In **P7**$_{133}$-*b*-**P9**$_{133}$, the PNPAM and PNEAM blocks have the same length. **P7**$_{133}$-*b*-**P9**$_{133}$ aggregates into micelles with a mixed star-/flower-like structure, whose PNEAM-shell reversibly collapses at temperatures beyond the second thermal transition (Scheme 12b). **P7**$_{34}$-*b*-**P9**$_{94}$ contains the shortest PNPAM block and the relatively

longest PNEAM block in the studied series. Here again, a mixed star-/flower-like structure is formed above the cloud point of the PNPAM block. However, the second phase transition results in reversible clustering of the micelles into well-defined, stable, larger aggregates (Scheme 12c). Consequently, the self-organization behavior as well as the size of the formed aggregates can be influenced by varying the relative length of the blocks within double thermosensitive diblock copolymers. Moreover, the nature of the end group may influence the aggregate formation additionally.

3.3.3 Triple Thermoresponsive Triblock Copolymers

In order to increase the complexity of the step-wise aggregation behavior, triple thermoresponsive triblock copolymers in which each block exhibits its own, distinct LCST, were synthesized by sequential RAFT-polymerization using CTA **1**. Such block copolymers can be switched from a hydrophilic into a hydrophobic state by passing at least two intermediate states at which amphiphilic block copolymers are formed (Scheme 13). With increasing temperature the hydrophilic-to-lipophilic balance (HLB) can be varied step-wise which is expected to lead to a rich and dynamic aggregation behavior of such terpolymer systems. Thus, the first transition will transform a triple hydrophilic polymer into an amphiphilic one with low-HLB followed by a transition into an amphiphilic triblock copolymer with high-HLB. The last transition then will convert the terpolymer into a triple hydrophobic state.

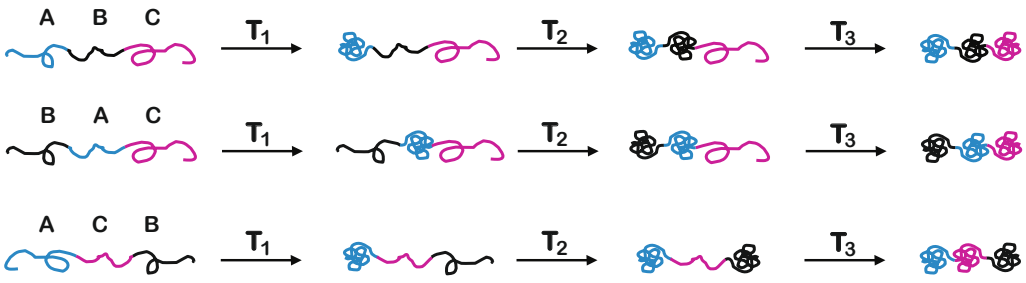

Scheme 13: Schematic representation of the sequential collapse of a triple thermosensitive terpolymer with different block sequence.

Triblock copolymers were synthesized in all possible block sequences, i.e., ABC, BAC and ACB bearing thermosensitive blocks from PNPAM (LCST about 22°C), poly(methoxydiethylene glycol acrylate) (LCST about 39°C) and PNEAM (LCST about 72°C).

$PNEAM_{90}$-*b*-$PMDEGA_{32}$-$PNPAM_{52}$ (**P9**$_{90}$-*b*-**P8**$_{32}$-*b*-**P7**$_{52}$ (CBA)), $PNEAM_{94}$-*b*-$PNPAM_{34}$-$PMDEGA_{52}$ (**P9**$_{94}$-*b*-**P7**$_{34}$-*b*-**P8**$_{54}$ (CAB)), and $PNPAM_{120}$-*b*-$PNEAM_{60}$-*b*-$PMDEGA_{13}$ (**P7**$_{120}$-*b*-**P9**$_{60}$-*b*-**P8**$_{13}$ (ACB)) were successfully prepared by sequential RAFT polymerization. Their structure and composition is given in Figure 37.

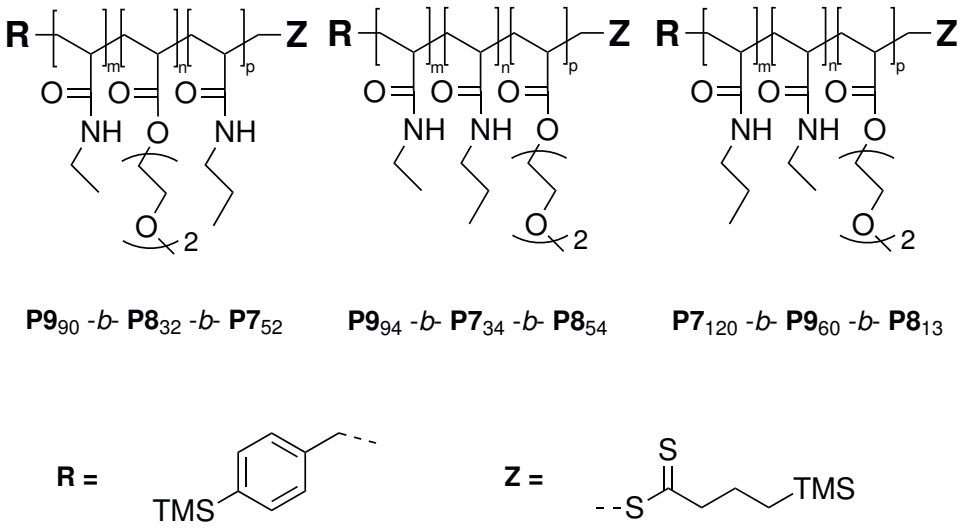

Figure 37: Structure of polymers **P9**$_{90}$-*b*-**P8**$_{32}$-*b*-**P7**$_{52}$, **P9**$_{94}$-*b*-**P7**$_{34}$-*b*-**P8**$_{54}$ and **P7**$_{120}$-*b*-**P9**$_{60}$-*b*-**P8**$_{13}$

With the use of the twofold TMS-labeled RAFT-agent CTA **1** the molar mass and end group functionality was determined directly from routine ^{1}H NMR spectroscopy throughout the subsequent polymerization steps. As for the diblock copolymers described above, monomers which show at least one distinct signal in ^{1}H NMR spectroscopy were chosen in order to ensure reliable molar mass determination. Accordingly, the PNPAM block displays a characteristic signal at 0.8 ppm for the CH_3-group in the propyl side chain, the PNEAM block shows the analogous signal of the ethyl side chain at 1.0 ppm, and the PMDEGA block exhibits a characteristic signal at 4.2 ppm of the $COOCH_2$-methylenes of the ester functionality. Comparative integration of the aryl bound TMS_R signal at about 0.2 ppm and of these three peaks provided average molar masses and polymer compositions as listed in Table 3.3. The values obtained from NMR spectroscopy and SEC analysis are in good agreement for the homopolymers **P9**$_{90}$, **P9**$_{94}$ and **P7**$_{120}$ and partially for the diblock copolymers while deviations were observed especially for the final triblock copolymers which may be explained by the calibration with linear polystyrene standards. Moreover, the use of two different monomer classes, namely acrylamides and acrylates, within one block copolymer may cause additional inaccuracies during SEC analysis.

Table 3.3: Synthesis data of **P9**$_{90}$-*b*-**P8**$_{32}$-*b*-**P7**$_{52}$, **P9**$_{94}$-*b*-**P7**$_{34}$-*b*-**P8**$_{54}$ and **P7**$_{120}$-*b*-**P9**$_{60}$-*b*-**P8**$_{13}$. All polymerizations were carried out in dry THF.

Polymer	CTA	Time	yield[a]	M_n[b]	Z/R	M_n[c]	PDI	DP
P9$_{90}$	**1**	5	50	9300	0.7	9400	1.48	90
P9$_{94}$	**1**	5.5	55	9700	0.9	10000	1.32	94
P7$_{120}$	**1**	5	63	13500	0.7	11700	1.41	120
P9$_{90}$-*b*-**P8**$_{32}$	**P9**$_{90}$	6	22	14900	0.4	14800	1.24	32
P9$_{94}$-*b*-**P7**$_{34}$	**P9**$_{94}$	4	81	13200	0.6	12800	1.44	34
P7$_{120}$-*b*-**P9**$_{60}$	**P7**$_{120}$	4	75	19500	0.5	14400	1.58	60
P9$_{90}$-*b*-**P8**$_{32}$-*b*-**P7**$_{52}$	**P9**$_{90}$-*b*-**P8**$_{32}$	16	34	20700	0.1	15300	1.24	52
P9$_{94}$-*b*-**P7**$_{34}$-*b*-**P8**$_{54}$	**P9**$_{94}$-*b*-**P7**$_{34}$	20	49	22600	0.1	11000	1.47	54
P7$_{120}$-*b*-**P9**$_{60}$-*b*-**P8**$_{13}$	**P7**$_{120}$-*b*-**P9**$_{60}$	24	41	24400	0.1	18000	1.43	13

[a]Yield in % and determined gravimetrically. [b] Calculated molar mass from ^{1}H NMR spectroscopy by integration or the TMS_R peak against a peak of the polymer (end group analysis). [c] Determined by size exclusion chromatography (SEC).

The TMS-labeled end groups revealed the increasing loss of active chain ends with the number of polymerization steps by ^{1}H NMR spectroscopy. While the homopolymers have an end group functionality of about 90%, roughly 50% of remaining Z-group was found after the second polymerization step. The final third polymerization step then led to a second drop to about 10%, to some extend also caused by the prolonged polymerization times of up to 24 h. However, detailed investigations indicated that the use of THF as solvent should be avoided when possible since such a loss of end group functionality was not observed when polymerizations of styrene were carried out in benzene or ethylacetate.[235]

An effective separation of homopolymers and diblock copolymers did not succeed before starting the third polymerization step. Therefore, the polymerization was continued toward the desired triblock copolymers and the reaction mixture was then purified by dialysis at 0°C using a membrane with a nominal cut off of 14.000-16.000 g mol^{-1}, well below the molar masses of the triblock copolymers. Hence, only homo- and diblock impurities are removed

from the reaction mixture. Indeed, the amounts of isolated triblock copolymer after dialysis corresponded well with the residual end group functionality (Z/R) of the diblock macroRAFT agents used, suggesting successful purification of the triblock copolymers (Table 3.4). In fact, the Z/R ratio of the macro RAFT agent inherently determines the maximum yield of triblock copolymers after the third polymerization step, as inactive chain ends cannot initiate a polymerization and, thus, lead to homopolymer and diblock copolymer impurities in the final product. Changes in the relative compositions within values obtained from NMR spectroscopy before and after dialysis additionally suggested removal of non-triblock copolymers (Table 3.4).

Table 3.4: Purification of **P9**$_{90}$-*b*-**P8**$_{32}$-*b*-**P7**$_{52}$ (CBA), **P9**$_{94}$-*b*-**P7**$_{34}$-*b*-**P8**$_{54}$ (CAB) and **P7**$_{120}$-*b*-**P9**$_{60}$-*b*-**P8**$_{13}$ (ACB) by dialysis at 0°C using a membrane with a cut off of 14.000-16.000 g mol^{-1} (A = PNPAM; B = PMDEGA; C = PNEAM).

Polymer	average composition according to ^{1}H NMR before dialysis	Z/R ratio of the diblock precursors	amount of polymer recovered after dialysis [%]	average composition according to ^{1}H NMR after dialysis
CBA	C_{90}-B_{27}-A_{47}	0.4	35	C_{90}-B_{32}-A_{52}
CAB	C_{90}-A_{29}-B_{47}	0.6	51	C_{94}-A_{34}-B_{54}
ACB	A_{122}-C_{49}-B_{11}	0.5	51	A_{120}-C_{60}-B_{13}

The integral of the first block was normalized in order to determine the changes in the integration before and after dialysis.

The temperature dependent aggregation behavior of the triblock copolymers **P9**$_{90}$-*b*-**P8**$_{32}$-*b*-**P7**$_{52}$, **P9**$_{94}$-*b*-**P7**$_{34}$-*b*-**P8**$_{54}$ and **P7**$_{120}$-*b*-**P9**$_{60}$-*b*-**P8**$_{13}$ was studied by a combination of turbidity and dynamic light scattering measurements in dilute aqueous solution at concentrations of 1.0 g mol^{-1}. Polymer **P9**$_{90}$-*b*-**P8**$_{32}$-*b*-**P7**$_{52}$, with an CBA block sequence, formed aggregates with a hydrodynamic diameter of 280 nm accompanied with a drastic drop in

transmittance above 22°C (Figure 38a). This phase transition temperature corresponds very well with the thermal collapse of the PNPAM (A) block. When heated further, a slight gradual decrease of D_h from 280 nm to 260 nm was observed between 30°C and 50°C, presumably due to ongoing dehydration of the PNPAM core. Simultaneously, the turbidity curve leveled off to reach a plateau value within this temperature range. Upon heating beyond 50°C, both the transmittance and the hydrodynamic diameter showed a second drop caused by the thermal collapse of the mid-LCST block PMDEGA which led to a shrinkage of the aggregates to about 200 nm. While the transmittance constantly decreased with increasing temperature, a third transition became visible in DLS measurements at 78°C, as indicated by a sudden increase of D_h by 25 nm to 225 nm. Although in increase of D_h by 25 nm may seem relatively small on the first sight, it reflects an increase of the particle volume by more than 40%.

The observed increase in D_h after the collapse of the PNEAM block is comparable to results reported on analogously built ABC copolymers by Zhu *et al.* [170] The authors argued that micellar clustering occurs, if the hydrated shell/corona is too short in comparison to the dehydrated core. In this case the collapse of the shell forming PNEAM block seems to induce further clustering, too. In contrast, for polymer **P9**$_{94}$-*b*-**P7**$_{34}$-*b*-**P8**$_{54}$ representing the CAB sequence with the low-LCST block PNPAM placed in the middle of the triblock copolymer, no aggregation could be observed below 38°C (Figure 38b). This finding is in line with studies by Tirrell *et al.* , reporting that amphiphilic BAB triblock copolymers with the hydrophobic B block in the center do not show aggregation if the length of the terminal, hydrophilic B blocks exceeds the length of the hydrophobic A block.[159] After passing the first cloud point of the PNPAM block, **P9**$_{94}$-*b*-**P7**$_{34}$-*b*-**P8**$_{54}$ is switched into a system similar to the aforementioned BAB block copolymers and, hence, may behave similar in dilute solution. In fact, **P9**$_{94}$-*b*-**P7**$_{34}$-*b*-**P8**$_{54}$ showed aggregation only at 38°C and above. At these relatively high temperatures, at which the thermal collapse of the PMDEGA block is expected, micellar aggregates with a D_h of 24 nm as well as clusters (D_h 160 nm) were found (38°C-46°C). Further heating enforced the clustering into particles of about 400 nm, which finally suffered a third increase of D_h to 430 nm above 68°C, which can be attributed to the collapse of the PNEAM shell. Again, this increase in D_h by 30 nm appears small but reflects an increase in particle volume of more than 24%. The turbidity curve for **P9**$_{94}$-*b*-**P7**$_{34}$-*b*-**P8**$_{54}$ showed a continuous decrease from about 43°C on displaying only one of the transition steps.

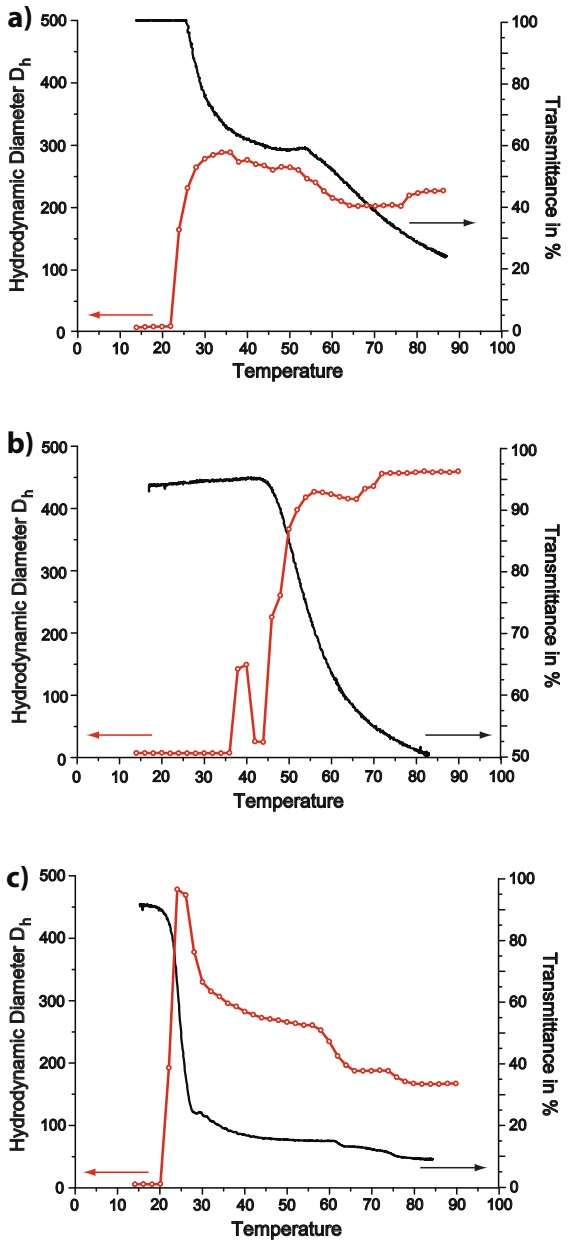

Figure 38: Dynamic light scattering and turbidity measurements of **P9**$_{90}$-*b*-**P8**$_{32}$-*b*-**P7**$_{52}$, **P9**$_{94}$-*b*-**P7**$_{34}$-*b*-**P8**$_{54}$ and **P7**$_{120}$-*b*-**P9**$_{60}$-*b*-**P8**$_{13}$ in aqueous solution at concentrations of 1 g L^{-1}.

The aggregation into particles of 400 nm due to the collapse of the PMDEGA block causes a drop in transmittance to 0% which does not allow further investigation of the polymer solution at higher temperatures by this measurement technique. Copolymer **P7**$_{120}$-*b*-**P9**$_{60}$-*b*-**P8**$_{13}$ of the CAB type, i. e., bearing the high-LCST (C) block in the center, showed a first temperature induced transition above 20°C in both DLS and turbidity measurements, due to the collapse of the PNPAM block (Figure 38c). After passing through an initial maximum, the

DLS curve leveled off and aggregates of 270 nm were observed. At about 60°C, turbidimety as well as DLS showed a decrease in transmittance and in D_h to 190 nm, respectively. These changes are attributed to a second phase transition, namely of the PMDEGA block. Upon increasing the temperature further, a third transition became visible at 76°C, which can be correlated to the collapse of the PNEAM block (C). This third transition led to another decrease of particle size from 190 nm to 167 nm. These different self-organization behaviors demonstrate that the block sequence has a major effect on the step-wise aggregation of such triple thermo-responsive triblock copolymers.

In order to gain more insight into the complex thermally induced aggregation behavior of copolymers **P9**$_{90}$-*b*-**P8**$_{32}$-*b*-**P7**$_{52}$, **P9**$_{94}$-*b*-**P7**$_{34}$-*b*-**P8**$_{54}$ and **P7**$_{120}$-*b*-**P9**$_{60}$-*b*-**P8**$_{13}$ on the molecular level, temperature dependent ^{1}H NMR studies were performed (Figure 39). The temperature induced desolvation of a given polymer block can be detected by comparing the relative peak integrals at 0.8 ppm of the methyl group in the propyl side chain as characteristic signal for the PNPAM block (A), the peak at 4.2 ppm of the $COOCH_2$ methylene group for the PMDEGA block (B), and the peak at 1.0 ppm of the methyl group in the ethyl side chain for the PNEAM block (C), as these signals can be distinctively resolved in the ^{1}H NMR spectrum. For all polymers studied, the consecutive attenuation of the NMR signals with increasing temperature was observed in the expected order A < B < C, i. e., from the low *via* the medium to the high LCST block (Figures 39 and 40). Individual differences become visible when looking at the changes in more detail. In the case of **P9**$_{90}$-*b*-**P8**$_{32}$-*b*-**P7**$_{52}$ with the block sequence CBA, the intensity of the methyl signal of the PNPAM block starts to decrease at 23°C (Figure 39a), indicating the collapse of the A domains accompanied with a decrease of the intensity of the signal at 1.4 ppm, having a strong contribution from the PNPAM block. The attenuation of the signals increases continuously with increasing temperature, but small residual signals are still visible even at 80°C. With increasing temperature, the water peak inevitably shifted[257,258] into the $COOCH_2$ resonance of the PMDEGA block. However, the decrease in signal intensity above 40°C for the signal at 3.2 ppm, representative for the CH_3O groups of PMDEGA, is still evident (Figure 39b). Likewise, the signal intensity of the methylene protons of the diethylene glycol side chains at 2.9 ppm decreased. The intensity losses for these three peaks reflect the collapse of the PMDEGA block above 50°C. As observed for the PNPAM block, the signals attenuated gradually with further increasing temperature.

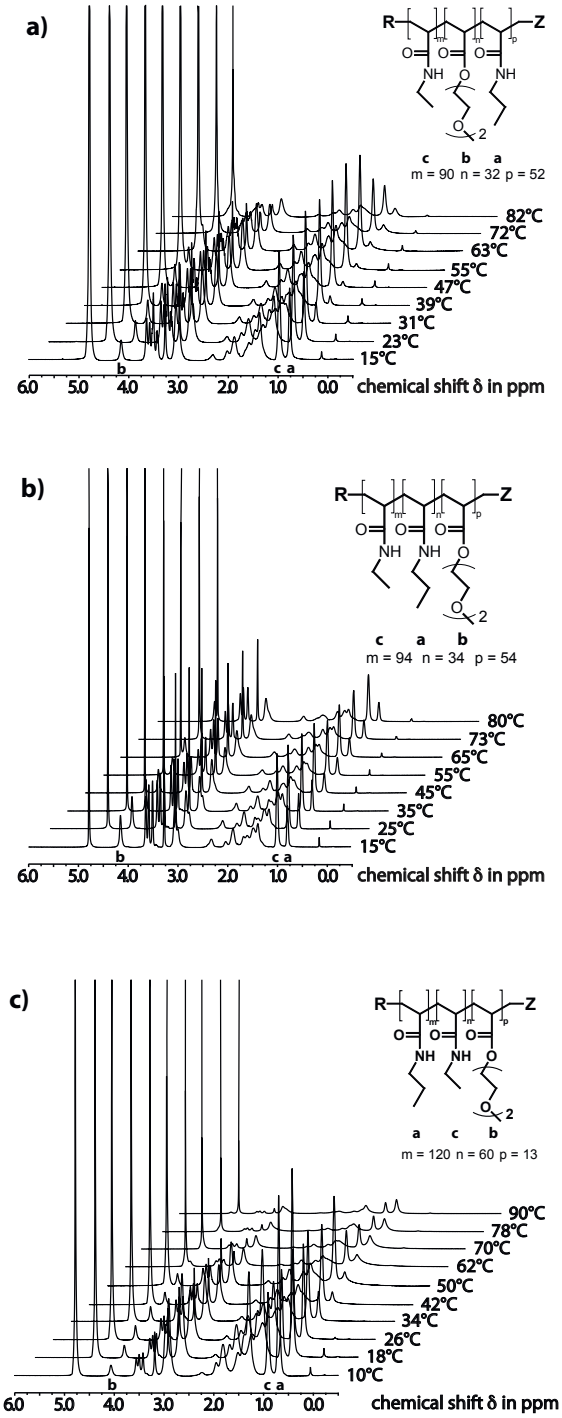

Figure 39: Temperature dependent ^{1}H NMR spectra of **P9**$_{90}$-*b*-**P8**$_{32}$-*b*-**P7**$_{52}$, **P9**$_{94}$-*b*-**P7**$_{34}$-*b*-**P8**$_{54}$ and **P7**$_{120}$-*b*-**P9**$_{60}$-*b*-**P8**$_{13}$ in D_2O at a concentration of 10 g L^{-1}.

Upon heating above 55°C, the relative signal intensity of the methyl group corresponding to the PNEAM block starts to decrease in comparison to the characteristic peaks of both PNPAM and PMDEGA blocks (Figure 40a,b). Thus, the turning points indicate the onset of the

collapse of the third block. In the case of **P9**$_{94}$-*b*-**P7**$_{34}$-*b*-**P8**$_{54}$ with the block sequence CAB, the onset of the attenuation of the PNPAM signals is observed at 25°C, while the signals of the PMDEGA block start to decrease at about 40°C, and the signals of the PNEAM block at about 55-60°C (Figure 40c,d). However, the changes are less pronounced than for **P9**$_{90}$-*b*-**P8**$_{32}$-*b*-**P7**$_{52}$. The relatively high remaining signal intensity even at high temperatures might point to a relatively high water content in the formed aggregates. For **P7**$_{120}$-*b*-**P9**$_{60}$-*b*-**P8**$_{13}$ with the block sequence ACB, the PNPAM signal intensities start to decrease at 22°C, whereas the signals of the PMDEGA block are attenuated above about 40°C, and the signals of the PNEAM block above 50-55°C (Figure 40e,f). The temperature dependent NMR spectra demonstrate that all terblock copolymers under investigation undergo indeed three successive phase transitions of the individual blocks A, B and C with low, medium and high LCST. Interestingly, a correlation between the cloud point temperatures obtained from ^{1}H NMR data on the one hand with turbidity changes and the onset of aggregation according to DLS measurements on the other hand is not always straightforward. However, these discrepancies cannot be explained by the known differences between phase transition temperatures in H_2O and D_2O, as these are small.[246,259] Whereas in the case of copolymers **P9**$_{90}$-*b*-**P8**$_{32}$-*b*-**P7**$_{52}$ and **P7**$_{120}$-*b*-**P9**$_{60}$-*b*-**P8**$_{13}$ with the block sequences CBA and ACB, the transition temperatures seen by the different methods coincide reasonably well, the NMR studies reveal an additional low temperature transition of the PNPAM block for **P9**$_{94}$-*b*-**P7**$_{34}$-*b*-**P8**$_{54}$ (CAB). This transition is not visible in turbidimetry or DLS. However, the two transitions found for **P9**$_{94}$-*b*-**P7**$_{34}$-*b*-**P8**$_{54}$ by the latter methods (Figure 38b) may be correlated with the collapses of the PMDEGA and the PNEAM blocks. ^{1}H NMR spectroscopy provides additional information about the thermally induced aggregation of the polymers by virtue of the TMS end groups introduced into the polymers *via* the RAFT agent. Due to the partial loss of Z-groups throughout the subsequent polymerization steps, only the TMS$_R$ signal was useful in order to obtain further information about the temperature induced aggregation processes of **P9**$_{90}$-*b*-**P8**$_{32}$-*b*-**P7**$_{52}$, **P9**$_{94}$-*b*-**P7**$_{34}$-*b*-**P8**$_{54}$ and **P7**$_{120}$-*b*-**P9**$_{60}$-*b*-**P8**$_{13}$. In polymers **P9**$_{90}$-*b*-**P8**$_{32}$-*b*-**P7**$_{52}$ and **P9**$_{94}$-*b*-**P7**$_{34}$-*b*-**P8**$_{54}$, the TMS moiety originating from the R-group is located at the PNEAM chain end, i. e., the block with the highest LCST, whereas in **P7**$_{120}$-*b*-**P9**$_{60}$-*b*-**P8**$_{13}$, the TMS$_R$ group is attached to the PNPAM chain end, i. e., at the block with the lowest LCST. For **P7**$_{120}$-*b*-**P9**$_{60}$-*b*-**P8**$_{13}$ indeed, the TMS$_R$ resonance showed a strong attenuation above 18°C and completely vanished above 26°C, revealing the formation of hydrophobic PNPAM domains (Figure 41c).

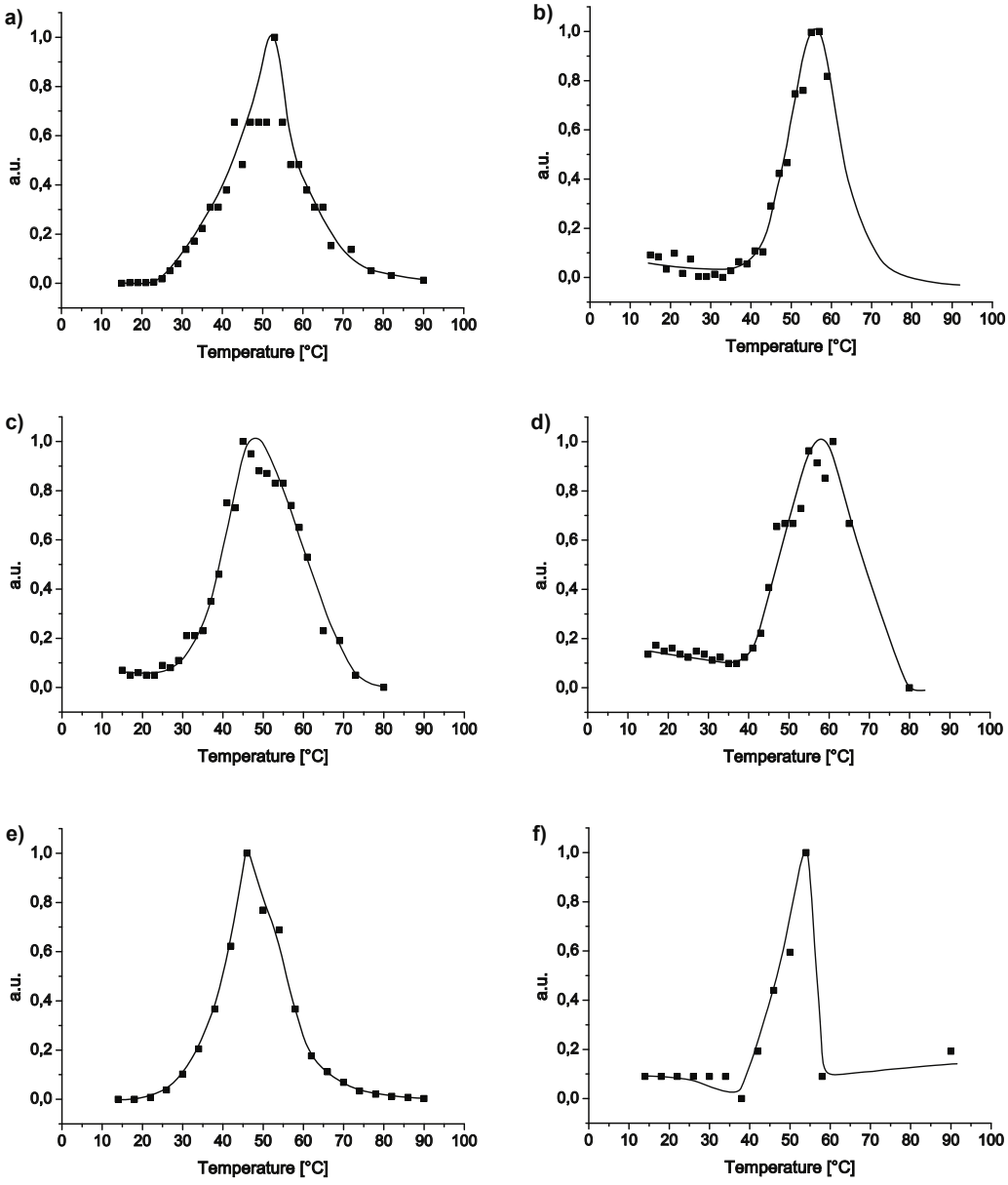

Figure 40: Ratio of the integrals of the signals of the methyl groups and the methylene group in the side chain of the PNEAM block compared to the ones of the PNPAM block (left column) and the PMDEGA block (right column), as function of the temperature for **P9**$_{90}$-*b*-**P8**$_{32}$-*b*-**P7**$_{52}$ (a,b), **P9**$_{94}$-*b*-**P7**$_{34}$-*b*-**P8**$_{54}$ (c,d), and **P7**$_{120}$-*b*-**P9**$_{60}$-*b*-**P8**$_{13}$ (e,f).

For polymers **P9**$_{90}$-*b*-**P8**$_{32}$-*b*-**P7**$_{52}$ and **P9**$_{94}$-*b*-**P7**$_{34}$-*b*-**P8**$_{54}$, the situation is more complex. In the case of **P9**$_{94}$-*b*-**P7**$_{34}$-*b*-**P8**$_{54}$ (sequence CAB), the TMS$_R$ signal remained unchanged until a small shoulder on the right flank appeared at 65°C (Figure 41b). With increasing temperature a peak with two maxima and finally a signal with a shoulder on the left flank

evolved. A similar peak splitting behavior was observed for the double thermoresponsive diblock copolymers (*vide supra*) and attributed to the incorporation of the hydrophobic end group into the hydrophobic core of micellar aggregates. For polymer **P9**$_{90}$-*b*-**P8**$_{32}$-*b*-**P7**$_{52}$ with block sequence CBA (Figure 41a) the TMS$_R$ peak remained unchanged until a decrease in signal intensity is observed above 63°C, indicating the collapse of the PNEAM corona.

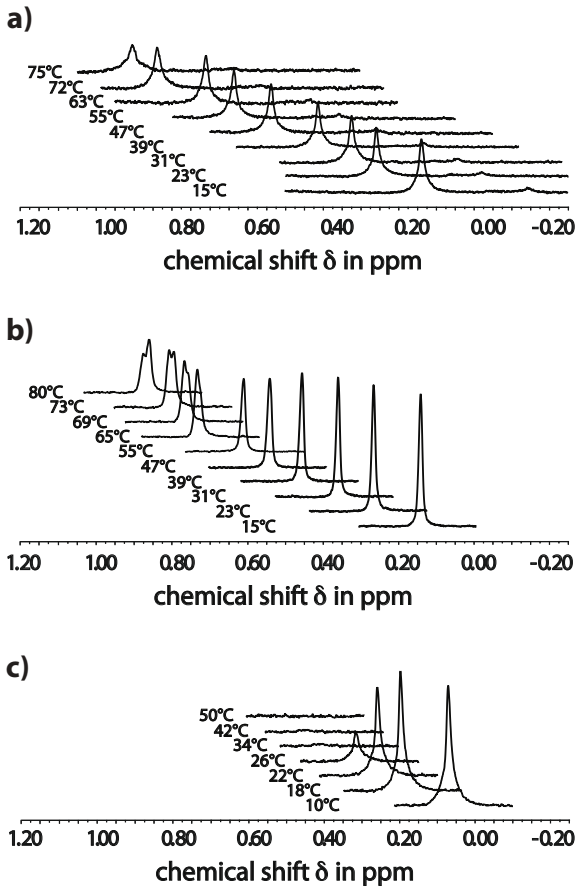

Figure 41: Temperature dependent ^{1}H NMR spectra of the TMS end groups of **P9**$_{90}$-*b*-**P8**$_{32}$-*b*-**P7**$_{52}$, **P9**$_{94}$-*b*-**P7**$_{34}$-*b*-**P8**$_{54}$ and **P7**$_{120}$-*b*-**P9**$_{60}$-*b*-**P8**$_{13}$ in D_2O at a concentration of 10 g L^{-1}.

In order to obtain more information about the thermally induced self-assembly process of these triple responsive terpolymers the fluorescence probe Nile Red was dissolved together with polymers **P9**$_{90}$-*b*-**P8**$_{32}$-*b*-**P7**$_{52}$, **P9**$_{94}$-*b*-**P7**$_{34}$-*b*-**P8**$_{54}$ and **P7**$_{120}$-*b*-**P9**$_{60}$-*b*-**P8**$_{13}$ in water (0.1 g L^{-1}) and studied in temperature dependent fluorescence spectroscopy. The spectral properties of Nile Red are sensitive to the polarity of its environment, and therefore, the dye is suited to detect the presence of hydrophobic domains.[260–262] When incorporated into hydrophobic domains of, e. g., polymer aggregates in water, the emission intensity typically

increases and the emission maximum shifts to smaller wavelengths. The shift of the emission maximum is attributed to changes in the excited state dipole moment, resulting from polarity-sensitive twisted intramolecular charge transfer (TICT) processes.[262,263] Control experiments of Nile Red in pure water, DMF and triethylene glycol dimethylether demonstrated that the emission maximum remained virtually unchanged between 20°C and 80°C at about 660 nm, 626 nm, and 608 nm, respectively (Figure 42). The emission intensity, however, increased with increasing temperature in pure water notably above 50°C, while it did not change when Nile Red was heated in DMF or triethylene glycol dimethylether solutions from 20°C to 80°C. Figure 43 illustrates the evolution of fluorescence intensity and emission maxima (λ_{max}) of Nile Red in the copolymer solutions with increasing temperature. Upon heating solutions of **P9**$_{90}$-*b*-**P8**$_{32}$-*b*-**P7**$_{52}$ and **P7**$_{120}$-*b*-**P9**$_{60}$-*b*-**P8**$_{13}$, the fluorescence emission increased markedly from 22°C to 54°C and 58°C, respectively (Figure 43a,c), where it reached a maximum. Further heating then in both cases led to a gradual decrease of emission intensity until 80°C. The onset temperature at 22°C agrees well with the collapse of the PNPAM block and the observed aggregation of **P9**$_{90}$-*b*-**P8**$_{32}$-*b*-**P7**$_{52}$ and **P7**$_{120}$-*b*-**P9**$_{60}$-*b*-**P8**$_{13}$ in DLS, thus, reflects the incorporation of Nile Red into the polymer aggregates formed. The observed decrease of emission intensity above 54°C (**P9**$_{90}$-*b*-**P8**$_{32}$-*b*-**P7**$_{52}$) and 58°C (**P7**$_{120}$-*b*-**P9**$_{60}$-*b*-**P8**$_{13}$), the temperatures at which the collapse of the PMDEGA block is observed, suggests that the solubilized probe Nile Red partitions between the more hydrophobic PNPAM cores and the additionally formed domains of collapsed PMDEGA that are somewhat less hydrophobic. In contrast, heating solutions of **P9**$_{94}$-*b*-**P7**$_{34}$-*b*-**P8**$_{54}$ resulted first in a slight and gradual increase of the emission intensity above 22°C, implying that small amounts of Nile Red are incorporated into the collapsed PNPAM middle blocks. Further heating led to a marked jump in emission intensity at 45°C. At this temperature, the PMDEGA block collapses and aggregation of **P9**$_{94}$-*b*-**P7**$_{34}$-*b*-**P8**$_{54}$ is observed in DLS. Hence, the evolution of the fluorescence intensity with temperature corroborates the picture that the initial collapse of the central A block results in the formation of unimolecular micelles. The increase of fluorescence intensity at about 22°C for the solutions of **P9**$_{90}$-*b*-**P8**$_{32}$-*b*-**P7**$_{52}$ and **P7**$_{120}$-*b*-**P9**$_{60}$-*b*-**P8**$_{13}$ is accompanied by a sudden hypsochromic shift of the emission maxima by about 9 nm (Figure 43a) and 20 nm (Figure 43c), respectively.

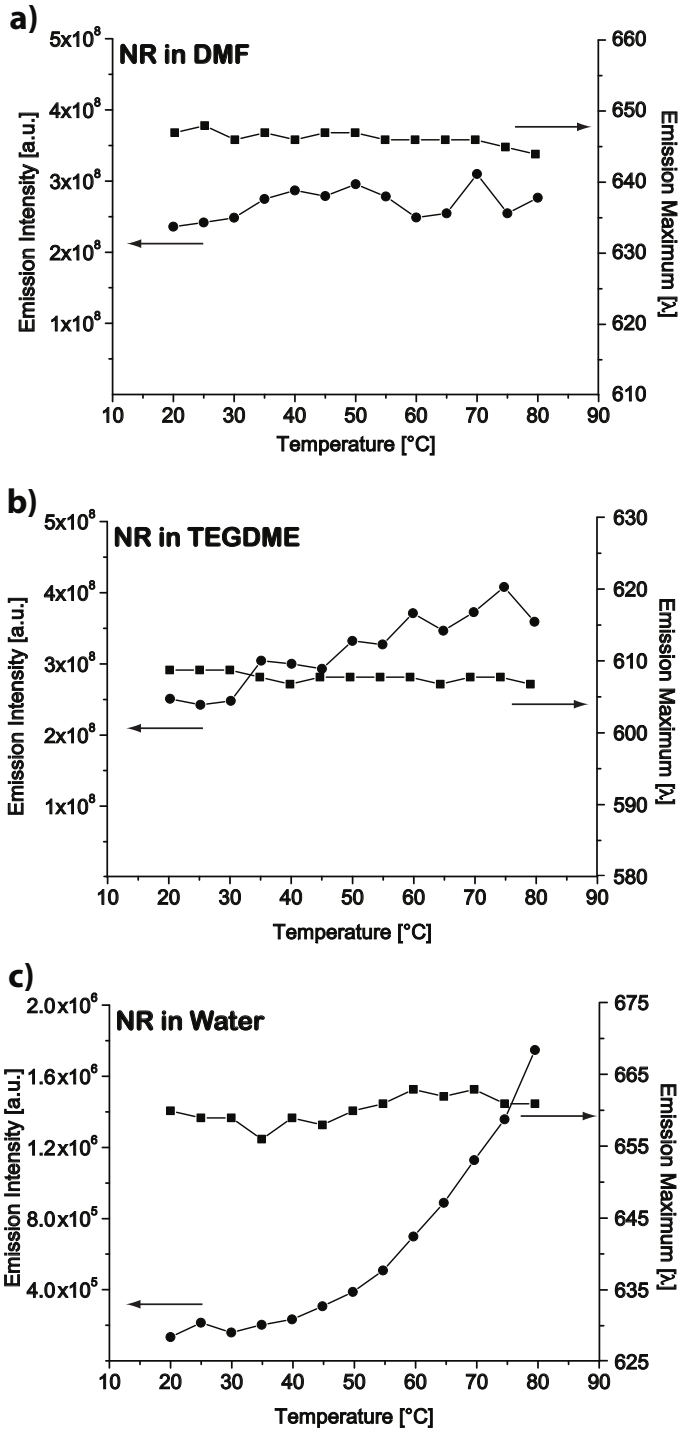

Figure 42: Fluorescence emission intensities (•) and maxia (■) of Nile Red in a) DMF, b) triethyleneglycol dimethylether, and c) distilled water.

The difference in the observed absolute hypsochromic shifts for **P9**$_{90}$-*b*-**P8**$_{32}$-*b*-**P7**$_{52}$ and **P7**$_{120}$-*b*-**P9**$_{60}$-*b*-**P8**$_{13}$ may be explained by the larger PNPAM blocks in **P7**$_{120}$-*b*-**P9**$_{60}$-*b*-**P8**$_{13}$, which can form larger and less hydrated aggregate cores and, therefore, provide a less polar

environment for Nile Red than the aggregates formed by **P9**$_{90}$-*b*-**P8**$_{32}$-*b*-**P7**$_{52}$. The emission maximum of Nile Red in solutions of **P7**$_{120}$-*b*-**P9**$_{60}$-*b*-**P8**$_{13}$ apparently increases slightly but continuously above 50°C, an effect which may point to a partitioning of the probe between the collapsed A and B blocks as already indicated by the intensity maximum occurring at about 55°C. For solutions of **P9**$_{90}$-*b*-**P8**$_{32}$-*b*-**P7**$_{52}$, no such shift above the collapse temperature of the second block is observed, but as the overall spectral shift is much smaller than for **P7**$_{120}$-*b*-**P9**$_{60}$-*b*-**P8**$_{13}$, one cannot decide whether the absence of an analogous bathochromic shift above the collapse of the B block is merely caused by a lack of spectral resolution. In contrast to the other copolymers, the emission maximum of solutions of **P9**$_{94}$-*b*-**P7**$_{34}$-*b*-**P8**$_{54}$ (Figure 43b) undergoes two distinct hypsochromic shifts at 22°C (by 6 nm) and 42°C (by another 12 nm). The first shift at 22°C reflects the incorporation of Nile Red into the collapsed PNPAM blocks of the supposedly formed unimer micelles of **P9**$_{94}$-*b*-**P7**$_{34}$-*b*-**P8**$_{54}$, while the second shift at 42°C reflects the collapse of the PMDEGA block and the subsequent polymer aggregation. The combination of all measurement data on the collapse points of each block as well as aggregation pathway and solubilization ability give a complex picture of the temperature induced self-assembly of the ternary block copolymers in water. Although three distinct, consecutive phase transitions were observed by NMR spectroscopy for all three polymers, their aggregation behavior and ability to accommodate hydrophobic compounds varied markedly. Obviously, the distribution of the A block with the low LCST, the B block with the intermediate LCST, and C block with the high LCST within the macromolecules plays an important role.

Copolymer **P9**$_{90}$-*b*-**P8**$_{32}$-*b*-**P7**$_{52}$ with the sequence CBA shows micellar aggregation already with the collapse of the terminal A block as schematically depicted in Scheme 14a. At this stage, the aggregates contain hydrophobic domains that can accommodate hydrophobic molecules such as Nile Red efficiently. Heating above the collapse temperature of the B block, which is localized in the center, makes the hydrodynamic diameter of the aggregates shrink. This decrease in size in attributed to the transition of the former hydrophilic B block from the hydrated shell into the hydrophobic core domains. However, this transition does not increase the hydrophobicity of the hydrophobic domains further, as indicated by the virtually unchanged emission wavelength of Nile Red. Nevertheless, when the aggregates' hydrophobic core is enlarged by the collapsed B block, the hydrophobic probe Nile Red seems to partition between collapsed PNPAM and PMDEGA segments.

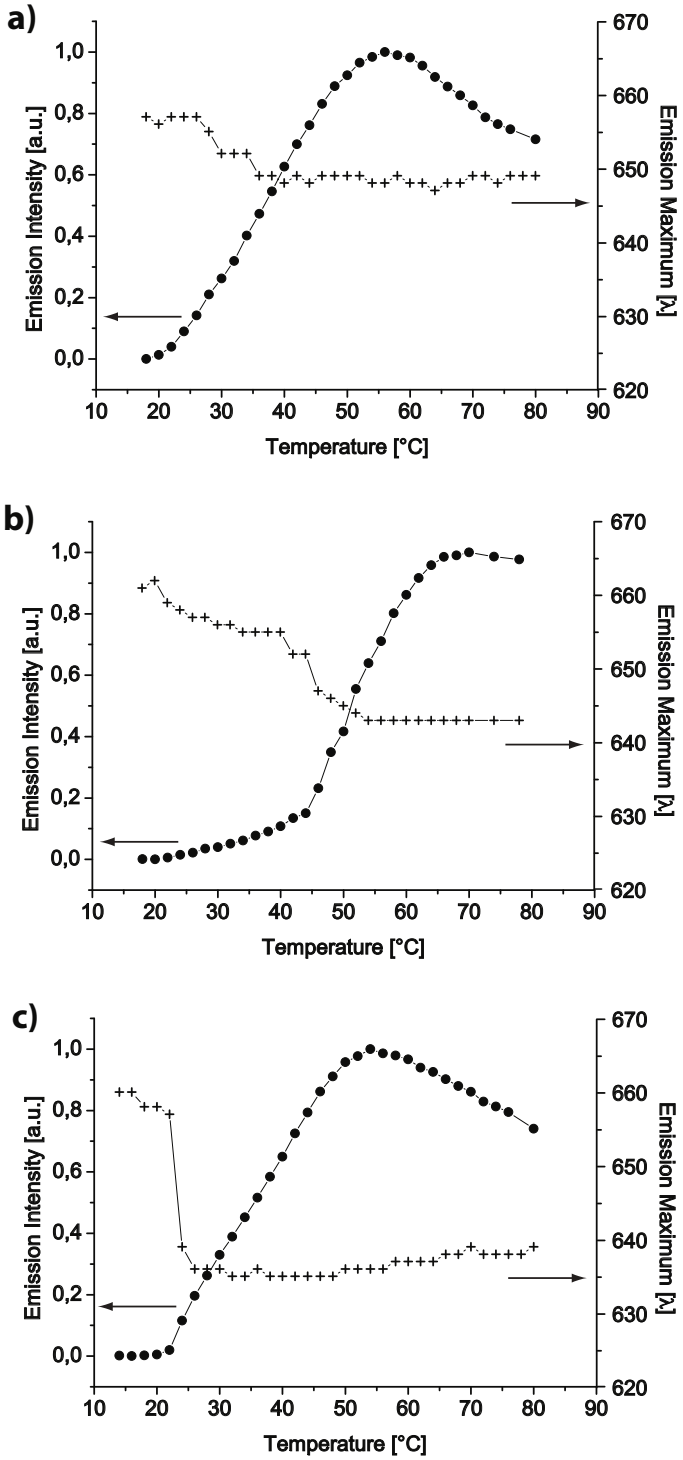

Figure 43: Fluorescence emission intensities (•) and maxima (+) of $\mathbf{P9}_{90}$-*b*-$\mathbf{P8}_{32}$-*b*-$\mathbf{P7}_{52}$, $\mathbf{P9}_{94}$-*b*-$\mathbf{P7}_{34}$-*b*-$\mathbf{P8}_{54}$ and $\mathbf{P7}_{120}$-*b*-$\mathbf{P9}_{60}$-*b*-$\mathbf{P8}_{13}$ as a function of temperature.

Further heating above the cloud point of the C block destabilizes the aggregates at least partially and results in secondary aggregation. This transition again leaves the emission wavelength of Nile Red unchanged, for analogous reasons as discussed for block B, as

PNEAM should be inherently more polar than PNPAM. Still, the collapse of the PNEAM block provides an additional, sufficiently attractive hydrophobic environment for the aryl-TMS end groups, thus corroborating the thermally induced third increase of the hydrophobic microdomains in the system.

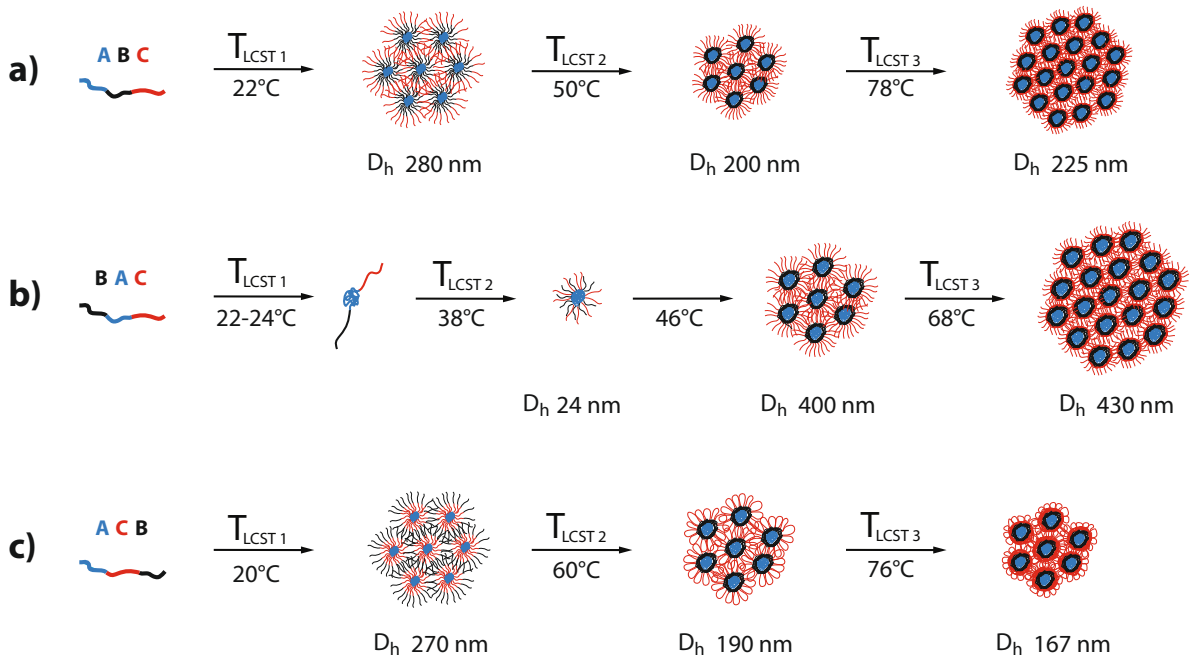

Scheme 14: Schematic aggregation pathway of a) **P9**$_{90}$-*b*-**P8**$_{32}$-*b*-**P7**$_{52}$, b) **P9**$_{94}$-*b*-**P7**$_{34}$-*b*-**P8**$_{54}$ and c) **P7**$_{120}$-*b*-**P9**$_{60}$-*b*-**P8**$_{13}$ in dilute aqueous solution.

Copolymer **P7**$_{120}$-*b*-**P9**$_{60}$-*b*-**P8**$_{13}$ with the sequence ACB, bearing the high LCST block in the center, behaves similar than **P9**$_{90}$-*b*-**P8**$_{32}$-*b*-**P7**$_{52}$ with the CBA sequence, at the first sight. **P7**$_{120}$-*b*-**P9**$_{60}$-*b*-**P8**$_{13}$ shows micellar aggregation already with the collapse of the terminal A block providing aggregates with a notably hydrophobic core, able to accommodate Nile Red. Moreover, the hydrophobic R-groups that are here directly attached to the PNPAM block find an attractive environment. Heating above the collapse of the B block, localized at the other end of the macromolecules, induces a decrease of the hydrodynamic diameter of the aggregates, as for the terpolymers with CBA sequence. The collapse of the B block presumably results in the formation of aggregates which may be best described as flower-like clusters. Likewise to flower-like micelles, the solubilizing coronal chains fold toward the inner hydrophobic domains of the formed particles causing loops of still hydrophilic C blocks at least on the periphery (Scheme 14c). Whether the terminal B blocks within the clusters

are incorporated into the own or into adjacent cores is unclear since non of the measurements allows to rule out one of these possibilities. Still, it seems that the modified ACB sequence shifts the second collapse transition to somewhat higher temperatures. As observed for **P9**$_{90}$-*b*-**P8**$_{32}$-*b*-**P7**$_{52}$, Nile Red apparently partitions between the collapsed PNPAM and PMDEGA chains. Further heating above the collapse point of the C block results in another decrease in size, without indication for secondary aggregation. The block sequence CAB, with the low LCST block in the center of the copolymers, is exemplified by **P9**$_{94}$-*b*-**P7**$_{34}$-*b*-**P8**$_{54}$. For this sequence, the collapse of the A block does not provoke polymer aggregation yet. Instead, it seems that at this temperature, the still hydrophilic, terminal B and C blocks shield the collapsed central A block from encountering other collapsed chains, thus suppressing aggregation (Scheme 14b). The individual collapsed A blocks are, nevertheless, able to solubilize small amounts of Nile Red. Aggregation occurs only, when the second phase transition temperature is reached and the collapse of the B block sets in, leading to non-centrosymmetric micelles due to the different lengths of the B and C block. A pronounced increase of emission intensity accompanied with a second distinct hypsochromic shift shows that after the second transition, hydrophobic molecules are efficiently solubilized by the now formed aggregates. It seems that with the ongoing collapse of the PMDEGA block first micelles are formed as long the HLB allows for the formation of stable micellar aggregates. Increasing temperature by only a few degrees and, thus, ongoing collapse of the B block leads to secondary aggregation. When reaching the collapse temperature of the C block, these aggregates get partially destabilized and show further aggregation. The hydrophobic microdomains formed by the collapsed polymers can accomodate the aromatic end groups at this stage, thus demonstrating that thermally induced hydrophobic microdomains are formed in the system. Nevertheless, in comparison to the other block sequences, the sequence CAB with the low LCST block in the polymer center, is clearly the least performing architecture for multi responsive polymeric amphiphiles if efficient solubilization at low temperatures is aimed at.

3.4 One-Step Synthesis of Multi Responsive Block Copolymers

The major drawback of sequentially synthesized block copolymers is the potential loss of end group functionality as observed throughout the subsequent polymerization of triple thermoresponsive triblock copolymers by RAFT (*vide supra*). Thus, it would be desirable to have the possibility to synthesize similar systems in a single polymerization step in order to minimize impurities from homo- and/or diblock copolymers in the final products. Furthermore, with view on potential applications, a one-step procedure would drastically reduce the costs for the production of smart multiblock copolymers. Recent reports on styrene/maleic anhydride, which undergo an alternating copolymerization under proper polymerization conditions, showed that diblock copolymers are indeed accessible in a one-pot procedure by using an excess of styrene.[202–204] A thermosensitive styrene derivative is expected to show similar polymerization characteristics than styrene and, in addition, its LCST may be varied upon copolymerization with differently substituted maleimides. An excess of such a styrene compound would then inevitably lead to diblock copolymers with two blocks exhibiting different cloud point temperatures, thus result in the formation of double thermoresponsive diblock copolymers within a single polymerization step. In addition, bifunctional initiators or sequential addition of differently substituted maleimides may even give rise to multi responsive terpolymers.

3.4.1 Synthesis of Monomers and ATRP Initiators

N-methylmaleimide (NMM, **10**), N-propylmaleimide (NPM, **11**), and N-PEG_{750}-maleimide (NPEGM, **12**) are commercially available. N-Decylmaleimide (NDM, **13**) was a gift of P. Hendlinger and used as obtained. Maleimides with uncommon residues were synthesized as follows. N-(3-Trimethylsilyl)propyl maleimide (NTMSM, **15**) was synthesized in two steps. First aminopropyltrimethylsilane was added to a solution of maleic anhydride in DMF followed by precipitation and recrystallization from water (Scheme 15a), giving N-(3-trimethylsilyl)propyl maleic acid (**14**) as colorless solid in quantitative yield. The second step is the ring closure of the monosubstituted maleamic acid into the corresponding maleimide.

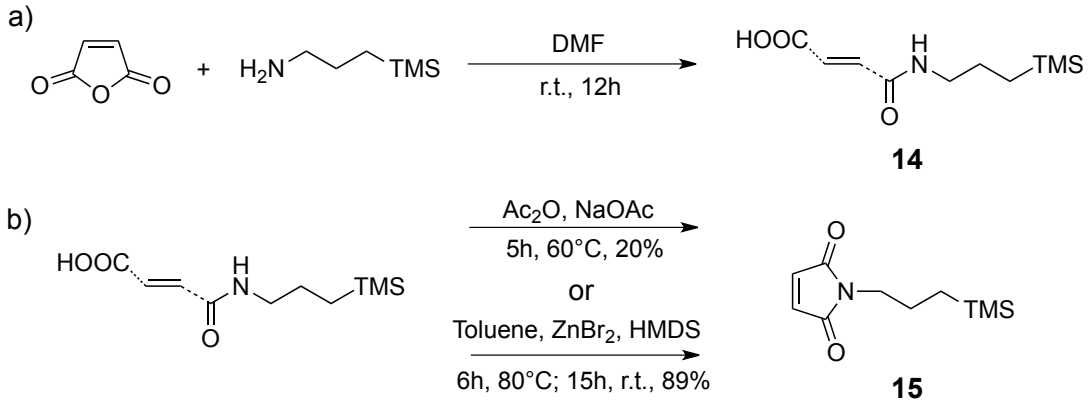

Scheme 15: Synthesis of N-(3-trimethylsilyl)propyl maleimide (**15**).

Whereas the classical route of addition of **14** to sodium acetate in acetic anhydride gave only 20% of the desired maleimide **15** after purification by column chromatography, the yield could be increased to 89% when **14** was reacted in toluene with $ZnBr_2$ and hexamethyl disilazane (HMDS) (Figure 15b).[264] The latter route allows for the one-pot synthesis of N-substituted maleimides since both the formation of the monosubstituted maleamic acid as well as the ring closure can be carried out in toluene using $ZnBr_2$ and HMDS. Consequently, N-(3-triethylsilyl)propargyl maleimide (NTESM, **17**) was synthesized in a one-pot reaction by first adding triethylsilyl protected propargylamine (Scheme 16a) to a solution of maleic anhydride in toluene at 60°C followed by the addition of $ZnBr_2$ and HMDS at 80°C (Scheme 16b). Purification by column chromatography (hexane/ethylacetate) gave N-(3-triethylsilyl)propargyl maleimide as slightly brown oil in about 20% isolated yield.

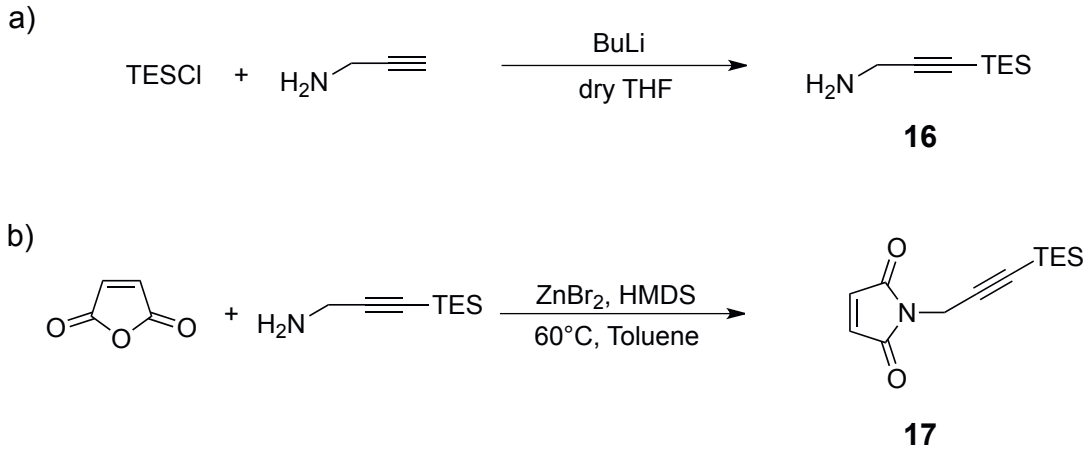

Scheme 16: Synthesis of N-(3-triethylsilyl)propargyl maleimide (**17**).

Furthermore, maleimides derived from glycine and alanine were synthesized. Surprisingly, addition of L-glycine *tert.*-butylester and L-alanine *tert.*-butylester to a solution of maleic anhydride and TEA in DMF did not lead to any reaction. The reason is the formation of charge-transfer complexes of TEA and maleic anhydride which further react under ring-opening of maleic anhydride and monosubstitution (Scheme 17).[265]

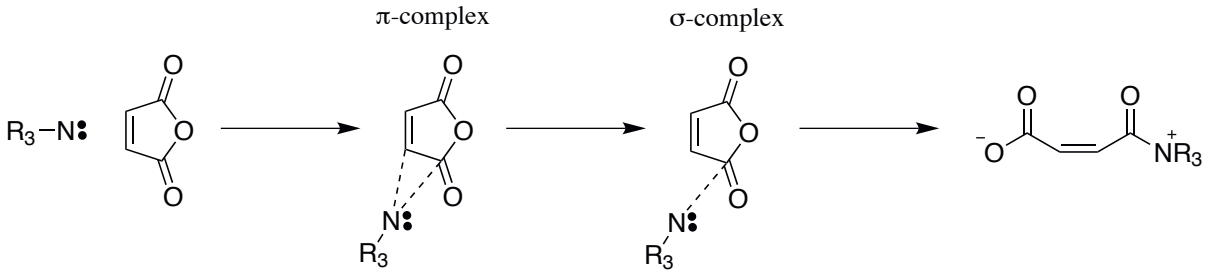

Scheme 17: Reaction of maleic anhydride with triethylamine.

Thus, L-glycine *tert.*-butylester and L-alanine *tert.*-butylester were dissolved in dry toluene and 1 eq. TEA followed by the addition of maleic anhydride.[264] Stirring for 6-8 h at 60°C and 12-15 h at room temperature was followed by the addition of $ZnBr_2$ and HMDS at 80°C. The reaction mixtures were again stirred for 8 h at 80°C and over night at room temperature (Scheme 18). After purification of the crude products by column chromatography (DCM/MeOH) N,N-maleoyl-L-glycine *tert.*-butylester (NtBGlyM, **18**) and N,N-maleoyl-L-alanine *tert.*-butylester (NtBAlaM, **19**) were obtained as colorless solids in moderate yield of about 70%.

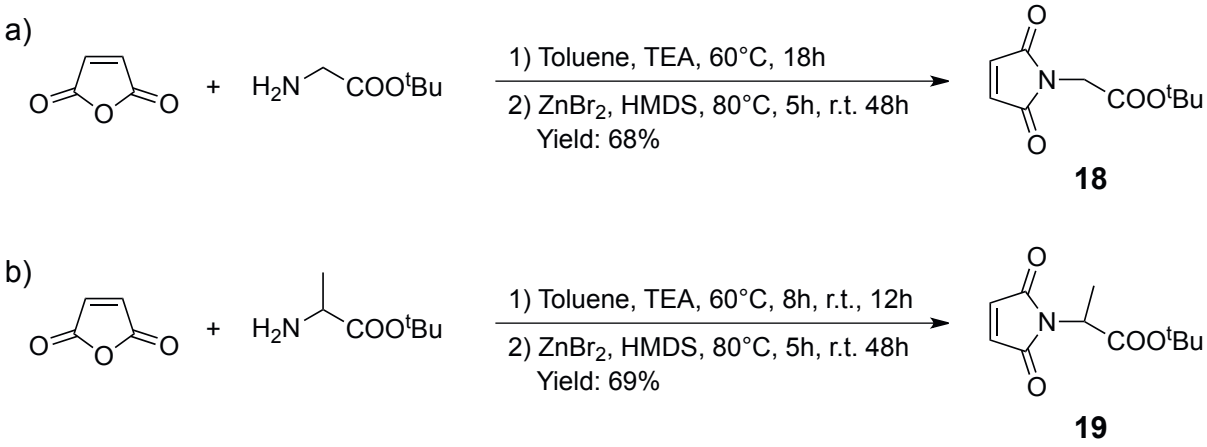

Scheme 18: Synthesis of maleimides **18** and **19**.

In addition, a maleimide containing a thioether moiety in the side chain (**20**) was synthesized following the one-step route catalyzed by $ZnBr_2$ and HMDS starting from methylthioethylamine and maleic anhydride (Figure 19a). After column chromatography N-ethylthiomethyl maleimide (**20**) was obtained as slightly yellow oil (24%). Subsequent oxidation of maleimide **20** to the corresponding sulfoxide was done using $NaIO_4$ in methanol. However, the reaction resulted not only in the formation of the monooxidized maleimide **21** (31%) but also in the formation of a side product, presumably the bisoxidized maleimide **22** (25%) which could be separated by column chromatography (Figure 19b).

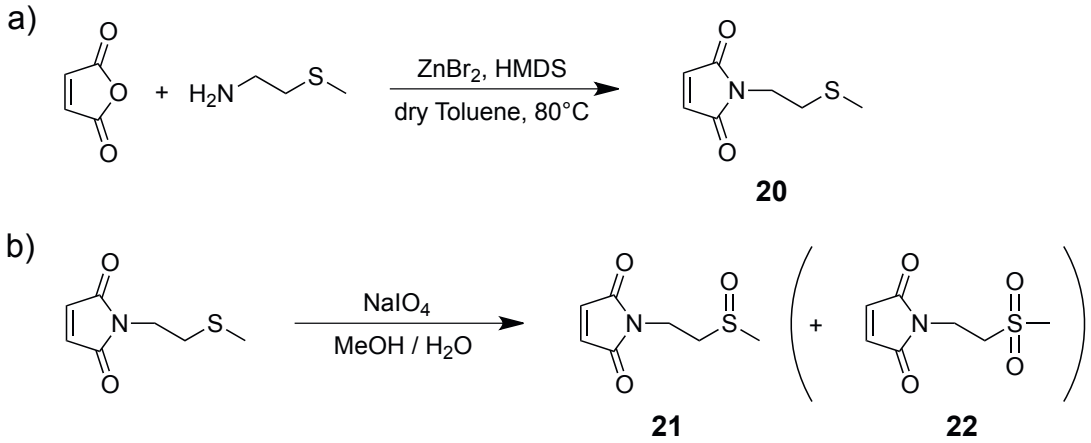

Scheme 19: a) Synthesis of N-ethylthiomethylmaleimide (**20**) and b) oxidation of **20** using $NaIO_4$ into **21** and **22**.

The synthesis of maleimides containing hydrophilic side chains starting from hydrophilic amines and maleic anhydride turned out to be challenging especially due to the difficulties during the purification process. Since all starting compounds were soluble only in water and methanol, neither column chromatography nor selective precipitation were possible.
In order to avoid at least impurities from $ZnBr_2$ and HMDS, a glycine derived maleimide was synthesized. For this purpose, glycine was added to a solution of maleic anhydride in acetic acid and stirred at room temperature over night to give the monosubstituted maleamic acid **23**. A comparison of the NMR spectra of the crude reaction mixture and the obtained product after recrystallization from water (100°C, 10 min) indicated that large amounts of **23** were already transfered into the corresponding maleimide **24**. Consequently, the reaction mixture was refluxed for 1-2 h in water to yield N,N-maleoyl-L-glycine (**24**) as colorless solid in almost quantitative yield (Scheme 20).

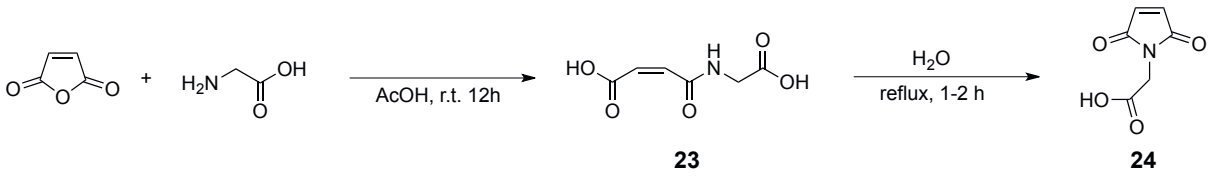

Scheme 20: Synthesis of N,N-maleoyl-L-glycine (**24**).

Maleimide **24** was then converted into the corresponding acid chloride **25** using oxalylchloride in dry THF and directly reacted with hydrophilic amines such as 2,3-aminopropandiol and diethanolamine. Unfortunately, the reactions led to many undesired side reactions as seen in TLC and NMR. Since purification by column chromatography did not succeed due to the limited solubility of the reaction mixture in organic solvents, the hydrophilic amines 2,3-aminopropandiol and diethanolamine were protected as triethylsilyl ethers using triethylsilylchloride in pyridine. The resulting TES-protected amines were then reacted with the acid chloride **25** in dry DCM. However, also these reactions suffered from undesired side reactions, as indicated by NMR spectroscopy, which cannot result from competition of free alcohol functionalities with the amine groups since the former were TES-protected. Another attempt toward a maleimide with hydrophilic side chains was adapted from the literature.[266] Glucosamine was reacted with maleic anhydride in dry methanol and NaOMe (Scheme 21). Precipitation in ethylacetate led to an slightly brown solid (64%).

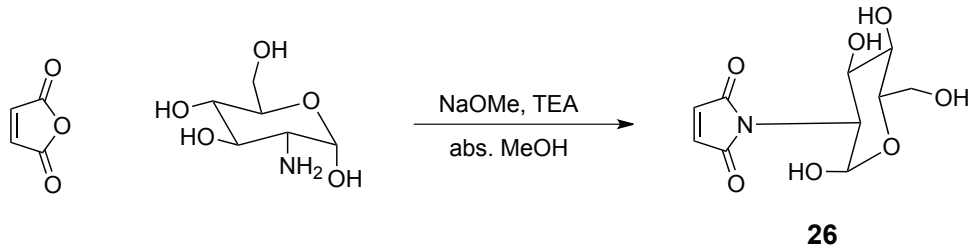

Scheme 21: Attempted synthesis of maleimide **26**.

However, NMR analysis after precipitation indicated that the majority of the obtained product consists of the monosubstituted maleamic acid rather than the desired maleimide **26**. Moreover, a comparison with the given NMR spectra in the literature showed that the obtained product was almost identical. Thus, the given synthesis protocol seems to be not suitable in order to obtain maleimides derived from glucoseamine *via* this synthesis route. Any attempt to induced cyclization by, e. g., temperature failed and the catalysis with $ZnBr_2$ and

HMDS will result in reaction mixtures which cannot be purified by column chromatography due to the insolubility of the product and the starting compounds in common organic solvents.

Finally, 4-vinylbenzyl methoxytetrakis(oxyethylene) ether (VBTOE, **27**), a styrene based monomer which gives water soluble homopolymers below 40°C, was synthesized according to a literature procedure.[267] Thus, 4-vinylbenzyl chloride was added dropwise to a solution of tetra(ethylene glycol) monomethyl ether and NaH in dry THF (Scheme 22). After stirring over night at 75°C, aqueous work up and purification by column chromatography, VBTOE was obtained as colorless liquid in good yield (76%).

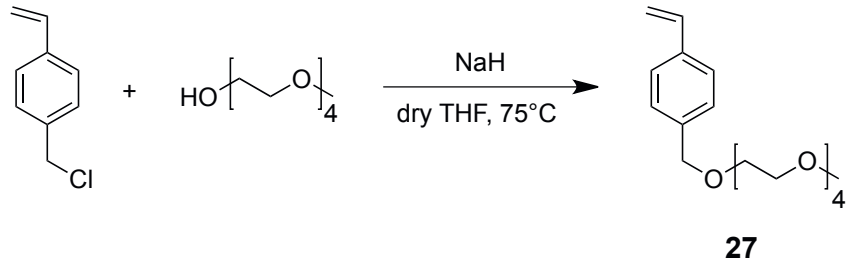

27

Scheme 22: Synthesis of 4-vinylbenzyl methoxytetrakis(oxyethylene) ether (**27**).

A bifunctional ATRP initiator was synthesized by dropwise addition of bromoisobutyrylbromide to a solution of hydrochinone in dry THF and TEA at 0°C. Recrystallization from methanol gave the ATRP initiator **28** as colorless solid in moderate yield of 58% (Scheme 23).

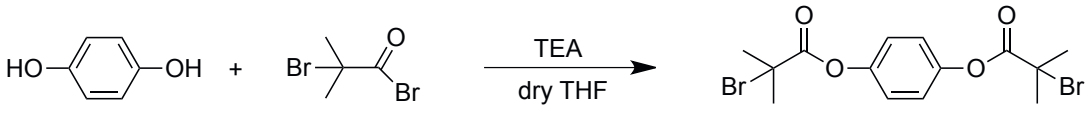

28

Scheme 23: Synthesis of the bifunctional ATRP initiator **28**.

Another bifunctional ATRP initiator (**29**) was synthesized by Ang Li[268] and used as obtained. Its structure is shown in Figure 44.

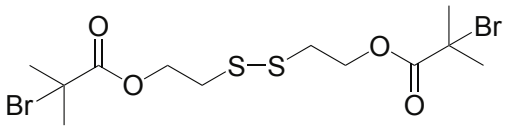

29

Figure 44: Structure of the bifuntional ATRP initiator bis[2-(2-bromoisobutyryloxy)ethyl] disulfide (**29**).

3.4.2 Homopolymers

Homopolymers of VBTOE (**27**) were synthesized by RAFT and ATRP with different molar masses using either CTA **3**, 3-(trimethylsilyl)benzylbromid (**6**), or 1-bromoethylbenzene (**30**). ATRP polymerizations were carried out at 110°C using CuBr and hexamethyltriethylenetetramine (HMTETA) as catalyst system. Since RAFT polymerizations of VBTOE at 60°C using AIBN as initiator did lot lead to high conversions, RAFT polymerizations were performed at 100°C using 1-[(1-cyano-1-methylethyl)azo]formamide (V30). The polymers were analyzed by a combination of ^{1}H NMR spectroscopy and SEC as summarized in Table 3.5.

Table 3.5: Synthesis data of homopolymers of VBTOE with varying degree of polymerization.

Polymer	CRP	Initiator/CTA	M_n, theor.[a]	M_n[b]	$M_{n,app}$[c]	PDI	CP[d]
P27$_6$	ATRP	**6**	2000	2200	2500	1.20	34°C
P27$_{16}$	RAFT	**3**	4600	5200	4000	1.47	39°C
P27$_{26}$	ATRP	**30**	6800		8600	1.66	44°C

[a] Determined gravimetrically. [b] Calculated molar mass from ^{1}H NMR spectroscopy by integration of the aromatic TMS-peak against a peak of the polymer (end group analysis). [c] Determined by size exclusion chromatography (SEC) in THF with linear polystyrene standards. [d] Cloud points (CP) were determined by turbidity measurements of dilute aqueous solutions at a concentration of 1.0 g L^{-1}.

The cloud point temperatures of **P27**$_6$, **P27**$_{16}$, and **P27**$_{26}$ were measured by turbidimetry at concentrations of 1 g L^{-1}. The onset of the drop in transmittance was taken as phase transition temperature. The measured turbidity curves (Figure 45a) indicate a shift to higher temperatures with increasing molar mass.

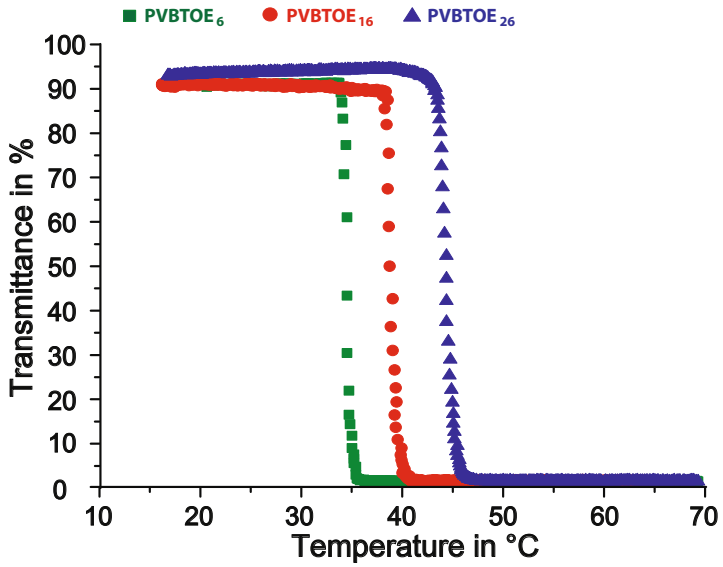

Figure 45: Plot of the turbidity measurements of **P27**$_6$ (■), **P27**$_{16}$ (•), and **P27**$_{26}$ (▲) in dilute aqueous solution.

This is not surprising. Especially for the very short **P27**$_6$ with an average molar mass of about 2000 g mol^{-1} the hydrophobic TMS-labeled aromatic end group may influence the solution behavior markedly.

3.4.3 Alternating Copolymers

Like styrene, VBTOE is expected to copolymerize with N-substituted maleimides in an almost alternating fashion since the methoxytetraethylene glycol substituent should not affect the copolymerization behavior.[269] Thus, alternating copolymers of VBTOE and differently substituted maleimides were synthesized by RAFT and ATRP (Figure 46).

The alternating nature of the synthesized copolymers was validated by ^{1}H NMR spectroscopy. Comparison of the benzylic CH_2 resonance of VBTOE with a characteristic signal of the maleimide side chains revealed 1 : 1 ratios within the obtained copolymers. Taking into account that a homopolymerization of the maleimides is virtually impossible under the given polymerization conditions, a 1 : 1 ratio can only be obtained when the polymerization proceeds alternatingly. Different alternating copolymers were synthesized in triethylene glycol at 110°C using CuBr and HMTETA as catalyst system for ATRP, or at 100°C using CTA **3** and V30 in the case of RAFT and analyzed by a combination of SEC and ^{1}H NMR spectroscopy (Table 3.6). Compared to the homopolymerization of VBTOE, the alternating copolymeriza-

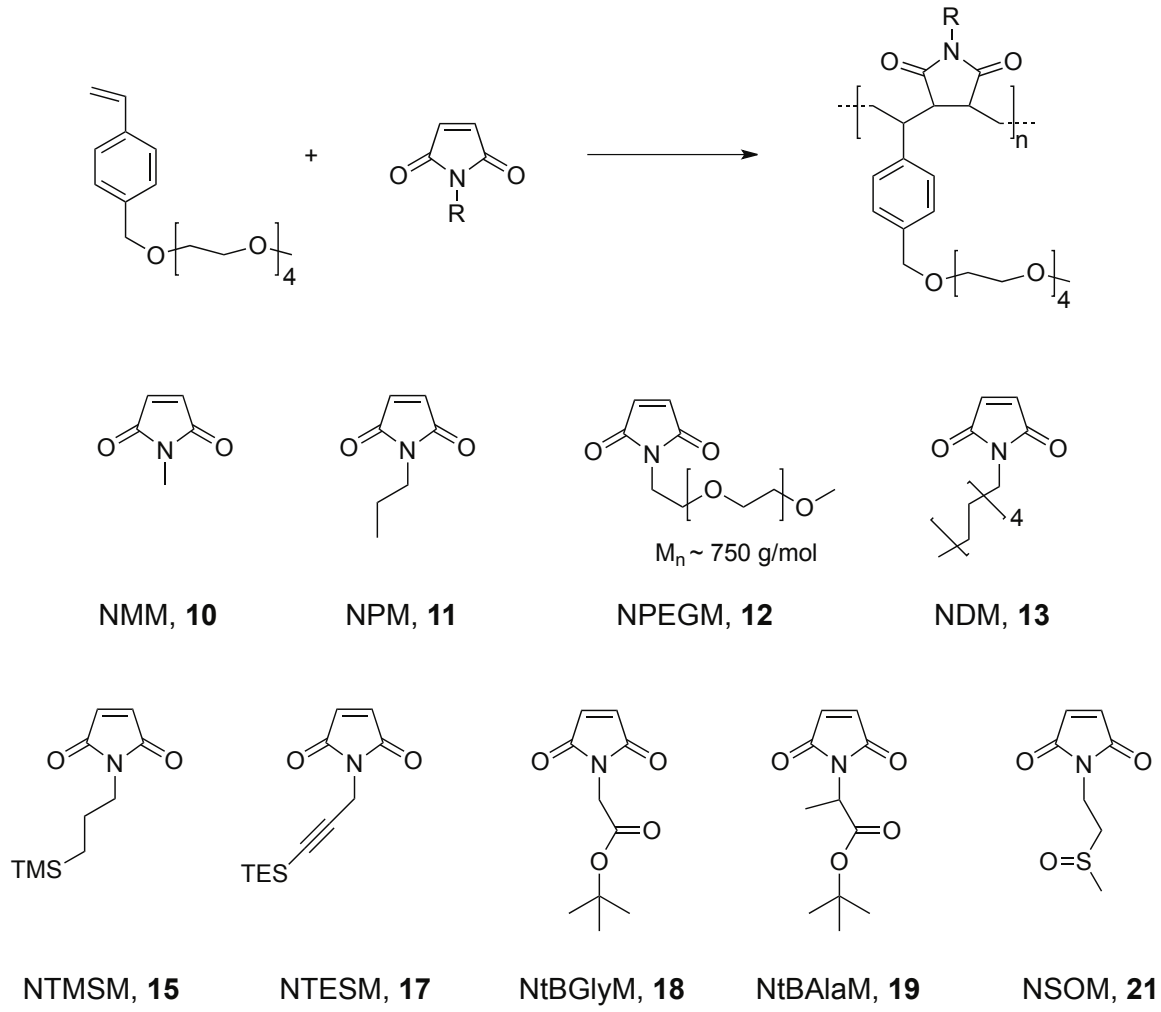

Figure 46: Alternating copolymers from VBTOE and different N-substituted maleimides.

tion proceeded much faster. This observation is not surprising since the formation of alternating copolymers from this monomer pair is based on the much faster crosspropagation compared to homopropagation of VBTOE.

Adjusting the hydrophilic-to-hydrophobic balance by different maleimide substituents influenced the phase transition temperatures of the resulting copolymers compared to the LCST of PVBTOE markedly. Furthermore, the LCST is adjustable by the choice of proper side chains within a relatively broad temperature window. For instance, the polymer P(VBTOE-*alt*-NMM)$_{45}$ (**P**(**27**-*alt*-**10**)$_{45}$) showed a cloud point of 28°C, thus about 10°C lower than PVBTOE with about 39°C. Longer alkyl side chains such as propyl led to a further decrease of the phase transition temperature of the resulting copolymer P(VBTOE-*alt*-NPM)$_{43}$ (**P**(**27**-*alt*-**11**)$_{43}$) to 17°C (Figure 47).

Table 3.6: Synthesis data of alternating copolymers of VBTOE and N-substituted maleimides. RAFT polymerizations were carried out at 100°C in triethylene glycol using V30 as initiator. ATRP polymerizations were carried out at 110°C in triethylene glycol.

Polymer	CRP	M_n, theor.[a]	M_n[b]	$M_{n,app}$[c]	PDI	CP[d]
P(VBTOE-*alt*-NPM)$_{43}$	RAFT (**3**)	16600	20300	11600	1.45	17°C
P(VBTOE-*alt*-NMM)$_{45}$	RAFT (**3**)	20100	17800	11000	1.49	28°C
P(VBTOE-*alt*-NtBGlyM)$_{34}$	ATRP (**30**)	18400		9300	1.83	20°C
P(VBTOE-*alt*-NtBAlaM)$_{23}$	ATRP (**30**)	14800		10900	1.70	34°C
P(VBTOE-*alt*-NTMSM)$_{13}$	ATRP (**30**)	7200		6100	1.62	not soluble
P(VBTOE-*alt*-NSOM)$_9$	ATRP (**30**)	4800		4900	3.44	36°C
P(VBTOE-*alt*-NPEGM)$_{24}$	ATRP (**30**)	29700		10800	4.66	>90°C

[a] Conversion determined gravimetrically. [b] Calculated molar mass from ^{1}H NMR spectroscopy by integration of the aromatic TMS-peak against a peak of the polymer (end group analysis). [c] Determined by size exclusion chromatography (SEC) in DMF + 0.1% LiBr using linear styrene standards. [d] Cloud points (CP) were determined by turbidity measurements of dilute aqueous solutions at a concentration of 1.0 g L^{-1}.

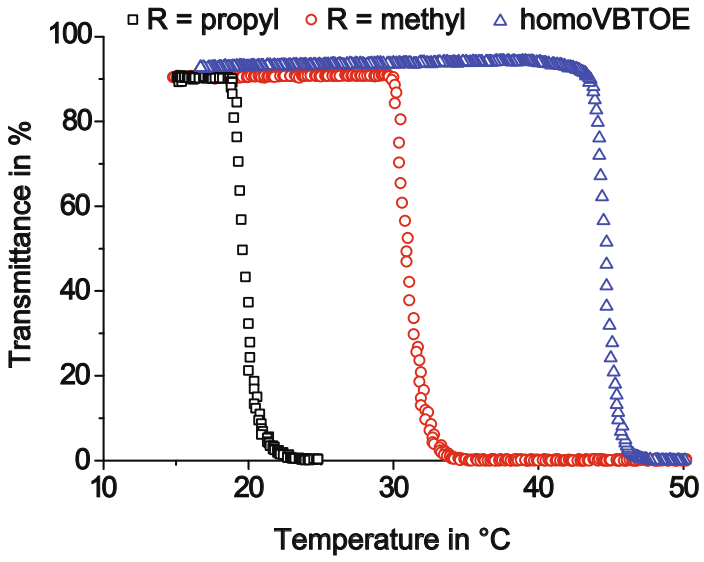

Figure 47: Cloud point temperatures of polymer **P**(**27**-*alt*-**11**)$_{43}$, **P**(**27**-*alt*-**10**)$_{45}$ and **P27**$_{26}$ (1 g L^{-1}).

However, exceeding the length of the alkyl residue further results in water insoluble copolymers as observed for a decyl substituent. Likewise, the use of aromatic substituents (e. g.benzyl) and propyl-TMS residues (P(VBTOE-*alt*-NTMSM)$_{13}$) led to copolymers which do not dissolve in water. Surprisingly, the use of maleimides derived from *tert.*-butyl protected glycine (**18**) and alanine (**19**) gave alternating copolymers P(VBTOE-*alt*-NtBGlyM)$_{34}$ (**P**(**27**-*alt*-**18**)$_{34}$) and P(VBTOE-*alt*-NtBAlaM)$_{23}$ (**P**(**27**-*alt*-**19**)$_{23}$), respectively, which gave clear solutions when dissolved in water (1.0 g L^{-1}) and did not show any changes in transmittance between 14°C and 90°C. Dynamic light scattering, however, revealed the temperature induced phase transitions of **P**(**27**-*alt*-**18**)$_{34}$ and **P**(**27**-*alt*-**19**)$_{23}$ at 20°C and 34°C, respectively (Figure 48). Both polymers showed aggregation above these temperatures into stable aggregates of 65 nm (**P**(**27**-*alt*-**18**)$_{34}$) and 76 nm (**P**(**27**-*alt*-**19**)$_{23}$). Surprisingly, **P**(**27**-*alt*-**19**)$_{23}$ showed a higher phase transition temperature then **P**(**27**-*alt*-**18**)$_{34}$. The reason for that is yet unclear.

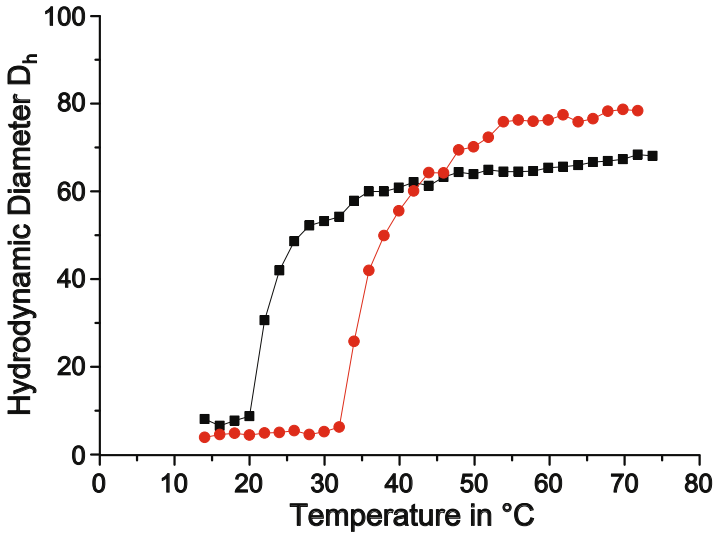

Figure 48: Dynamic light scattering of aqueous solutions of **P**(**27**-*alt*-**18**)$_{34}$ (■) and **P**(**27**-*alt*-**19**)$_{23}$ (•) at concentrations of 1 g L^{-1}.

Also **P**(**27**-*alt*-**11**)$_{43}$ with a propyl substituent on the maleimide units showed stable aggregates of about 200 nm while shorter side chains such as methyl residues led to macroscopic phase separation above the cloud point. This behavior can be explained by the concept of mesoglobules.[116] Presumably, the hydrophobic side chains of the maleimide units form a dense hydrophobic core surrounded by the less hydrophobic oligoethylene glycol chains of

the VBTOE units which stabilize the formed particles. If the hydrophobic chains become to short as in the case of **P**(**27**-*alt*-**10**)$_{45}$, the polymers cannot assemble into mesoglobular particles but precipitate from solution. The latter is the expected behavior of thermosensitive homopolymers about their LCST and was also observed for homopolymers of VBTOE.
The copolymerization of VBTOE with hydrophilic maleimides such as the sulfoxide containing maleimide NSOM (**21**) or the PEG-substituted maleimide NPEGM (**12**) did not result in a controlled increase of the phase transition temperature of the resulting copolymers. While P(VBTOE-*alt*-NSOM)$_9$ (**P**(**27**-*alt*-**21**)$_9$) showed a cloud point at 36°C, thus within the temperature range of PVBTOE, the copolymer P(VBTOE-*alt*-NPEGM)$_{24}$ (**P**(**27**-*alt*-**12**)$_{24}$) had a LCST above 90°C, the detection limit of the turbidity photometer and DLS. In addition, both polymers showed very broad distributions in SEC measurement which cannot be explained by interactions of the polymers with the column material alone as well as a shoulder at higher molecular weight in the case of **P**(**27**-*alt*-**12**)$_{24}$, indicating side reactions during the polymerization such as chain transfer or disproportionation. A possible explanation is the chelating of the copper catalyst system during the ATRP by the sulfoxide moiety or by the long PEG-substituents of NPEGM which may cause a certain loss in control.

3.4.4 Diblock Copolymers

The use of an excess of VBTOE in the copolymerization with a given maleimide consequently leads to the formation of diblock copolymers in a single polymerization step. During the initial stages of the polymerization alternating copolymers are formed. Once all of the maleimide is consumed, homopolymerization of VBTOE starts (Scheme 24). This results in the formation of diblock copolymers of the form P(VBTOE-*alt*-Maleimide)-*b*-PVBTOE with two blocks exhibiting different phase transition temperatures.

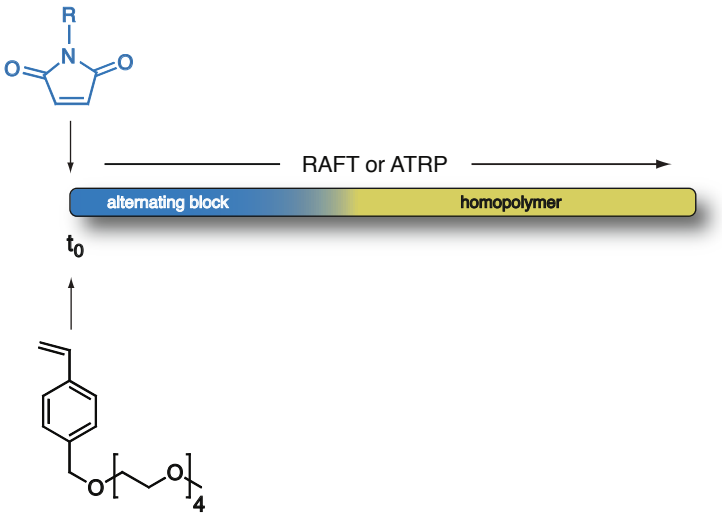

Scheme 24: General scheme of the one-step synthesis of double thermosensitive diblock copolymers from VBTOE and N-substituted maleimides.

A series of double thermosensitive diblock copolymers was synthesized by ATRP as well as RAFT polymerization using different N-substituted maleimides. Polymer characterization was done by a combination of SEC and ^{1}H NMR spectroscopy (Table 3.7).

For instance, the copolymerization of VBTOE (**27**) with NMM (**10**) led to double thermoresponsive tapered diblock copolymers with an alternating P(VBTOE-*alt*-NPM) (**P**(**27**-*alt*-**11**)) block (LCST around 28°C) and a PVBTOE block (LCST about 39°C). **P**(**27**-*alt*-**10**)$_8$-*b*-**P27**$_{31}$, with a ratio of alternating block to homopolymer block of 1 : 2, showed aggregation above 36°C due to the collapse of the P(VBTOE-*alt*-NMM) block (Figure 49). After an initial maximum, P(VBTOE-*alt*-NMM)-core PVBTOE-shell micelles of about 75 nm were formed which underwent secondary aggregation when the dilute aqueous solutions of **P**(**27**-*alt*-**10**)$_8$-*b*-**P27**$_{31}$ were heated to 41°C and above.

Table 3.7: Synthesis data of diblock copolymers obtained *via* a one-step procedure.

Polymer[a]	CRP	M_n, theor.[b]	M_n[c]	$M_{n,app}$[d]	PDI
P(VBTOE-*alt*-NMM)$_8$-*b*-PVBTOE$_{31}$	ATRP (**30**)	13600		13600	1.61
P(VBTOE-*alt*-NPM)$_6$-*b*-PVBTOE$_{16}$	ATRP (**30**)	8200		7600	1.82
P(VBTOE-*alt*-NPM)$_{12}$-*b*-PVBTOE$_{52}$	RAFT (**3**)	9000	22800	7700	1.43
P(VBTOE-*alt*-NDM)$_{26}$-*b*-PVBTOE$_{63}$	ATRP (**6**)	10300	35300	14300	1.98
P(VBTOE-*alt*-NTMSM)$_6$-*b*-PVBTOE$_{20}$	ATRP (**6**)	15100	11900	12300	2.39
P(VBTOE-*alt*-NTESM)$_7$-*b*-PVBTOE$_{23}$	ATRP (**30**)	11700		13300	1.70

[a] Determined by ^{1}H NMR spectroscopy by integration of the benzylic CH_2 signal against a characteristic signal of the maleimide side chains. [b] Determined gravimetrically. [c] Calculated molar mass from ^{1}H NMR spectroscopy by integration of the aromatic TMS-peak against a peak of the polymer (end group analysis). [d] Determined by size exclusion chromatography (SEC).

The still hydrated clusters with a D_h of 500-600 nm shrank due to ongoing dehydration and resulted in stable particles of about 180 nm above 46°C. Surprisingly, no changes of transmittance were observed within this temperature range.

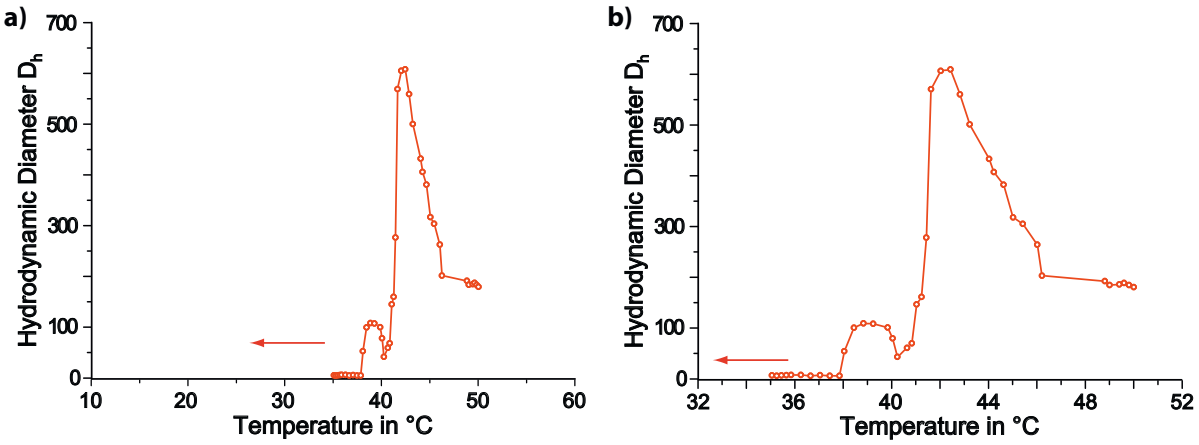

Figure 49: Dynamic light scattering measurements of a) P(VBTOE-*alt*-NMM)$_8$-*b*-PVBTOE$_{31}$ (**P**(**27**-*alt*-**10**)$_8$-*b*-**P27**$_{31}$) in dilute aqueous solutions (0.5 g L^{-1}); b) Plot of the same measurement with a differently scaled X-axis.

Upon increasing the length of the hydrophobic maleimide side chains by copolymerization of VBTOE (**27**) with NPM (**11**), double thermoresponsive tapered diblock copolymers with an alternating P(VBTOE-*alt*-NPM) (**P**(**27**-*alt*-**11**)) block (LCST around 18°C) and a PVBTOE block (LCST about 39°C) were obtained. Their relative composition was determined by ^{1}H NMR spectroscopy comparing the benzylic CH_2 resonance of the VBTOE units at about 4.5 ppm with the CH_3 signals of the NPM units at about 0.8 ppm. An indirect proof for the formation of double responsive copolymers was obtained by turbidity and DLS measurements of dilute aqueous solutions (0.5 g L^{-1}). **P**(**27**-*alt*-**11**)$_6$-*b*-**P27**$_{16}$ showed aggregates in DLS above 25°C accompanied with a sudden drop in transmittance above 33°C (Figure 50b). The observed shift to higher temperatures of the cloud point temperature of the alternating low-LCST block by about 8°C is similar to observations made for block copolymers obtained from sequential RAFT polymerization and can be explained with the adjacent PVBTOE block. After passing through a maximum both the DLS and the turbidity curve leveled off above 46°C to give aggregates with a hydrodynamic diameter of about 60 nm. Thus, the formation of P(VBTOE-*alt*-NPM)-core PVBTOE-shell micelles is expected for **P**(**27**-*alt*-**11**)$_6$-*b*-**P27**$_{16}$ in this temperature range. Further heating then induced the collapse of the PVBTOE shell and led to secondary aggregation into particles with a D_h of 340 nm. This second transition is also reflected by a drastic drop in transmittance above 38°C. The resulting aggregates presumably consist of clustered micelles. As explained above, the collapse of the solubilizing shell may lead to secondary aggregation when the formed aggregates are not longer stabilized and either the formation of mesoglobules or clustering is observed. The temperature induced aggregation behavior of this diblock copolymer obtained by a one-pot procedure is, hence, comparable with the one of diblock copolymers obtained by a classical step-wise synthesis. The relatively broad maximum of D_h found for both polymers above the first phase transition can be explained by the chemical similarity in both blocks. VBTOE units can be found in both blocks which makes microphase separation of the two blocks more difficult and, hence, broadens the temperature range in which loose, larger aggregates are present. Ongoing dehydration, however, leads to complete phase separation of the two blocks and the formation of stable micelles at higher temperatures. Compared to **P**(**27**-*alt*-**11**)$_6$-*b*-**P27**$_{16}$, **P**(**27**-*alt*-**11**)$_{12}$-*b*-**P27**$_{52}$ showed the formation of aggregates of about 45 nm above 18°C, in good agreement with the expected cloud point of the P(VBTOE-*alt*-NPM) block (Figure 50c). Further heating then led to a shrinkage of the hydrodynamic diameter to 17 nm above 38°C,

the phase transition temperature of the PVBTOE block, followed by secondary aggregation into particles with a D_h of about 680 nm above 44°C. Hence, **P**(**27**-*alt*-**11**)$_{12}$-*b*-**P27**$_{52}$ is expected to form P(VBTOE-*alt*-NPM)-core PVBTOE-shell micelles above 18°C. Further heating then induces the collapse of the PVBTOE shell above 38°C followed by clustering of the formed micelles at higher temperatures than 44°C.

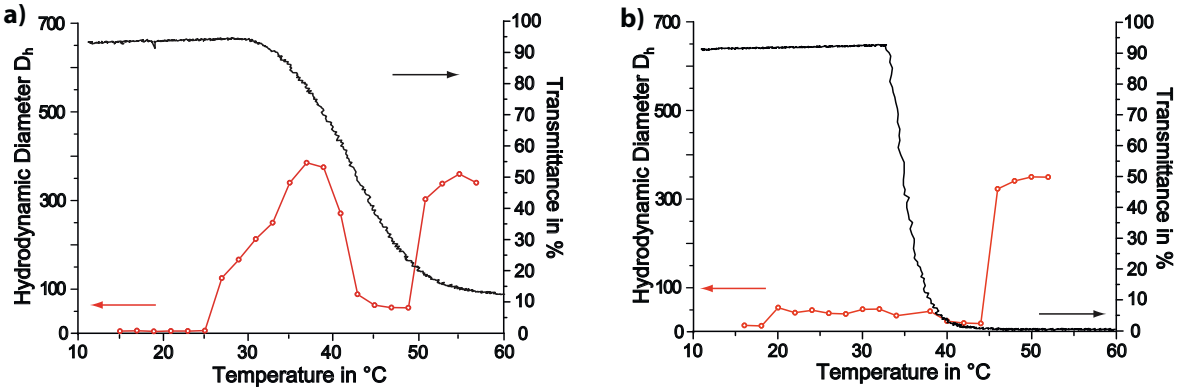

Figure 50: Dynamic light scattering and turbidity measurements of a) P(VBTOE-*alt*-NPM)$_6$-*b*-PVBTOE$_{16}$ (**P**(**27**-*alt*-**11**)$_6$-*b*-**P27**$_{16}$) and b) P(VBTOE-*alt*-NPM)$_{12}$-*b*-PVBTOE$_{52}$ (**P**(**27**-*alt*-**11**)$_{12}$-*b*-**P27**$_{52}$) in dilute aqueous solutions (0.5 g L^{-1}).

Further increase in the hydrophobicity of the maleimide side chains was obtained by the synthesis of diblock copolymers from VBTOE (**27**) and NDM (**13**) or NTMSM (**15**). Although the corresponding alternating copolymers were insoluble in water, a relatively long PVBTOE block led to block copolymers **P**(**27**-*alt*-**15**)$_6$-*b*-**P27**$_{20}$ and **P**(**27**-*alt*-**13**)$_{26}$-*b*-**P27**$_{63}$ which gave clear solutions below 20°C without any indication for aggregation as confirmed by DLS measurements (Figure 52). A comparison of the ^{1}H NMR spectra of **P**(**27**-*alt*-**15**)$_6$-*b*-**P27**$_{20}$ and **P**(**27**-*alt*-**13**)$_{26}$-*b*-**P27**$_{63}$ in DMSO-d$_6$ and D_2O (Figure 51a,b) showed the strong attenuation of the signals corresponding to the hydrophobic maleimide side chains when dissolved in water at temperatures below 20°. Since no aggregation is visible for both polymers within this temperature range in DLS (Figure 52a,b), the findings made in NMR spectroscopy suggest that the alternating blocks are not fully solubilized in D_2O even below 20°C.

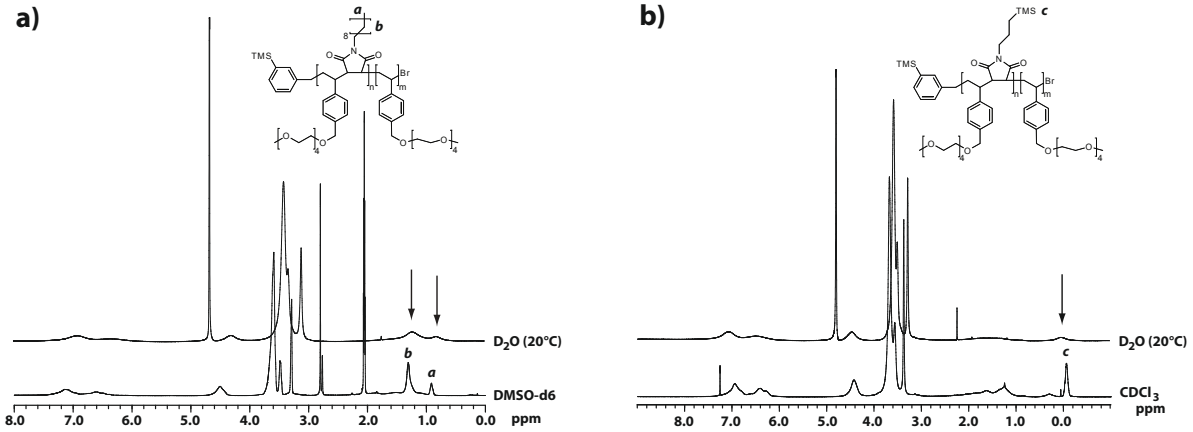

Figure 51: ^{1}H NMR spectra of a) P(VBTOE-*alt*-NDM)$_{26}$-*b*-PVBTOE$_{63}$ (**P**(**27**-*alt*-**13**)$_{26}$-*b*-**P27**$_{63}$) in $CDCl_3$ and D_2O and b) P(VBTOE-*alt*-NTMSM)$_6$-*b*-PVBTOE$_{20}$ (**P**(**27**-*alt*-**15**)$_6$-*b*-**P27**$_{20}$) in DMSO-d_6 and D_2O at concentrations of 10 g L^{-1}.

A possible explanation is the formation of a kind of polysoap[270] by the alternating blocks. The hydrophobic maleimide residues possibly undergo microphase separation along the polymer chain forming hydrophobic domains which are shielded by the hydrophilic methoxytetraethylene glycol side chains of the VBTOE units as schematically depicted in Scheme 25. Since the corresponding alternating copolymers were not soluble in water at any temperature, the relatively long PVBTOE block must prevent these diblock copolymers from aggregation below 20°C. The onset of aggregation observed in DLS was found for both polymers to be above 20°C. Since a decyl side chains is expected to be more hydrophobic than a TMS-propyl residue, the cloud point temperature of the P(VBTOE-*alt*-NTMSM) and P(VBTOE-*alt*-NDM) block seems to be independent of the chemical structure of the maleimide substituent. This indicates that once the maleimide side chains become too hydrophobic and result in the formation of a polysoap-like structure, the temperature at which aggregation sets in is no longer determined by the maleimide substituent but by the hydrophobic microdomains.

Dilute aqueous solutions (1.0 g L^{-1}) of **P**(**27**-*alt*-**15**)$_6$-*b*-**P27**$_{20}$ and **P**(**27**-*alt*-**13**)$_{26}$-*b*-**P27**$_{63}$ studied by turbidity and DLS measurements showed two thermally induced transitions in both cases. A first thermal transition was observed for the two block copolymers at 20°C due to the collapse of the alternating block as seen by an increase of the hydrodynamic diameter accompanied with a drop in transmittance. Above 20°C, **P**(**27**-*alt*-**15**)$_6$-*b*-**P27**$_{20}$ and **P**(**27**-*alt*-**13**)$_{26}$-*b*-**P27**$_{63}$ initially form relatively small aggregates of 100-120 nm and 35-45 nm, re-

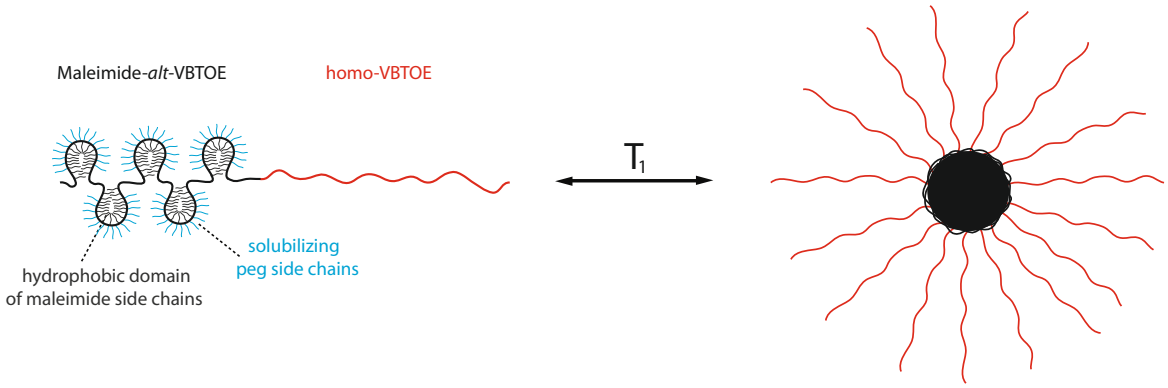

Scheme 25: Proposed solution behavior of P(VBTOE-*alt*-NDM)$_{26}$-*b*-PVBTOE$_{63}$ (**P**(**27**-*alt*-**13**)$_{26}$-*b*-**P27**$_{63}$) and P(VBTOE-*alt*-NTMSM)$_6$-*b*-PVBTOE$_{20}$ (**P**(**27**-*alt*-**15**)$_6$-*b*-**P27**$_{20}$) below and above the first cloud point (20°C).

spectively (Figure 52a,b). Presumably these aggregates consist of collapsed hydrophobic alternating blocks forming the core and a solubilizing PVBTOE shell. In both cases the transmittance decreased gradually within this temperature range. After a slight gradual increase of the D_h with increasing temperature, **P**(**27**-*alt*-**15**)$_6$-*b*-**P27**$_{20}$ and **P**(**27**-*alt*-**13**)$_{26}$-*b*-**P27**$_{63}$ showed a second drastic increase of the hydrodynamic diameter above 31°C. This transition is attributed to the collapse of the PVBTOE shell. The observed secondary aggregation above 31°C led to the formation of particles with a D_h of about 630 nm and was accompanied with a drastic drop in transmittance for both polymer solutions. Compared to polymers from VBTOE and NPM or NMM, the phase transition temperature of the PVBTOE block is lowered by about 10°C which can be explained by the more hydrophobic alternating block and, consequently, more hydrophobic micellar cores formed above the first cloud point.

By the maleimide units virtually any functional side chain can be introduced into such block copolymers. For instance, alkine functionalities within one block open potential possibilities for postmodification of the obtained block copolymers by, e. g., click-chemistry[271] or C-C coupling reactions such as Glaser[272] or Sonogashira coupling.[273] Furthermore, self-assembled block copolymer micelles bearing alkine functions allow for facile formation of core- or shell-crosslinked micelles. The copolymerization of styrene with N-propargyl maleimide was, however, reported to lead to side reactions, e. g., crosslinking, during the ATRP polymerization.[181] Moreover, TMS protecting groups may be cleaved under certain reaction conditions. Thus, diblock copolymers of VBTOE (**27**) and NTESM (**17**) were synthe-

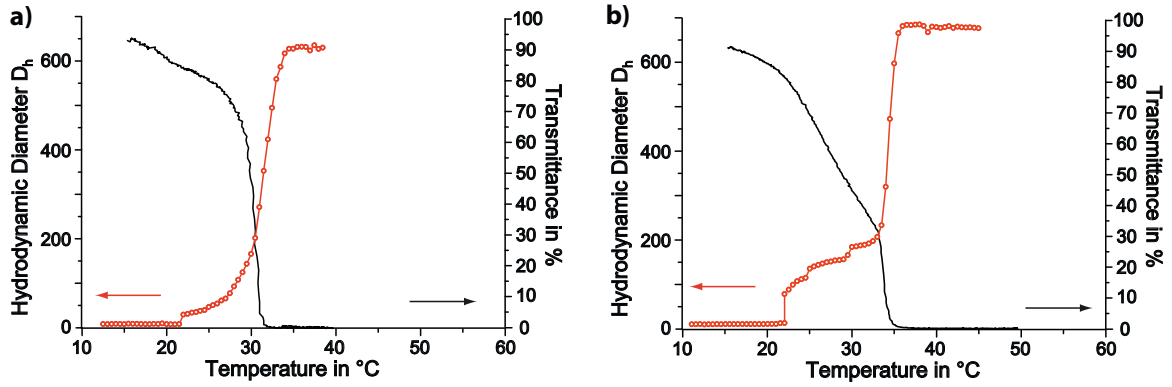

Figure 52: Dynamic light scattering and turbidity measurements of a) P(VBTOE-*alt*-NDM)$_{26}$-*b*-PVBTOE$_{63}$ (**P**(**27**-*alt*-**13**)$_{26}$-*b*-**P27**$_{63}$) and b) P(VBTOE-*alt*-NTMSM)$_6$-*b*-PVBTOE$_{20}$ (**P**(**27**-*alt*-**15**)$_6$-*b*-**P27**$_{20}$) in dilute aqueous solutions (1 g L^{-1}).

sized by ATRP since the TES group is more stable under the given polymerization conditions. The obtained polymer **P**(**27**-*alt*-**17**)$_7$-*b*-**P27**$_{23}$ was then TES-deprotected in dry THF using an excess of tetra-n-butylammonium fluoride (TBAF) at room temperature over night to give a diblock copolymer of VBTOE and N-propargyl maleimide (NPPGM, **31**), **P**(**27**-*alt*-**31**)$_7$-*b*-**P27**$_{23}$. Quantitative deprotection of the alternating block was revealed by the complete disappearance of the TES signals around 0 ppm in NMR spectroscopy (Figure 53).

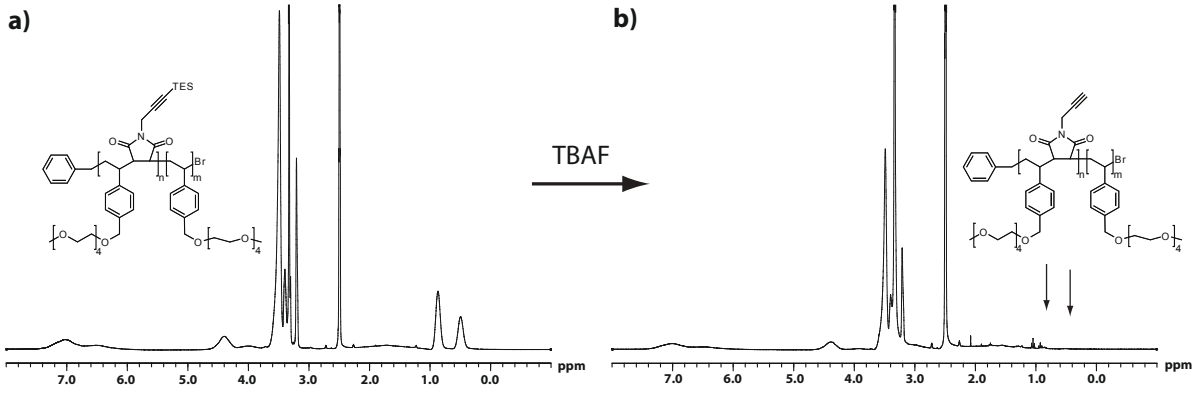

Figure 53: ^{1}H NMR spectra of a) P(VBTOE-*alt*-NTESM)$_7$-*b*-PVBTOE$_{23}$ (**P**(**27**-*alt*-**17**)$_7$-*b*-**P27**$_{23}$) bearing TES-protected propargyl side chains in the alternating block and b) P(VBTOE-*alt*-NPPGM)$_7$-*b*-PVBTOE$_{23}$ (**P**(**27**-*alt*-**31**)$_7$-*b*-**P27**$_{23}$) after TES deprotection by TBAF.

Both polymers were studied in dilute aqueous solution (1.0 g L^{-1}) by turbidimetry and DLS. Like the alternating copolymers of VBTOE with NTMSM and NDM, the alternating

polymers of VBTOE and NTESM were not soluble in water. However, once embedded in a diblock copolymer with a relatively long, hydrophilic PVBTOE block, **P**(**27**-*alt*-**17**)$_7$-*b*-**P27**$_{23}$ gave clear solutions below 22°C without any indication for aggregate formation in DLS (Figure 54a). The reason for the absence of aggregation may be the same than for diblock copolymers from VBTOE and NTMSM or NDM (*vide supra*). Above 22°C **P**(**27**-*alt*-**17**)$_7$-*b*-**P27**$_{23}$ showed the formation of aggregates with a hydrodynamic diameter of 190 nm accompanied with a drop in transmittance (Figure 54a) due to the collapse of the P(VBTOE-*alt*-NTESM) block. Again, the cloud point observed for the alternating block is at about 20°C, thus similar to the one of **P**(**27**-*alt*-**15**)$_6$-*b*-**P27**$_{20}$ and **P**(**27**-*alt*-**13**)$_{26}$-*b*-**P27**$_{63}$ indicating that indeed the hydrophobic microdomains determine the onset of aggregation. After passing the initial and relatively broad maximum the D_h dropped to about 70 nm between 40°C and 46°C. The explanation is the same than for the diblock copolymers from VBTOE and NPM (*vide supra*). While turbidity measurements display only one thermally induced transition, DLS showed secondary aggregation at 46°C into particles of about 150 nm as result of the collapse of the PVBTOE shell.

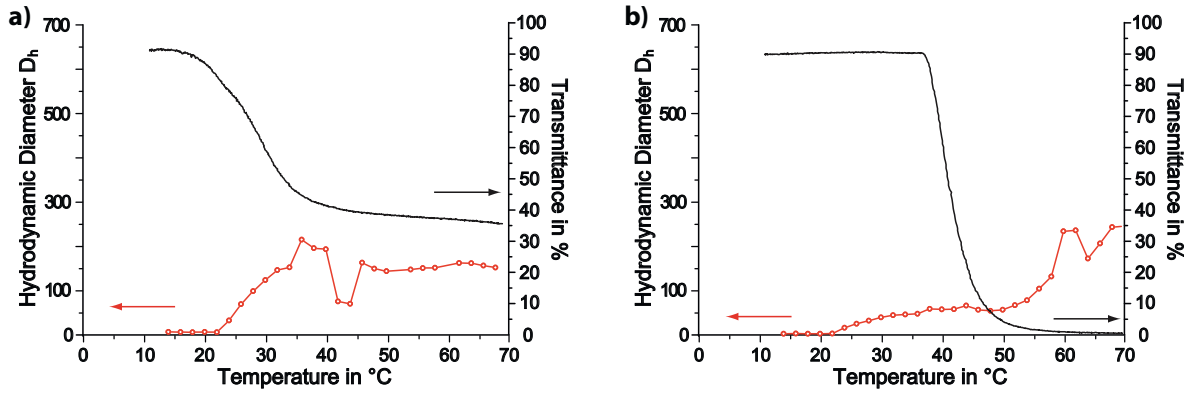

Figure 54: Dynamic light scattering and turbidity measurements of a) P(VBTOE-*alt*-NTESM)$_7$-*b*-PVBTOE$_{23}$ (**P**(**27**-*alt*-**17**)$_7$-*b*-**P27**$_{23}$) and b) P(VBTOE-*alt*-NPPGM)$_7$-*b*-PVBTOE$_{23}$ (**P**(**27**-*alt*-**31**)$_7$-*b*-**P27**$_{23}$) in dilute aqueous solutions (1 g L^{-1}).

The aggregation behavior of **P**(**27**-*alt*-**31**)$_7$-*b*-**P27**$_{23}$ in dilute aqueous solution (1.0 g L^{-1}) was similar to the one of **P**(**27**-*alt*-**17**)$_7$-*b*-**P27**$_{23}$ at least within the low temperature regime (15-35°C). While completely soluble below 22°C, **P**(**27**-*alt*-**31**)$_7$-*b*-**P27**$_{23}$ showed the formation of P(VBTOE-*alt*-NPGM)-core PVBTOE-shell micelles with a hydrodynamic diameter of about 60 nm by passing the first cloud point (Figure 54b). In addition, at about 37°C, the

temperature were the hydrodynamic diameter leveled off to reach a plateau, a single, sharp drop in transmittance was observed. With increasing temperature the aggregation pathway of **P**(**27**-*alt*-**31**)$_7$-*b*-**P27**$_{23}$ differed from the one of **P**(**27**-*alt*-**17**)$_7$-*b*-**P27**$_{23}$. The second phase transition, the collapse of the PVBTOE shell, was observed only at 56°C, hence 14°C above the one of **P**(**27**-*alt*-**31**)$_7$-*b*-**P27**$_{23}$ and induced a drastic increase of D_h from 60 nm to about 230 nm. Again, the observed clustering of the initially formed micelles results from destabilization of the aggregates after the phase transition of the solubilizing shell.

3.4.5 ABA and BAB Triblock Copolymers

Taking this general synthetic protocol for the one-step formation of double thermosensitive diblock copolymers, similar binary triblock copolymers can be synthesized using a bifunctional initiator (Scheme 26). Starting with a reaction mixture of VBTOE and a maleimide, double thermoresponsive BAB triblock copolymers can be synthesized within a single polymerization step. Here B represents the PVBTOE and A the alternating block.

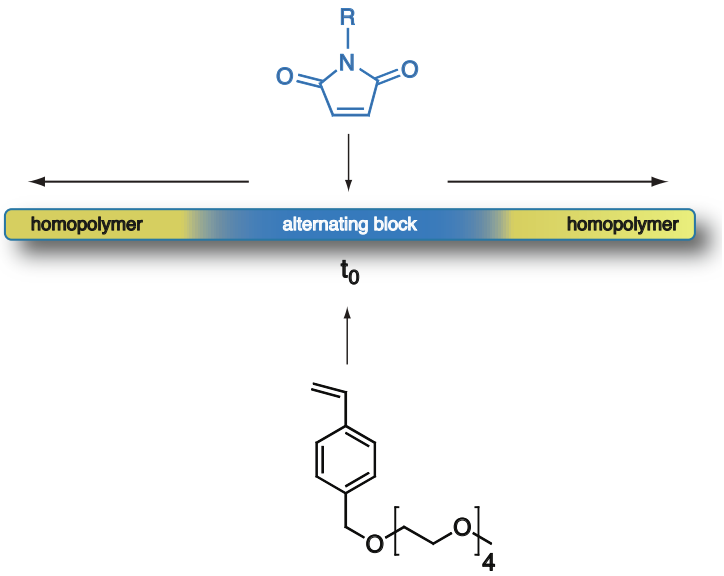

Scheme 26: Schematically shown one-step synthesis of BAB triblock copolymers with two different LCST. A represents the alternating block; B represents the homopolymer block of VBTOE

With the bifunctional ATRP initiator **29** a double thermoresponsive BAB triblock copolymers from VBTOE and NPM was synthesized (Table 3.8). The block copolymer was analyzed by a combination of ^{1}H NMR spectroscopy and SEC.

Table 3.8: Synthesis data of binary BAB triblock copolymers obtained by a one-step polymerization.

Polymer	CRP	M_n, theor.[a]	M_n[b]	$M_{n,app}$[c]	PDI
P27$_{10}$-*b*-**P**(**27**-*alt*-**11**)$_8$-*b*-**P27**$_{10}$	ATRP (**29**)	8900		11000	1.84

[a] Determined gravimetrically. [b] Calculated molar mass from ^{1}H NMR spectroscopy by integration of the aromatic TMS-peak against a peak of the polymer (end group analysis). [c] Determined by size exclusion chromatography (SEC).

The aggregation behavior of **P27**$_{10}$-*b*-**P**(**27**-*alt*-**11**)$_8$-*b*-**P27**$_{10}$ in dilute aqueous solution was found to be similar to the one usually observed for block copolymers obtained from sequential controlled radical polymerization techniques. Hence, **P27**$_{10}$-*b*-**P**(**27**-*alt*-**11**)$_8$-*b*-**P27**$_{10}$ showed the collapse of the middle P(VBTOE-*alt*-NPM) block and aggregation when dissolved in water (1.0 g mol^{-1}) and heated above 24-26°C. After passing an initial maximum the DLS curved dropped and showed aggregates with a D_h of 140 nm together with a drop in transmittance (Figure 55). Before the DLS curve leveled off at a certain value, a second pronounced increase in D_h is seen at 44°C leading to particles with a hydrodynamic diameter of about 540 nm.

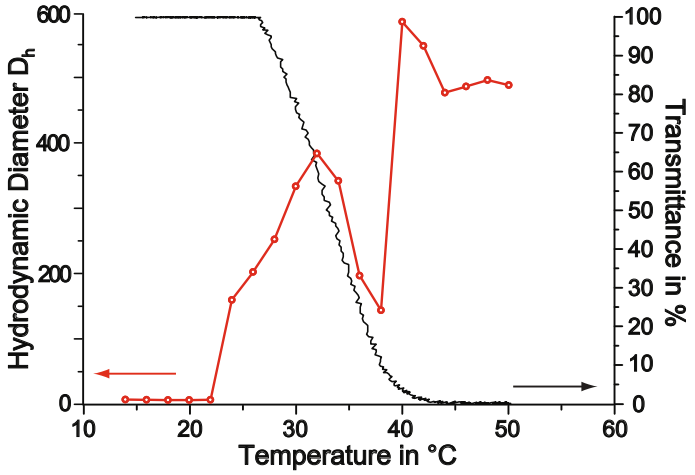

Figure 55: Turbidimetry and dynamic light scattering measurements of **P27**$_{10}$-*b*-**P**(**27**-*alt*-**11**)$_8$-*b*-**P27**$_{10}$ in dilute aqueous solution at concentrations of 1.0 g L^{-1}.

Due to the blurring of the two phase transition temperatures in this case it can not be decided whether the collapse of the alternating middle block leads to the formation of mi-

celles or clusters. The phase transition of the PVBTOE shell above 44°C induced secondary aggregation due to destabilization of the formed particles. Likewise, ABA triblock copolymers could be obtained by carrying out first the homopolymerization of VBTOE with a bifunctional initiator followed by the addition of a maleimide at time t_1 (Scheme 27).

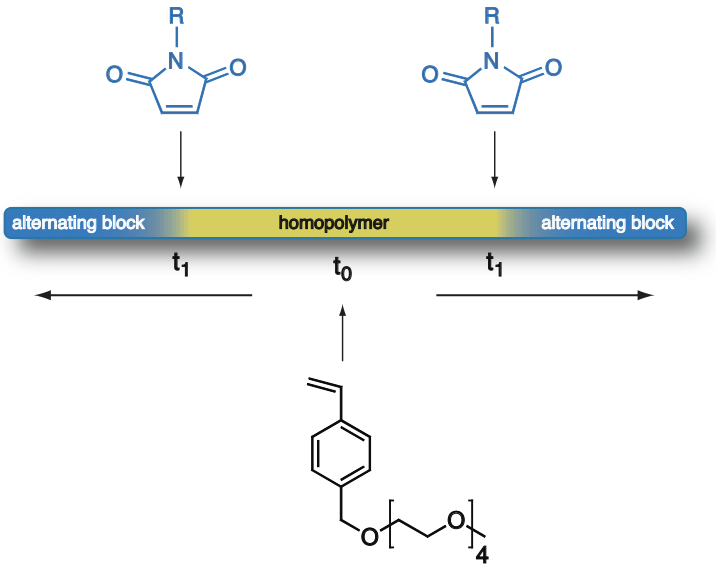

Scheme 27: Schematically shown one-step synthesis of ABA triblock copolymers with two different LCST. A represents the alternating block; B represents the homopolymer block of VBTOE

Here an excess of added maleimide was used to avoid the complete consumption of the maleimide and possible formation of an additional terminal PVBTOE block. However, the polymerization turned out to be relatively slow in the final stages that only few maleimide monomers were consumed resulting in ABA triblock copolymers with very short alternating low-LCST blocks at each terminus. Furthermore, SEC analysis showed a bimodal molar mass distribution. The ATRP initiator **28** (Scheme 23) may be prone to hydrolytic or alcoholytic cleavage during the polymerization in triethylene glycol at 110°C. However, the SEC curve showed a second maximum at ten times higher molar masses, indicating that chain transfer or disproportionation reactions take place rather than cleavage of the initiator which would result in halving of the molar mass.

Table 3.9: Synthesis data of binary ABA triblock copolymers obtained by a one-step protocol.

Polymer	CRP	M_n, theor.[a]	M_n[b]	$M_{n,app}$[c]	PDI
P(**27**-*alt*-**11**)$_2$-*b*-**P27**$_{80}$-*b*-**P**(**27**-*alt*-**11**)$_2$	ATRP (**28**)	27000		13600	5.87

[a] Determined gravimetrically. [b] Calculated molar mass from ^{1}H NMR spectroscopy by integration of the aromatic TMS-peak against a peak of the polymer (end group analysis). [c] Determined by size exclusion chromatography (SEC).

However, although only 1-2 maleimide units were incorporated into both ends aggregation above 20°C was observed for **P**(**27**-*alt*-**11**)$_2$-*b*-**P27**$_{80}$-*b*-**P**(**27**-*alt*-**11**)$_2$. Dynamic light scattering of aqueous solutions at a concentration of 1.0 g L^{-1} revealed the formation of aggregates of about 20 nm (Figure 56). Presumably, the maleimide units induce a thermal collapse of very short segments at each terminus resulting in looping of the long PVBTOE middle blocks as known from amphiphilic ABA terpolymers obtained by a classical stepwise synthesis. At this temperature no changes in transmittance were observed. Further heating then led to secondary aggregation into micellar clusters of 500-600 nm above 36°C accompanied with a drop in transmittance due to the collapse of the PVBTOE block.

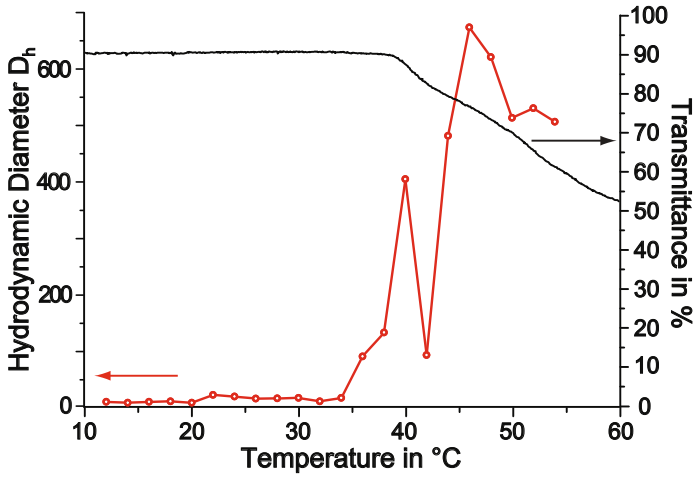

Figure 56: Turbidimetry and dynamic light scattering measurements of **P**(**27**-*alt*-**11**)$_2$-*b*-**P27**$_{80}$-*b*-**P**(**27**-*alt*-**11**)$_2$ in dilute aqueous solution at concentrations of 1.0 g L^{-1}.

Thus, above the first phase transition temperature of the two chain ends of **P**(**27**-*alt*-**11**)$_2$-*b*-**P27**$_{80}$-*b*-**P**(**27**-*alt*-**11**)$_2$ the formation of flower-like micelles is assumed. Such aggregation behavior is not surprising since several reports on PS-PNIPAM-PS show that even very short polystyrene ends are able to induce the formation of flower-like micelles. Taking the contour length of **P**(**27**-*alt*-**11**)$_2$-*b*-**P27**$_{80}$-*b*-**P**(**27**-*alt*-**11**)$_2$ with about 20 nm into account the resulting aggregates show about half of the expected size for star-like micelles. Consequently, **P**(**27**-*alt*-**11**)$_2$-*b*-**P27**$_{80}$-*b*-**P**(**27**-*alt*-**11**)$_2$ indeed seems to form flower-like micelles which cluster into larger particles above the cloud point of the PVBTOE block (Scheme 28).

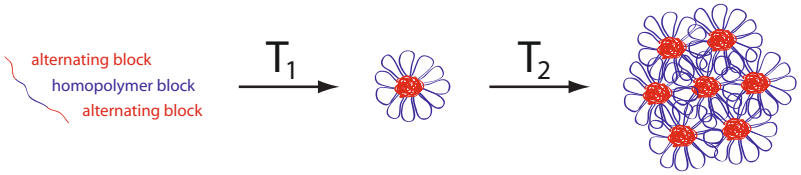

Scheme 28: Schematic representation of the suggested aggregation pathway of **P**(**27**-*alt*-**11**)$_2$-*b*-**P27**$_{80}$-*b*-**P**(**27**-*alt*-**11**)$_2$.

4 Conclusions

The synthesis of double thermosensitive diblock copolymers as well as triple thermoresponsive triblock copolymers was successful and multi-step aggregation behavior could be observed in dilute solution for all polymers. The twofold TMS-labeled RAFT agents used for the synthesis of multiple thermoresponsive block copolymers turned out to be a very powerful tool for the determination of the molar mass and the residual end group functionality *via* routine ^{1}H NMR spectroscopy. By a proper choice of monomers, which show distinct singlet signals in ^{1}H NMR spectroscopy, not only the relative but the absolute composition could be determined. The increasing loss of end group functionality became obvious during the subsequent polymerization toward triblock copolymers which would not be visible from commonly used RAFT agents. This information is crucial in order to synthesize high quality block copolymers. Especially for the study of the self-assembly in dilute aqueous solution of such multi responsive block copolymers it is desirable to minimize homo- and diblock copolymer impurities in the final products since these will inevitably distort the aggregation behavior.

The double thermoresponsive diblock copolymers obtained by RAFT polymerization showed two distinct transitions corresponding to the cloud points of the blocks within the polymers. Furthermore, the relative length of the block was found to be crucial in order to obtain micellar aggregates over cluster formation. In the non-ionic diblock copolymers obtained from RAFT polymerization, a minimum ratio of 1 : 1 between the hydrophilic and hydrophobic blocks seems necessary for efficient micellar stabilization. Beside turbidimetry and DLS, temperature dependent NMR spectroscopy was suitable for further investigations of the step-wise aggregation process on a molecular level. The measurements revealed that the phase transitions proceed gradually. Instead of an all-or-none transition, the dehydration of the polymer blocks continues over a relatively broad temperature range and fully dehydrated states were not even found at temperatures around 90°C. This suggests that even the collapsed cores of block copolymer micelles contain a certain amount of water. In addition, the TMS-labeled end groups could be used to gain more information about the aggregation behavior of these block copolymers in water. Especially for the diblock copoly-

mers of PNPAM and PNEAM, the NMR resonances corresponding to the two complementary TMS-labeled end groups showed attenuation and peak splitting which could be correlated with the self-organization process. Thus, the twofold TMS-labeled RAFT agents used are not only efficient for the determination of the molar mass and residual end group functionality but act also as temperature sensitive NMR-probe for the step-wise self-assembly of the diblock copolymers under investigation.

Due to the increasing loss of functional end groups during the synthesis of triple thermosensitive triblock copolymers in all possible block sequences, the crude products were purified by dialysis before studying their self-assembly in aqueous solution. The observed multistep self-assembly of these triple thermoresponsive triblock copolymers in dilute solution was found to depend sensitively on the block sequence. The collapse of the low-LCST block only resulted in aggregation when it was placed at one terminus of the triblock copolymers. Placed in the middle, the collapse of the PNPAM block led to the formation of unimolecular micelles, stabilized by the two terminal hydrophilic blocks. Above the second thermal transition, all polymers showed particles consisting presumably of clustered micelles, reflecting the high tendency for cluster formation. As observed for the diblock copolymers, the TMS-labeled end group provided further information about the self-organization process also for the terpolymers, although the interpretation of the NMR data was complicated due to clustering. In addition, the carrier abilities of the triple responsive triblock copolymers for hydrophobic agents were probed with the solvatochromic fluorescence dye Nile Red. Upon passing the first thermal transition, the block copolymers are capable of solubilizing Nile Red. In the case of block copolymers with sequences ABC or ACB, which bear the low-LCST block at one terminus, notable amounts of dye are solubilized already at this stage. In contrast, the hydrophobic probe is much less efficiently incorporated by the BAC triblock copolymer, which forms unimolecular micelles. Only after the collapse of the B block, when reaching the second phase transition, aggregation occurred and solubilization became efficient. Thus, in comparison to the other block sequences, the sequence BAC with the low LCST block in the polymer center, is clearly the least performing architecture for multi responsive polymeric amphiphiles if efficient solubilization at low temperatures is aimed at.

The interplay between block sequence and relative block length within the triblock copolymers is complex and further work is needed in order to obtain triple thermoresponsive triblock copolymers in all sequences which show three distinct transitions without clustering.

As found for the diblock copolymers, a 1 : 1 ratio is necessary to avoid cluster formation. Hence, the high-LCST block should be at least twice as long as the mid- and low-LCST block. Accordingly, a minimum ratio of 1 : 1 : 2 with a long high-LCST block may give triple thermoresponsive terpolymers which show the formation of single micelles.

Due to the observed increasing loss in end group functionality during the successive polymerization of triblock copolymers, a novel concept for the one-step synthesis of multi responsive block copolymers was developed. This allowed to synthesize double thermoresponsive di- and triblock copolymers in a single polymerization step. Since the phase transition temperature of a thermoresponsive styrene derivative could be varied upon copolymerization with different N-substituted maleimides, an excess of the styrene compound gave double thermoresponsive tapered block copolymers by a one-pot procedure. These block copolymers showed temperature induced aggregation behavior in dilute aqueous solution similar to block copolymers obtained by the classical sequential approach, thus indirectly proving the formation of diblock copolymers bearing two blocks with different LCST. Interestingly, by the use of long hydrophobic maleimide residues, the alternating chains formed a kind of polysoap-like structure when dissolved in water, which showed cloud points no longer dependent on the chemical nature of the substituent but on the hydrophobic microdomains. In addition, the use of bifunctional ATRP initiators and an excess of 4-vinylbenzyl methoxytetrakis(oxyethylene) ether (VBTOE) led to double thermosensitive binary triblock copolymers in one step, too. Also these block copolymers showed temperature induced two-step aggregation behavior comparable to classical systems. With this concept in hand, also the one-step synthesis of triblock copolymers bearing three different LCST can be envisioned. Sequential addition of two differently substituted maleimides in the beginning and at the end of the polymerization, will result in a tapered triblock copolymer with two different alternating terminal blocks and a homopolymer block in the middle. Taking potential applications of “smart“ block copolymers into account, the one-step synthesis is of particular interest in terms of reducing the costs for the production. Furthermore, this approach is not limited to styrene(derivatives) and maleimides but can be applied to any monomer pair which undergoes alternating copolymerization.

5 Experimental

5.1 Instrumentation

SEC Measurements. The set-up of size exclusion chromatography (SEC) consisted of an Agilent 1200 isocratic pump, an Agilent 1200 refractive index detector and two GRAM columns (10μm, 8 mm * 300 mm, pore sizes 100 and 1000; PSS GmbH, Mainz/Germany), eluent N,N-dimethylacetamide containing 0.1% LiBr, column temperature of 45°C, calibration by low polydispersity polystyrene standards (PSS GmbH, Mainz/Germany).

Turbidity Measurements. Turbidity measurements were performed on a Tepper TP1 photometer (= 670 nm) with a heating rate of 1°C per min at concentrations of 1 gL^{-1}.

DLS Measurements. Dynamic light scattering was performed on a Malvern HPPS-ET equipped with a He-Ne laser (= 633 nm) at concentrations of 1 gL^{-1}, using the backscattering mode at a fixed angle of 173°.

TEM Measurements. Transmission electron micrographs were taken with a Philips Tecnai F20 transmission electron microscope (FEI company, Oregon, USA). Samples were prepared at ambient temperature of 45°C and saturated humidity, by placing droplets of the polymer solutions on hydrophilized carbon filmed copper grids, staining with phosphotungstic acid, and air-drying in one set of preparation or kept unstained, but shadowed with platinum/carbon.

Temperature Dependent NMR Spectroscopy. Temperature dependent NMR spectroscopy was done on a Bruker 500 spectrometer from 16°C to 80°C with an interval of 2°C, an equilibration time of 10 min, at a concentration of 10 gL^{-1}.

Temperature Dependent Fluorescence Spectroscopy. Fluorescence spectroscopy used an instrument FL920 (Edinburgh Instruments) equipped with a Xe900 source; excitation wavelength 550 nm, slit width 2.0 nm. Scans were performed from 560-760 nm in 1 nm steps with a dwell time of 0.30 s. Emission spectra were measured with temperature intervals of 2°C and an equilibration time of 10 min between each measurement. The polymer samples were prepared by agitating 4 mL of dilute solutions of 0.1 g L^{-1} in the presence of 1 mg of Nile Red for 12 h before filtering the dye off, all operations being performed at 14°C.

5.2 General Procedures

General Procedures. Unless otherwise noted, all reactions were carried out in dried Schlenk glassware in an inert N_2 atmosphere. All reagents were purchased as reagent grade and used without further purification. Solvents were purchased as reagent grade and distilled prior to use. Ether, toluene and THF were dried over sodium/benzophenone, dichloromethane over CaH_2. The solvents were freshly distilled and stored over molecular sieves prior to use. NMR spectroscopy was carried out on a Bruker Avance 300 spectrometer operating at a frequency of 300.23 MHz for ^{1}H and 75.49 MHz for ^{13}C nuclei.

General Sequential RAFT Polymerization. In a typical procedure, N-propylacrylamide (3.0 g, 26.5 mmol), 4-(trimethylsilyl)benzyl 4'-(trimethylsilyl)butanedithioate (45 mg, 0.13 mmol) and AIBN (2.0 mg, 0.012 mmol) were dissolved in dry THF (15 mL) in a 10 mL Schlenk tube. The mixture was degassed by three freeze-pump-thaw cycles, and polymerized for 5 h at 65°C. Then, the collected reaction mixture was precipitated twice into diethylether to yield poly(N-propylacrylamide)$_{137}$ as slightly yellow solid (1.9 g, 63%).
Block copolymers were obtained following similar protocol using the homo- and diblock copolymers as macroRAFT agents.

General One-Step RAFT Polymerization of Alternating and Diblock Copolymers. In a typical procedure, 4-vinylbenzyl methoxytetrakis(oxyethylene) ether (200 mg, 0.62 mmol), 4-(trimethylsilyl)benzyl 3'-(trimethylsilyl)propyl trithiocarbonate (4.8 mg, 0.012 mmol), N-propylmaleimide (NPM) (86 mg, 0.62 mmol) and V30 (0.5 mg, 0.004 mmol) were dissolved

in triethylene glycol (1.4 g) and purged with nitrogen for 20 min. The polymerization was carried out at 100°C for 4 d before the reaction mixture was purified by dialysis using a nominal cut off of 4000-6000 g mol^{-1}. P(VBTOE-*alt*-NPM)$_{43}$ was obtained as brown viscous oil (70%).
Tapered diblock copolymers obtained by RAFT polymerization followed the same protocol using an excess of VBTOE.

General ATRP Polymerization. In a 5 mL round bottom flask, styrene (1.0 g, 9.60 mmol) and 3- or 4-(trimethylsilyl)benzylbromide (23.4 mg, 0.096 mmol) were degassed by purging with N_2 for 15 min. Then, the mixture was transferred under N_2 into a 10 mL round bottom flask with CuBr (13.8 mg, 0.096 mmol) and 4,4'-dinonyl-2,2'-bipyridine (78.5 mg, 0.192 mmol). The brown solution was polymerized at 110°C for given temperatures, diluted with THF (1.0 mL) and precipitated three times into MeOH to yield polystyrene as a colorless solid.

General One-Step ATRP Polymerization of Alternating and Diblock Copolymers. In a 5 mL round bottom flask 4-vinylbenzyl methoxytetrakis(oxyethylene) ether (260 mg, 0.80 mmol), 1-bromoethylbenzene (1.3 mg, 0.007 mmol), and HMTETA (2.1 mg, 0.019 mmol) were dissolved in triethylene glycol (520 mg) and purged with N_2 for 20 min. Then, the mixture was transferred under N_2 into a 5 mL round bottom flask with CuBr (2.9 mg, 0.01 mmol) and N,N-maleoyl-L-glycine *tert.*-butylester (126 mg, 0.6 mmol). The polymerization was carried out at 110°C for 60 h. The reaction mixture was purified by dialysis (cut off 4000-6000 g mol^{-1}) to yield P(VBTOE-*alt*-NtBGlyM)$_{34}$ as brown oil (130 mg, 34%).
Diblock copolymers were obtained using an excess of 4-vinylbenzyl methoxytetrakis(oxyethylene) ether. Binary triblock copolymers were obtained using an excess of 4-vinylbenzyl methoxytetrakis(oxyethylene) ether and an bifunctional ATRP initiator.

5.3 RAFT-Agents and ATRP Initiators

Tri(methylsilyl)propyl magnesiumchloride.[234] Dry THF (20 mL) was placed in a three-neck flask under argon atmosphere. Then, magnesium swarf (0.62 g, 25 mmol) and catalytic amounts of iodine were added. The reaction mixture was stirred for 30 min at r. t. After the addition of 3-chloropropyl trimethylsilane (3.79 g, 25 mmol) the solution was stirred for 1 h at r. t. Since no reaction took place two drops of 1,2-dibromoethane was added to the reaction without stirring and led for 20 min. Afterward, the reaction mixture was stirred another 24 h at r.t. until most of the magnesium was consumed. The formed tri(methylsilyl)propyl magnesiumchloride in dry THF was taken up with a syringe and used in the next step without purification.

4-(Trimethylsilyl)benzyl-3'-(trimethylsilyl)propyl-dithioate (1).[234] Tri(methylsilyl)-propyl magnesiumchloride (12.5 mmol) in dry THF (20 mL) was added to a Schlenk flask and carbondisulfide (0.90 g, 11.8 mmol) was added dropwise via a syringe. The solution was stirred at r.t. for 90 min and m-(trimethylsilyl)benzylbromid (1.81 g, 7.44 mmol) was added dropwise via a syringe. Then, the reaction mixture was stirred at r.t. over night. After addition of distilled water and hexane the residual THF was removed in vacuo, the formed colorless precipitate ($MgX_2 \cdot 4THF$) was filtered off, the organic phase was separated, and the aqueous phase was extracted three times with hexane (50 mL). Then, the combined organic phases were washed with distilled water (20 mL), dried over $MgSO_4$, and concentrated in vacuo. The crude product (red-brown oil) was purified by column chromatography (silica gel, hexane/toluene 5:1) affording 4-(trimethylsilyl)benzyl 4'-(trimethylsilyl)propyl-dithioate (1.81 g, 68.6%) as a yellow-brown oil.

^{1}HNMR (300 MHz, $CDCl_3$): δ = 0.0 (s, 9H, $CH_2Si(CH_3)_3$), 0.27 (s, 9H, $ArSi(CH_3)_3$), 0.55-0.61 (m, 2H, $CH_2Si(CH_3)_3$), 1.81-1.92 (m, 2H, $CH_2CH_2Si(CH_3)_3$), 3.05 (t, J = 7.35 Hz, 2H, $CSCH_2$), 4.47 (s, 2H, CH_2SCS), 7.17-7.46 (m, 4H, aryl*H*). R_f: 0.5-0.6 (Hexane/Toluene 4:1).

3-(Trimethylsilyl)benzyl-3'-(trimethylsilyl)propyl dithioate (2).[234] Tri(methylsilyl)-propyl magnesiumchloride (12.5 mmol) in dry THF (20 mL) was added to a Schlenk flask and carbondisulfide (0.91 g, 12 mmol) was added dropwise via a syringe. The solution was stirred at r. t. for 90 min and m-(trimethylsilyl)benzylbromid (1.80 g, 7.40 mmol) was added dropwise via a syringe. Then, the reaction mixture was stirred at r. t. over night. After addition of distilled water and hexane the residual THF was removed in vacuo, the formed colorless precipitate ($MgX_2 \cdot 4THF$) was filtered off, the organic phase was separated, and the aqueous phase was extracted three times with hexane (50 mL). Then, the combined organic phases were washed with distilled water (20 mL), dried over $MgSO_4$, and concentrated in vacuo. The crude product (red-brown oil) was purified by column chromatography (silica gel, hexane/toluene 5:1) affording 3-(trimethylsilyl)benzyl-3'-(trimethylsilyl)propyl dithioate (2.0 g, 76.6%) as a yellow-brown oil.
^{1}HNMR (300 MHz, $CDCl_3$): δ = 0.00 (s, 9H, $CH_2Si(CH_3)_3$), 0.27 (s, 9H, $ArSi(CH_3)_3$), 0.55-0.61 (m, 2H, $CH_2Si(CH_3)_3$), 1.81-1.92 (m, 2H, $CH_2CH_2Si(CH_3)_3$), 3.05 (t, J = 7.5 Hz, 2H, $CSCH_2$), 4.46 (s, 2H, CH_2SCS), 7.17-7.50 (m, 4H, aryl*H*). R_f: 0.5-0.6 (Hexane/Toluene 4:1).

Bis[1-(4-bromoisobutyryloxy)] benzene (28). In a 100 mL three-neck flask hydrochinone (1.1 g, 10 mol) was dissolved in 40 mL dry THF, triethylamine (2.33 g, 23 mol) was added and the reaction mixture was cooled to 0°C. Then, bromoisobutyrylbromide (4.68 g, 20.4 mol) was added and the reaction was stirred at room temperature for 16 h, quenched with MeOH, filtrated and concentrated in vacuo. The obtained solid was recrystallized two times from MeOH to yield bis[1-(4-bromoisobutyryloxy)] benzeneas colorless solid (2.37 g, 58%).
^{1}HNMR (300 MHz, $CDCl_3$): δ = 2.06 (s, 12H, CCH_3), 7.18 (s, 4H, aryl*H*). ^{13}CNMR (75MHz, $CDCl_3$): δ = 30.4 (4 CCH_3), 55.0 (2 CCH_3), 121.8 (4 aryl*C*H), 148.2 (2 aryl*C*O), 169.8 (*C*=O).

5.4 Monomers

5.4.1 Acrylamides

N-Ethylacrylamide (9). Ethylamine(9.20 g, 0.20 mol) was cooled to -25°C, transferred into a dried 250 mL Schlenk flask and cooled to -40°C. Then, 80 mL dry dichloromethane and dry triethylamine (21.10 g, 0.21 mol) were added. After the mixture reached -40°C, acryloyl chloride(18.35 g, 0.20 mol) in 40 mL dry dichloromethane were added dropwise. The reaction was stirred at -40°C over night, heated to room temperature and stirred for additional 2 h. The precipitated salt was filtered off and the solvents were removed in vacuo. The crude product was distilled in vacuo at 100°C to yield N-ethylacrylamide as a slightly brown liquid (10.40 g, 53%) which solidified upon storage in the freezer.
^{1}HNMR (300 MHz, $CDCl_3$): δ = 1.07 (t, J = 7.2 Hz, 3H, CH_2CH_3), 3.23-3.27 (m, 2H, CH_2CH_3), 5.50 (dd, J = 7.2 Hz, 1H, CH_2CH), 6.13-6.15 (m, 2H, CH_2CH, CH_2CH), 6.98 (bs, 1H, NH). ^{13}CNMR (75MHz, $CDCl_3$): δ = 14.5 (CH_3), 34.3 (CH_2CH_3), 125.5 (CH_2CH), 131.2 (CH_2CH), 165.8 (C=O).

N-Propylacrylamide (7). Acryloyl chloride (9.11 g, 0.10 mol) was dissolved in 20 mL dry benzene and cooled in a dried 250 mL Schlenk flask to 0°C. Then, dry triethylamine (11.36 g, 0.11 mol), propylamine (5.91 g, 0.10 mol) in 20 mLdry benzene were added dropwise. The solution was allowed to reach room temperature and stirred for 1 h. The precipitated salt was filtered off and the solvents were removed in vacuo. The crude product was distilled in vacuo at 105°C to give N-propylacrylamide as a slightly yellow liquid (6.54 g, 58%) which solidifies upon storage in the freezer.
^{1}HNMR (300 MHz, $CDCl_3$): δ = 0.89 (t, J = 7.4 Hz, 3H, CH_2CH_3), 1.46-1.58 (m, 2H, CH_2CH_3), 3.20-3.27 (m, 2H, $CH_2CH_2CH_3$), 5.54-5.58 (m, 1H, CH_2CH), 6.08-6.25 (m, 2H, CH_2CH, CH_2CH), 6.41 (bs, 1H, NH). ^{13}CNMR (75MHz, $CDCl_3$): δ = 11.4 (CH_3), 22.8 (CH_2CH_3), 41.4 ($CH_2CH_2CH_3$), 125.8 (CH_2CH), 131.3 (CH_2CH), 165.9 (C=O).

5.4.2 Acrylates

Methoxydi(ethylene glycol) acrylate (8).[240] Di(ethylene glycol) monomethyl ether (10.40 g, 0.09 mol) and dry triethylamine (10.00 g, 0.10 mol) were dissolved in dry dichloromethane (80 mL) and cooled to 0°C. Then, acryloyl chloride (7.98 g, 0.09 mol) in 30 mL of dry dichloromethane was added dropwise. The reaction was stirred at 0°C for 30 min, allowed to reach room temperature and stirred over night. The precipitated salt was filtered off, the solution was washed three times with H_2O and three times with aq. $NaHCO_3$. The solvent was removed in vacuo and the crude product was purified by column chromatography (silica gel, ethylacetate) to give methoxydi(ethylene glycol) acrylate as a colorless liquid (14.66 g, 96%).

^{1}HNMR (300 MHz, $CDCl_3$): δ = 3.35 (s, 3H, OCH_3), 3.53 (m, 2H, CH_2OCH$_3$), 3.63 (m, 2H, CH_2CH$_2$OCH$_3$), 3.72 (m, 2H, CH_2O(CH$_2$)$_2$OCH$_3$), 4.30 (m, 2H, CH$_2$CHCOOCH_2), 5.80 (dd, J = 10.4 Hz, 1H, CH_2CHCO), 6.12 (dd, J = 17.3 Hz, 1H, CH$_2$CH), 6.40 (dd, J = 17.4 Hz, 1H, CH_2CH). ^{13}CNMR (75 MHz, DMSO-d$_6$): d = 59.2 (OCH$_3$), 63.8 (CH$_2$COO), 69.3 (CH$_2$CH$_2$COO), 70.7 (CH$_2$CH$_2$OCH$_3$), 72.1 (CH$_2$OCH$_3$), 128.5 (CHCH$_2$), 131.1 (CH$_2$CH), 166.3 (C=O). R$_f$: 0.6 (Ethylacetate).

5.4.3 Styrenics

4-Vinylbenzyl methoxytetrakis(oxyethylene) ether (27).[267] In a 250 mL Schlenk flask tetra(ethylene glycol) monomethyl ether (10.0 g, 48 mmol) and NaH (1.8 g, 71 mmol) were dissolved in dry THF (100 mL) and stirred for 1 h at room temperature. Then, 4-vinylbenzyl chloride was added dropwise and the reaction mixture was stirred at 75°C over night. The reaction was quenched with water, extracted three times with $CHCl_3$ and concentrated in vacuo. The crude product was purified by column chromatography (EE:Hex 10:1) to yield 4-vinylbenzyl methoxytetrakis(oxyethylene) ether as slightly yellow oil (11.8 g, 76%).
^{1}HNMR (300 MHz,): δ = 3.36 (s, 3H, OCH_3), 3.52-3.65 (m, 16H, 8 OCH_2), 4.54 (s, 2H, ArCH_2), 5.22 (dd, J = 10.95 Hz, 1H, CH_2CH), 5.73 (dd, J = 17.55 Hz, 1H, CH_2CH), 6.69 (dd, J = 17.7 Hz, 1H, CH_2CH), 7.28 (d, J = 8.1 Hz, 2H, ArH), 7.37 (d, J = 8.1 Hz, 2H, ArH). ^{13}CNMR (75 Mhz, $CDCl_3$): δ = 59.0 (OCH_3), 69.4-70.6 (7 CH_2), 71.9 (CH_2OMe), 72.9 (ArCH_2), 113.7 (CH_2CH), 126.2 (2 ArC), 127.9 (2 ArC), 136.5 (ArCCH), 136.9 (ArCCH_2), 137.9 (CH_2CH). R_f: 0.3 (EE).

5.4.4 Maleimides

N-(3-trimethylsilyl)propyl maleic acid (14). Maleic anhydride (1.9 g, 19.5 mmol) was dissolved in DMF (5 mL) and aminopropyltrimethylsilane (2.5 g, 19.1 mmol) was added. The solution was stirred at room temperature over night, precipitated into H_2O, filtrated and washed three times with H_2O. The crude product was recrystallized three times from H_2O to yield N-(3-trimethylsilyl)propyl maleic acid as colorless solid (4.35 g, 100%).
^{1}HNMR (300 MHz, $CDCl_3$): δ = 0.01 (s, 9H, Si(CH_3)$_3$), 0.48-0.54 (m, 2H, CH_2Si), 1.53-1.63 (m, 2H, CH_2CH_2), 3.30-3.37 (m, 2H, NCH_2), 6.30 (d, J = 12.9 Hz, 1H, CHCOOH), 6.51 (d, J = 12.6 Hz, 1H, CHCO), 8.12 (bs, 1H, NH). ^{13}CNMR (75 MHz, $CDCl_3$): δ = -1.7 (Si(CH$_3$)$_3$), 13.9 (CH$_2$Si(CH$_3$)$_3$), 23.5 (NHCH$_2$$CH_2$), 43.7 (NH$CH_2$), 132.4 ($C$HCO), 135.7 ($C$HCOOH), 166.2 ($C$OOH), 166.5 ($C$O). Anal. calcd for $C_{10}H_{19}NO_3Si$: C, 52.37%; H, 8.35%; N, 6.11%; found: C, 51.70%; H, 8.89%; N, 6.09%. HRMS (ESI): calcd for $C_{10}H_{20}NO_3Si$ ([MH$^+$]) 230.1212; found 230.1216.

N-(3-trimethylsilyl)propyl maleimide (15).[264] N-(3-Trimethylsilyl)propyl maleic acid (500 mg, 2.2 mmol) was dissolved in toluene (20 mL) under argon atmosphere. The solution was heated to 80°C and $ZnBr_2$ (500 mg, 2.2 mmol) was added. Then, hexamethyl disilazane (720 mg, 4.4 mmol) in toluene (10 mL) was added dropwise and the reaction mixture was stirred at 80°C for 6 h and at room temperature for 15 h. The solution was concentrated in vacuo and the crude product was purified by column chromatography (DCM:MeOH 24:1) to yield N-(3-trimethylsilyl)propyl maleimide (410 mg, 89%) as slightly brown solid.
^{1}HNMR (300 MHz, $CDCl_3$): δ = -0.03 (s, 9H, Si(CH_3)$_3$), 0.42-0.47 (m, 2H, CH_2Si(CH$_3$)$_3$), 1.50-1.61 (m, 2H, NHCH$_2$CH_2), 3.49 (t, J = 7.35 Hz, 2H, NHCH_2), 6.68 (s, 2H, 2 C*H*CO). ^{13}CNMR (75 MHz, $CDCl_3$): δ = -2.1 (Si(*C*H$_3$)$_3$), 13.4 (*C*H$_2$Si(CH$_3$)$_3$), 23.0 (NHCH$_2$*C*H$_2$), 40.7 (N*C*H$_2$), 133.8 (2 *C*H), 170.7 (2 *C*O). Anal. calcd for $C_{10}H_{17}NO_2Si$: C, 56.83%; H, 8.04%; N, 6.62%; found: C, 56.30%; H, 8.02%; N, 6.36%. HRMS (ESI): calcd for $C_{10}H_{18}NO_2Si$ ([MH$^+$]) 212.1107; found 212.1122. R_f: 0.8 (DCM/MeOH 10:1).

Triethylsilylpropargylamine (16). In a 50 mL Schlenk flask proparylamine (1.0 g, 18.1 mmol) was dissolved in dry THF (20 mL) and cooled to -78°C. The solution was stirred for 15 min, *n*-butyl lithium 1.6M in hexane (11.7 mL) was added and the reaction mixture was allowed to reach 0°C. Then, chlorotriethylsilane (1.3 g, 8.6 mmol) was added dropwise and the solution was stirred at room temperature for 2 h. After quenching the reaction with aq. NH_4Cl the THF was removed in vacuo, 1M HCl (50 mL) was added and extracted three times with ethylacetate. The crude product was purified by column chromatography (DCM:MeOH 24:1) to yield triethylsilyl-protected propargylamine (530 mg, 36%) as brown oil.
^{1}HNMR (300 MHz, DMSO-d$_6$): δ = 0.53-0.55 (q, 6H, J = 7.8 Hz, 3 SiCH_2CH$_3$), 0.94 (t, J = 7.8 Hz, 9H, 3 SiCH$_2$CH_3), 3.29 (s, 2H, CH_2NH$_2$). ^{13}CNMR (75 MHz, $CDCl_3$): δ = 3.9 (3 Si*C*H$_2$), 7.1 (3 SiCH$_2$*C*H$_3$), 30.8 (N*C*H$_2$), 88.1 (SiC*C*), 101.5 (Si*C*C). R_f: 0.2 (DCM/MeOH 10:1).

N-(3-Triethylsilyl)propargyl maleimide (17).[264] In a 250 mL Schlenk flask triethylsilylpropargylamine (530 mg, 3.1 mmol) and maleic anhydride (350 mg, 3.5 mmol) were dissolved in toluene (50 mL), stirred at 60°C for 6 h and at room temperature for 12 h. Then, $ZnBr_2$ (710 g, 3.1 mmol) was added, the reaction mixture was heated to 80°C and hexamethyl disilazane (1.25 g, 7.7 mmol) was added dropwise. The solution was stirred for 6 h, cooled to room temperature and stirred for another 12 h. The solvent was removed in vacuo and the crude reaction mixture was purified by column chromatography (EE:Hex 95:5) to yield N-(3-triethylsilyl)propargyl maleimide (150 mg, 19%) as brownish oil.
^{1}HNMR (300 MHz, $CDCl_3$): δ = 0.56 (q, J = 7.6 Hz, 6H, 3 CH_2CH$_3$), 0.95 (t, J = 7.5 Hz, 9H, 3CH_3), 4.30 (s, 2H, NCH_2), 6.74 (s, 2H, 2 C*H*CO). ^{13}CNMR (75 MHz, $CDCl_3$): δ = 3.9 (3 Si*C*H$_2$), 7.1 (3 CH$_2$*C*H$_3$), 27.6 (N*C*H$_2$), 85.6 (SiC*C*), 99.2 (Si*C*C), 134.2 (2 CO*C*H), 169.0 (2 *C*O). Anal. calcd for $C_{13}H_{19}NO_2Si$: C, 62.56%; H, 7.62%; N, 5.61%; found: C, 62.33%; H, 7.56%; N, 5.66%. HRMS (EI): calcd for $C_{13}H_{19}NO_2Si$ ([M$^+$]) 249.1180; found 249.1178. R_f: 0.3 (DCM/MeOH 10:1).

N,N-maleoyl-L-glycine *tert.*-butylester (18).[264] In a 50 mL round bottom flask L-glycine *tert.*-butylester (500 mg, 3.0 mmol) and triethylamine (300 mg, 3.0 mmol) were dissolved in toluene (20 mL), maleic anhydride (293 mg, 2.99 mmol) was added and the reaction mixture was stirred at 60°C for 6 h and at room temperature for 15 h. Then, $ZnBr_2$ (685 mg, 3.0 mmol) was added in one portion, the solution was heated to 80°C and hexamethyl disilazane (1.04 g, 6.4 mmol) in toluene (10 mL) was added dropwise. The reaction mixture was stirred at 80°C for 6 h and at room temperature for 20 h. The solution was concentrated in vacuo and the crude product was purified by column chromatography (DCM:MeOH 24:1) to yield N,N-maleoyl-L-glycine *tert.*-butylester (430 mg, 68%) as colorless solid.
^{1}HNMR (300 MHz, $CDCl_3$): δ = 1.45 (s, 9H, C(CH_3)$_3$), 4.16 (s, 2H, CH_2), 6.77 (s, 2H, 2 C*H*). ^{13}CNMR (75MHz, $CDCl_3$): δ = 27.7 (C(*C*H$_3$)$_3$), 39.2 (*C*H$_2$), 82.6 (*C*(CH$_3$)$_3$), 134.2 (2 *C*H), 165.9 (*C*OO), 169.7 (2 *C*O). Anal. calcd for $C_{10}H_{13}NO_4$: C, 56.87%; H, 6.20%; N, 6.63%; found: C, 56.75%; H, 6.01%; N, 6.64%. HRMS (ESI): calcd for $C_{10}H_{14}NO_4$ ([MH$^+$]) 212.0923; found 212.0930. R_f: 0.7 (DCM/MeOH 10:1).

N,N-maleoyl-L-alanine *tert.*-butylester (19).[264] In a 250 mL round bottom flask L-alanine *tert.*-butylester (2.0 g, 11.3 mmol) and triethylamine (1.1 g, 11.2 mmol) were dissolved in toluene (80 mL) and stirred for 30 min at room temperature. Then, the solution was heated to 60°C, maleic anhydride (1.1 g, 11.3 mmol) was added and the reaction mixture was stirred at 60°C for 8 h and at room temperature for 12 h. After the addition of $ZnBr_2$ the solution was heated to 80°C, hexamethyl disilazane (3.6 g, 22.4 mmol) in toluene (20 mL) was added dropwise and the reaction was stirred for 6 h, cooled to room temperature and stirred for another 12 h. The solution was concentrated in vacuo and the crude product was purified by column chromatography (DCM:MeOH 24:1) to yield N,N-maleoyl-L-alanine *tert.*-butylester (1.75 g, 69%) as colorless solid.

^{1}HNMR (300 MHz, $CDCl_3$): δ = 1.42 (s, 9H, C(CH_3)$_3$), 1.58 (d, J = 7.5 Hz, 3H, CHCH_3), 4.67 (q, J = 7.2 Hz, 1H, CHCH$_3$), 6.71 (s, 2H, 2 CHCO). ^{13}CNMR (75 MHz, $CDCl_3$): δ = 14.9 (*C*H$_3$CH), 27.6 (C(*C*H$_3$)$_3$), 48.0 (*C*HCH$_3$), 82.1 (*C*(CH$_3$)$_3$), 134.0 (2 *C*HCO), 168.3 (2 N*C*O), 169.8 (*C*OO).

N-Ethylthiomethyl maleimide (20).[264] In a 250 mL Schlenk flask methylthioethylamine (2.5 g, 27.4 mmol) and maleic anhydride (2.7 g, 27.4 mmol) were dissolved in toluene (150 mL), stirred at 60°C for 8 h and at room temperature for 12 h. Then, $ZnBr_2$ (6.2 g, 27.4 mmol) was added, the reaction mixture was heated to 80°C and hexamethyl disilazane (8.85 g, 54.8 mmol) was added dropwise. The solution was stirred for 12 h, cooled to room temperature and stirred for another 12 h. The solvent was removed in vacuo and the crude reaction mixture was purified by column chromatography (DCM:MeOH 24:1) to yield N-ethylthiomethyl maleimide (1.1 g, 24%) as yellow oil.

^{1}HNMR (300 MHz, $CDCl_3$): δ = 2.12 (s, 3H, SCH_3), 2.70 (t, J = 6.9 Hz, 2H, SCH_2), 3.73 (t, J = 6.9 Hz, 2H, NCH_2), 6.70 (s, 2H, 2 CHCO). ^{13}CNMR (75 MHz, $CDCl_3$): δ = 14.8 (S*C*H$_3$), 31.9 (S*C*H$_2$), 36.0 (N*C*H$_2$), 133.9 (2 CO*C*H), 170.3 (2 *C*O). R_f: 0.8 (DCM/MeOH 10:1).

N-Ethylsulfoxymethyl maleimide (21).[274] In a 50 mL round bottom flask N-ethylthiomethyl maleimide (500 mg, 2.9 mmol) was added to a 0.5 M solution of $NaIO_4$ in methanol/water (8 mL/22 mL) and stirred at room temperature over night. Then, the solvent was removed in vacuo and the crude reaction mixture was purified by column chromatography (DCM:MeOH 24:1) to yield N-ethylsulfoxymethyl maleimide (170 mg, 31%) as colorless solid.

^{1}HNMR (300 MHz, $CDCl_3$): δ = 2.99 (s, 3H, SOCH_3), 3.33 (t, J = 6.6 Hz, 2H, SOCH_2), 4.04 (t, J = 6.6 Hz, 2H, NCH_2), 6.76 (s, 2H, 2 CHCO). ^{13}CNMR (75 MHz, $CDCl_3$): δ = 31.3 (SOCH$_3$), 40.4 (SOCH$_2$), 51.3 (NCH$_2$), 134.3 (2 COCH), 169.7 (2 CO).

6 References

1. Lakes, R. *Nature* **1993,** *361,* 511-515.
2. Lutz, J.-F. *Polym. Int.* **2006,** *55,* 979-993.
3. Tu, R. S.; Tirrell, M. *Adv. Drug Delivery Rev.* **2004,** *56,* 1537-1563.
4. Förster, S.; Plantenberg, T. *Angew. Chem. Int. Ed.* **2002,** *41,* 688-714.
5. Zhang, L.; Eisenberg, A. *Science* **1995,** *268,* 1728-1731.
6. Förster, S.; Antonietti, M. *Adv. Mater.* **1998,** *10,* 195-217.
7. Won, Y.; Davis, H. T.; Bates, F. S. *Science* **1999,** *283,* 960-963.
8. Discher, D. E.; A., E. *Science* **2002,** *297,* 967-973.
9. Pochan, D. J.; Chen, Z.; Cui, H.; Hales, K.; Qi, K.; Wooley, K. L. *Science* **2004,** *306,* 94-97.
10. Rodriguez-Hernandez, J.; Checot, F.; Gnanou, Y.; Lecommandoux, S. *Prog. Polym. Sci.* **2005,** *30,* 691-724.
11. Moad, G.; Solomon, D. H. *The Chemistry of Free Radical Polymerization;* Pergamon: Oxford, England: 1995.
12. Hawker, C. J.; Bosman, A. W.; Harth, E. *Chem. Rev.* **2001,** *101,* 3661-3688.
13. Matyjaszewski, K.; Xia, J. *Chem. Rev.* **2001,** *101,* 2921-2990.
14. Lowe, A. B.; McCormick, C. L. *Prog. Polym. Sci.* **2007,** *32,* 283-351.
15. Quirk, R. P.; Kinning, D. J.; Fetters, L. J. *Comprehensive Polymer Science;* Pergamon Press, London: 1989.
16. Hammouch, S. O.; Catala, J. M. *Macromol. Rapid Commun.* **1996,** *17,* 149-154.
17. Li, I. Q.; Howell, B. A.; Koster, R. A.; Priddy, D. B. *Macromolecules* **1996,** *29,* 8554-8555.
18. Fukuda, T.; Terauchi, T.; Goto, A.; Ohno, K.; Tsujii, Y.; Yamada, B. *Macromolecules* **1996,** *29,* 6393-6398.
19. Moad, G.; Rizzardo, E. *Macromolecules* **1995,** *28,* 8722-8728.
20. Solomon, D. H. *J. Polym. Sci. Part A: Polym. Chem.* **2005,** *43,* 5748-5764.

21. Moad, G.; Rizzardo, E.; Solomon, D. H. *Macromolecules* **1982,** *15,* 909-914.

22. Solomon, D. H.; Rizzardo, E.; Cacioli, P. **1986,** U.S. Patent, 4.581.429.

23. Georges, M. K.; Veregin, R. P. N.; Kazmaier, P. M.; Hamer, G. K. *Macromolecules* **1993,** *26,* 2987-2988.

24. Fischer, H. *Chem. Rev.* **2001,** *101,* 3581-3610.

25. Benoit, D.; Chaplinski, V.; Braslau, R.; Hawker, C. J. *J. Am. Chem. Soc.* **1999,** *121,* 3904-3920.

26. Kato, M.; Kamigaito, M.; Sawamoto, M.; Higashimura, T. *Macromolecules* **1995,** *28,* 1721-1723.

27. Wang, J.; Matyjaszewski, K. *J. Am. Chem. Soc.* **1995,** *117,* 5614-5615.

28. Matyjaszewski, K.; Davis, K.; Patten, T.; Wei, M. *Tetrahedron* **1997,** *53,* 15321-15329.

29. Wang, J.; Matyjaszewski, K. *Macromolecules* **1995,** *28,* 7572-7573.

30. Wang, W.; Dong, Z.; Xia, P.; Zhang, Q. *Macromol. Rapid Commun.* **1998,** *19,* 647-649.

31. Xia, J.; Matyjaszewski, K. *Macromolecules* **1999,** *32,* 5199-5202.

32. Goto, A.; Fukuda, T. *Macromol. Rapid Commun.* **1999,** *20,* 633-636.

33. Matyjaszewski, K.; Goebelt, B.; Paik, H.-J.; Horwitz, C. P. *Macromolecules* **2001,** *34,* 430-440.

34. Matyjaszewski, K.; Paik, H.-J.; Zhou, P.; Diamanti, S. J. *Macromolecules* **2001,** *34,* 5125-5131.

35. Matyjaszewski, K.; Gaynor, S. G.; Wang, J.-S. *Macromolecules* **1995,** *28,* 2093-2095.

36. Singha, N. K.; Klumperman, B. *Macromol. Rapid Commun.* **2000,** *21,* 1116-1120.

37. Xia, J.; Zhang, X.; Matyjaszewski, K. *ACS Symp. Ser.* **2000,** *760,* 207-223.

38. Jakubowski, W.; Matyjaszewski, K. *Macromolecules* **2005,** *38,* 4139-4146.

39. Jakubowski, W.; Matyjaszewski, K. *Angew. Chem. Int. Ed.* **2006,** *45,* 4482-4486.

40. Mayadunne, R. T. A.; E., R.; Chiefari, J.; Chong, Y. K.; Moad, G.; Thang, S. H. *Macromolecules* **1999,** *32,* 6977-6980.

41. Chong, Y. K.; Le, T. P. T.; Moad, G.; Rizzardo, E.; Thang, S. H. *Macromolecules* **1999,** *32,* 2071-2074.

42. Moad, G.; Chiefari, J.; Chong, Y. K.; Krstina, J.; Mayadunne, R. T. A. Postma, A. *Polym. Int.* **2000,** *49,* 993-1001.

43. Delduc, P.; Tailhan, C.; Zard, S. Z. *J. Chem. Soc. Chem. Commun.* **1988,** 308-310.

44. Zard, S. Z. *Angew. Chem. Int. Ed.* **1997,** *36,* 672-685.

45. Favier, A.; Charreyre, M.-T. *Macromol. Rapid. Commun* **2006,** *27,* 653-692.

46. Schilli, C.; Lanzendorfer, M. G.; Müller, A. H. E. *Macromolecules* **2002,** *35,* 6819-6827.

47. Coote, M.; Izgorodina, E. I.; Cavigliasso, G. E.; Roth, M.; Busch, M.; Barner-Kowollik, C. *Macromolecules* **2006,** *39,* 4585-4591.

48. Thies, A.; Stenzel, M. H.; Davis, T. P.; Coote, M. L.; Barner-Kowollik, C. *Aust. J. Chem.* **2005,** *58,* 437-441.

49. Chong, Y. K.; Krstina, J.; Le, T. P. T.; Moad, G.; Postma, A.; Rizzardo, E. *Macromolecules* **2003,** *36,* 2256-2272.

50. Chiefari, J.; Mayadunne, R. T. A.; Moad, C. L.; Moad, G.; Rizzardo, E.; Postma, A. *Macromolecules* **2003,** *36,* 2273-2283.

51. Francis, R.; Ajayaghosh, A. *Macromolecules* **2000,** *33,* 4699-4704.

52. Donovan, M. S.; Lowe, A. B.; Sumerlin, B. S.; McCormick, C. L. *Macromolecules* **2002,** *35,* 4123-4132.

53. Donovan, M. S.; Lowe, A. B.; Sanford, T. A.; McCormick, C. L. *J. Polym. Sci. Part A: Polym. Chem.* **2003,** *41,* 1262-1281.

54. Baussard, J.-F.; Habib-Jiwan, J.-L.; Laschewsky, A.; Mertoglu, M.; Storsberg, J. *Polymer* **2004,** *45,* 3615-3626.

55. Mertoglu, M.; Laschewsky, A.; Skrabania, K.; Wieland, C. *Macromolecules* **2005,** *38,* 3601-3614.

56. Bivigou-Koumba, A. M.; Kristen, J.; Laschewsky, A.; Müller-Buschbaum, P.; Papadakis, C. M. *Macromol. Chem. Phys.* **2009,** *210,* 565-578.

57. Quinn, J. F.; Barner, L.; Davis, T. P.; Thang, S. H.; Rizzardo, E. *Macromol. Rapid Commun.* **2002,** *23,* 717-721.

58. Quinn, J. F.; Barner, L.; Rizzardo, E.; Davis, T. P. *J. Polym. Sci. Part A: Polym. Chem.* **2002,** *40,* 19-25.

59. Barner-Kowollik, C.; Vana, P.; Quinn, J. F.; Davis, T. P. *J. Polym. Sci. Part A: Polym. Chem.* **2002,** *40,* 1058-1063.

60. Barner-Kowollik, C.; Buback, M.; Charleux, B.; Coote, M. L.; Drache, M.; Fukuda, T.; Goto, A.; Klumperman, B.; Lowe, A. B.; McLeary, J. B.; Moad, G.; Monteiro, M. J.; Sanderson, R. D.; Tonge, M. P.; Vana, P. *J. Polym. Sci. Part A: Polym. Chem.* **2006,** *44,* 5809-5831.

61. Monteiro, M. J.; Bussels, R.; Beuermann, S.; Buback, M. *Aust. J. Chem.* **2002,** *55,* 433-437.

62. Barner-Kowollik, C.; Quinn, J. F.; Nguyen, T. L. U.; Heuts, J. P. A.; Davis, T. P. *Macromolecules* **2001,** *34,* 7849-7857.

63. Davis, T. P.; Barner-Kowollik, C.; Nguyen, T. L. U.; Stenzel, M. H.; Quinn, J. F.; Vana, P. *ACS Symp. Ser.* **2003,** *854,* 551-569.

64. Vana, P.; Quinn, J. F.; Davis, T. P.; Barner-Kowollik, C. *Aust. J. Chem.* **2002,** *55,* 425-431.

65. Prescott, S. W.; Ballard, M. J.; Rizzardo, E.; Gilbert, R. G. *Macromolecules* **2005,** *38,* 4901-4912.

66. Toy, A. A.; Vana, P.; Davis, T. P.; Barner-Kowollik, C. *Macromolecules* **2004,** *37,* 744-751.

67. Feldermann, A.; Toy, A. A.; Davis, T. P.; Stenzel, M. H.; Barner-Kowollik, C. *Polymer* **2005,** *46,* 8448-8457.

68. Calitz, F. M.; McLeary, J. B.; McKenzie, J. M.; Tonge, M. P.; Klumperman, B.; Sanderson, R. D. *Macromolecules* **2003,** *36,* 9687-9690.

69. Buback, M.; Vana, P. *Macromol. Rapid Commum.* **2006,** *27,* 1299-1305.

70. Konkolewicz, D.; Hawkett, B. S.; Gray-Weale, A.; Perrier, S. *Macromolecules* **2008,** *41,* 6400-6412.

71. *Macromol. Rapid Commun.* **2007,** *28,* 856-862.

72. Konkolewicz, D.; Hawkett, B. S.; Gray-Weale, A.; Perrier, S. *J. Polym. Sci. Part A: Polym. Chem.* **2009,** *47,* 3455-3466.

73. Israelachvili, J. *Intermolecular and Surface Forces;* Academic Press Inc.: 1991.

74. Israelachvili, J. N.; Mitchel, D. J.; Ninham, B. W. *J. Chem. Soc. Faraday Trans. I* **1976,** *72,* 1525-1568.

75. Puvvada, S.; Blanckstein, D. *J. Chem. Phys.* **1990,** *92,* 3710-3724.

76. Herrington, T. M.; Sahi, S. S. *J. Colloid Interface Sci.* **1988,** *121,* 107-120.

77. Kato, T.; Seimiya, T. *J. Phys. Chem.* **1986,** *90,* 3159-3167.

78. Missel, P. J.; Mazer, N. A.; Benedek, G. B.; Young, C. Y.; Carey, M. C. *J. Phys. Chem.* **1980,** *84,* 1044-1057.

79. Riess, G. *Prog. Polym. Sci.* **2003,** *28,* 1107-1170.

80. Gohy, J.-F. *Adv. Polym. Sci.* **2005,** *190,* 65-136.

81. Holder, S. J.; Sommerdijk, N. A. J. M. *Polym. Chem.* **2011,** DOI: 10.1039/c0py00379d.

82. Denkova, A. G.; Mendes, E.; Coppens, M.-O. *Soft Matter* **2010,** *6,* 2351-2357.

83. Mortensen, K.; Pedersen, J. S. *Macromolecules* **1993,** *26,* 805-812.

84. Khan, T. N.; Mobbs, R. H.; Price, C.; Quintana, J. R.; Stubbersfield, R. B. *Eur. Polym. J.* **1987,** *23,* 191-194.

85. Xu, R.; Winnik, M. A.; Riess, G.; Chu, G.; Croucher, M. D. *Macromolecules* **1992,** *25,* 644-652.

86. Mortensen, K.; Brown, W.; Almdal, K.; Alami, E.; Jada, A. *Langmuir* **1997,** *13,* 3635-3645.

87. Bronstein, L. M.; Chernyshov, D. M.; Timofeeva, G. I.; Dubrovina, L. V.; Valetsky, P. M.; Khokhlov, A. R. *Langmuir* **1999,** *15,* 6195-6200.

88. Gohy, J.-F.; Lohmeijer, B. G. G.; Varshney, S. K.; Schubert, U. S. *Macromolecules* **2002,** *35,* 7427-7435.

89. Polik, W. F.; Burchard, W. *Macromolecules* **1983,** *16,* 978-982.

90. Nagarajan, R.; Ganesh, K. *Macromolecules* **1989,** *22,* 4312-4325.

91. Halperin, A. *Macromolecules* **1987,** *20,* 2943-2946.

92. Skrabania, K. *The multifarious self-assembly of triblock copolymers: From multiresponsive polymers and multi-compartment micelles,* Thesis, University of Potsdam, 2008.

93. Kriz, J.; Masar, B.; Plestil, J.; Tuzar, Z.; Pospisil, H.; Doskocilova, D. *Macromolecules* **1998,** *31,* 41-51.

94. Ishizone, T.; Sugiyama, K.; Sakano, Y.; Mori, H.; Hirao, A.; Nakahama, S. *Polymer J.* **1999,** *31,* 983-988.

95. Yu, G.; Eisenberg, A. *Macromolecules* **1998,** *31,* 5546-5549.

96. Willet, N.; Gohy, J.-F.; Auvray, L.; Varshney, S.; Jerome, R.; Leyh, B. *Langmuir* **2008,** *24,* 3009-3015.

97. Stupp, S. I.; LeBonheur, V.; Walker, K.; Li, L. S.; Huggins, K. E.; Keser, M.; Amstutz, A. *Science* **1997,** *276,* 384-389.

98. Erhardt, R.; Böker, A.; Zettl, H.; Kaya, H.; Pyckhout-Hintzen, W.; Krausch, G.; Abetz, V.; Müller, A. H. E. *Macromolecules* **2001,** *34,* 1069-1104.

99. Kubowicz, S.; Baussard, J.-F.; Lutz, J.-F.; Thünemann, A. F.; von Berlepsch, H.; Laschewsky, A. *Angew. Chem. Int. Ed.* **2005,** *44,* 5262-5265.

100. von Berlepsch, H.; Böttcher, C.; Skrabania, K.; Laschewsky, A. *Chem. Commun.* **2009,** 2290-2292.

101. Lodge, T. P.; Rasdal, A.; Li, Z.; Hillmyer, M. A. *J. Am. Chem. Soc.* **2005,** *127,* 17608-17609.

102. Marsat, J.-N.; Heydenreich, M.; Kleinpeter, E.; Berlepsch, H. v.; Böttcher, C.; Laschewsky, A. *Macromolecules* **2011,** asap.

103. Laschewsky, A.; Marsat, J.-N.; Skrabania, K.; Berlepsch, H. v.; Böttcher, C. *Macromol. Chem. Phys.* **2010,** *211,* 215-221.

104. Cornelissen, J. J. L. M.; Rowan, A. E.; Nolte, R. J. M.; Sommerdijk, N. A. J. M. *Chem. Rev.* **2001,** *101,* 4039-4070.

105. Dou, H.; Liu, G.; Dupont, J.; Hong, L. *Soft Matter* **2010,** *6,* 4214-4222.

106. Yamamoto, S.; Pietrasik, J.; Matyjaszewski, K. *J. Polym Sci. Part A: Polym. Chem.* **2007,** *46,* 194-202.

107. Luna-Barcenas, G.; Gromov, D. G.; Meredith, C.; Sanchez, I. C.; de Pablo, J. J.; Johnston, K. P. *Chem. Phys. Lett.* **1997,** *278,* 302-306.

108. Rushbrooke, G. H. *Proc. Camb. Phil. Soc.* **1938,** *34,* 424.

109. Freeman, P. I.; Rowlinson, J. S. *Polymer* **1960,** *1,* 20-26.

110. Flory, P. J.; Orwoll, R. A.; Vrij, A. *J. Am. Chem. Soc.* **1964,** *86,* 3515-3520.

111. Flory, P. J. *J. Am. Chem. Soc.* **1965,** *87,* 1833-1838.

112. Flory, P. J. *Discuss. Faraday Soc.* **1970,** *49,* 7-29.

113. Schild, H. G. *Prog. Polym. Sci.* **1992,** *17,* 163-249.

114. Aoshima, S.; Kanaoka, S. *Adv. Polym. Sci.* **2007,** *210,* 169-208.

115. Liu, R.; Fraylich, M.; Saunders, B. R. *Colloid Polym. Sci.* **2009,** *287,* 627-643.

116. Aseyev, V.; Tenhu, H.; Winnik, F. *Adv. Polym. Sci.* **2010,** doi 10.1007/12.2010.57.

117. Plate, N. A.; Lebedeva, T. L.; Valuev, L. I. *Polymer J. Jpn.* **1999,** *31,* 21-27.

118. Laschewsky, A.; Rekai, E. D.; Wischerhoff, E. *Macromol. Chem. Phys.* **2001,** *202,* 276-286.

119. Myrat, C. D.; Rowlinson, J. S. *Polymer* **1965,** *6,* 645.

120. Delmas, G.; Patterson, D. *J. Polym. Sci., Part C* **1970,** *30,* 1-8.

121. Xue, W.; Huglin, M. B.; Jones, T. G. J. *Macromol. Chem. Phys.* **2003,** *204,* 1956-1965.

122. Ray, B.; Okamoto, Y.; Kamigaito, M.; Sawamoto, M.; Seno, K.; Kanaoka, S.; Aoshima, S. *Polym. J.* **2005,** *37,* 234.

123. Hirano, T.; Okumura, Y.; Kitajima, H.; Seno, M.; Sato, T. J. *J. Polym. Sci. Part A: Polym. Chem.* **2006,** *44,* 4450.

124. Katsumoto, Y.; Kubosaki, N. *Macromolecules* **2008,** *41,* 5955-5956.

125. Zhao, J.; Zhang, G.; Pispas, S. *J. Polym. Sci. Part A: Polym. Chem.* **2009,** *47,* 4099-4110.

126. Lessard, D. G.; Ousalem, M.; Zhu, X. X. *Can. J. Chem.* **2001,** *79,* 1870-1874.

127. Zhang, G.; Wu, C. *Adv. Polym. Sci.* **2006,** *195,* 101-176.

128. Wu, C.; Zhou, S. *Phys. Rev. Lett.* **1996,** *77,* 3053-3055.

129. Kujawa, P.; Aseyev, V.; Tenhu, H.; Winnik, F. M. *Macromolecules* **2006,** *39,* 7686-7693.

130. Wang, X.; Qui, X.; Wu, C. *Macromolecules* **1998,** *31,* 2972-2976.

131. Wu, C.; Wang, X. *Phys. Rev. Lett.* **1998,** *80,* 4092-4094.

132. Xu, J.; Zhu, Z.; Luo, S.; Wu, C.; Liu, S. *Phys. Rev. Lett* **2006,** *96,* 1-4.

133. Aseyev, V.; Hietala, S.; Laukkanen, A.; Nuopponen, M.; Confortini, O.; Du Prez, F. E.; Tenhu, H. *Polymer* **2005,** *46,* 7118-7131.

134. Vasilevskaya, V. V.; Khalatur, P. G.; Khokhlov, A. R. *Macromolecules* **2003,** *36,* 10103-10111.

135. Liu, B.; Perrier, S. *J. Polym. Sci. Part A: Polym. Chem.* **2005,** *43,* 3643-3654.

136. Convertine, A. J.; Lokitz, B. S.; Vasileva, Y.; Myrick, L. J.; Scales, C. W.; McCormick, C. L. *Macromolecules* **2006,** *39,* 1724.

137. Nuopponen, M.; Ojala, J.; Tenhu, H. *Polymer* **2004,** *45,* 3643-3650.

138. Sistach, S.; Beija, M.; Rahal, V.; Brulet, A.; Marty, J.-D.; Destarac, M.; Mingotaud, C. *Chem. Mater.* **2010,** *22,* 3712-3724.

139. Forder, C.; Patrickios, C. S.; Armes, S. P.; Billingham, N. C. *Macromolecules* **1996,** *29,* 8160-8169.

140. Qin, S.; Geng, Y.; Discher, D. E.; Yang, S. *Adv. Mater.* **2006,** *18,* 2905-2909.

141. Topp, M. D. C.; Dijkstra, P. J.; Talsma, H.; Feijen, J. *Macromolecules* **1997,** *30,* 8518-8520.

142. Zhang, W.; Shi, L.; Wu, K.; An, K. *Macromolecules* **2005,** *38,* 5743-5747.

143. Zhang, Q.; Ye, J.; Lu, Y.; Nie, T.; Xie, D.; Song, Q.; Chen, H.; Zhang, G.; Tang, Y.; Wu, C.; Xie, Z. *Macromolecules* **2008,** *41,* 2228-2234.

144. Klouda, L.; Mikos, A. G. *Eur. J. Pharm. Biopharm.* **2008,** *68,* 34-45.

145. Kirkland, S. E.; Hensarling, R. M.; McConaughy, S. D.; Guo, Y.; Jarrett, W. L.; McCormick, C. L. *Biomacromolecules* **2008,** *9,* 481-486.

146. Wang, H.; An, Y.; Huang, N.; Ma, R.; Li, J.; Shi, L. *Macromol. Rapid Commun.* **2008,** *29,* 1410-1414.

147. York, A. W.; Kirkland, S. E.; McCormick, C. L. *Adv. Drug Deliv. Rev.* **2008,** *60,* 1018-1036.

148. Schmaljohann, D. *Adv. Drug Deliv. Rev.* **2006,** *58,* 1655-1670.

149. Bajpai, A.; Shukla, S. K.; Bhanu, S.; Kankane, S. *Prog. Polym. Sci.* **2008,** *33,* 1088-1118.

150. Neradovic, D.; Soga, O.; Van Nostrum, C.; Hennink, W. *Biomaterials* **2004,** *25,* 2409-2418.

151. Arotcarena, M.; Heise, B.; Ishaya, S.; Laschewsky, A. *J. Am. Chem. Soc.* **2002,** *124,* 3787-3793.

152. Maeda, Y.; Mochiduki, H.; Ikeda, I. *Macromol. Rapid Commum.* **2004,** *25,* 1330-1334.

153. Weaver, J. V. M.; Armes, S. P.; Bütün, V. *Chem. Commun.* **2002,** 2122-2123.

154. Liu, S.; Armes, S. *Langmuir* **2003,** *19,* 4432-4438.

155. Klaikherd, A.; Nagamani, C.; Thayumanavan, S. *J. Am. Chem. Soc.* **2009,** *131,* 4830-4838.

156. Roy, D.; Cambre, J. N.; Sumerlin, B. S. *Chem. Commun.* **2008,** 2477-2479.

157. Roy, D.; Cambre, J. N.; Sumerlin, B. S. *Chem. Commun.* **2009,** 2106-2108.

158. Smith, A. E.; Xu, X.; Kirkland-York, S. E.; Savin, D. A.; McCormick, C. L. *Macromolecules* **2010,** *43,* 1210-1217.

159. Balsara, N. P.; Tirrell, M.; Lodge, T. P. *Macromolecules* **1991,** *24,* 1975-1986.

160. Leibler, L.; Orland, H.; Wheeler, J. C. *J. Chem. Phys.* **1983,** *79,* 3550-3557.

161. Zhou, J.; Wang, L.; Yang, Q.; Liu, Q.; Yu, H.; Zhao, Z. *J. Phys. Chem. B* **2007,** *111,* 5573-5580.

162. Liu, F.; Eisenberg, A. *J. Am. Chem. Soc.* **2003,** *125,* 15059-15064.

163. Tsitsilianis, C.; Roiter, Y.; Katsampas, I.; Minko, S. *Macromolecules* **2008,** *41,* 925-934.

164. Zhang, W.; Shi, L.; Ma, R.; An, Y.; Xu, Y.; Wu, K. *Macromolecules* **2005,** *38,* 8850-8852.

165. Walther, A.; Millard, P.-E.; Goldmann, A. S.; Lovestead, T. M.; Schacher, F.; Barner-Kowollik, C.; Müller, A. H. E. *Macromolecules* **2008,** *41,* 8608-8619.

166. Bütün, V.; Top, R. B.; Ufuklar, S. *Macromolecules* **2006,** *39,* 1216-1225.

167. Dupont, J.; Liu, G. *Soft Matter* **2010,** *6,* 3654-3661.

168. Sugihara, S.; Kanaoka, S.; Aoshima, S. *J. Polym. Sci. Part A: Polym. Chem.* **2004,** *42,* 2601-2611.

169. Cao, Y.; Zhao, N.; Wu, K.; Zhu, X. X. *Langmuir* **2009,** *25,* 1699-1704.

170. Xie, D.; Ye, X.; Ding, Y.; Zhang, G.; Zhao, N.; Wu, K.; Cao, Y.; Zhu, X. X. *Macromolecules* **2009,** *42,* 2715-2720.

171. Alfrey, T.; Lavin, E. *J. Am. Chem. Soc.* **1945,** *67,* 2044-2045.

172. Shirota, Y.; Yoshimura, M.; Matsumoto, A.; Mikawa, H. *Macromolecules* **1974,** *7,* 4-11.

173. Yoshimura, M.; Mikawa, H.; Shirota, Y. *Macromolecules* **1978,** *11,* 1085-1091.

174. Zeng, W.; Shirota, Y. *Macromolecules* **1989,** *22,* 4204-4208.

175. Mayo, F. R. *Discuss. Faraday Soc.* **1947,** *2,* 304-309.

176. Ebdon, J. R.; Towns, C. R.; Dodgson, K. *Polymer Reviews* **1986,** *26,* 523-550.

177. Rzaev, Z. *Prog. Polym. Sci.* **2000,** *25,* 163-217.

178. Tsuchida, E.; Tomono, T. *Macromol. Chem.* **1971,** *141,* 265-298.

179. Fleming, I. *Grenzorbitale und Reaktionen organischer Verbindungen;* VCH, Weinheim: 1990.

180. Pfeifer, S.; Lutz, J.-F. *J. Am. Chem. Soc.* **2007,** *129,* 9542-9543.

181. Pfeifer, S.; Lutz, J.-F. *Chem. Eur. J.* **2008,** *14,* 10949-10957.

182. Deb, P. C.; Meyerhoff, G. *Eur. Polym. J.* **1984,** *20,* 713-719.

183. Bevington, J. C. *Trans. Faraday Soc.* **1957,** *53,* 997-1002.

184. Bevington, J. C.; Johnson, M. *Eur. Polym. J.* **1966,** *2,* 185-188.

185. Sato, T.; Abe, M.; Otsu, T. *Makromol. Chem.* **1977,** *178,* 1061-1075.

186. Klumperman, B. *Polym. Chem.* **2010,** *1,* 558-562.

187. Sanayei, R. A.; O'Driscoll, K. F.; Klumperman, B. *Macromolecules* **1994,** *27,* 5577-5582.

188. Prementine, G. S.; Jones, S. A.; Tirrell, D. A. *Macromolecules* **1989,** *22,* 770-775.

189. van den Dungen, E. T. A.; Rinquest, J.; Pretorius, N. O.; McKenzie, J. M.; McLeary, J. B.; Sanderson, R. D.; Klumperman, B. *Aust. J. Chem.* **2006,** *59,* 742-748.

190. Chen, G.-Q.; Wu, Z.-Q.; Wu, J.-R.; Li, Z.-C.; Li, F.-M. *Macromolecules* **2000,** *33,* 232-234.

191. Zhao, Y.-L.; Chen, C.-F.; Xi, F. *J. Polym. Sci. Part A: Polym. Chem.* **2003,** *41,* 2156-2165.

192. Lutz, J.-F.; Kirci, B.; Matyjaszewski, K. *Macromolecules* **2003,** *36,* 3136-3145.

193. Nakayama, Y.; Smets, G. *J. Polym. Sci. Part A: Polym. Chem.* **1967,** *5,* 1619-1633.

194. Hagiwara, T.; Mizota, J.; Hamana, H.; Narita, T. *Macromol. Rapid Commun.* **1985,** *6,* 169-174.

195. Hagiwara, T.; Someno, T.; Hamana, H.; Narita, T. *J. Polym. Sci. Part A: Polym. Chem.* **1988,** *26,* 1011-1020.

196. Matsumoto, A.; Kubota, T.; Otsu, T. *Macromolecules* **1990,** *23,* 4508-4513.

197. El-Guweri, M.; Hendlinger, P.; Laschewsky, A. *Macromol. Chem. Phys.* **1997,** *198,* 401-418.

198. Lutz, J.-F.; Matyjaszewski, K. *Macromol. Chem. Phys.* **2002,** *203,* 1385-1395.

199. Lutz, J.-F. *Polym. Chem.* **2010,** *1,* 55-62.

200. Lutz, J.-F. *Nature Chemistry* **2010,** *2,* 84-85.

201. Lutz, J.-F.; Schmidt, B. V. K. J.; Pfeifer, S. *Macromol. Rapid Commum.* **2011,** *32,* 127-135.

202. Benoit, D.; Hawker, C. J.; Huang, E. E.; Lin, Z.; Russell, T. P. *Macromolecules* **2000,** *33,* 1505-1507.

203. Zhu, M.-Q.; Wei, L.-H.; Li, M.; Jiang, L.; Du, F.-S.; Li, Z.-C.; Li, F.-M. *Chem. Commun.* **2001,** 365-366.

204. Lessard, B.; Maric, M. *Macromolecules* **2010,** *43,* 879-885.

205. Lazzari, M.; Liu, G.; Lecommandoux, S. *Block Copolymers in Nanoscience;* Wiley-VCH, Weinheim: 2006.

206. Barner-Kowollik, C. *Handbook of RAFT Polymerization.;* Wiley-VCH, Weinheim: 2008.

207. Favier, A.; Charreyre, M.-T.; Chaumont, P.; Pichot, C. *Macromolecules* **2002,** *35,* 8217-8280.

208. Thomas, D. B.; Convertine, A. J.; Hester, R. D.; Lowe, A. B.; McCormick, C. L. *Macromolecules* **2004,** *37,* 1735-1741.

209. Albertin, L.; Stenzela, M. H.; Barner-Kowollik, C.; Davis, T. *Polymer* **2006,** *47,* 1011-1019.

210. Gruendling, T.; Pickford, R.; Guilhaus, M.; Barner-Kowollik, C. *J. Polym. Sci. Part A: Polym. Chem.* **2008,** *46,* 7447-7461.

211. Chen, M.; Ghiggino, K. P.; Mau, A. W. H.; Rizzardo, E.; Thang, S. H.; Wilson, G. J. *Chem. Commun.* **2002,** *19,* 2276-2277.

212. Chen, M.; Ghiggino, K. P.; Launikonis, A.; Mau, A. W. H.; Rizzardo, E.; Sasse, W. H. F.; Thang, S. H.; Wilson, G. J. *J. Mater. Chem.* **2003,** *13,* 2696-2700.

213. Mertoglu, M.; Garnier, S.; Laschewsky, A.; Skrabania, K.; Storsberg, J. *Polymer* **2005,** *46,* 7726-7740.

214. Bivigou-Koumba, A. M.; Görnitz, E.; Laschewsky, A.; Müller-Buschbaum, P.; Papadakis, C. M. *Colloid. Polym. Sci.* **2010,** *288,* 499-517.

215. Skrabania, K.; Berlepsch, H. v.; Böttcher, C.; Laschewsky, A. *Macromolecules* **2010,** *43,* 271-281.

216. Hahn, T. D.; Thomaides, J. S.; Huey, A.; Morales, J.; Meng, S. *PMSE Preprints* **2006,** *95,* 490-491.

217. Liu, J.; Hong, C.-Y.; Pan, C.-Y. *Polymer* **2004,** *45,* 4413-4421.

218. Skrabania, K.; Li, W.; Laschewsky, A. *Macromol. Chem. Phys.* **2008,** *209,* 1389-1403.

219. Albertin, L.; Stenzel, M.; Barner-Kowollik, C.; Foster, L. J. R.; Davis, T. *Macromolecules* **2004,** *37,* 7530-7537.

220. Lebreton, P.; Ameduri, B.; Boutevin, B.; Corpart, J.-M. *Macromol. Chem. Phys.* **2002,** *203,* 522-537.

221. Roth, P. J.; Kessler, D.; Zentel, R.; Theato, P. *Macromolecules* **2008,** *41,* 8316-8319.

222. Tang, C.; Kowalewski, T.; Matyjaszewski, K. *Macromolecules* **2003,** *36,* 8587-8589.

223. Ray, B.; Isobe, Y.; Matsumoto, K.; Habaue, S.; Okamoto, Y.; Kamigaito, M.; Sawamoto, M. *Macromolecules* **2004,** *37,* 1702-1710.

224. Wan, X.; Zhu, X.; Zhu, J.; Zhang, Z.; Cheng, Z. *J. Polym. Sci. Part A: Polym. Chem.* **2007,** *45,* 2886-2896.

225. Goldmann, A. S.; Quémener, D.; Millard, P.-E.; Davis, T. P.; Stenzel, M. H.; Barner-Kowollik, C.; Müller, A. H. E. *Polymer* **2008,** *49,* 2274-2281.

226. Troll, K.; Kulkarni, A.; Wang, W.; Darko, C.; Bivigou-Koumba, A. M.; Laschewsky, A.; Müller-Buschbaum, P.; Papadakis, C. M. *Colloid Polym. Sci.* **2008,** *286,* 1079-1092.

227. Gibson, M. I.; Fröhlich, E.; Klok, H. A. *J. Polym. Sci. Part A: Polym. Chem.* **2009,** *47,* 4332-4345.

228. Li, H.; Yu, B.; Matsushima, H.; Hoyle, C. E.; Lowe, A. B. *Macromolecules* **2009,** *42,* 6537-6542.

229. Zhou, N.; Zhang, Z.; Zhu, J.; Cheng, Z.; Zhu, X. *Macromolecules* **2009,** *42,* 3898-3905.

230. Ribaut, T.; Lacroix-Desmazes, P.; Fournel, B.; Sarrade, S. *J. Polym. Sci. Part A: Polym. Chem.* **2009,** *47,* 5448-5460.

231. Ma, Z.; Lacroix-Desmazes, P. *J. Polym. Sci. Part A: Polym. Chem.* **2004,** *42,* 2405-2415.

232. Hu, Y.-C.; Liu, Y.; Pan, C.-Y. *J. Polym. Sci. Part A: Polym. Chem.* **2004,** *42,* 4862-4872.

233. Dambowski, I. "Darstellung und Anwendung Trimethylsilyl-markierter RAFT-Agenzien", Master's thesis, University of Potsdam, 2009.

234. Lange, M. "Synthesis and Application of Trimethylsilyl-marked RAFT-Reagent for End group determination by 1H-NMR-Spectroscopy", Master's thesis, University of Potsdam, 2007.

235. Päch, M.; Zehm, D.; Lange, M.; Dambowski, I.; Weiss, J.; Laschewsky, A. *J. Am. Chem. Soc.* **2010,** *132,* 8757-8765.

236. Furyk, S.; Zhang, Y.; Oritz-Acosta, D.; Cremer, P. S.; Bergbreiter, D. E. *J. Polym. Sci. Part A: Polym. Chem.* **2006,** *44,* 1492-1501.

237. Klod, S.; Kleinpeter, E. *J. Chem. Soc., Perkin Trans. 2* **2001,** *10,* 1893-1898.

238. Viglione, R. G.; Zanasi, R.; Lazzeretti, P. *Org. Lett.* **2004,** *6,* 2265-2267.

239. Skrabania, K.; Kristen, J.; Laschewsky, A.; Akdemir, Ö.; Hoth, A.; Lutz, J.-F. *Langmuir* **2007,** *23,* 84-93.

240. Hua, F.; Jiang, X.; Li, D.; Zhao, B. *J. Polym* **2006,** *44,* 2454-2467.

241. Tanaka, Y.; Sato, H.; Saito, K.; Miyashita, K. *Macromol. Rapid Commun.* **1980,** *1,* 551-555.

242. Soum, A. H.; Hogen-Esch, T. E. *Macromolecules* **1985,** *18,* 691-694.

243. Bheda, M. C.; Gibson, H. W. *Macromolecules* **1991,** *24,* 2703-2708.

244. Viglione, R. G.; Zanasi, R. *Org. Lett.* **2004,** *6,* 2265-2267.

245. Xu, J.; Jiang, X.; Liu, S. *J. Polym. Sci. Part A: Polym. Chem.* **2008,** *46,* 60-69.

246. Mao, H.; Li, C.; Zhang, Y.; Furyk, S.; Cremer, P. S.; Bergbreiter, D. E. *Macromolecules* **2004,** *37,* 1031-1036.

247. Ito, D.; Kubota, K. *Macromolecules* **1997,** *30,* 7828-7834.

248. Maki, Y.; Mori, H.; Endo, T. *Macromol. Chem. Phys.* **2010,** *211,* 45-56.

249. Garnier, S.; Laschewsky, A. *Colloid Polym. Sci.* **2006,** *284,* 1243-1254.

250. Garnier, S.; Laschewsky, A. *Langmuir* **2006,** *22,* 4044-4053.

251. Zhang, L.; Eisenberg, A. *J. Am. Chem. Soc.* **1996,** *118,* 3168-3181.

252. Cameron, N. S.; Corbierre, M. K.; Eisenberg, A. *Can. J. Chem.* **1999,** *77,* 1311-1326.

253. Koh, H.-D.; Changez, M.; Rahman, M. S.; Lee, J.-S. *Langmuir* **2009,** *25,* 7188-7192.

254. Dimitrov, I.; Trzebicka, B.; Müller, A. H. E.; Dworak, A.; Tsvetanov, C. B. *Prog. Polym. Sci.* **2007,** *32,* 1275-1343.

255. Semenov, A. N.; Nyrkova, I. A.; Khokhlov, A. R. *Macromolecules* **1995,** *28,* 7491-7500.

256. Halperin, A. *Polym. Rev.* **2006,** *46,* 173-214.

257. Hindman, J. C. *J. Chem. Phys.* **1965,** *44,* 4582.

258. Muller, N.; Reiter, R. C. *J. Chem. Phys.* **1964,** *42,* 3265-3269.

259. Shirota, H.; Ohkawa, K.; Kuwabara, N.; Endo, N.; Horie, K. *Macromol. Chem. Phys.* **2000,** *201,* 2210-2219.

260. Basting, D.; Ouw, D.; Schäfer, F. P. *Opt. Commun.* **1976,** *18,* 260-262.

261. Kawski, A.; Bojarski, P.; Kuklinski, B. *Chem. Phys. Lett.* **2008,** *463,* 410-412.

262. Dutta, A. K.; Kamada, K.; Ohta, K. *J. Photochem. Photobiol. A: Chem.* **1996,** *93,* 57-64.

263. Golini, C. M.; Williams, B. W.; Foresman, J. B. *J. Fluoresc.* **1998,** *8,* 395-404.

264. Bodtke, A.; Otto, H.-H. *Pharmazie* **2005,** *60,* 803-813.

265. Mayahi, M. F.; El-Bermani, M. F. *Can. J. Chem.* **1973,** *51,* 3539-3540.

266. Jin, X.; Zhang, X.; Wu, Z.; Teng, D.; Zhang, X.; Wang, Y.; Wang, Z.; Li, C. *Biomacromolecules* **2009,** *10,* 1337-1345.

267. Zhao, B.; Li, D.; Hua, F.; Green, D. R. *Macromolecules* **2005,** *38,* 9509-9517.

268. Li, A. "Properties of Thermo-Responsive Polymers in Aqueous Phase and at the Interface", Master's thesis, University of Potsdam, 2009.

269. Beuermann, S.; Buback, M.; Davis, T. P.; Gilbert, R. G.; Hutchinson, R. A.; Kajiwara, A.; Klumpermann, B.; Russell, G. T. *Macromol. Chem. Phys.* **2000,** *201,* 1355.

270. Laschewsky, A. *Molecular concepts, self-organisation and properties of polysoaps;* Adv. Polym. Sci.: 1995.

271. Kolb, H. C.; Finn, M. G.; Sharpless, K. B. *Angew. Chem.* **2001,** *113,* 2056-2075.

272. Brückner, R. *Reaktionsmechanismen* **2003,** 2nd Edition, Spektrum Akademischer Verlag, Heidelberg-Berlin, Germany.

273. Chinchilla, R.; Najera, C. *Chem. Rev.* **2007,** *107,* 874-922.

274. Leonard, N. J.; Johnson, C. R. *J. Org. Chem.* **1962,** *27,* 282-284.

7 Appendix

^{1}H- and ^{13}CNMR spectra of 1 and 2

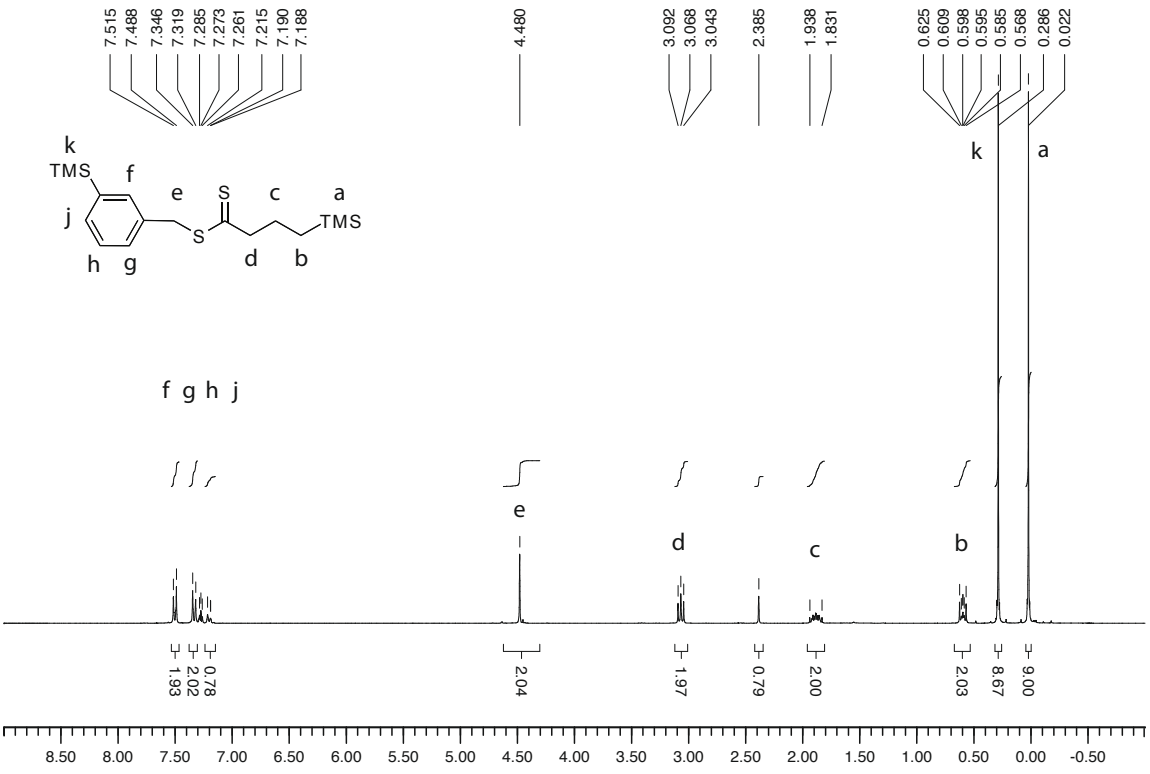

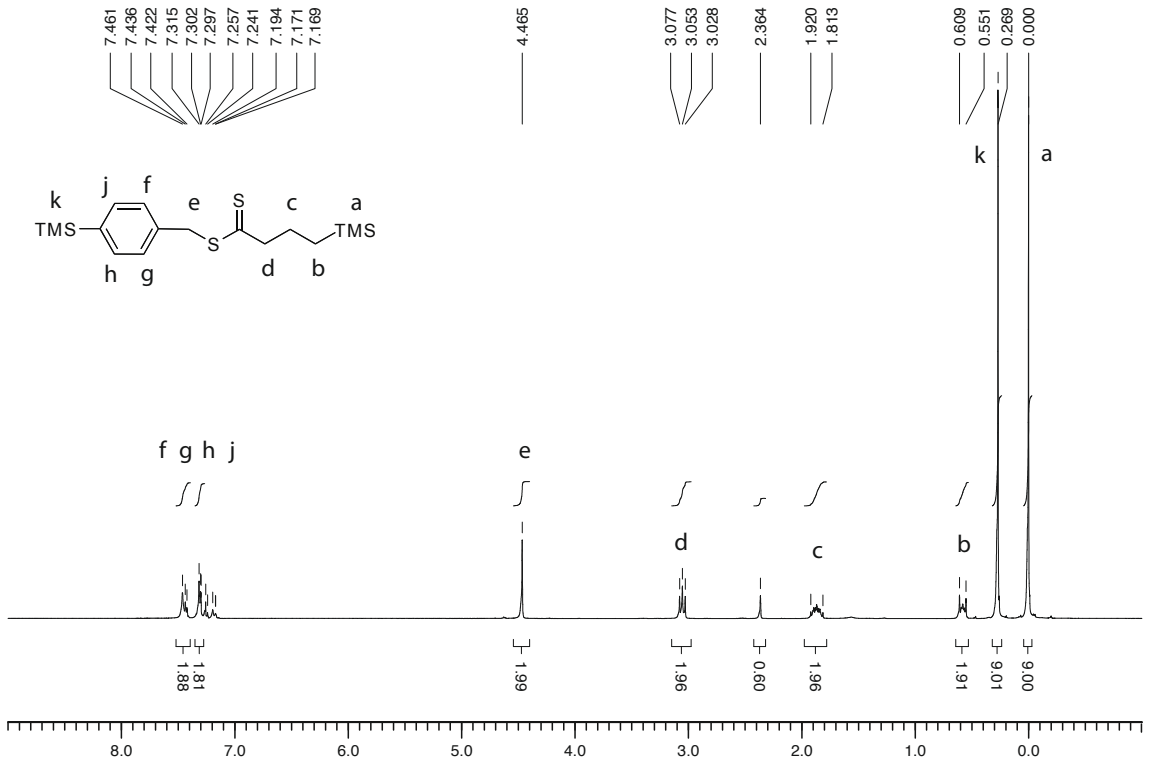

^{1}H- and ^{13}CNMR spectra of 7

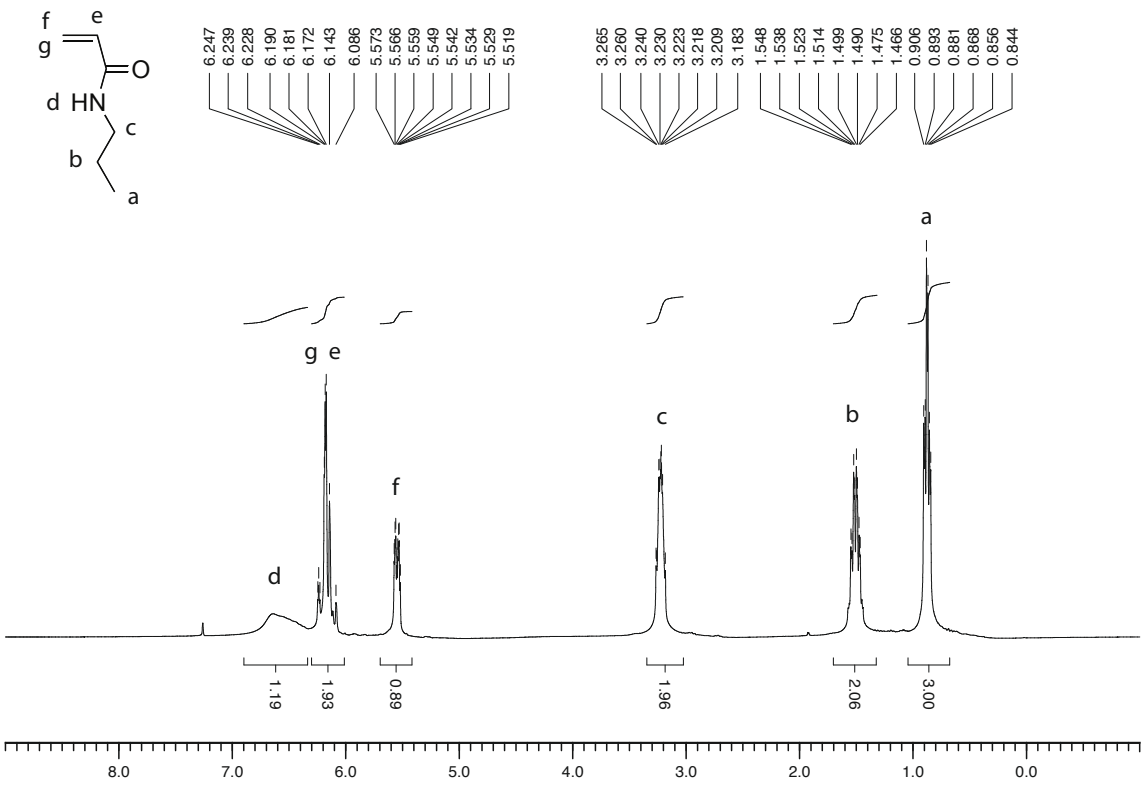

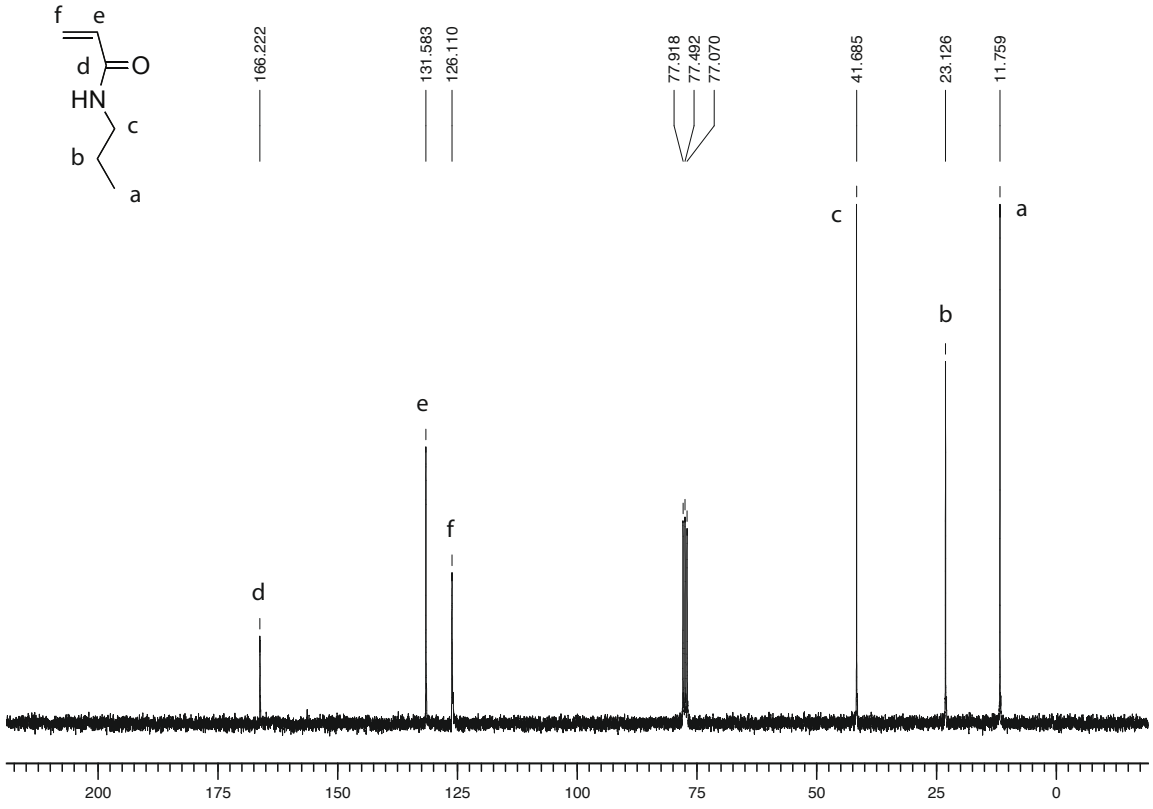

^{1}H- and ^{13}CNMR spectra of 8

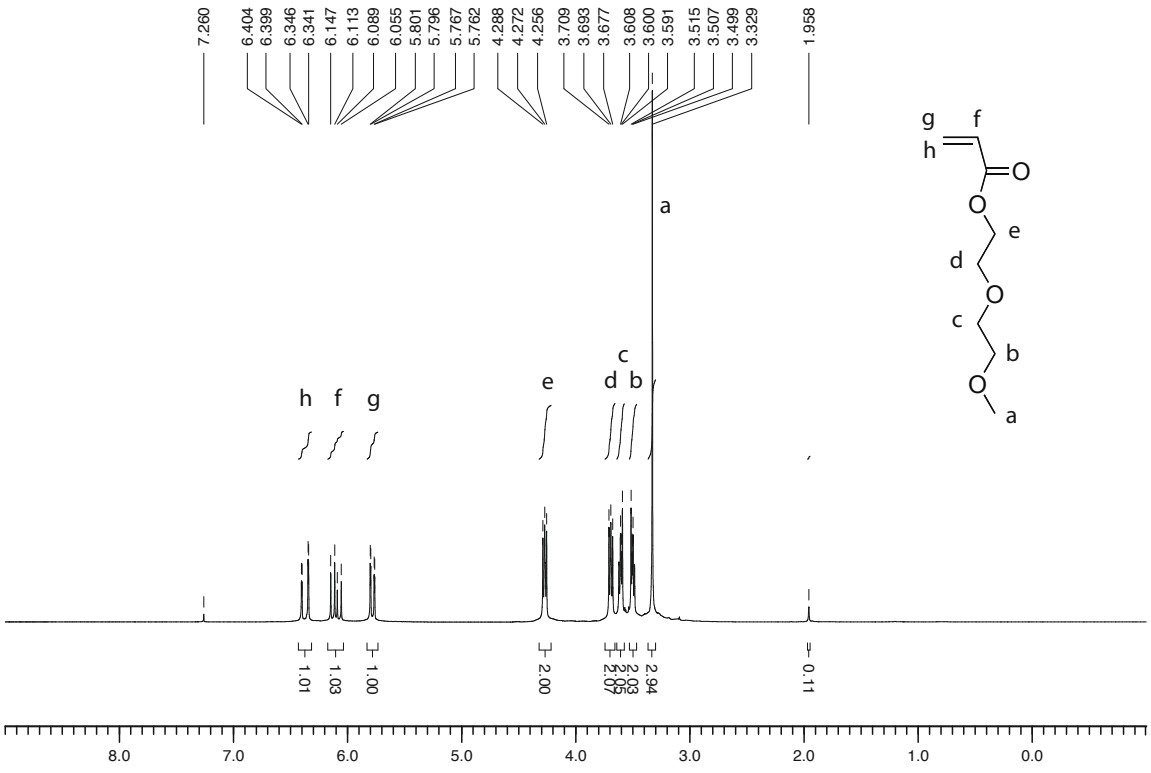

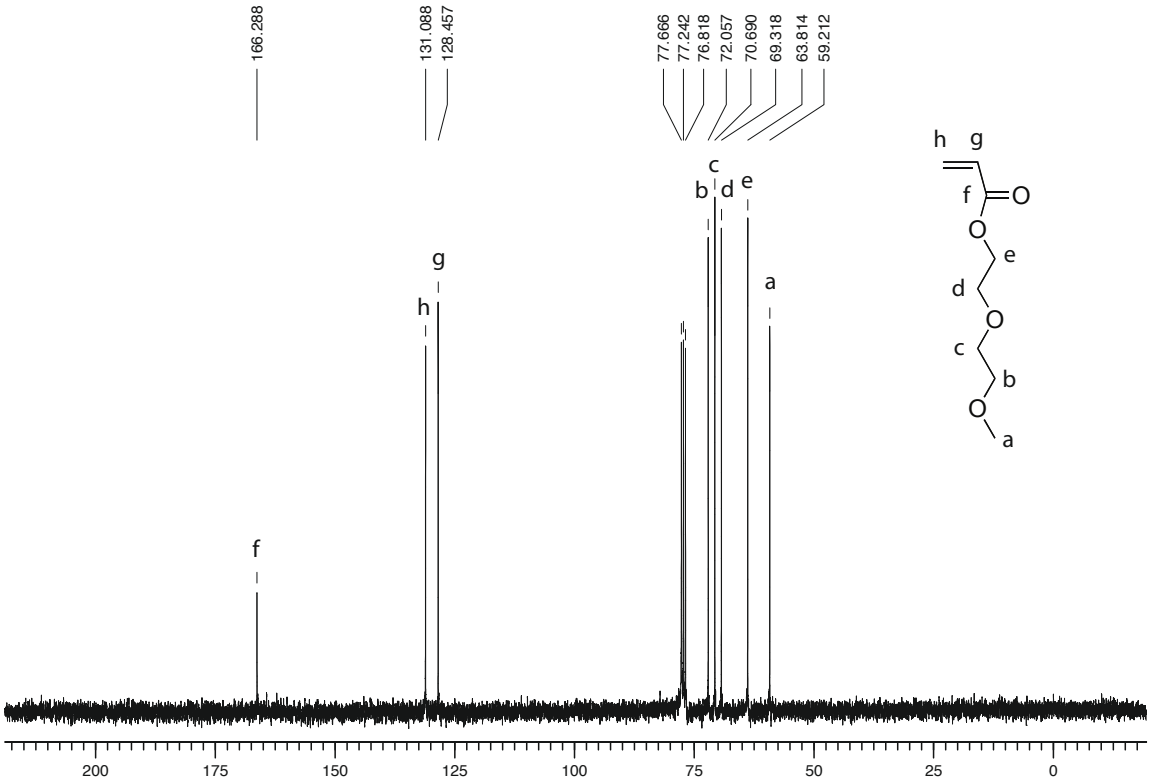

^{1}H- and ^{13}CNMR spectra of 9

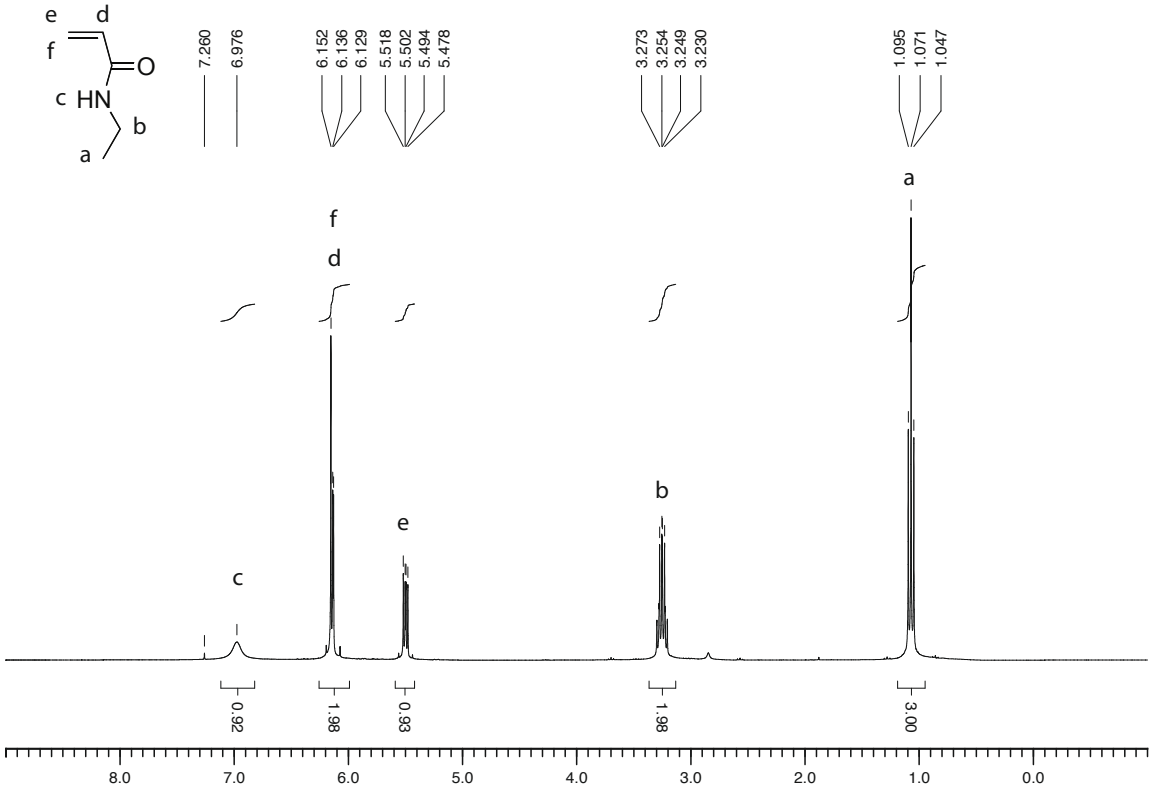

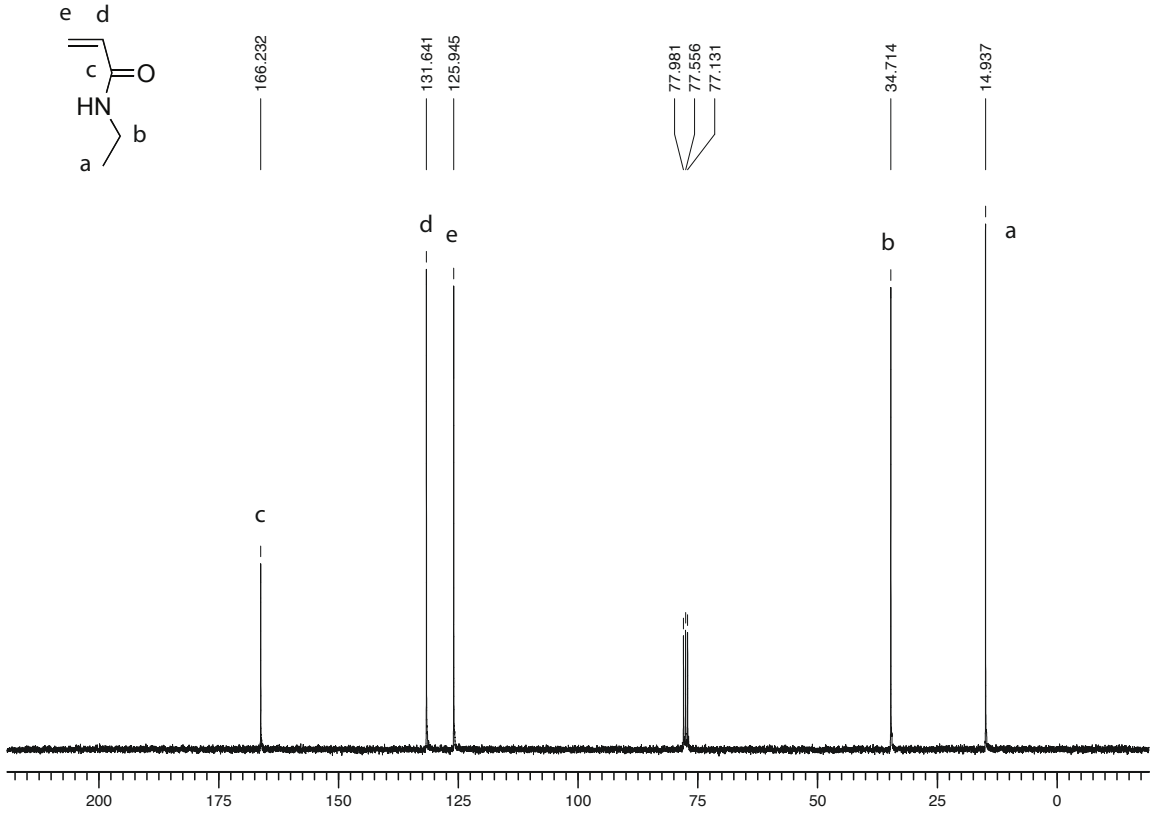

^{1}H- and ^{13}CNMR spectra of 14

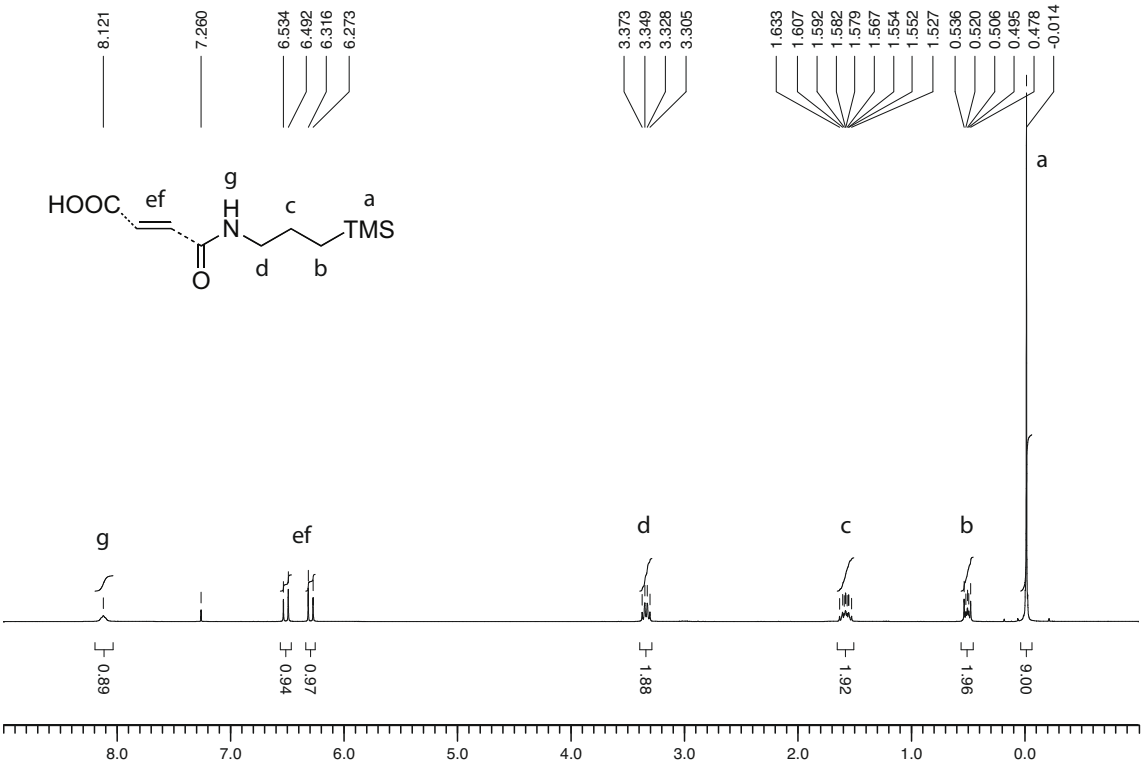

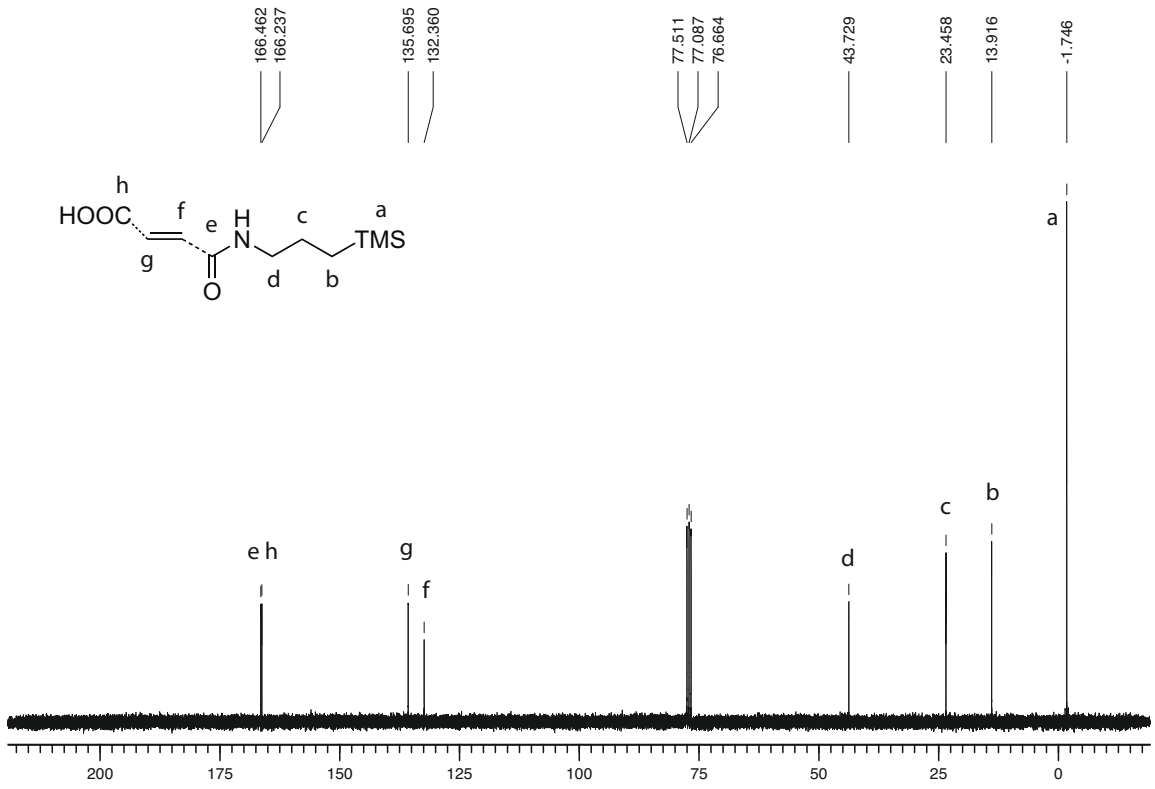

^{1}H- and ^{13}CNMR spectra of 15

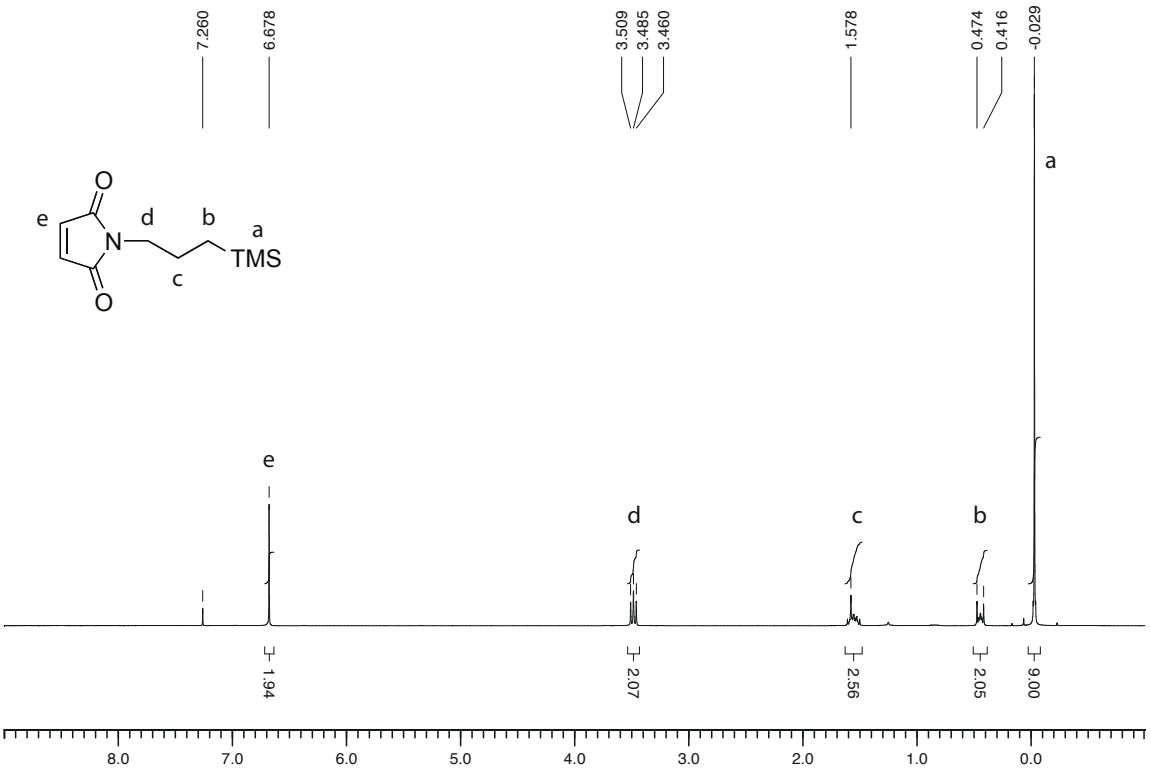

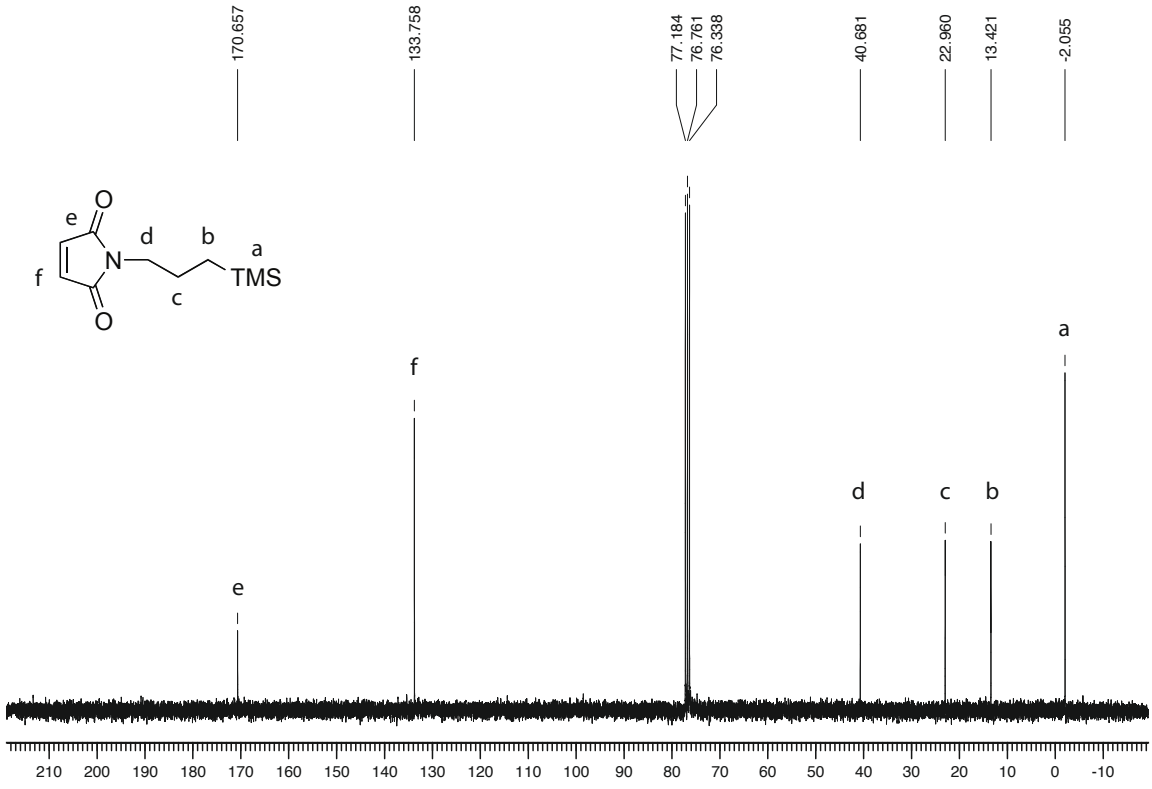

^{1}H- and ^{13}CNMR spectra of 16

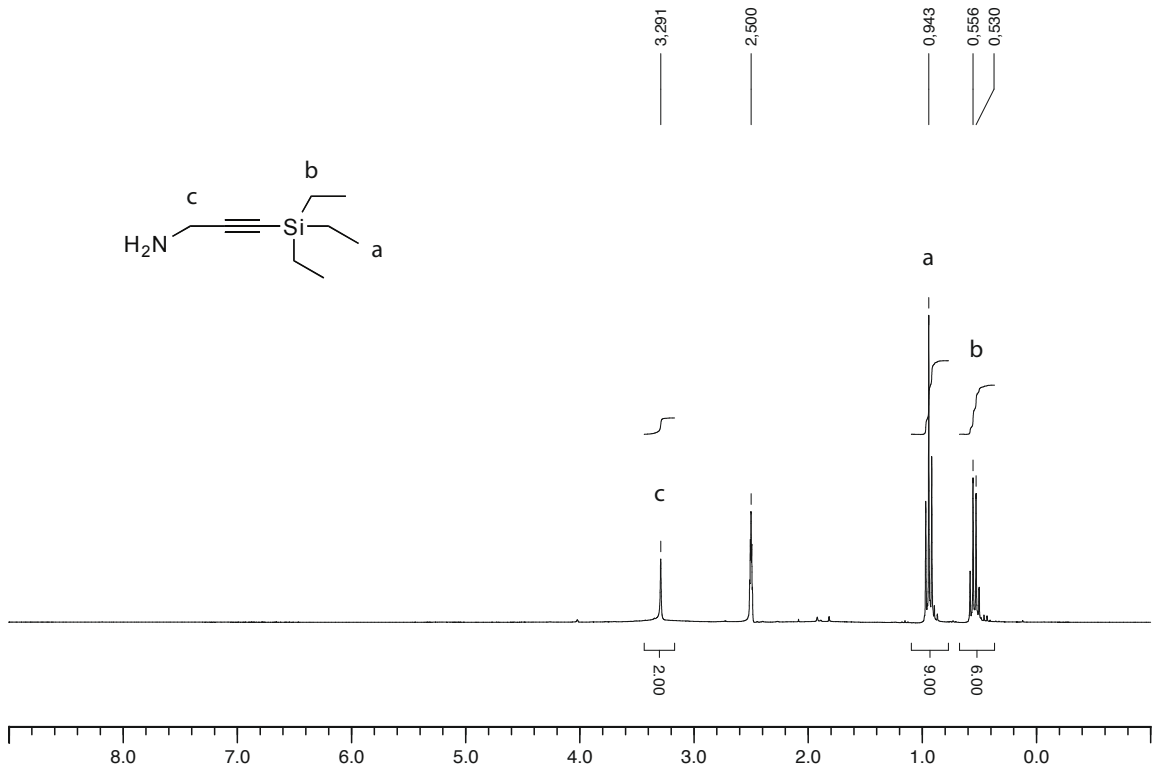

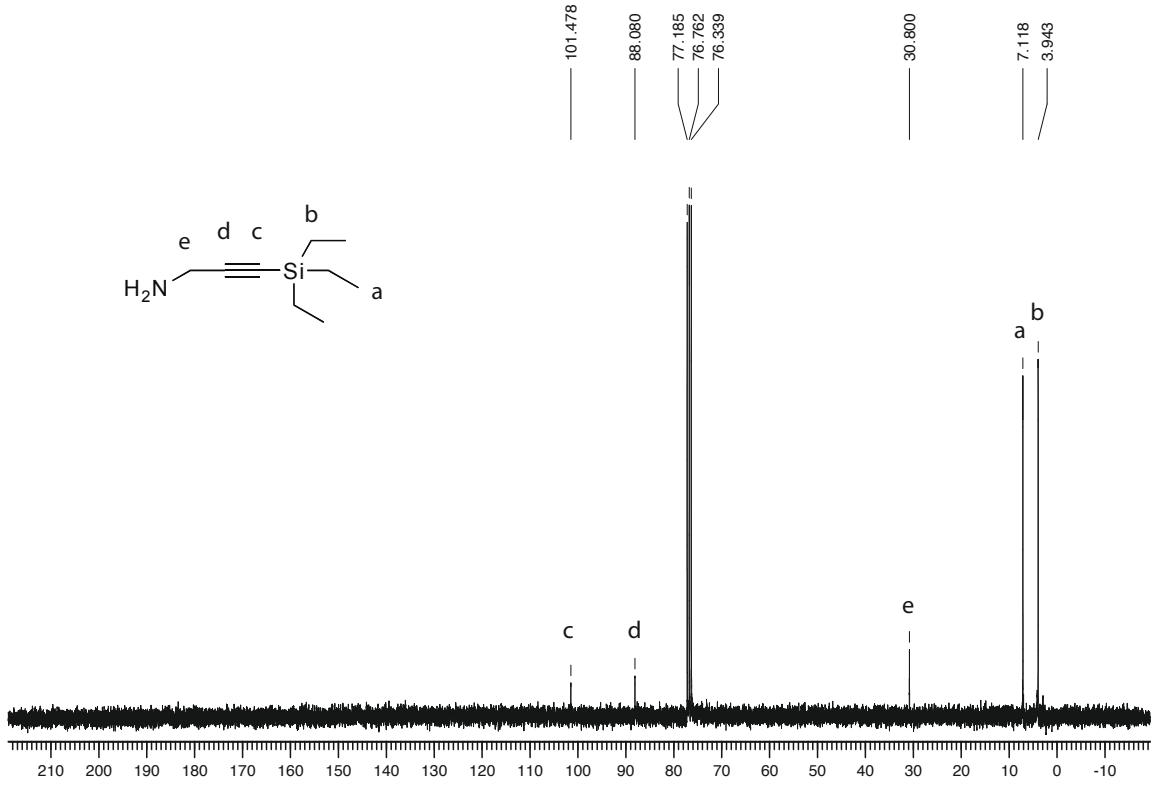

^{1}H- and ^{13}CNMR spectra of 17

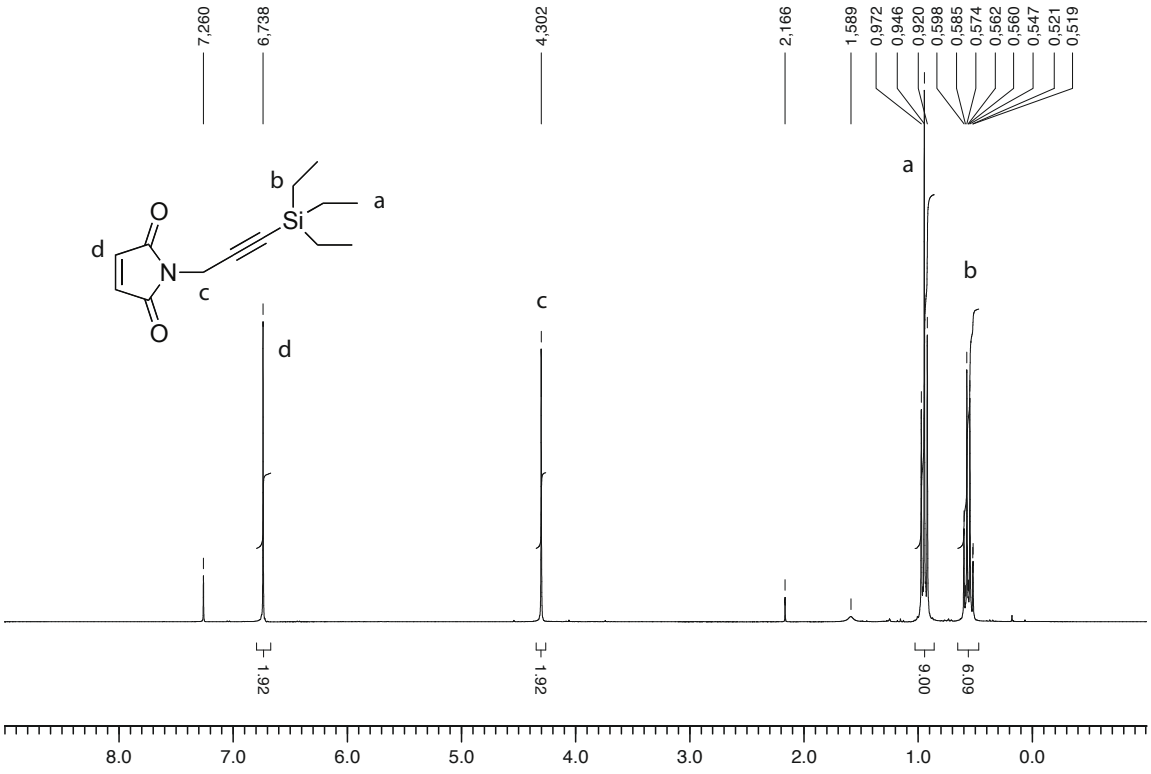

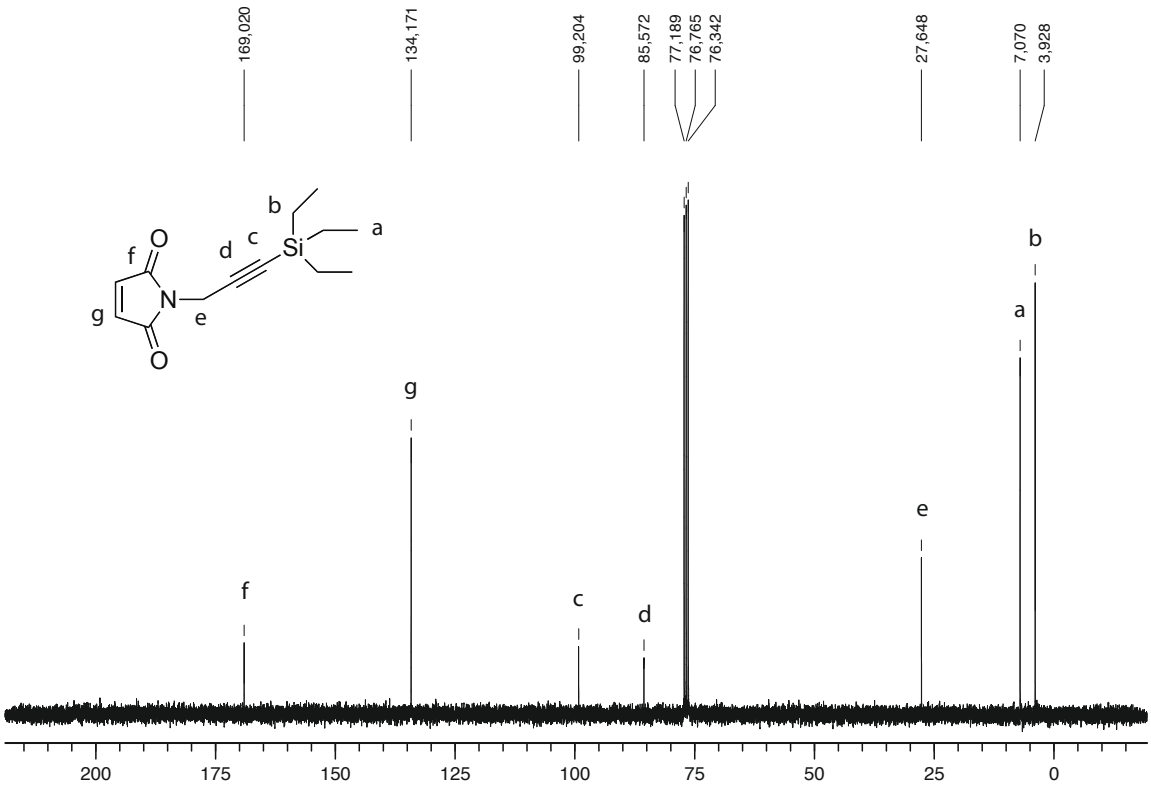

^{1}H- and ^{13}CNMR spectra of 18

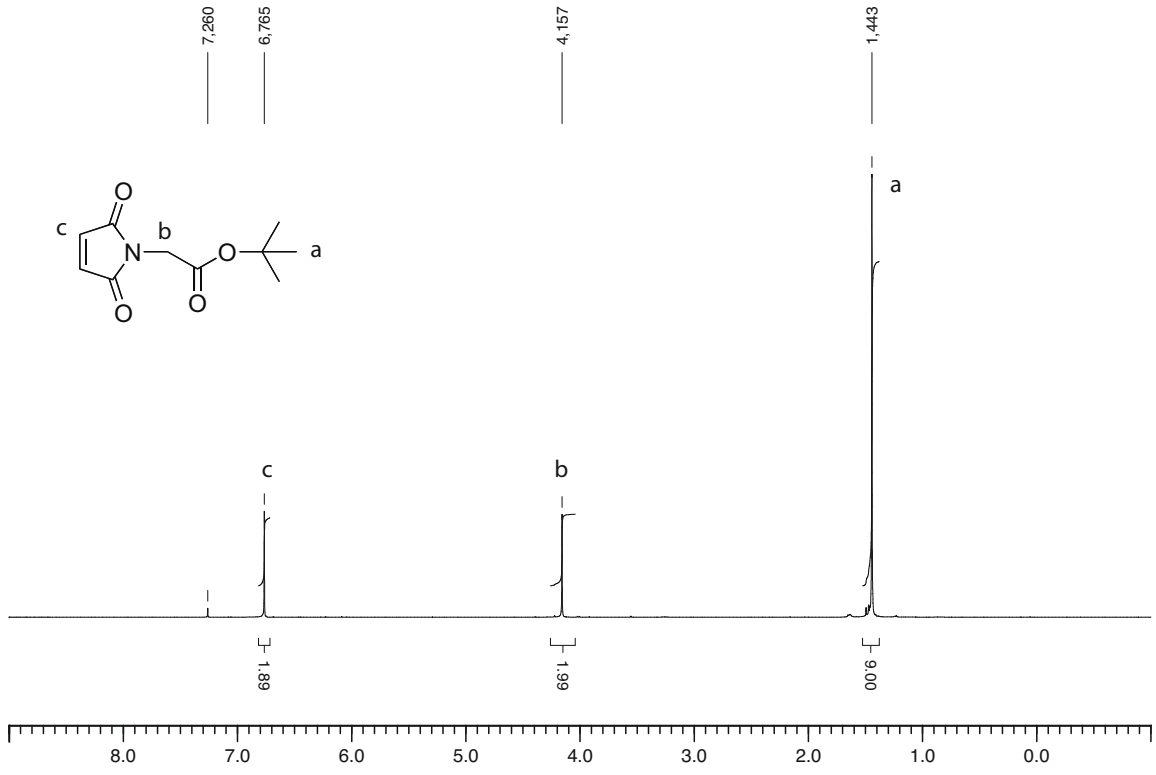

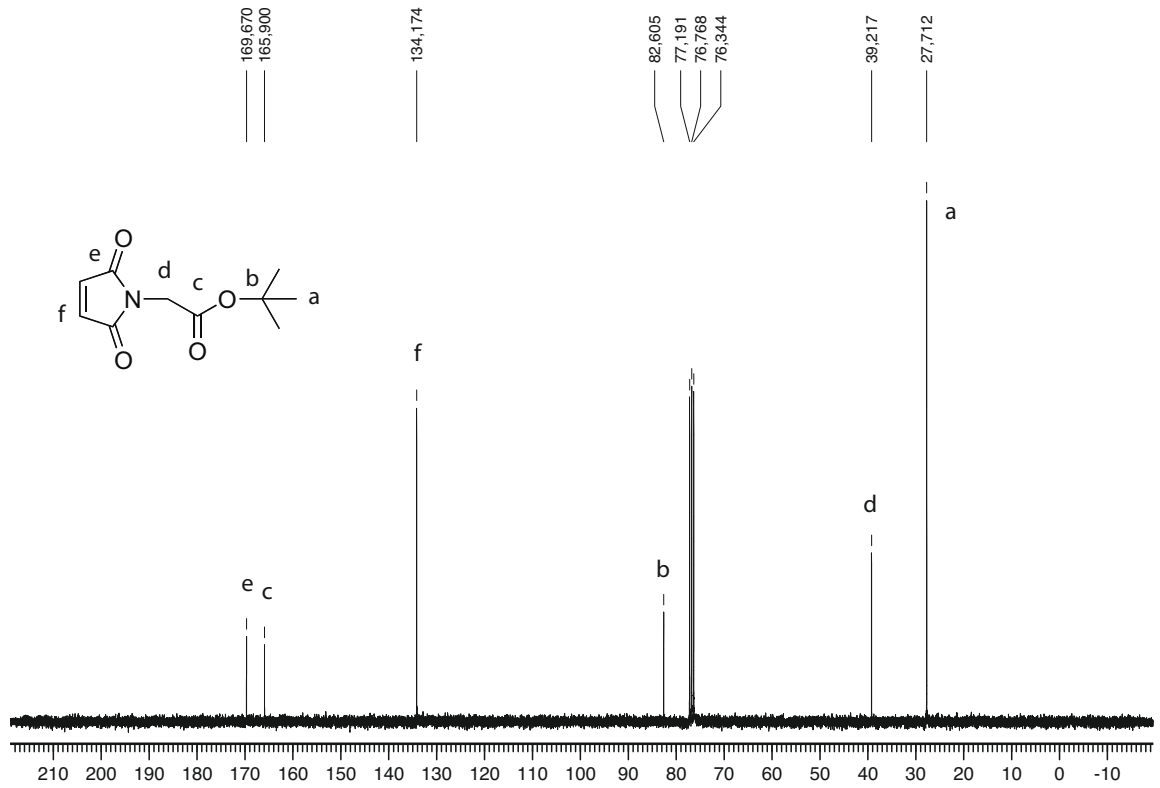

^{1}H- and ^{13}CNMR spectra of 19

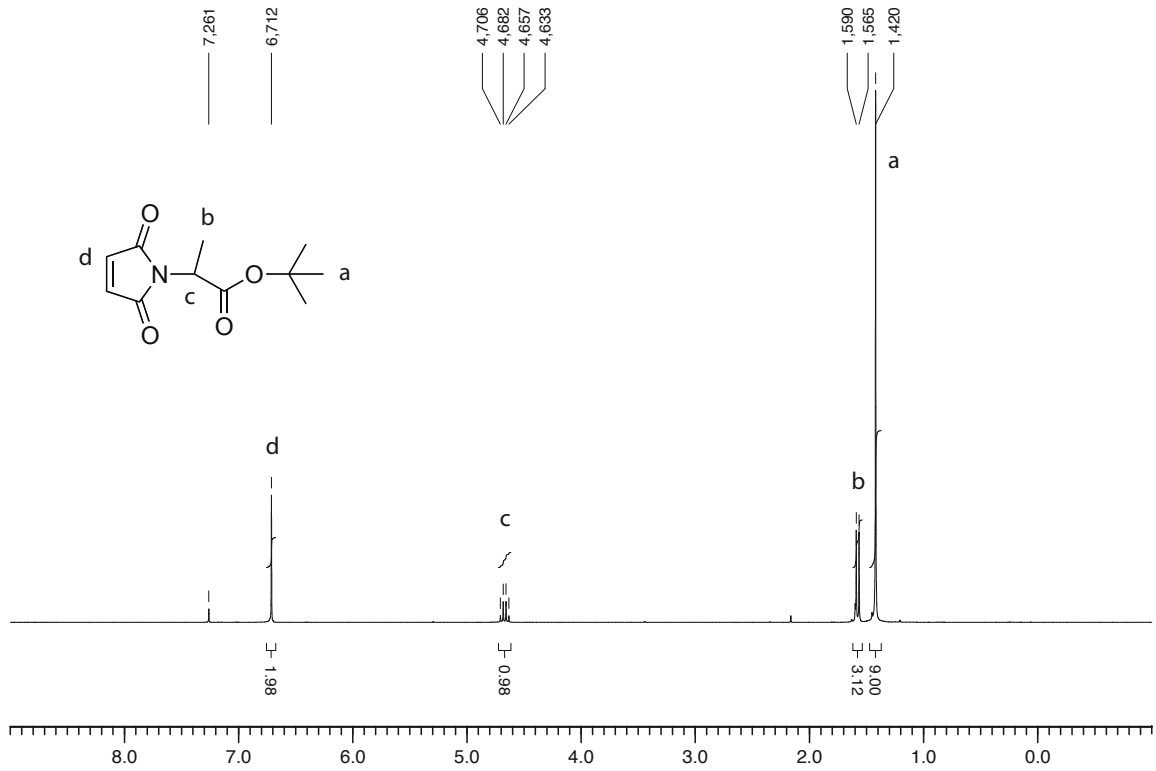

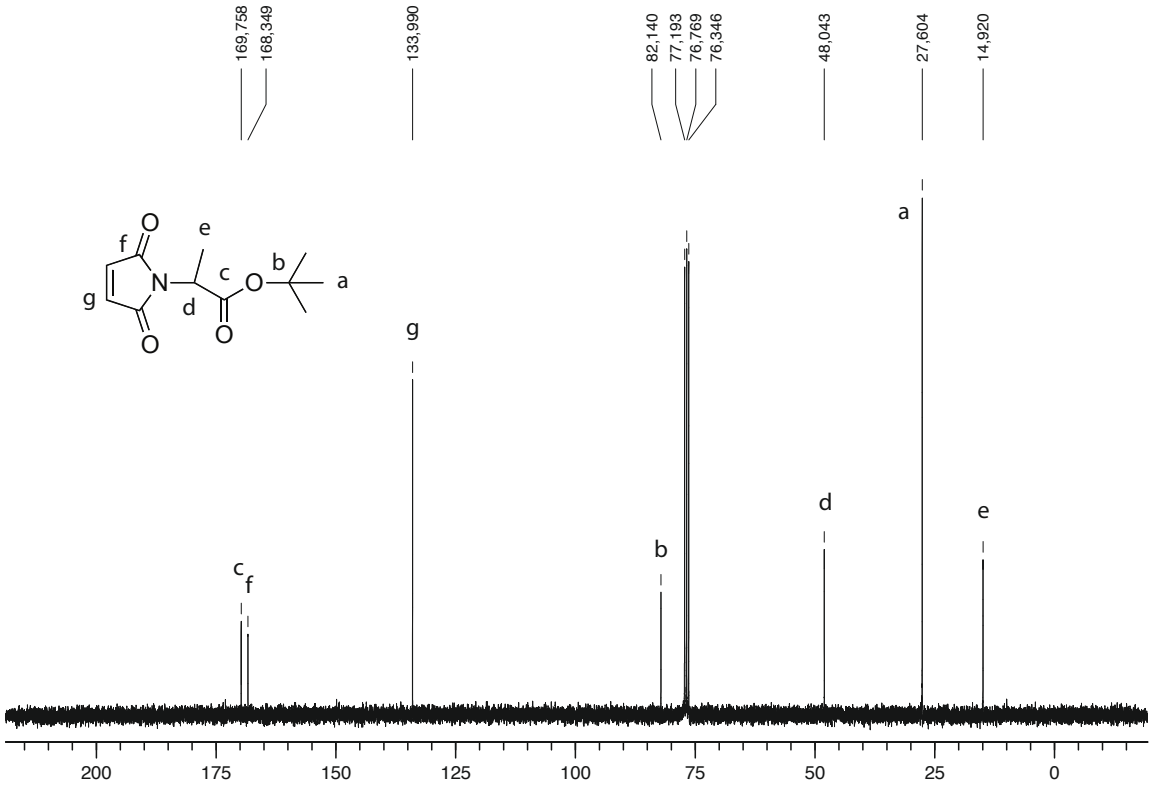

^{1}H- and ^{13}CNMR spectra of 20

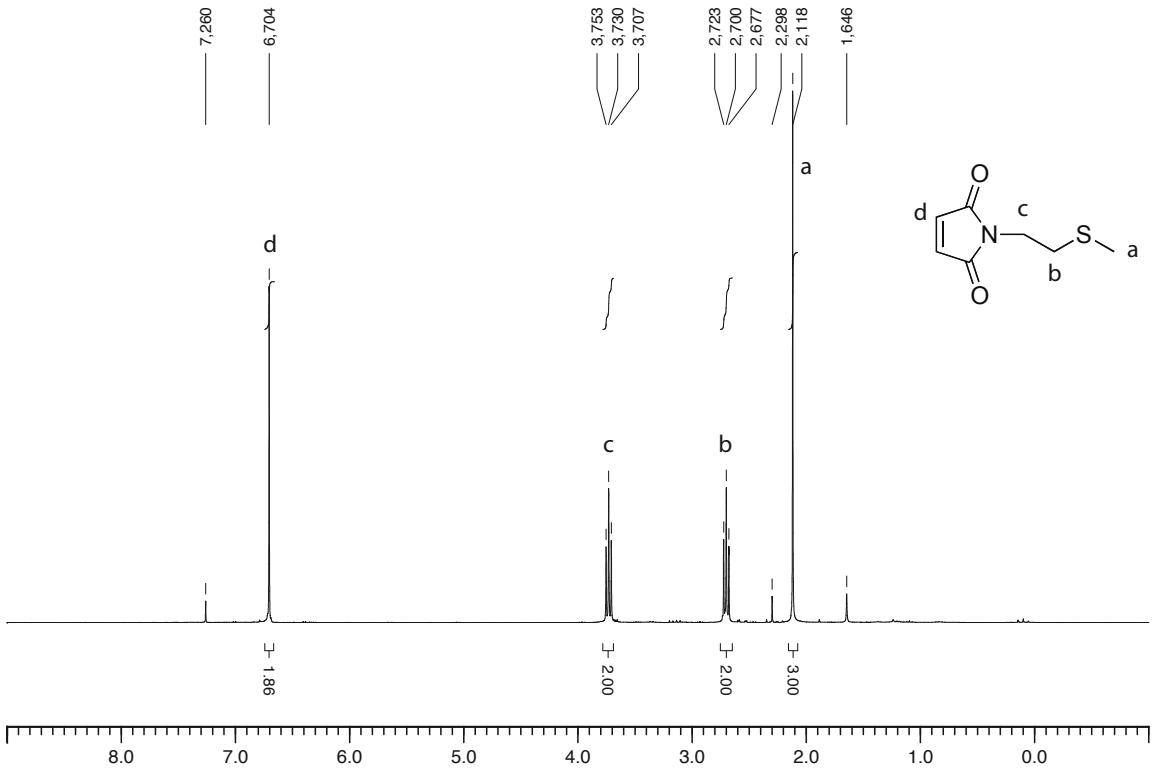

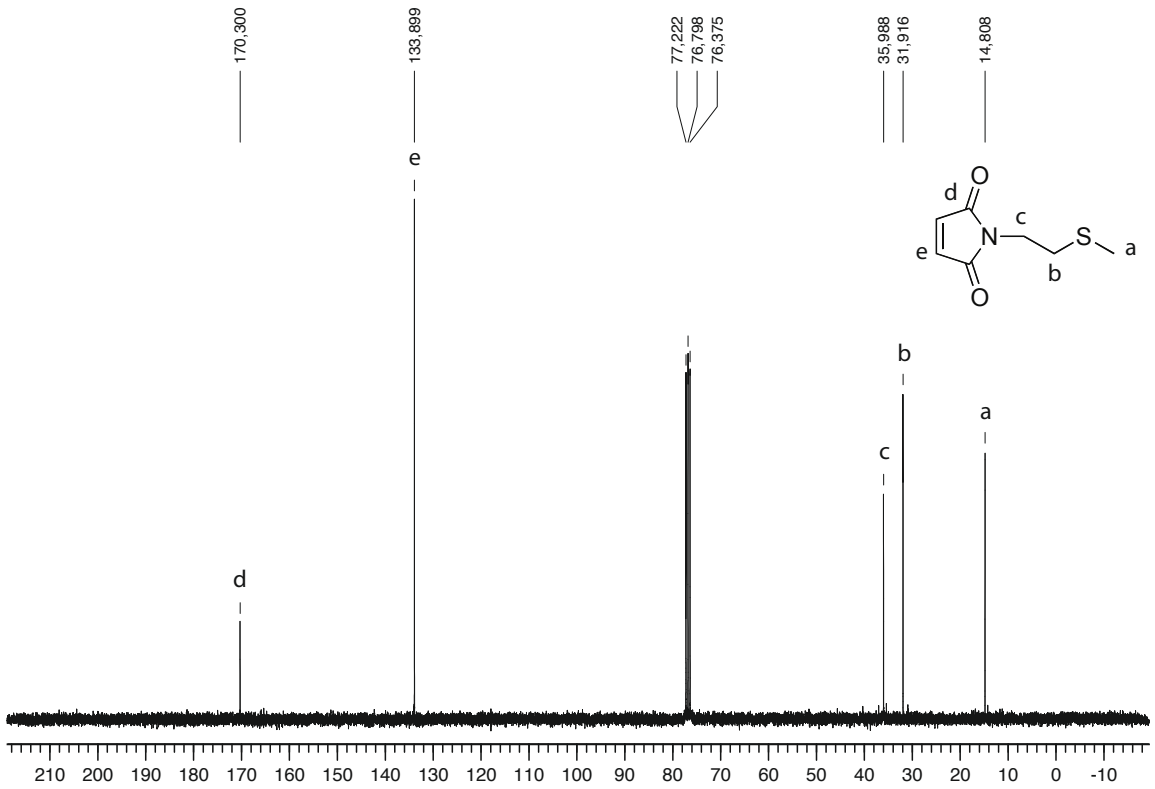

^{1}H- and ^{13}CNMR spectra of 21

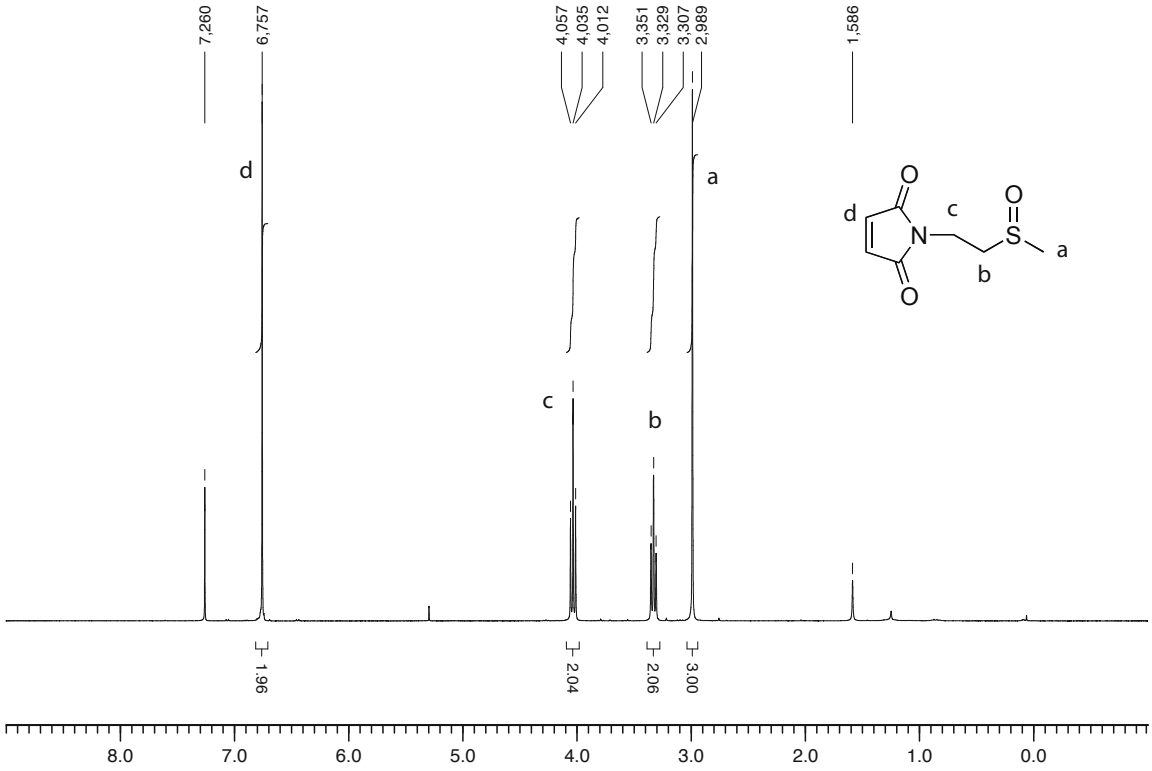

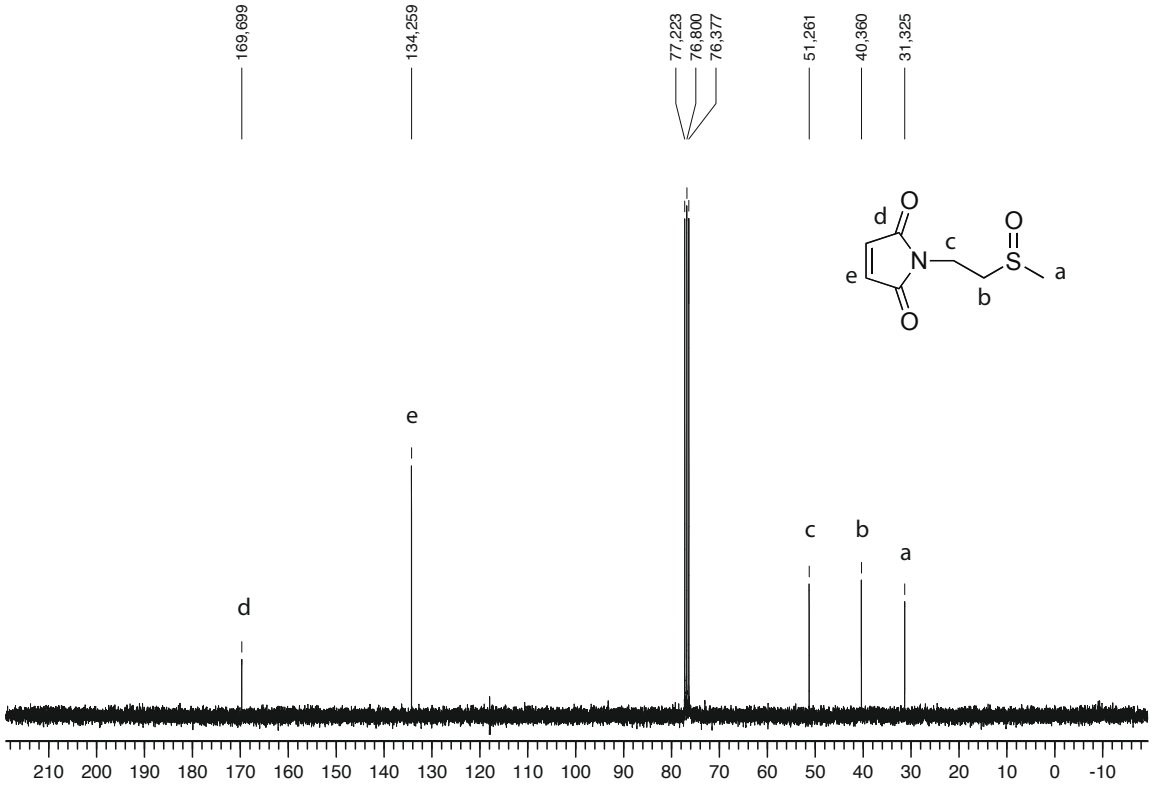

^{1}H- and ^{13}CNMR spectra of 27

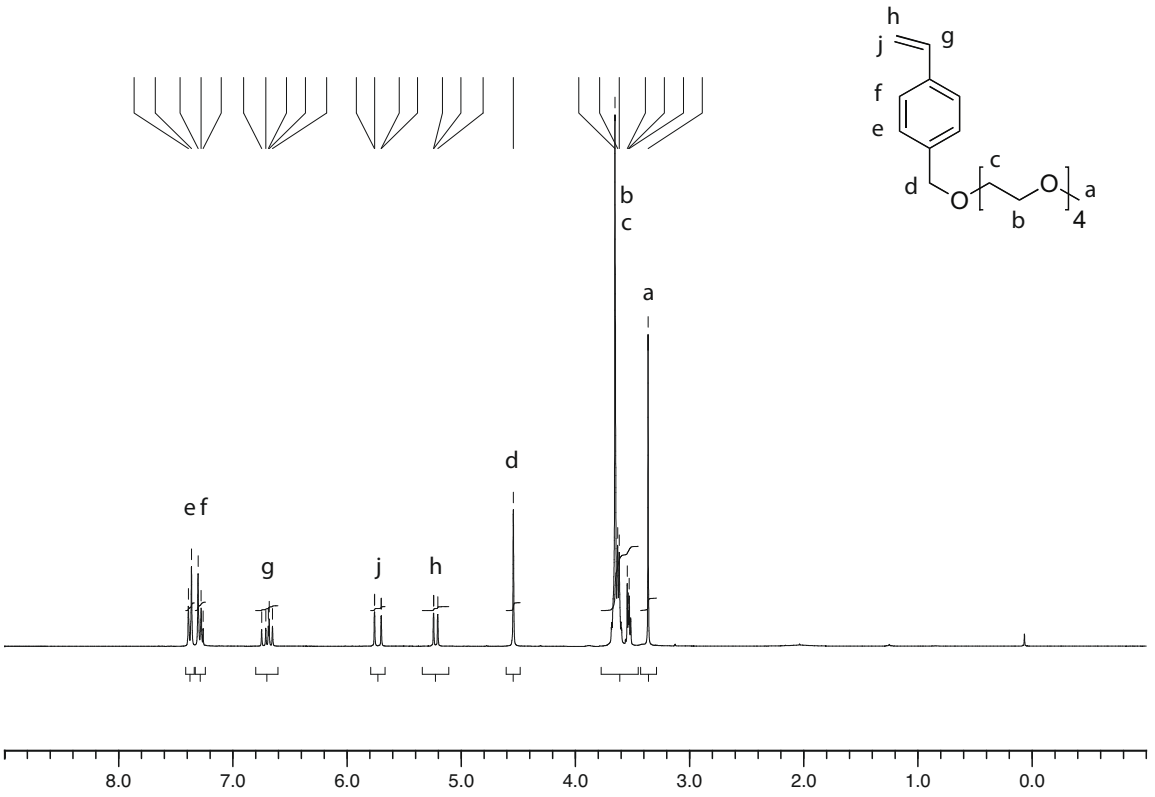

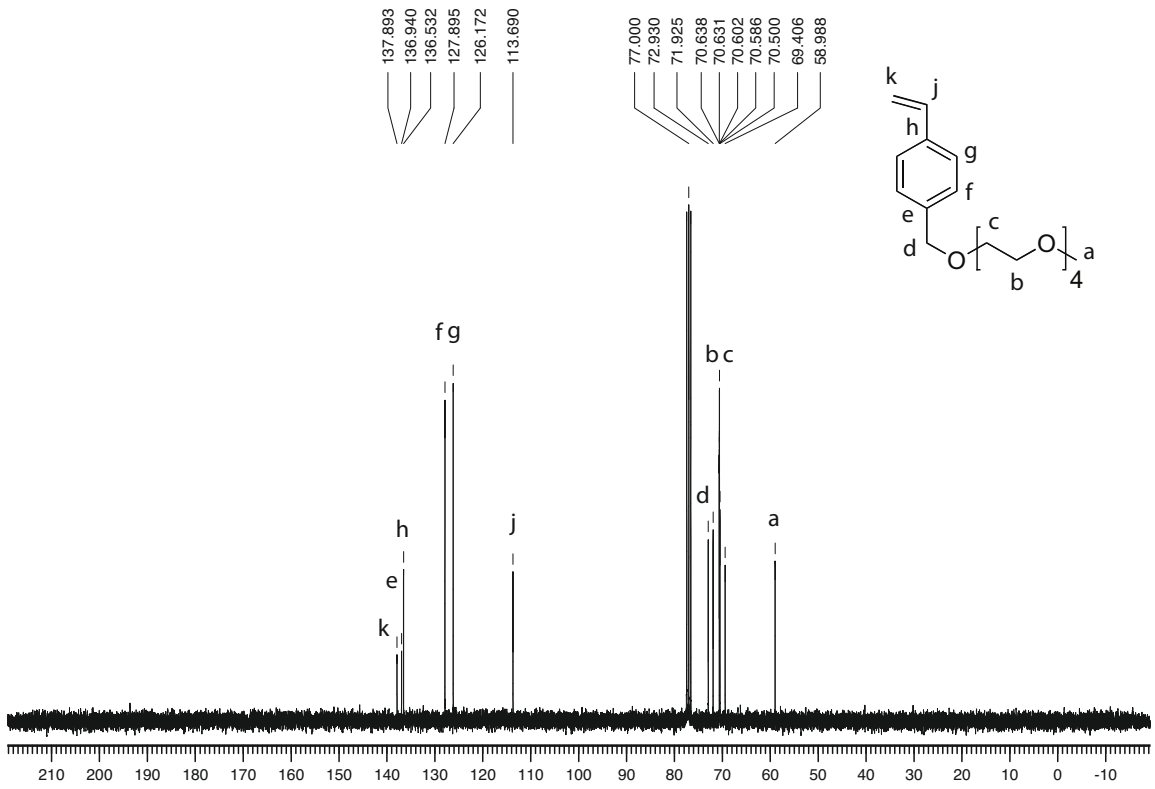

^{1}H- and ^{13}CNMR spectra of 28